PROCESSES AND PRODUCTS IN KIMBERLITIC CRATER FACIES OF THE SOUTH LOBE, JWANENG MINE, BOTSWANA

Kimberley Machin

November 2000

Thesis submitted in fulfilment of the requirements for the degree of

Master of Science in the Department of Geology,

Rhodes University

Declaration

I hereby declare that all the work presented in this thesis is my own, except where otherwise stated in the text.

K.J. Machin

"However much you knock at Nature's door, she will never answer you in comprehensible words."

Ivan Turgenev

ABSTRACT

The Permian (~ 245 Ma) Jwaneng kimberlite, situated in southern Botswana, comprises three steep-sided pipes that coalesce approximately 100m below the present day surface to form a 54ha body. These pipes have been labelled the South, Centre and North Lobes. The kimberlites intruded a thick sequence of Proterozoic shales, dolomites and sandstones and a thin veneer of consolidated to poorly consolidated mudstones and siltstones of the Karoo Supergroup. Although the shapes of these pipes are comparable to other southern African pipes, they are filled predominantly with crater facies volcaniclastic kimberlite. No tuffisitic kimberlite breccia, the characteristic rock type of the diatremes of other southern African pipes, has yet been identified. The Jwaneng kimberlite thus represents an exception to the standard model for southern African kimberlites, implying that different processes need to be invoked to explain its formation.

The present study involves a detailed volcanological and sedimentological analysis of the volcaniclastic fill of the Jwaneng South Lobe. Two principal and distinct lithofacies have been identified: the quartz-free RVK facies and the quartz-bearing QRVK facies. Both facies include fine to coarse grained, predominantly massive and subordinate chaotically-bedded deposits. The volcaniclastic rocks have been classified as resedimented volcaniclastic kimberlite (RVK), since their deposition is ascribed to mechanisms dominated by mass flow processes. Based on certain characteristics and differences between the two principal facies, and their spatial distribution within the pipe, they are interpreted as being the products of at least two separate eruption episodes.

Certain characteristics (e.g. shape, granularity) of the juvenile magma clasts in the volcaniclastic kimberlite suggest complete crystallisation and devolatilisation of the

magma at depth prior to explosive fragmentation. A scenario in which this might have occurred, and which led to catastrophic explosive eruption and pipe excavation is proposed. Explosive eruption and associated tuff cone formation is followed by resedimentation of the material back into the pipe by mass flow processes. Mass flow processes are dominated by debris flow, with lesser grain flow, hyperconcentrated flow and subaqueous mud flow and suspension settling of muddy kimberlitic sediments. Geochemical analyses of the latter indicate a high degree of contamination and weathering, and mixing between pristine kimberlite and silicic shale/mud compositions. Failure and collapse of parts of the underlying pipe walls yielded megablocks of poorly consolidated Permian Karoo mudstone in the peripheral zone of the pipe. This source of the megablocks is supported by their bulk chemical composition.

Minor phreatic/phreatomagmatic eruptions are suggested by the presence of rare accretionary and armoured lapilli within both the QRVK and RVK facies. Subsidence of the volcaniclastic pipe fill, inferred mainly from the oversteepened dips of the bedded QRVK and RVK facies, may be related to gravity-induced compaction, late-stage phreatomagmatic eruptions or eruption of the adjacent Centre Lobe.

TABLE OF CONTENTS

LIST OF TABLES

LIST OF FIGURES

APPENDIX 1: Tables

Table A1: List of core samples and corresponding depths in drillholes DD15, DD68 and DD88.

Table A2: Maximum clast size measurements for the samples from drillcores DD15, DD68 and DD88.

Table A3: The results of modal analysis by macro-pointcounting and micro-pointcounting methods for the sample set.

Table A4: Sample numbers, logging codes, modal proportions and facies codes for drillhole DD15. Modal analyses by point counting are in bold.

Table A5: Sample numbers, logging codes, modal proportions and facies codes for drillhole DD68. Modal analyses by point counting are in bold.

Table A6: Sample numbers, logging codes, modal proportions and facies codes for drillhole DD88. Modal analyses by point counting are in bold.

Table A7: The results of the magma clast shape analysis.

Table A8: Major and trace element compositions of the nine samples analysed in this study (total Fe as Fe2O3; all volatiles as LOI).

Table A9: Major and trace element data for the nine samples normalised to 100% free of volatiles. This data used in all manipulations.

APPENDIX 1: Figures

Key: The shading and pattern fills used in the graphic logs of the three drillholes to denote the grain-matrix relationship, degree of sorting and nature of bedding and other structures of the various facies. The symbols used to indicate the modal abundances of olivine and country rock xenoliths are also shown.

Log of drillhole DD15.

Log of drillhole DD68.

Log of drillhole DD88.

I. INTRODUCTION

Kimberlites are volatile-rich potassic ultrabasic igneous rocks and are the products of continental intra-cratonic magmatism. They differ from most other volcanic rocks in that no extrusive magmatic or plutonic equivalents have been found. Unique styles of emplacement have been postulated for kimberlites occuring mainly in southern Africa (Clement and Skinner 1979, 1985; Clement 1982; Clement and Reid 1989), and these differ from processes associated with maar-diatreme volcanoes, tuff cones and tuff rings, which some authors (Lorenz 1975, 1985, 1999) have suggested are analagous to the upper parts of kimberlite pipes. The present study of the Jwaneng kimberlite, as well as research on recent kimberlite discoveries in Canada (e.g. Field and Scott-Smith, 1999), indicate that the spectrum of kimberlite pipe types and emplacement styles is greater than that previously described from southern Africa.

The concept of a kimberlite pipe model was first published by Hawthorne (1975) and later developed by Clement (1982). The model was based on a number of Cretaceous southern African kimberlite pipes, many of which had been exposed through mining activities. The model was based on the observation that, regardless of depth of erosion, all of the pipes have a similar gross morphology and distinct depth zones, each of which is filled with a characteristic textural variety of kimberlite. Three varieties are recognised: crater facies, diatreme facies and hypabyssal facies and each is associated with a specific style of magmatic activity (Clement and Skinner 1979, 1985, Clement and Reid, 1989). The latter is discussed further in Chapter IV. Further discoveries and investigation of Cretaceous kimberlites in southern Africa, including the less eroded pipes in Botswana (e.g. Orapa, Field et al. 1997), indicated that the large majority of southern African kimberlites conform to this model. It has also been demonstrated that the model is equally applicable to older southern African kimberlites, such as the Ordovician Venetia kimberlite and the Precambrian Premier kimberlite (Field and Scott-Smith, 1999).

However, the Jwaneng kimberlite, situated in southern Botswana (Figure 1), represents an exception to this standard model. The Jwaneng kimberlite comprises three steep-sided pipes that coalesce approximately 100m below the present day surface to form a 54 ha body. These pipes have been labelled the South, Centre and North Lobes, in recognition of their lobate surface expression in plan view (Figure 2).

FIGURE 1: LOCALITY AND REGIONAL GEOLOGY MAP

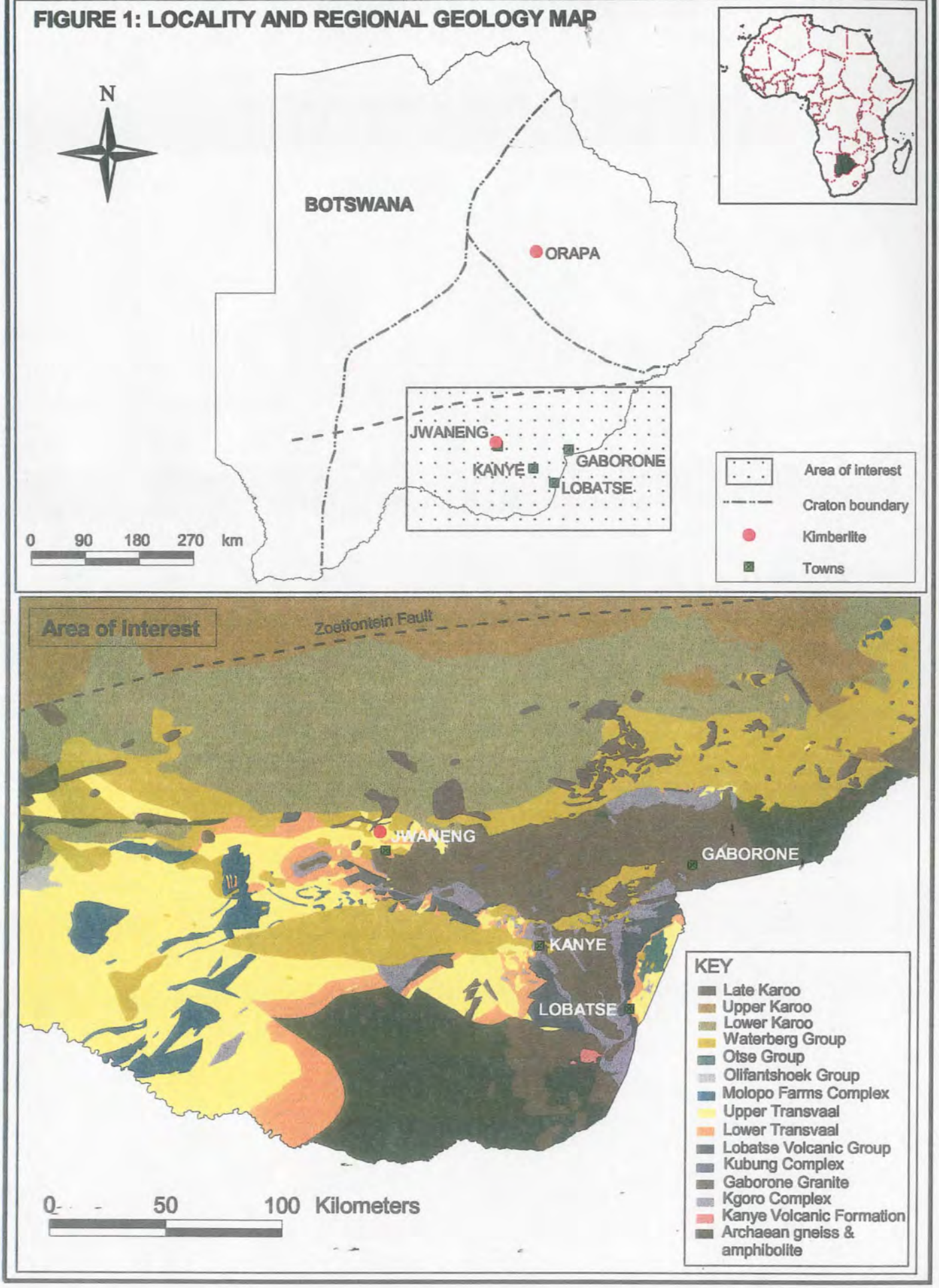

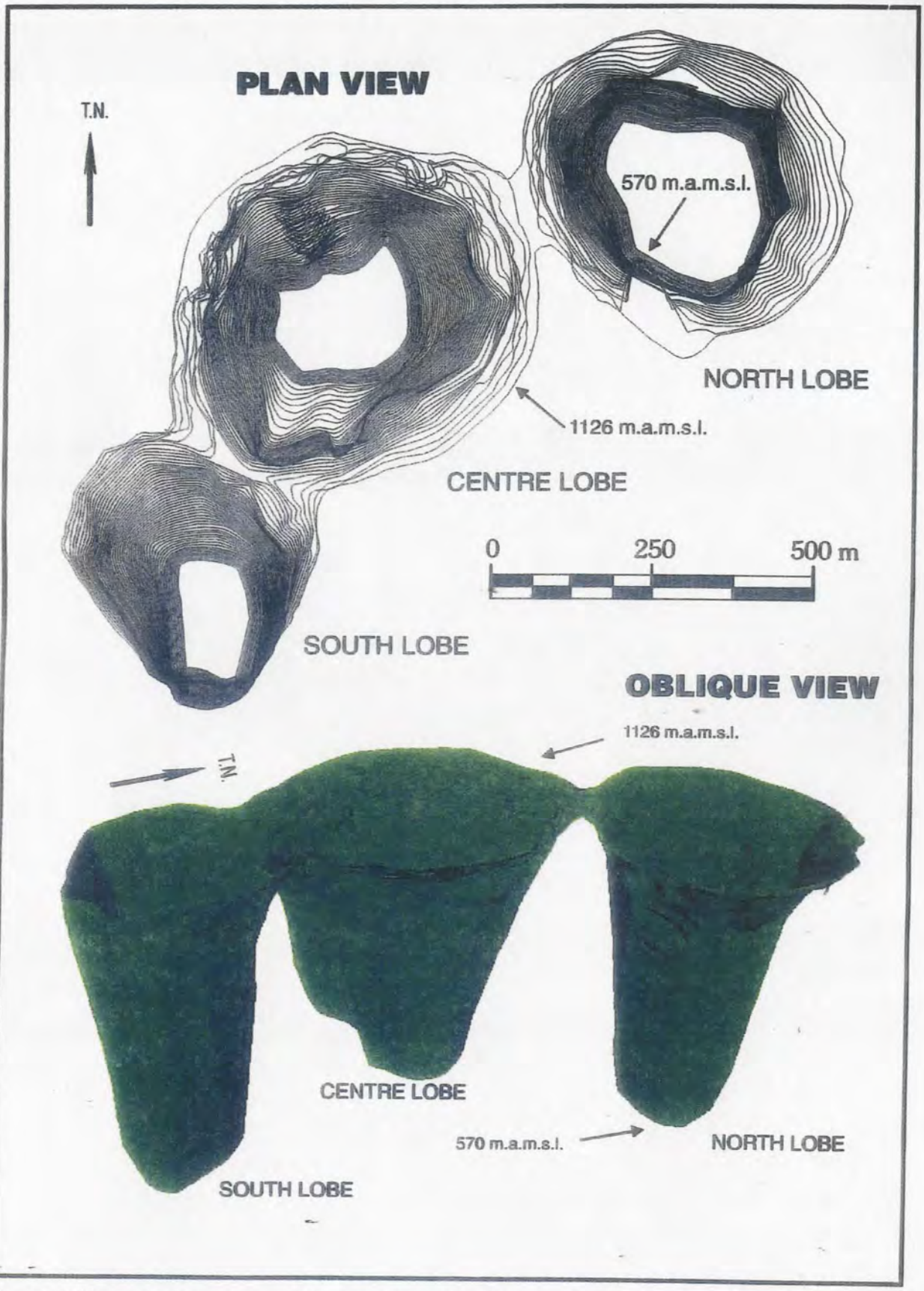

Figure 2: Plan and oblique view of the three pipes of the Jwaneng kimberlite, termed the South, Centre and North Lobes.

Although the shapes of the pipes are comparable to other southern African kimberlite pipes, they are filled virtually exclusively with crater facies volcaniclastic kimberlite. No diatreme facies tuffisitic kimberlite breccia (TKB) has yet been identified. The kimberlite is Permian in age (Kinney et al. 1989), and was emplaced into Early Proterozoic Transvaal Supergroup dolomites and shales, with the cover rocks at the time of emplacement including poorly consolidated Karoo Supergroup mudstones and siltstones, now removed by erosion (Figure 1). The Jwaneng kimberlite thus represents an exception to the standard model for southern African kimberlites, implying that different processes need to be invoked to explain its formation.

Since its discovery in 1973, research on the Jwaneng kimberlite has been limited and thus its geology and emplacement history are poorly understood. However, a recent broad-scale petrographic and modelling project focused on the Centre and North Lobes has revealed that both of these pipes are filled predominantly with chaotically-bedded, resedimented volcaniclastic kimberlite (crater facies), to depths in excess of 600m in the case of the Centre Lobe, and that the North Lobe may also contain some primary pyroclastic kimberlite deposits (Stiefenhofer, 1999).

The present study involves a detailed volcanological and sedimentological analysis of the volcaniclastic fill of the South Lobe of the Jwaneng kimberlite and was initiated in order to gain a broader understanding of the full spectrum of kimberlite pipe types and emplacement styles, particularly in view of the recent work conducted on the Centre and North Lobes of the kimberlite, as well as the discovery in Canada of a number of kimberlite pipes which also do not conform to the emplacement models developed for southern African kimberlites.

1. PREVIOUS WORK ON THE JWANENG KIMBERLITE

Very little research relating to the geology and emplacement of the Jwaneng kimberlite has been published, with the majority of work having been conducted and reported internally by De Beers Consolidated Mines Ltd and Debswana Diamond Mining Company geologists. The discovery of the Jwaneng kimberlite in 1973 was followed by an extensive drilling programme, in addition to the sinking of a number of shafts on the property. This enabled an assessment of the nature of the kimberlite in the upper part of the kimberlite

body. The early petrological characterisation of the kimberlite revealed the presence of stuctureless and bedded fragmental volcaniclastic kimberlite beneath approximately 40m of Kalahari beds (Clement and Skinner, 1978).

During an orebody delineation programme in the 1980's a total of 75 boreholes were drilled within the three pipes (termed Lobes) which constitute the Jwaneng kimberlite. Of the 17 boreholes drilled within the South Lobe, approximately one third were logged and sampled during or soon after the drilling programme was completed (Figure 3). This work and subsequent petrographic examination of the drillcore samples (Field 1988a,b; 1989a-d, 1991) largely substantiates and complements the findings of the present study. However, despite these and similar studies conducted in the Centre and North Lobes, the internal geology of the Jwaneng kimberlite remained poorly understood, due to the unusual nature of the kimberlite and the lack of any detailed research.

In 1998 a broad-scale petrographic investigation and modelling project commenced at the Mine (Stiefenhofer, 1999). The project focused exclusively on the Centre and North Lobes of the Jwaneng kimberlite, and aimed to identify and document geological units, correlate the geology with diamond grades and develop emplacement models for the two Lobes. Key issues revealed by this study include the following: the Centre Lobe is filled predominantly with resedimented volcaniclastic kimberlite, whereas the North Lobe comprises both resedimented volcaniclastic kimberlite and pyroclastic kimberlite deposits.

The age of the Jwaneng kimberlite has been determined by both U-Pb ion microprobe analysis of zircons and Rb-Sr analysis of micas, which yielded ages of 235±4 Ma and 250±17 Ma, respectively (Kinney et al. 1989). Attempts to substantiate the radiometric emplacement age and to elucidate the palaeoenvironment have included limited palynological studies and identification of fossil wood specimens derived from the kimberlite (Stiefenhofer, 1999). Palynological work has been conducted during this study on selected mudstone samples from the South Lobe and the results are discussed in Chapter III, Section 6.

Field and Scott-Smith (1999) briefly outline the geology of the Jwaneng kimberlite as part of a comprehensive review which compares and contrasts the geology and near-surface emplacement of kimberlites in southern Africa and Canada. Additional accounts of crater

facies kimberlite preserved in kimberlite pipes in Botswana, Tanzania, and Canada are given by Field et al. (1997), Edwards and Howkins (1966), and Carlson et al. (1999).

2. AIMS AND SCOPE OF THE PROJECT

Considering the lack of any comprehensive study of the South Lobe of the Jwaneng kimberlite the aims of the project were as follows:

i) to determine the volcanological and sedimentological character of the volcaniclastic fill of the South Lobe through a detailed analysis of clast size and shape, clast size distribution and juvenile and xenolithic modal abundances
ii) to determine the relative distribution and petrological character of the various lithofacies which constitute the fill
iii) to determine the petrological variety and possible origin of the xenolithic megablocks which occur in the peripheral zones of the Lobes
iv) to attempt to constrain the palaeoenvironment at the time of eruption
v) to investigate possible eruption mechanisms and crater filling processes based on the results obtained and by comparison with other kimberlites and similar non-kimberlitic volcanic centres
vi) to propose an emplacement model for the South Lobe to account for the origin of the pipe and its fill
vii) to highlight any implications of the latter for kimberlite pipe emplacement mechanisms in general.

Although there is little doubt that the processes involved in the emplacement of the three pipes which constitute the Jwaneng kimberlite are closely related, it is beyond the scope of this study to propose or expand upon emplacement models for the Centre and North Lobes, or to attempt to interpret the relative evolution of the Jwaneng kimberlite as a whole. However, it would be shortsighted to completely disregard the nature of the other two Lobes, and thus gross comparisons of the South Lobe in relation to the other two Lobes will be made.

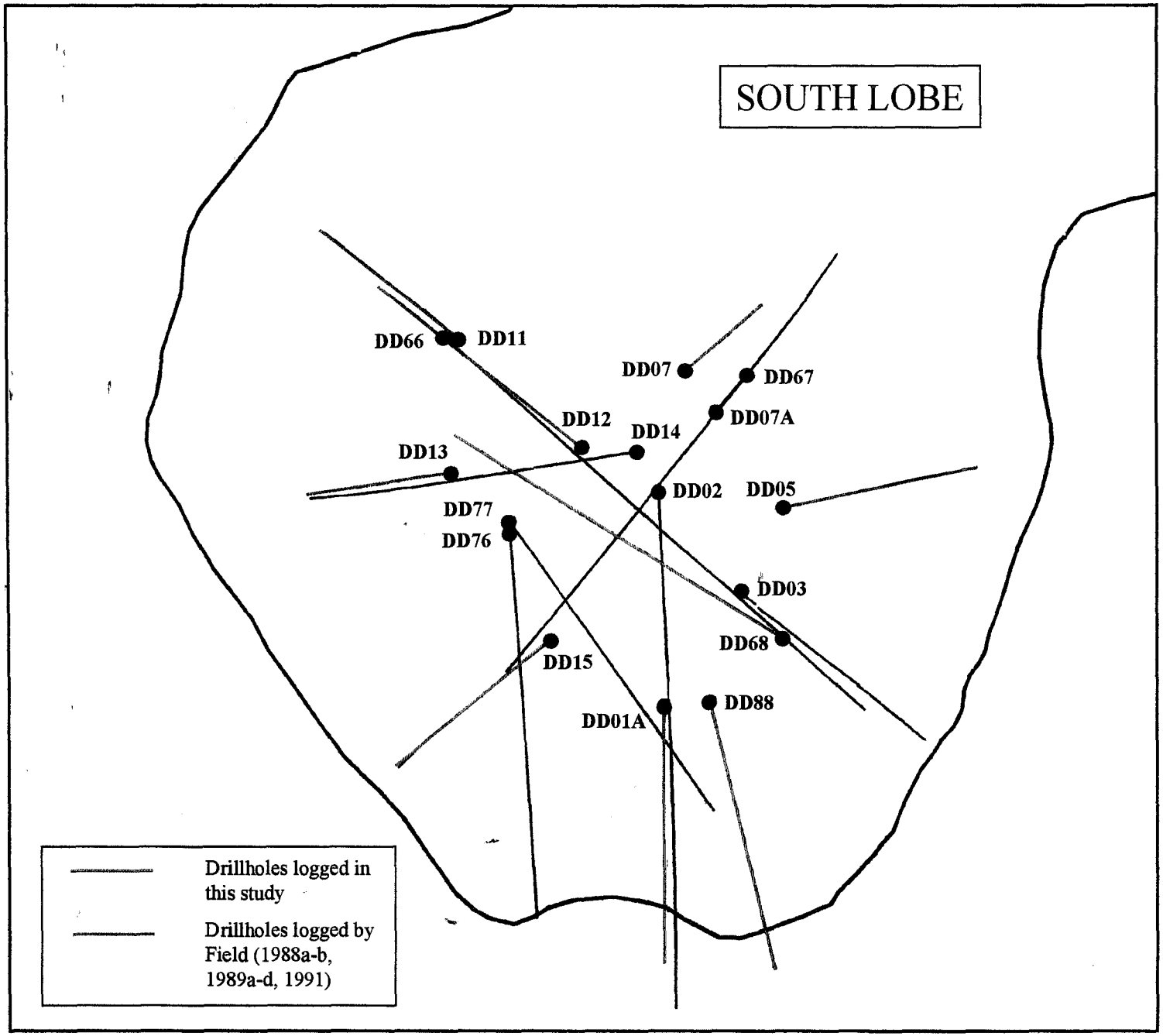

Figure 3: Plan view of the Jwaneng South Lobe showing the boreholes drilled, and indicating those logged in the present study and those logged by Field (1988a-b, 1989a-d, 1991).

3. GEOLOGICAL SETTING

The Jwaneng kimberlite is situated approximately 120 km north-west of Kanye in southern Botswana (Figure 1), and is the largest of a cluster of 11 kimberlites discovered in the area. The Jwaneng kimberlite consists of three steep-sided kimberlite pipes which coalesce approximately 100m below the present day surface to form a 54 ha body. The three pipes have been labelled the South, Centre and North Lobes (Figure 2). A fourth, much smaller pipe, is situated close to the eastern margin of the South Lobe, but is not currently being mined. Of the other kimberlites in the cluster, the 5 ha bilobate DK7 kimberlite, situated approximately 7 km to the east of Jwaneng Mine, is the only other body of economic significance. Most of the Jwaneng kimberlites are overlain by 35 – 45m of sand, silcrete and calcrete of the Kalahari beds (Carney et al. 1994). It is not clear how much the pipes have been eroded since emplacement, although estimations in the order of 250 to 300m seem reasonable (see Chapter IV, Section 1).

The Jwaneng kimberlite cluster occurs in an on-craton setting and is located in the northwestern part of the Kaapvaal Craton, approximately 55km south of the east-northeast trending Zoetfontein Fault (Figure 1). The Kaapvaal Craton, Zimbabwe Craton and Limpopo Belt together constitute the Archaean-age basement sequences of Botswana. In the Jwaneng area the Kaapvaal Craton comprises the Gaborone Granite, which is a texturally varied assemblage of alkali granites that dominates the geology of southeastern Botswana (Carney et al. 1994).

The basement granite complex is unconformably overlain by local equivalents of the Early Proterozoic Transvaal Supergroup, namely the Segwagwa Group (upper Transvaal Supergroup) and the Taupone Dolomite Group (lower Transvaal Supergroup; Table 1). At Jwaneng Mine, the various shale formations of the Segwagwa Group, which are equivalents of the Rooihoogte and Timeball Hill Formations of the Pretoria Group, are currently exposed in the walls of the open pit. The shales constitute the dominant country rock xenolith lithology within the kimberlite. Two prominent marker horizons of the Segwagwa Group are also exposed in the pit walls: the Bevets Conglomerate Member, which is a distinctive chert-clast conglomerate, and a medium- to coarse-grained arenite known as the Polo Ground Quartzite Member. The Taupone Dolomite Group has been intersected in drillcore, but has not yet been exposed in the pit. It occurs as less abundant

xenoliths in the kimberlite and is composed predominantly of massive dolomites interlayered with chert bands. Proterozoic dolerite and syenite sills and dykes can also be observed in the pit walls.

The Waterberg Group is an assemblage of sandstones, conglomerates and siltstones, and is one of the oldest occurrences of continental red-beds sedimentation on Earth. In Botswana the main outcrop lies within a west-southwest trending belt south of the Zoetfontein Fault (Carney et al. 1994). The Waterberg Group is not exposed within the Jwaneng Mine open pit, but pockets of Waterberg Group sandstones and conglomerates unconformably overlie Transvaal Supergroup rocks in the Kgome Quarry to the south-west of Jwaneng (Stiefenhofer, 1999). This, together with the occurrence of probable Waterberg quartzite xenoliths within the kimberlite, suggests that the Waterberg Group was present at the time of intrusion of the kimberlite, although its thickness is difficult to estimate.

The Karoo Supergroup is an extensive Carboniferous to Jurassic sequence comprising sedimentary and volcanic successions which have a widespread outcrop within the southern African subcontinent. In Botswana it unconformably overlies Archaean and Proterozoic rocks over approximately 70 percent of the area (Carney et al. 1994). It is poorly exposed, however, being in turn overlain unconformably by the Cretaceous to Recent Kalahari beds. The Dwyka Group occurs at the base of the Karoo Supergroup and was deposited during a major Permo-Carboniferous glaciation. It is succeeded by the Ecca and Beaufort Groups which comprise shallow marine to fluviatile sediments that reflect conditions of increasing continentality and a change to warmer, more arid palaeoclimates. The Lower Jurassic Stormberg Lava Group (equivalent of Drakensberg Group in the main Karoo Basin of South Africa) marked the end of the Karoo sedimentation. The flood basalts were deposited onto a desert landscape consisting of aeolian sands (Ntane/Clarens Formation) of the Lebung Group. According to Smith (1984) and Carney et al. (1994), these Groups (excluding the Stormberg Lava Group) will in part be diachronous in terms of the southern African subcontinent, since they evolved at a time when Gondwana was 'drifting' northwards into lower latitudes.

Estimates of the age of intrusion of the Jwaneng kimberlite include the following: (1) an age of 235 ± 4 Ma was obtained from an average of nine U-Pb ion microprobe analyses of zircons from the Jwaneng kimberlite, and (2) Rb-Sr analyses of macrocrystal phlogopite

mica separated from a hypabyssal intrusion in the adjacent DK7 kimberlite yielded an isochron age of 250 ± 17 Ma (Kinney et al. 1989). A Permian age of emplacement (~ 245 Ma) for the Jwaneng kimberlite cluster (at least the Jwaneng kimberlite and DK7) extends the age range of the known Mesozoic and younger kimberlites of southern Africa (Smith et al., 1985a).

The ~ 245 Ma emplacement age of the Jwaneng kimberlite places it within the depositional period of Karoo sediments (Beaufort Group). The presence of significant quantities of consolidated and unconsolidated mudstone xenoliths in the volcaniclastic kimberlite further indicates that the cover rocks at the time of emplacement included poorly consolidated Karoo mudstones and siltstones. However, exposures of the Karoo Supergroup are no longer present in the Jwaneng area. Jwaneng Mine lies approximately 20 km south of the Southern Belt of the Central Kalahari Sub-basin, as defined by Smith (1984) in his lithostratigraphic scheme for the Karoo Supergroup in Botswana. The Southern Belt lies between the pre-Karoo outcrop or subcrop to the south and the Zoetfontein Fault in the north. There is no evidence to suggest that the Dwyka Group (Dukwi Formation) was present in the Jwaneng area at the time of kimberlite emplacement. It may have occurred only locally and thickened away from the sub-basin margins. Taking into account the complete erosion of the Karoo Supergroup in the Jwaneng area and considering its location on the extreme southern margin of the sub-basin, the combined thickness of the Karoo Supergroup at the time of kimberlite emplacement could not have been extensive, and was probably less than 100m. Certain of the xenolithic megablocks which occur within the Jwaneng kimberlite are inferred to represent downrafted masses of the original land surface present at the time of eruption, and can thus provide an idea of the nature of Karoo sedimentation at that time. The megablocks are discussed further in Chapter III, Section 5.

The Lower Ecca subgroup (Bori Formation) is composed predominantly of argillites and carbonaceous argillites with subordinate sandstone intercalations. The Middle Ecca subgroup (Kweneng Formation) comprises a predominantly medium- to coarse-grained feldspathic sandstone succession with intercalated dull coal bands and coaly mudstones. The Upper Ecca subgroup (Boritse Formation) consists of a sequence of alternating coals, mudstones, siltstones and finer-grained sandstones. Whereas the Lower Ecca subgroup was deposited in a post-glacial lacustrine and deltaic environment, the Middle and Upper

subgroups of the Ecca were mostly formed in fluviodeltaic and swamp environments under subarctic to cool temperate conditions. The presence of the Ecca Group (at least the Middle and Upper subgroups) in the Jwaneng area at the time of kimberlite emplacement is indicated by the occurrence of coal fragments within the volcaniclastic kimberlite of the South Lobe.

The possible existence in Botswana of beds equivalent to the Beaufort Group in South Africa was recognised in the scheme of Smith (1984). In the Southern Belt of the Central Kalahari Sub-basin, the thick succession of non-carbonaceous mudstones and silty mudstones which occurs above the carbonaceous beds of the Ecca Group and below the Lebung Group is termed the Kwetla Formation. Smith (1994) suggests deposition of the Kwetla Formation in a fluvio-lacustrine environment under semi-arid conditions.

Table 1: The stratigraphy of the Jwaneng area at the time of kimberlite emplacement, and equivalent stratigraphic units in South Africa.

Stratigraphy in Jwaneng area, Botswana	**Equivalent stratigraphy in South Africa**		**Age**	**Thickness**	**Consolidation at time of kimberlite eruption**
Kwetla Formation	Beaufort Group	Karoo Supergroup	Permian-Triassic	~ 100m ?	Poorly consolidated
Boritse Formation	Upper Ecca		Permian		Partly consolidated
Kweneng Formation	Middle Ecca		Permian		Consolidated
Bori Formation	Lower Ecca		Permian		Consolidated
Waterberg Group	Waterberg Group		Mid-Proterozoic	~ 100m ?	Consolidated
Segwagwa Group	Upper Transvaal Supergroup	Transvaal Supergroup	Early Proterozoic	1000m ?	Consolidated
Taupone Dolomite Group	Lower Transvaal Supergroup			1700m ?	Consolidated
Gaborone Granite			Archaean	?	Consolidated

II. METHODOLOGY

1. TERMINOLOGY

The terms used to describe the textural variants of kimberlite and the pipe zones in which they occur are generally used in a kimberlite-specific sense and require definition.

The extensive mineralogical and textural variations exhibited by kimberlites have led to the development of numerous classification schemes (Wagner 1914, Dawson 1971, Clement and Skinner 1979, Clement 1982 and Clement and Skinner 1985, Mitchell 1995) which, until recently, has resulted in considerable nomenclatural confusion. Classification of kimberlites is based on the understanding that the textural variations result primarily from different near-surface emplacement processes. The textural-genetic classification scheme developed by Clement and Skinner (1979, 1985) recognised three textural-genetic groups of kimberlite, each associated with a specific style of magmatic activity, namely crater, diatreme and hypabyssal facies kimberlite. Shortcomings of this classification scheme, mainly in regard to its genetic aspect, have recently been recognised by Field and Scott-Smith (1998, 1999). These authors propose a new textural classification scheme based on five descriptive textural categories, namely: juvenile magma texture, structure, clast/grain size, xenolith/autolith content and type, and cognate olivine content. This scheme thus enables an initial non-genetic descriptive classification of the rock, which can then be used to derive a genetic classification when possible.

A further contribution of the new classification scheme is the clarification of concepts relating to pipe shape and pipe zones. Field and Scott-Smith (1998, 1999) suggest that kimberlite *pipe* be used as a non-genetic term to describe a body that is not tabular or sheet-like in shape, and that the term *diatreme* should only be used if the pipe can be shown to have formed by the fluidisation processes of the southern African kimberlite model, as described by Field and Scott-Smith (1999). Furthermore, since the textural types of kimberlite are typical of, but not exclusive to, certain pipe zones, the terms crater facies, diatreme facies and hypabyssal facies should only be used if the main fill of a pipe zone is characteristic of that zone. The latter is of particular relevance to Jwaneng.

Brief definitions of the terms used to describe the various textural kimberlite types and pipe fills are given below (after Field and Scott-Smith, 1999):

The texture of the juvenile kimberlite magma is the fundamental feature that reflects the mode of emplacement. *Magmatic* kimberlites display textural features indicative of crystallisation from coherent magmas, while *magmaclastic* kimberlites are those derived from disrupted magmas. Magmaclastic rocks are characterised by the presence of *juvenile magma clasts* which are set in a contrasting *inter-clast matrix* of either *magmatic* or *non-magmatic* origin.

Volcaniclastic Kimberlite (VK) describes extrusively formed fragmental kimberlite deposits for which the mode of deposition is unknown. The general non-genetic term 'volcaniclastic' is used in the sense proposed by Fisher (1961).

Resedimented Volcaniclastic Kimberlite (RVK) is used here to describe VK for which depositional mechanisms can be ascribed to mass flow redeposition processes involving little textural modification. Gravitational *resedimentation* should be distinguished from tractional *reworking* which may involve abrasion and rounding of clasts. RVK replaces the term 'epiclastic kimberlite' in the classification scheme of Clement and Skinner (1985).

Pyroclastic Kimberlite (PK) describes VK for which *prima facie* evidence shows direct deposition by explosive volcanic processes. Standard pyroclastic terminology (Fisher and Schmincke 1984, Cas and Wright 1987) may be applied to pyroclastic kimberlites.

VK, RVK and PK typically dominate the crater zone of most kimberlite pipes.

Tuffisitic Kimberlite Breccia (TKB) or Tuffisitic Kimberlite (TK) are terms originally introduced by Clement and Skinner (1979, 1985), and are used to describe the intrusive filling that is typical of the diatreme zone of many kimberlite pipes. TKB/TK is a very specific textural variety of kimberlite composed predominantly of rounded juvenile magma clasts termed pelletal lapilli, mixed country rock xenoliths and serpentinised macrocrysts and phenocrysts of olivine set in a fine-grained interclast matrix. The detailed nature of the pelletal lapilli and inter-clast matrix, such as the presence of abundant diopside microlites and the absence of matrix carbonate, are diagnostic of this rock type and its emplacement process.

Hypabyssal kimberlite (HK) describes the intrusive rock formed by crystallisation of a non-disrupted kimberlite magma, that is, magma which has not been subjected to fluidisation or pyroclastic eruption. HK commonly has a uniform texture, although segregationary textures may form under certain conditions. HK typically occurs in the root zones of pipes, but can also occur in tabular and sheet-like bodies.

The Jwaneng pipe, as well as a number of Canadian occurrences (Kirkley et al. 1998, Berg and Carlson 1998, Carlson et al. 1999, Field and Scott-Smith 1999, Graham et al. 1999), are good examples of cases where a specific textural variety of kimberlite is not exclusive to the corresponding pipe zone, implying different emplacement mechanisms to those of the standard model (Hawthorne 1975, Clement 1982, Mitchell, 1986).

2. GRAIN/CLAST SIZE CLASSIFICATION

One of the most important textural features of any rock is the grain or clast size. Because size is a continuous variable and many particles are required for a good estimate, a grain size or grade scale is always necessary. Selection of a suitable grain size scale should be based on the nature of the rocks being studied, the type of analyses to be conducted and the objectives of the study.

The most commonly applied grain size scale in studies of volcaniclastic rocks (Fisher and Schmincke 1984, Cas and Wright 1987, McPhie et al. 1993) is the Udden-Wentworth grain size scale (Udden 1914, Wentworth 1922). Although originally devised as the standard for objective description of non-volcanic clastic sediments, it has been modified for use by volcanologists by varying the boundaries of the size class subdivisions and the terms assigned to these subclasses. A similar approach has been adopted in this study in the selection of grain size classes used in the description and analysis of the South Lobe RVK. The grain size classes are indicated in Table 2.

Table 2: The grain size scale and classes used to describe and classify the South Lobe RVK and the equivalent size classes of the modified Udden-Wentworth grain size scale (Blair and McPherson, 1999).

Grain size (mm)	RVK size class	Equivalent Udden-Wentworth size class
< 2	fine	clay, silt, sand
2 – 4	*fine*-medium	granule
> 4 - 8	medium	fine pebbles
> 8 - 16	coarse	medium pebbles
> 16	very coarse	coarse and very coarse pebbles

The grain size recorded is the mean grain size of the non-juvenile lithic component, rather than the juvenile component (olivine and magma clasts) of the RVK. The decision to conduct clast size measurements on the lithic clasts was based on the poor resolution of the juvenile component in the rough uncut drillcore and pit exposures, as a result of the high degree of alteration and poor competency.

Since a volumetrically minor proportion of the RVK displays mean grain sizes less than 2mm (the clay, silt and sand size fraction), these deposits are grouped into a single size class, and are termed **fine grained**. The mean grain size of the majority of the RVK falls within the gravel fraction of the Udden-Wentworth grain size scale, particularly the granule (2 – 4mm) and pebble (4 – 64mm) size classes. To facilitate a detailed analysis, these deposits are subdivided into four separate size classes, namely ***fine*-medium grained** (2 – 4mm), **medium grained** (> 4 – 8mm), **coarse grained** (> 8 – 16mm) and **very coarse grained** (> 16mm). These size classes correlate with the granule, fine pebble, medium pebble and coarse and very coarse pebble grades (respectively) of the modified Udden-Wentworth grain size scheme. This modification, proposed by Blair and McPherson (1999), involves the extension of the Udden-Wentworth scheme into the gravel fraction to produce more detailed grades, as well as the introduction of a megagravel fraction for particles coarser than boulders (see Chapter III, Section 5).

It should be noted that the grain size classes described above differ from those used in previous studies of the Jwaneng crater facies kimberlite (Field 1988a-b, 1989a-d, 1991; Stiefenhofer 1999), mainly in terms of the boundaries used to define the subclasses. Furthermore, whereas Field (1988a-b, 1989a-d, 1991) measured the average grain size of the lithic clasts, Stiefenhofer (1999) subdivided the RVK according to the mean grain size of the juvenile constituents.

3. LITHOFACIES CLASSIFICATION AND CODES

The lithofacies approach is a convenient way of identifying, describing and interpreting distinctive intervals and/or associations of rocks within a particular succession. Although the concept is most commonly used in non-volcanic sediments, it is also applicable in volcaniclastic successions (Cas and Wright, 1987). The attempt to subdivide a rock body into constituent facies is a classification procedure, and the scale of subdivision is dependant not only on the objectives, but also on the abundance and variability of physical structures in the rocks.

With respect to facies nomenclature, the development of a Logical-Letter Coding (LLC) system facilitates a rapid but standardised description of the deposits and their internal structures. A classic example of a LLC scheme is that proposed by Miall (1977, 1978) for facies nomenclature related to the braided stream depositional environment. Logical-letter coding entails the grouping of letters that are representative of certain physical attributes within the rock or sediment that constitute a designated lithofacies. This concept has been adopted and applied to the lithofacies subdivision and description of the Jwaneng South Lobe RVK. A similar approach has been taken by workers in other fields of research (e.g. Le Blanc Smith, 1980).

Although the South Lobe RVK displays considerable variation on a small-scale, it is megascopically relatively homogenous and as a result, the scale of lithofacies subdivision is fairly limited. The designated lithofacies codes comprise a cluster of letters that respectively constitute: the mineralogical composition, the internal structure (bedding) and the mean grain size of the rock. The composition and internal structure parameters are portrayed in upper-case lettering, with any subdivisions of these being appended in lower-case lettering. The grain size qualifier occurs at the end of the code in lower-case lettering. Subordinate qualifying criteria, specifically the grain-matrix relationship and degree of sorting, are not included in the code, but rather indicated on the graphic logs by way of various shading or pattern fills. The reason for this is largely to avoid the facies code from becoming too long and cumbersome (also, since the majority of the deposits are clast-supported and poorly sorted, the inclusion of these criteria in the facies code would be unnecessarily repetitive). Any additional variations to a facies are appended to the code in subscript format.

The principle lithofacies of the South Lobe crater fill are as follows: the quartz-free RVK facies (**RVK**) and the quartz-bearing RVK facies (**QRVK**). The QRVK facies is subdivided into two lower-case lithofacies subcategories based on the proportion of quartz present. These are termed the quartz facies (**q**), in which quartz predominates, and the juvenile/quartz facies (**j/q**), in which the juvenile component is dominant, but quartz is present. These lithofacies were similarly coded by Field (1988a-b, 1989a-d, 1991), using an earlier, less comprehensive code scheme than that described here.

With respect to internal structure, both the RVK and the QRVK facies include deposits which are either massive (**M**) or bedded (**B**). The QRVK facies also comprises deposits which display evidence of soft sediment deformation, possibly resulting from slumping (**S**). The bedding in the RVK facies is either vague (**v**) or distinct (**d**). These subdivisions are excluded from the QRVK facies code since all the bedding observed in this facies is distinct. To avoid confusion between the bedding subqualifiers and the grain size qualifiers, the letters denoting the nature of bedding are given as subscripts.

The letter codes used for the grain size classes of the principle lithofacies are: fine grained (**f**), *fine*-medium grained (***fm***), medium grained (**m**), coarse grained (**c**) and very coarse grained (**vc**).

An example of the manner in which the LLC is built up is as follows: a vaguely bedded medium grained RVK deposit would be coded as RVK-B_vm. The lithofacies subdivisions and the corresponding codes are indicated in Table 3. The shading and pattern fills used in the graphic logs to denote the grain-matrix relationship and degree of sorting may be found in Appendix 1. The spatial and petrographic characteristics of the lithofacies are described in Chapter III.

The code devised and utilized by Field (1988a-b, 1989a-d, 1991) for the Jwaneng crater facies is useful for rapid logging of drillcore, but lacks detailed information such as composition and the nature of bedding. The logical-letter code scheme adopted from Miall (1977, 1978) and modified in this study has the merit of being hierarchical and readily memorised. It also has the potential to be expanded and refined.

Table 3: The lithofacies classification and facies codes used in this study.

COMPOSITION		BEDDING		GRAIN SIZE	FACIES CODE
RVK		MASSIVE		fine	RVK-Mf
				fine-medium	RVK-M*f*m
				medium	RVK-Mm
				coarse	RVK-Mc
					RVK-Mc_{srb}
		BEDDED	vague	*fine*-medium	RVK-B_v*f*m
				medium	RVK-B_vm
				coarse	RVK-B_vc
			distinct	fine	RVK-B_df
				fine-medium	RVK-B_d*f*m
				medium	RVK-B_dm
				coarse	RVK-B_dc
QRVK	**quartz**	MASSIVE		*fine*-medium	QRVKq-M*f*m
				medium	QRVKq-Mm
				coarse	QRVKq-Mc
		BEDDED		*fine*-medium	QRVKq-B*f*m
				medium	QRVKq-Bm
		SLUMPED		fine	QRVKq-Sf
	juvenile/quartz	MASSIVE		*fine*-medium	QRVKj/q-M*f*m
				medium	QRVKj/q-Mm
		BEDDED		*fine*-medium	QRVKj/q-B*f*m
				medium	QRVKj/q-Bm

4. IN-PIT MAPPING

Field data for this study was collected by: (1) mapping of exposures within the open pit and (2) logging of drillcore (see Section 5) during three separate visits to the mine, each three to six months apart (May 1999, September 1999 and April 2000). Of the three pipes which constitute Jwaneng Mine, the South Lobe has been the least actively mined, with the depths to mining levels from surface for the South, Centre and North Lobes at the commencement of the project being 128m, 224m and 188m, respectively. The advantage of mapping in an active mine is the continual availability of new exposures and benches, although accessibility is variable and in some instances impossible. During the three phases of fieldwork, the following South Lobe benches contained exposures that were partially or totally accessible for mapping purposes: Bench 11, Bench 12 and Bench 14, in addition to a veneer of kimberlite along the wall-rock contact on Bench 13. The orientation of the bench faces mapped is variable and is indicated in Figures 5 – 7 (Chapter III, Section 1) . The benches expose vertical faces approximately 12m in height.

The principal aims of the in-pit mapping exercise were as follows:

(i) to examine and describe the lateral and vertical variation of the lithofacies in terms of composition, juvenile and xenolithic content, internal structure and grain size

(ii) to examine the nature and lateral continuity of bedding

(iii) to examine the nature of contacts between the various lithofacies and the kimberlite-wallrock contact

(iv) to identify any possible marker horizons

(v) to identify and describe any megablocks in the peripheral zones of the pipe

(vi) to compare the marginal and central zones of the pipe

(vii) to observe and describe any features and/or structures which might correlate with those recorded during drillcore logging or which may have been undetected or misinterpreted in the drillcore

(viii) to collect handspecimens for petrographic analysis, whole-rock geochemical analysis and palynology.

The basic procedure followed during mapping of the pit exposures is outlined below:

(i) photograph the exposure and construct a photo-mosaic

(ii) traverse the face making detailed observations and descriptions and marking any contacts or features on the photo-mosaic

(iii) carry out more detailed photographing and documentation of distinctive features

(iv) collect handspecimens where relevant

5. DRILLCORE LOGGING AND SAMPLE COLLECTION

A total of 17 boreholes were drilled within the South Lobe as part of an orebody delineation programme at Jwaneng Mine during the 1980's (Figure 3). The majority of boreholes were drilled from the center of the pipe towards the kimberlite-wallrock contact, in an attempt to delineate the geometry of the pipe between the 200m and 350m levels. Approximately one third of the drillcores were logged and sampled during or soon after completion of the drilling programme (Field 1988a-b, 1989a-d, 1991).

The drillcores logged during this study were selected in order to: (1) obtain coverage of both the central and peripheral zones of the pipe, and (2) complement rather than duplicate previous work (Field 1988b; 1989a-d, 1991). Due to the fact that the core was drilled more than ten years ago, it was also necessary to base the selection on the relative degree of preservation of the drillcores. Details of the three drillholes selected are listed in Table 4 below.

Table 4: Details of the drillholes selected for logging purposes.

Drillhole No.	Depth (m)	Bearing	Dip
DD15	251.57	230	70
DD68	376.30	301	71
DD88	427.25	166	74

The drillcore was logged using the strategy outlined by Field (1988a), although different grain size classes were utilised, as discussed in Section 2 of this chapter. This scheme operates on a four-letter code, for example Mcpm (1234), in which letter 1 refers to the mean grain size, letter 2 to the grain-matrix relationship (clast-supported (**c**) or matrix-supported (**m**)), letter 3 to the degree of sorting (well (**w**) or poorly (**p**) sorted) and letter 4

to the fabric (massive (**m**) or bedded (**b**)). Additional features recorded to substantiate this information include:

(i) colour and competency

(ii) maximum clast size

(iii) nature of the juvenile constituents (olivine and magma clasts), e.g. shape, size and distribution

(iv) nature of the xenolithic components e.g. clast types, shapes and distribution

(v) visual estimation of percentage composition of the juvenile and lithic components

(vi) nature of the bedding (note that core was not orientated when drilled, so dip angles of bedding have not been recorded)

(vii) nature of contacts

(viii) other features such as autoliths, mantle nodules, etc.

It should be noted that the modal abundances of the juvenile and lithic components were estimated using standard visual estimation charts (Terry & Chilingar, 1955). Since many of the observations were hampered by the rough outer core surfaces, and in some cases poor levels of core competency, some of these values were later adjusted, based on the results of modal analysis of selected polished core samples (see Section 7, this chapter).

A total of 109 handspecimens were selected from the three drillcores. Samples were taken at intervals of approximately eight to ten meters through each drillcore (Table A1), and an attempt was made to include the full range of rock types and textures represented within the drillcores. The majority of samples were cut and polished and/or thin sectioned for detailed macroscopic and microscopic examination, and modal analysis.

6. MAXIMUM CLAST SIZE MEASURMENTS

Measurement of the maximum juvenile and lithic clast size involves measuring the long axis of several of the largest clasts, and can yield important information relating to the origin of a deposit or lithofacies (Cas and Wright, 1987). The maximum sizes of olivine, magma clasts and country rock xenoliths have been measured in all the samples collected from the three drillcores. Assuming that the suite of samples is representative of the range of lithofacies and grain sizes present, the maximum clast size measurements may provide an indication of: (1) the coarsest fraction in the grain size spectrum of the lithofacies, (2)

the relationship between the lithic and juvenile components in terms of the variation in coarsest grain size, (3) a rough measure of the fragmentation intensity of the eruption mechanism and the relative degree of reworking of the deposits, and (4) the relative proportions of coarser-grained and finer-grained material. Results of the measurements are presented in Table A2, and discussed in Chapter III, Section 3.1.

7. MODAL ANALYSIS

A total of 12 samples were selected for modal analysis by point counting. The sample suite includes four representative samples from each of the three drillcores (Table 5). The main objectives of the modal analysis were: (1) to obtain quantitative estimates of the abundances of the main constituents of the principal lithofacies, which could be used to refine and where necessary adjust the visual estimations of juvenile and lithic component modal proportions made during core logging, and (2) to compare the results obtained from macro-pointcounting and micro-pointcounting methods, and in so doing assess the relative accuracy of each technique in its application to volcaniclastic rocks.

Macro-pointcounting was conducted on polished slabs of the samples using a 3mm grid. Micro-pointcounting was carried out on thin sections of the samples utilising a 0.4 x 2mm grid. In all cases 500 points per sample were counted. The number of counts for each constituent were recorded after every 100 points counted in order to test the repeatability of the data (Table A3).

Table 5: The 12 samples selected for modal analysis and their respective lithofacies codes.

Sample number	Lithofacies code
DD15/5	RVK-Mm
DD15/14	RVK-Mm
DD15/17	QRVKq-B*f*m
DD15/27	QRVKq-Mm
DD68/11	RVK-M*f*m
DD68/16	RVK-Mc
DD68/21	RVK-Mm
DD68/25	RVK-Mc
DD88/9	RVK-Mm
DD88/19	QRVKq-Sf
DD88/28	QRVKj/q-B*f*m
DD88/41	RVK-Mc

The constituents counted were as follows: macrocrystal and phenocrystal olivine (OL), both as discrete grains and as coarse inclusions within magma clasts; other xenocrysts (Xc) such as garnet, ilmenite, phlogopite and diopside; magmaclastic material (MC-x), that is, the magmatic material comprising the magma clasts, but excluding any coarse inclusions such as olivine macrocrysts or lithic clasts; country rock xenoliths (CRX); inter-clast matrix (ICM) and, where applicable, quartz and feldspar (Qtz/Fspar), which were counted together. The inter-clast matrix of these rocks is considered to comprise the ultrafine interstitial material including clay minerals and finely comminuted juvenile and lithic fragments, i.e. all material with grain sizes less than 0.01mm. The results of the modal analysis are discussed in Chapter III, Section 3.2.

Some clasts (e.g. olivine macrocrysts, xenoliths) are mantled by a juvenile magmatic selvage. These selvages vary in thickness from 0.1 to 1mm. The clasts (coarse inclusions) have not been included in the magma clast population (MC-x) during point counting for the following reasons: (i) the methodology did not allow reliable quantification of these selvages, (ii) it was often not possible to determine whether a clast has a selvage or not due to very narrow selvages in some cases and the high degree of alteration of the rocks, and (iii) the aim of the point counting was not to determine the proportion of clasts with and without juvenile selvages, but to determine and compare the modal abundances of the various components of the different facies.

8. MAGMA CLAST SHAPE CLASSIFICATION

The magma clast shape classification scheme used in this study was developed specifically for the analysis of the Jwaneng volcaniclastic rocks. The magma clasts in these rocks differ from those in volcaniclastic rocks of other kimberlite pipes in many respects, particularly in terms of the range of shapes displayed by the discrete magma bodies.

Shape is an assessment of the three-dimensional form of a clast or grain, and is often described in terms of sphericity (Prothero & Schwab, 1996). Since an accurate measure of sphericity is difficult in the two-dimensional plane of a thin section, this parameter has not been included as a fundamental feature of the classification. This is possibly a short-coming of the classification scheme which may require rectification in the future. It

should be noted however that, in general, the magma clasts appear to display low sphericity, that is, the majority appear to be subdiscoidal or subprismoidal (Powers, 1953).

The *roundness* or angularity of a clast or grain is concerned with the curvature (sharpness or smoothness) of its corners (Pettijohn, et al. 1987). The roundness or angularity of a magma clast is significant since it may reflect: (1) the mode of fragmentation of the magma and other pyroclastic processes such as in-vent milling (Cas and Wright, 1987), and (2) the degree of abrasion resulting from transportation and/or deposition.

In most sedimentological studies, standard sets of images are used to estimate differing degrees of roundness (Wadell 1935, Krumbein 1934). A similar set of grain silhouettes has been devised for use in this study (Figure 4), in accordance with the range of clast shapes/roundness present in the sample suite. The classification scheme comprises five main shape/roundness categories, namely: rounded, subrounded, irregular, subangular and angular. *Rounded* magma clasts are those which have completely smooth edges; *subrounded* is used for magma clasts characterised by scalloped margins; *irregular* magma clasts have slightly curvilinear but smooth margins; *subangular* is used to describe magma clasts with at least two sharp corners; and *angular* magma clasts are those which have no smooth margins, i.e. all corners are sharp. It should be noted that the term irregular is used here to denote angularity derived from clastic processes (abrasion of original sharp corners), and that the curvilinear margins do not suggest a fluidal (amoeboid) origin for the magma clasts. The classification scheme was applied to thin sections of the same suite of 12 samples that was used for the modal analysis. A total of 20 magma clasts in each sample were categorised. In order to avoid visual size bias, the magma clasts categorised in each sample included 10 clasts greater than 0.5mm and 10 less than 0.5mm in size.

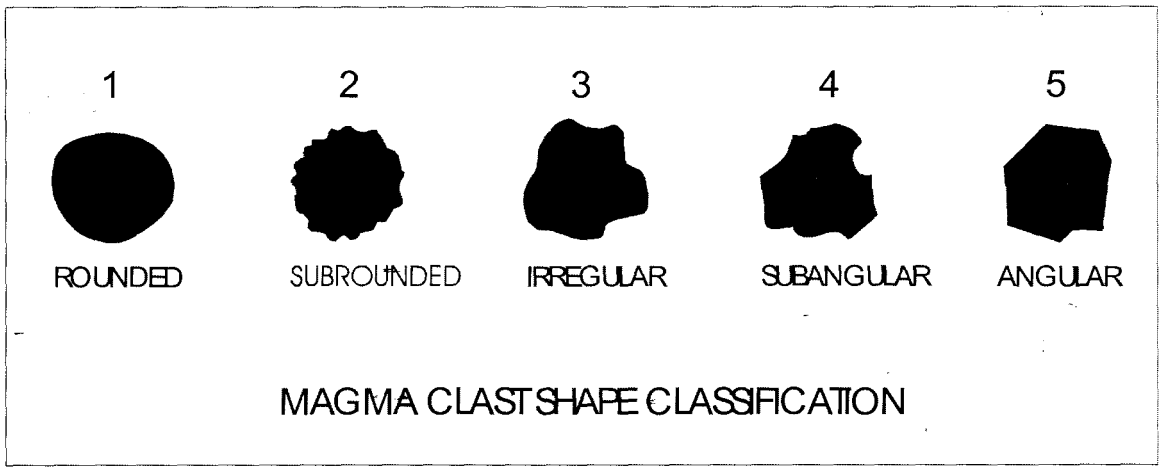

Figure 4: Grain silhouettes depicting the five categories of the magma clast shape classification scheme devised for use in this study.

III. OBSERVATIONS

1. OVERVIEW OF IN-PIT GEOLOGY

This section provides a brief review of the main geological features of the Jwaneng South Lobe as observed within the open pit. A more detailed spatial and petrographic description of the lithofacies is given in Section 2. Oblique views of the South Lobe from surface as it appeared during the three phases of pit work are indicated in Figures 5 - 7.

The South Lobe of Jwaneng Mine has a surface area of approximately 10 hectares, and at the commencement of this study in May 1999 had been mined to a depth of 128m (Bench 11). Based on the then current exposures within the open pit, as well as available borehole data, the pipe appears to be filled predominantly with resedimented volcaniclastic kimberlite (RVK). No pyroclastic kimberlite (PK) or tuffisitic kimberlite breccia (TKB) have thus far been identified and no hypabyssal facies kimberlite has been intersected to date.

One of the most striking features of the RVK is its extremely homogenous nature on a megascopic scale. However, it does exhibit considerable variation on a small-scale, particularly in terms of grain size, texture and internal structure. Two principal lithofacies have been identified, namely the quartz-free RVK facies and the quartz-bearing QRVK facies. The RVK facies occupies the central portion of the pipe, whereas the QRVK facies is restricted to a discontinuous marginal zone which, where present, has a thickness of 7 to 15 meters adjacent to the wall-rock contact. Both lithofacies are predominantly massive and chaotic with the presence of lesser bedded zones. The RVK is typically clast-supported and poorly sorted, although localised zones and subfacies displaying increased degrees of sorting and/or matrix support do occur.

Where bedding is present it is in all cases laterally discontinuous, occuring in distinct, sharply bounded blocks or less obvious zones of only a few meters in maximum dimension (Figure 8). All bedding observed is planar, and no tractional bedforms such as cross bedding have been found. In all instances bedding displays steep dips, generally greater than 60°, which considerably exceeds the angle of repose for clastic sediments (Cas and

Wright, 1987). The dip directions of the beds are variable, that is, although the bedding commonly dips towards the centre of the pipe, a number of bedded blocks displaying other orientations are also present. The majority of the beds examined appear to be undisturbed, with little or no evidence of slumping or deformation of individual layers within the blocks and zones. Two main types of bedding have been identified, and are termed *vague* and *distinct* bedding. Where the bedding is *vague* an internal fabric is imparted by the subparallel alignment of elongate clasts, particularly shale xenoliths (Figure 9). No obvious clast imbrication has been identified. Large-scale vague bedding may also be defined by a very gradual increase or decrease in the country rock xenolith content over a few meters. *Distinct* bedding is defined by the presence of narrow randomly or regularly spaced layers displaying an increase in grain size, sorting and lithic content. Prefered alignment of elongate clasts may be present in these beds, as well as in the alternate finer-grained beds. Distinctly bedded zones may also contain thin intercalated, fine grained mud-rich layers (Figure 10).

In addition to the bedded blocks and zones, careful examination of the pit exposures reveals the presence of relatively common slickenside-bound, rotated blocks of massive RVK, or QRVK in the case of the marginal zones. These can be identified by the concentration of variably orientated slickenside planes, and on closer inspection are seen to exhibit a variation in grain size and/or lithic, mud, or autolith content in comparison to the immediately adjacent rocks (Figure 11). The contrast between the rotated blocks and the host is often quite subtle. The presence of these, as well as the bedded blocks, results in random and abrupt variations in lithofacies over relatively short distances. This, combined with the lack of marker horizons, severely complicates lateral and vertical correlation of facies and units (Figures 8 and 12).

The RVK and QRVK facies are further characterised by the common presence, in localised areas, of a fine grained, mud-rich kimberlite facies. This facies occurs as irregular blebs or 'clots', ranging up to a few meters in size, within medium or coarse grained massive RVK/QRVK facies, and in many cases contains micro-structures such as slumping and faulting (Figures 13 and 14). Less common are fine grained kimberlitic muds which occur as thin interbedded layers within some of the bedded facies.

Both the bedded and massive RVK and QRVK facies are characterised by the presence of relatively abundant country rock xenoliths of various lithologies and sizes, although the majority do not exceed 150 mm. The xenolithic clasts appear to display an homogenous distribution within the RVK/QRVK facies. It is not possible to correlate the distribution of xenolithic types with the stratigraphy of the host rocks. Although Transvaal Supergroup shale is the dominant country rock xenolith throughout most of the RVK/QRVK facies, localised zones displaying a dominance of a particular xenolith type other than shale occur in places, and subrounded quartzite clasts appear to occur only in the QRVK facies. All three of the Lobes contain large included wall-rock masses or megablocks, which range up to 30 meters in size and consist predominantly of mudstone or siltstone/sandstone packages. These megablocks occur exclusively around the periphery of the Lobes, close to the wall-rock contact. Only one such megablock was observed in the South Lobe during this study (Figure 12) and this, in addition to two others, which occur in the Centre and the North Lobes, is discussed in more detail in Section 5 of this Chapter.

Despite the fact that Transvaal Supergroup shales are the dominant wall-rock lithology and constitute the most common xenolithic clast type within the RVK/QRVK facies, megablocks of shale appear to be absent, with only rare blocks up to a maximum of 1m in size having been observed. Of interest is the relatively common occurrence of coal within the QRVK facies. It is probably derived from the Ecca Group (Kweneng and Boritse Formations) of the Karoo Supergroup and ranges from small fragments up to blocks of a meter or more in size (Figure 15). Rare fossilised wood fragments are also present (Figure 16), particularly within the QRVK facies, and are discussed further in Section 6.

The kimberlite-wall rock contact zones may contain localised shale-rich breccias, although these are not a widespread feature (Figures 17 and 18). These comprise abundant medium to coarse grained angular shale clasts set in a finer-grained kimberlitic matrix. The wall-rock contacts are either sharp, with minor in-situ fracturing of the shales (Figure 19), or gradational with a transition from slightly to highly fractured shale, to clast-rotated breccias with a matrix of shale fragments, to admixed shale/kimberlite breccias closest to the kimberlite contact.

An additional feature of the RVK and QRVK facies is the abundance of variably coloured mudstone clasts of apparent non-kimberlitic nature. These appear to be particularly

common in the QRVK facies, and are an important diagnostic feature. They vary from a few millimeters up to a meter in size, and display a range of shapes from subrounded to irregular to highly contorted. They either lack internal stratification or contain highly disturbed fine laminations (Figures 20 and 21) and soft sediment deformation structures. These mudstones probably represent poorly consolidated Karoo sediments incorporated into the kimberlite during eruption or resedimentation.

Figure 5: Oblique view of the South Lobe in May 1999.

Figure 6: Oblique view of the South Lobe in September 1999.

Figure 7: Oblique view of the South Lobe in April 2000.

Figure 8: Photomosaic showing one of the exposed faces on Bench 12 of the South Lobe. It is orientated approximately east-west across the centre of the Lobe.

Figure 9: Vague bedding in medium-grained RVK facies (RVK-B_vm).

Figure 10: Distinctly bedded *fine*-medium and medium grained RVK facies (RVK-B_d *f*m-m) with thin intercalated beds of mud-rich, fine grained RVK facies (RVK-B_df).

Figure 11: Slickenside-bound rotated block of coarse grained, mud-poor massive RVK facies (RVK-Mc), at centre, within coarse grained, mud-rich and comparatively lithic-rich massive RVK facies (RVK-Mc). Approximate scale: 1cm = 0.3m.

Figure 12: Photomosaic showing one of the exposed faces on Bench 14 of the South Lobe. It has an approximate northwest-southeast orientation and is located close to the southwestern and western margins of the Lobe.

Figure 5.

Figure 6.

Figure 7.

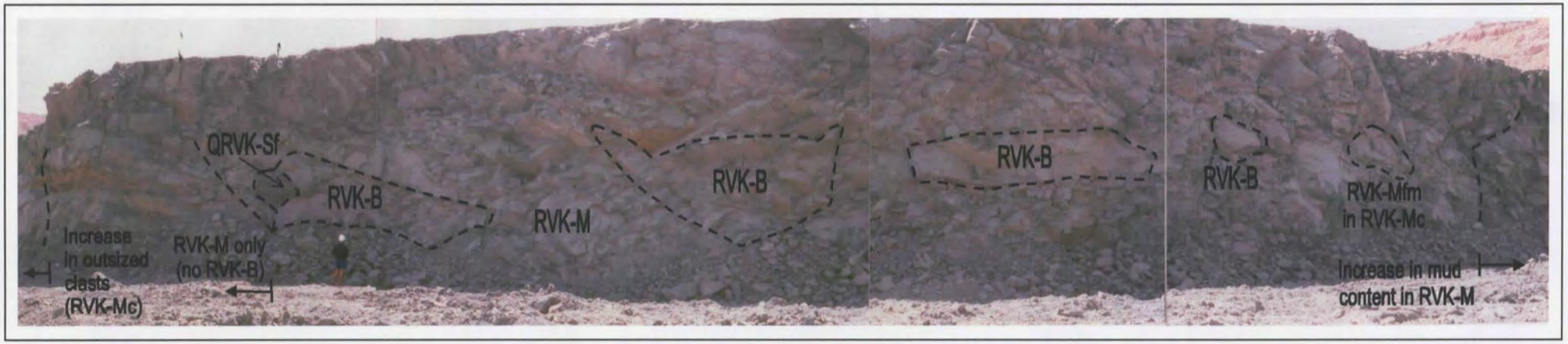
QRVK-Sf
RVK-B
RVK-M
RVK-B
RVK-B
RVK-B
RVK-Mfm
in RVK-Mc
Increase
in outsized
clasts
(RVK-Mc)
RVK-M only
(no RVK-B)
Increase in mud
content in RVK-M

Figure 8

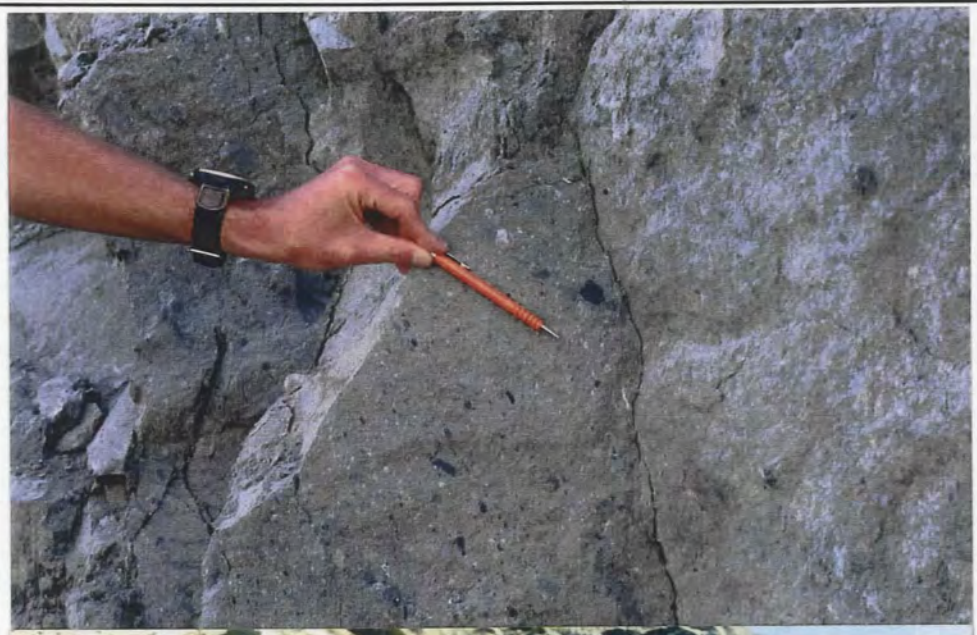

Figure 9.

Figure 10.

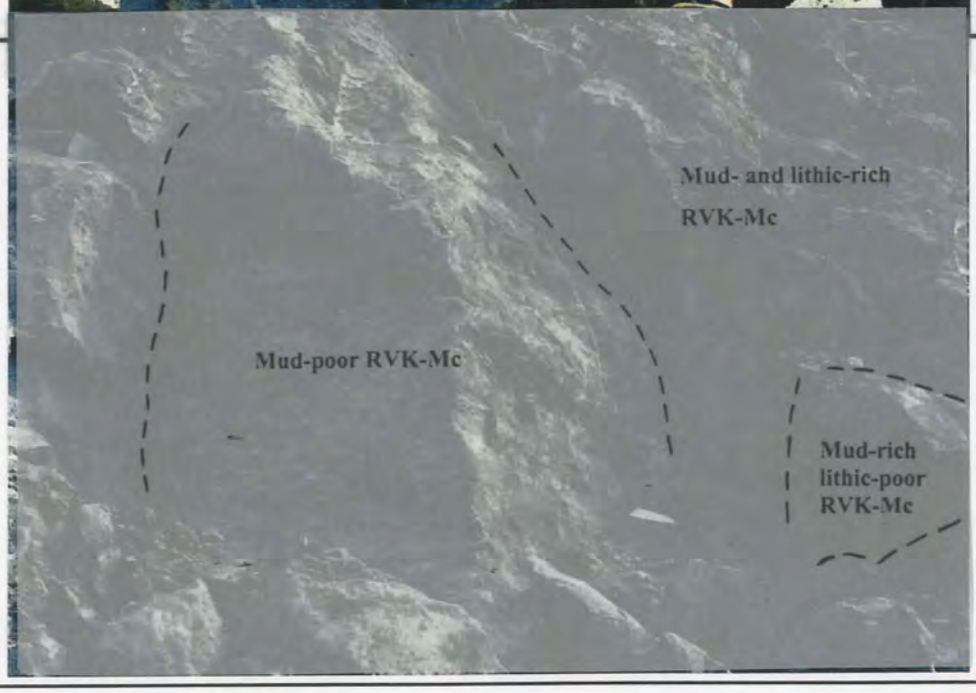

Figure 11.


Decreased mud content in RVK-M
RVK-B
Increased mud content in RVK-M
RVK-Mm in RVK-Mc
Zone of common outsized shale clasts
RVK
QRVK
Green mudstone megablock
QRVK-B
Zone of common QRVK-Sf & autoliths in QRVK-M
Quartzite boulder
Coal xenolith
QRVK-Sf
QRVK-B
QRVK-Mc in QRVK-Mm
Wallrock contact
Shale

Figure 12

Figure 13: Dark grey fine grained, mud-rich QRVK facies (QRVKq-Sf) displaying micro-faulting.

Figure 14: Dark grey fine grained, mud-rich QRVK facies (QRVKq-Sf) within coarse grained massive RVK facies. Note the sharp, but irregular contacts.

Figure 15: Large (1.2m) coal xenolith within massive QRVK facies close to the wall-rock contact.

Figure 16: Fossilised wood fragment within medium grained massive QRVK facies.

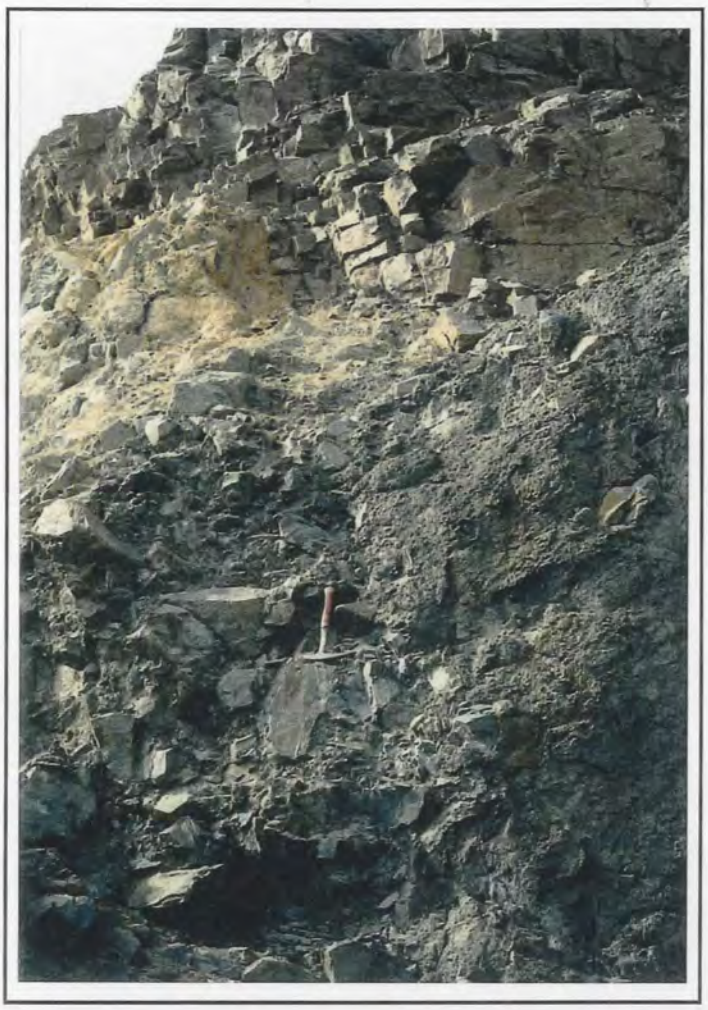

Figure 17: Kimberlite-wall rock contact zone along the southern margin of the South Lobe with localised zone of the shale-rich breccia facies (RVK-Mc_{srb}).

Figure 18: Kimberlite-wall rock contact zone along the southern margin of the South Lobe showing weathered zone at the contact and distinct absence of shale-rich breccia facies or outsized shale xenoliths.

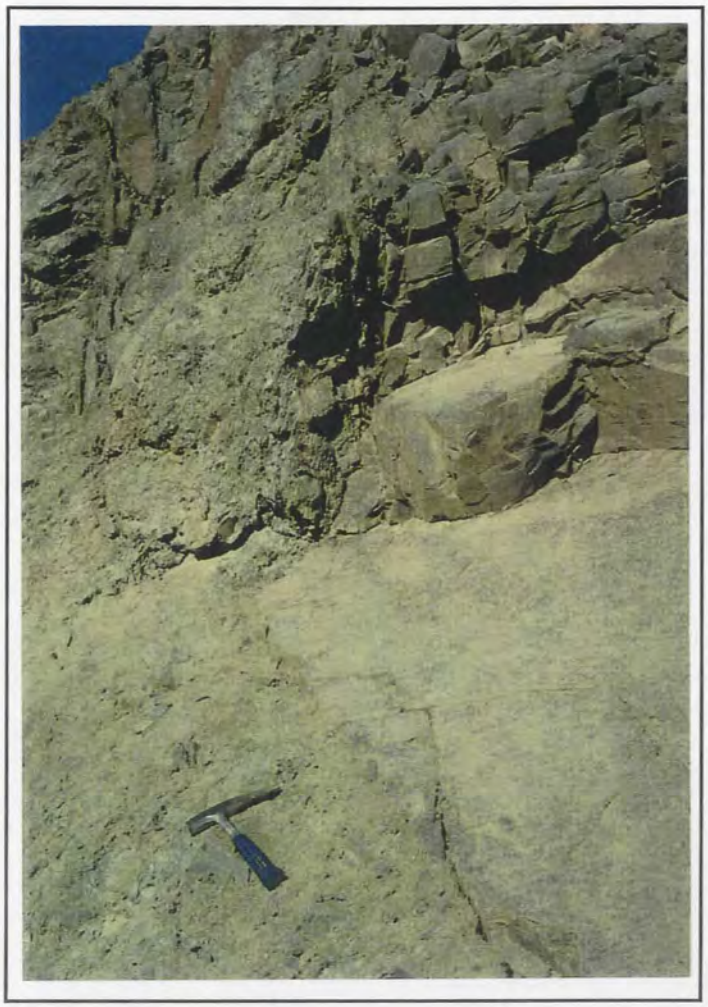

Figure 19: Kimberlite-wall rock contact zone showing sharp nature of the contact with minor in-situ fracturing of the shales.

Figure 20: Irregular mudstone xenolith displaying highly disturbed laminations within massive coarse grained QRVK facies.

Figure 21: Contorted green mudstone xenolith within medium grained massive QRVK facies.

2. DESCRIPTIONS OF THE LITHOFACIES

This section includes detailed descriptions of the lithofacies which comprise the volcaniclastic fill of the South Lobe of Jwaneng Mine. The relative distribution of each lithofacies and characteristic macroscopic and microscopic features of representative samples are described. The lithofacies subdivision and facies code scheme used in this sttudy are outlined in Chapter II, Section 3. Graphic logs of the three drillcores studied (DD15, DD68 and DD88) are presented in Appendix I.

2.1. The RVK Facies

The quartz-free RVK facies is the dominant lithofacies in the South Lobe, and occupies the majority of the pipe, excluding a relatively narrow discontinuous marginal zone. The lithofacies includes both the **massive RVK** facies (RVK-M facies) and the vaguely to distinctly **bedded RVK** facies (RVK-B_v and RVK-B_d facies). These facies display a wide range in grain size, including fine, *fine*-medium, medium and coarse grained deposits. The characteristic features of the facies are summarised in Table 6.

2.1.1. Massive RVK Facies (RVK-M)

The massive RVK facies dominates the South Lobe, both in the pit exposures examined and in the three drillcores, where borehole intersections of up to 100m or more of massive RVK have been recorded. The RVK-M facies has been subdivided according to the mean grain size of the lithic component into: (i) fine grained (RVK-Mf), (ii) *fine*-medium grained (RVK-M*f*m), (iii) medium grained (RVK-Mm), and (iv) coarse grained (RVK-Mc) subfacies (see Chapter II, Section 2 for grade scale classes). In terms of relative proportions, the RVK-Mc and RVK-Mm subfacies appear to dominate over the RVK-M*f*m and RVK-Mf subfacies. These subfacies may occur in any sequence in the drillcores, and contacts between them are usually gradational. Sharp contacts are present in some cases however, generally between the RVK-Mc and RVK-M*f*m subfacies, where the contact between the coarser-grained and finer-grained material may also be associated with a sharp contrast in the juvenile and/or lithic content. For example, the contact between RVK-Mc and RVK-M*f*m subfacies at 129.55m depth in borehole DD15 is sharp and is associated with a lower juvenile and lithic content within the RVK*f*m subfacies. Contacts between the

massive RVK facies and the bedded RVK facies (RVK-B) may be gradational or sharp, depending on the nature of the bedded deposits. In general, the contacts are gradational only where the bedding of the RVK-B facies is vague. Contacts between the massive RVK facies and the quartz-bearing QRVK facies in the marginal zones of the pipe may be sharp or gradational (Section 2.2).

The main distinguishing feature of this facies is its apparent absence of internal structure (bedding), hence the use of the term 'massive'. Variations in the mean grain size, lithic content and/or juvenile content do occur, although for the most part they appear to be broad-scale and gradational. For example, in borehole DD68 the mean grain size and lithic content increase to 9mm and 28 volume %, respectively, and then decrease again to 5mm and 10 volume % over approximately 10m, between depths of 267.68m and 276.38m. Smaller-scale variations also occur, in the form of narrow (< 1m thick), sharply bounded zones displaying an increase in lithic content or an increase/decrease in mean grain size, with or without variation in associated lithic or juvenile content. Although these variations were recorded during detailed core logging and were often difficult to detect in the pit exposures, they do not appear to define distinct bedding. In many cases they appear to represent localised, laterally impersistent lithic-rich lenses or pods.

The rocks of this facies are typically medium greenish-grey in colour, except in the uppermost highly calcretised zone, where they are pale cream to creamy-brown. They are generally competent, although friable zones do occur. The reduced competency tends to be associated with slickensided fracture planes and in areas adjacent to the fine grained mud-rich QRVK facies (QRVKq-Sf facies). The rocks display good textural preservation, despite a moderate to high degree of alteration, which includes alteration to clay minerals, serpentine and carbonate.

The massive RVK facies displays a distinctly fragmental, inequigranular texture resulting from the presence of angular to subrounded coarser constituents (olivine, country rock xenoliths, juvenile magma clasts, autoliths and xenocrysts) which are set in a very fine grained inter-clast matrix (Figure 22). The close-packed arrangement of the juvenile and lithic components in the majority of deposits imparts a clast-supported texture to the rocks. The *fine*-medium and medium grained subfacies (RVK-M*f*m; RVK-Mm) may display a matrix-supported texture in places (e.g. 110.28 – 111.60m and 147.96 – 149.13m in

borehole DD88), although in most cases this can only be determined microscopically. The rocks are predominantly poorly sorted, although minor localised zones of RVK-M*f*m and RVK-Mm subfacies are moderately well sorted (e.g. 155.80 – 160.10m and 185.75 – 187.50m in borehole DD68). It should be noted, however, that even these finer-grained, macroscopically well sorted deposits are poorly sorted on a microscopic scale, due to the polymodal size distribution of the constituent juvenile and lithic clasts. In the majority of deposits outsized clasts of various sizes, in rare cases up to 150mm, are present. These outsized clasts are generally country rock xenoliths, but may also be autolithic VK and hypabyssal facies kimberlite clasts.

Macrocrystal and phenocrystal olivine forms the dominant constituent of the massive RVK facies, with modal abundances ranging from 40 to 52 volume %. The olivine ranges in shape from subrounded to angular and is totally altered to serpentine, carbonate and clay minerals (Figure 23). The abundance of angular, broken grains contributes to the fragmental texture of the rocks and complicates the distinction between macrocrystal and phenocrystal olivine. Although in some of the deposits, particularly the RVK-M*f*m subfacies, the olivine appears to be relatively well sorted, closer examination reveals a very wide range in grain size, from coarse macrocrysts (up to 20mm) to small crystal fragments less than 0.5mm in size. The olivine occurs both discretely within the inter-clast matrix and as coarse inclusions within magma clasts.

One of the most striking features of the massive RVK facies is the predominance of xenoliths of green shale, as well as lesser amounts of green and grey-brown, fine grained quartz and micaceous wackes of the Segwagwa Group (upper Transvaal Supergroup). Other country rock xenolith lithologies present, in approximate decreasing order of abundance (although variations do occur) include: black and pale khaki shale (Segwagwa Group), grey-white dolomite and chert of the Taupone Dolomite Group (lower Transvaal Supergroup), chloritised and amphibolitised dolerite, quartzite/sandstone (Segwagwa Group and Waterberg Group) and rare amphibolitised basement granitoids, biotite schist, and red-brown (oxidised) shale. Mudstone clasts of probable Karoo age are also common within the massive RVK facies, and range in colour from pale or dark green to grey-brown to red-brown.

The majority of lithic clasts range in shape from subrounded to angular with sharp contacts, although a number of the mudstone clasts display irregular to highly contorted shapes, with diffuse contacts in places. Zonal alteration and evidence of kimberlitization of the clasts are rare or absent. The lithic component in each subfacies exhibits a polymodal size distribution, covering an entire spectrum from small fragments less than 0.5mm to larger clasts up to 150mm in size, and in rare cases up to 1m. The modal abundance of country rock xenolithic material varies from 10 to 25 volume %, with localised increases of up to 45 volume %, most commonly within the shale-rich breccia facies (Section 2.1.1.1.).

The modal abundance of juvenile magmaclastic material in the massive RVK facies ranges between 10 and 20 volume %. The juvenile magma clasts are often quite indistinct and difficult to recognise in uncut core and in the pit exposures. This is probably a result of the uniform colour of the magmaclastic material and the inter-clast matrix, and it is generally only the coarser examples which are readily recognisable.

The magma clasts display a wide range in size and shape. Sizes vary from 0.15mm up to 40mm, i.e. ash to lapilli size in standard volcanological terminology. The population includes predominantly rounded and subrounded clasts, as well as lesser, but significant proportions of irregular and subangular varieties. Rare examples of angular magma clasts were observed in a few handspecimens (e.g. DD88/22, DD88/39). Magma clast shape categories are described in Chapter II, Section 8, and the results of the magma clast shape classification scheme are presented in Section 3.3 of this Chapter. The magma clasts commonly contain a coarse inclusion, consisting of an olivine crystal, country rock xenolith, mantle- or crustal-derived xenocryst or autolithic clast. In the majority of cases these coarse inclusions are not centrally positioned within the magma clast.

Microscopic examination reveals the presence of two distinct mineralogical types of magma clast, namely monticellite and monticellite-calcite kimberlite (Figure 24). Both types comprise serpentinised olivine macrocryst and phenocryst pseudomorphs set in a groundmass composed of relict monticellite, fine grained spinel, turbid relicts of perovskite and rare phlogopite and apatite, with the presence of calcite laths in the one variety. The calcite laths may be primary or a secondary replacement of melilite. Despite ubiquitous alteration of the groundmass to turbid cryptocrystalline carbonate, which overprints the

monticellite in the majority of cases, the groundmass is texturally well-preserved, even in many of the smaller clasts. No microlitic diopside has been observed in any of the samples examined. The granularity of the magmaclastic material approximates that of typical hypabyssal facies kimberlite, in contrast to the much finer grain size of the groundmass constituents of pelletal lapilli in volcaniclastic rocks from other southern African kimberlite pipes (e.g. Orapa). The relative proportions of the monticellite and monticellite-calcite magma clast types is variable, and there does not appear to be any preferential stratigraphic correlation of the two varieties.

The massive RVK facies contains up to 5 volume % mantle-derived xenocrysts, including ilmenite, garnet, chrome diopside and rare spinel, phlogopite and rutile. These occur either discretely within the inter-clast matrix or as coarse inclusions within juvenile magma clasts. Rare, highly altered small peridotite xenoliths are also present (e.g. sample DD68/26). The inter-clast matrix has a brown turbid appearance and is composed of clay minerals, very finely comminuted juvenile and lithic fragments and serpentine, in variable proportions.

A variety of unequivocal autolithic clasts occur within the massive RVK facies. Autoliths of volcaniclastic kimberlite (VK) range from a few millimeters up to 200mm in size. They are recognisable in handspecimen by their darker grey-green or reddish-brown colour. Microscopically they are seen to be highly altered with a high inter-clast matrix mud content, but are otherwise texturally and compositionally similar to the host RVK facies. They are subrounded to irregular in shape, and contacts with the host RVK facies are mostly sharp, but may be irregular. Figures 25 and 26 show examples of VK autoliths as they appear in the pit exposures. Figure 27 shows a VK autolith within RVK-Mm subfacies in drillcore DD15 (sample DD15/8). It is also likely that the very narrow (9 – 27cm) intersections at 116.72m, 116.96m, 121.19m, 122.35m, 128.06m, 128.28m and 129.55m in DD15 represent intersections of the drillcore with VK autoliths.

Subrounded to irregular hypabyssal facies autoliths, up to 130mm in size, are pale grey-brown in colour and exhibit a uniform, highly macrocrystic texture (Figure 27). They are composed of abundant altered macrocrystic and phenocrystic olivine, rare lithic clasts and scattered coarse grained garnet, ilmenite and diopside xenocrysts set in a fine grained groundmass consisting of relict monticellite, uniformly distributed spinel and lesser

amounts of relict perovskite, in addition to abundant fine calcite laths in some cases. The groundmass constituents occur in a base of serpentine and cryptocrystalline carbonate. Irregular segregations of calcite occur in some examples and others display a weakly developed globular segregationary texture, e.g. samples DD15/15 and DD88/23 (Figure 28).

An interesting feature of the massive RVK facies is the presence of accreted non-magmatic rims on a variety of clasts, including country rock xenoliths, juvenile magma clasts, autoliths (VK and hypabyssal) and individual olivine macrocrysts (Figure 29). These rims are not a widespread feature, and were observed in certain samples only (e.g. DD15/14, DD88/8, DD88/10, DD88/18, DD88/43). The rims are composed of clays and very fine grained lithic and juvenile fragments, i.e. mud, or fine ash in standard volcanological terminology. These clasts resemble armoured lapilli (Cas and Wright 1987, Schumacher and Schmincke 1991).

2.1.1.1. Shale-rich Breccia Facies

The shale-rich breccia facies (RVK-Mc_{srb}) is a subfacies of the massive RVK facies, which is characterised by a high modal abundance of country rock xenoliths, particularly Transvaal Supergroup shales, and a coarse to very coarse mean grain size. The facies appears to be restricted to the marginal zones of the pipe, close to the wall-rock contact. The breccias are not abundant, and were observed in only a few localised zones of the pit exposures. The best exposure of the facies occurs in a 4m wide zone located along the southern margin of the pipe (Figure 17). The RVK-Mc_{srb} facies was intersected in drillcores DD15 and DD68 (Figure 30). In DD15, the 2.6m intersection of the shale-rich breccia facies is followed with depth by approximately 12 m of massive QRVKq facies before intersection with the wall-rock shale. In DD68, three narrow intersections (207cm, 41cm and 31cm) of the shale-rich breccia facies occur at depths of 315.17m, 318.54m and 320.06m (respectively), and are separated by approximately one meter wide intervals of RVK-Mc facies.

The lithic component of the RVK-Mc_{srb} facies is dominated by subangular and angular green and black Transvaal Supergroup shales. Minor proportions of dolomite, various wackes and altered dolerite may also be present. The country rock xenoliths together

constitute 35 – 45 volume % of the rocks, and range in size up to 120mm. Rare boulders up to 1m in size were observed in the pit exposures. Subrounded to subangular altered olivine macrocrysts and phenocrysts (30 – 40 volume %) and juvenile magma clasts (15 – 20 volume %) occur in a close-packed arrangement between the lithic clasts. The juvenile components range in size from 0.05mm to 10mm. The coarser constituents are set in a very fine grained clay- and serpentine-rich matrix.

Figure 22: Massive RVK facies: core samples (a) DD15/5, (b) DD88/9 and (c) DD88/27. Note the fragmental, poorly sorted texture and abundant green shale xenoliths. Sample DD15/5 is from the uppermost highly calcretised zone. Scale in centimeters.

Figure 23: Photomicrograph of RVK-M facies (sample DD88/21) showing typical poorly sorted, clast-supported texture. Abundant altered olivine (Ol) macrocryst and phenocryst fragments, juvenile magma clasts (MC) and dolomite (Dol) and shale (Sh) xenoliths are set in a fine grained, clay and serpentine inter-clast matrix. Plane polarised light (PPL). Field of view (FOV) = 5.2 mm.

Figure 24: Photomicrograph of RVK-M facies (sample DD88/43) showing the two mineralogical types of magma clasts, namely monticellite kimberlite (rounded to subrounded magma clasts at left and right) and monticellite-calcite kimberlite (irregular magma clast at centre right). PPL. FOV = 5.2mm.

Figure 22:

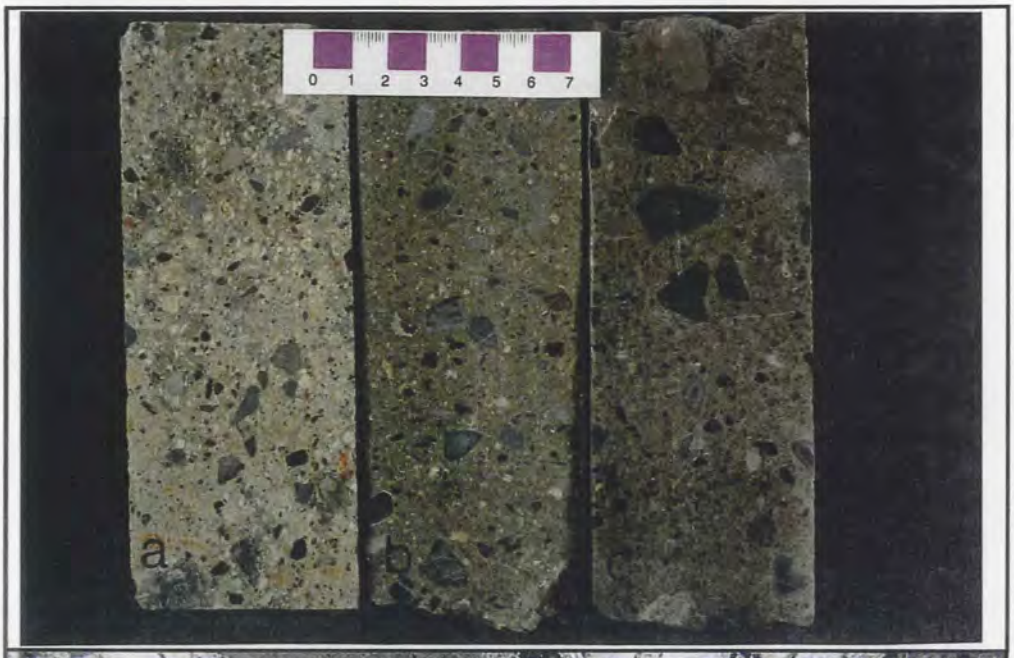

Figure 23:

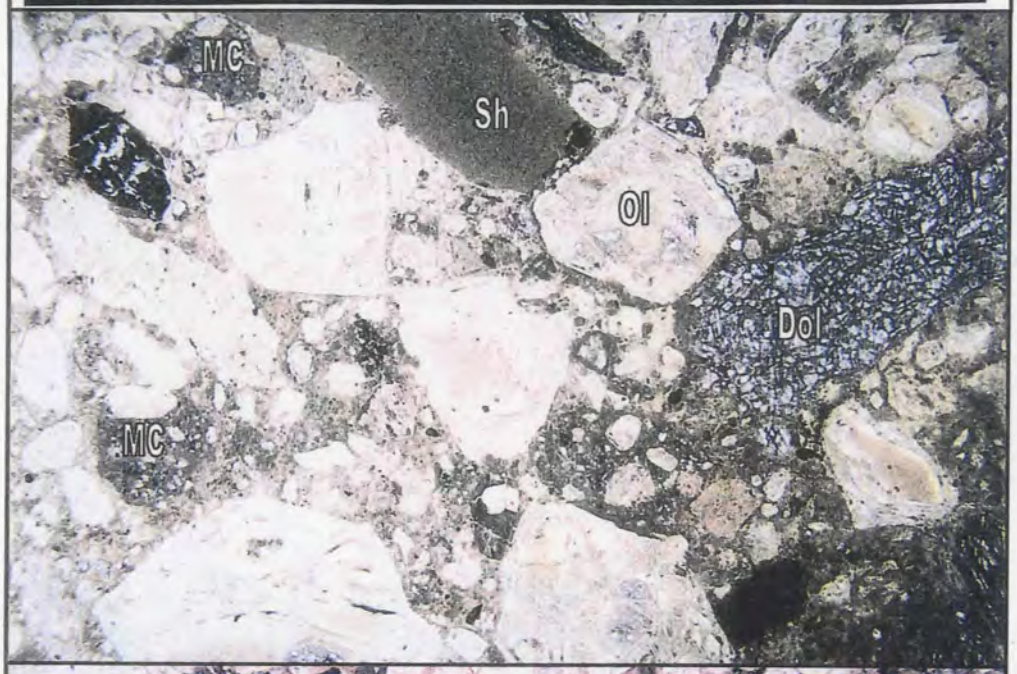

Figure 24:

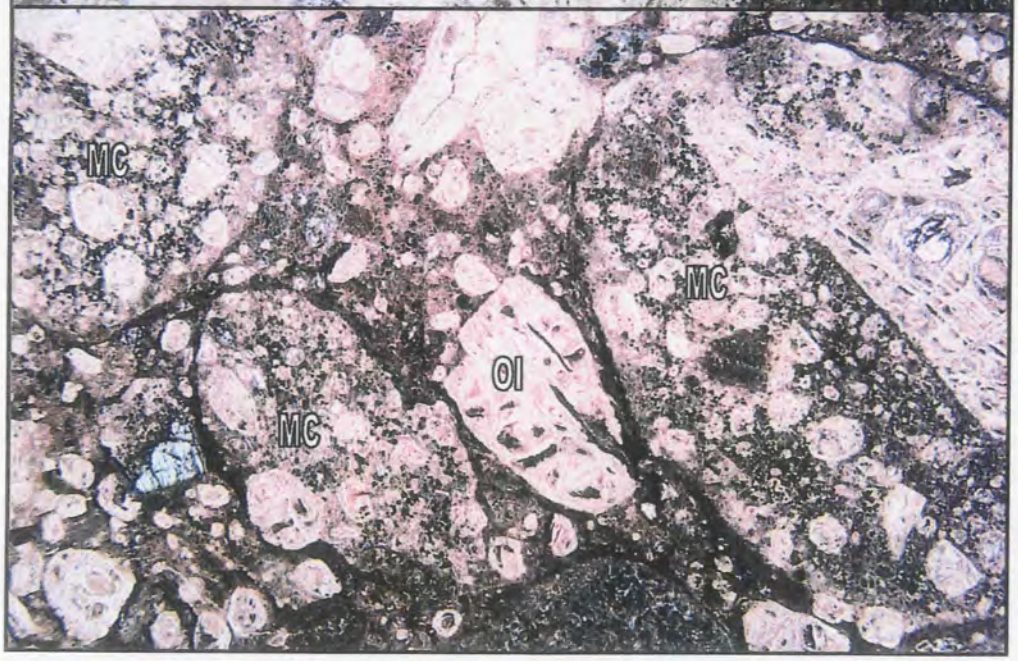

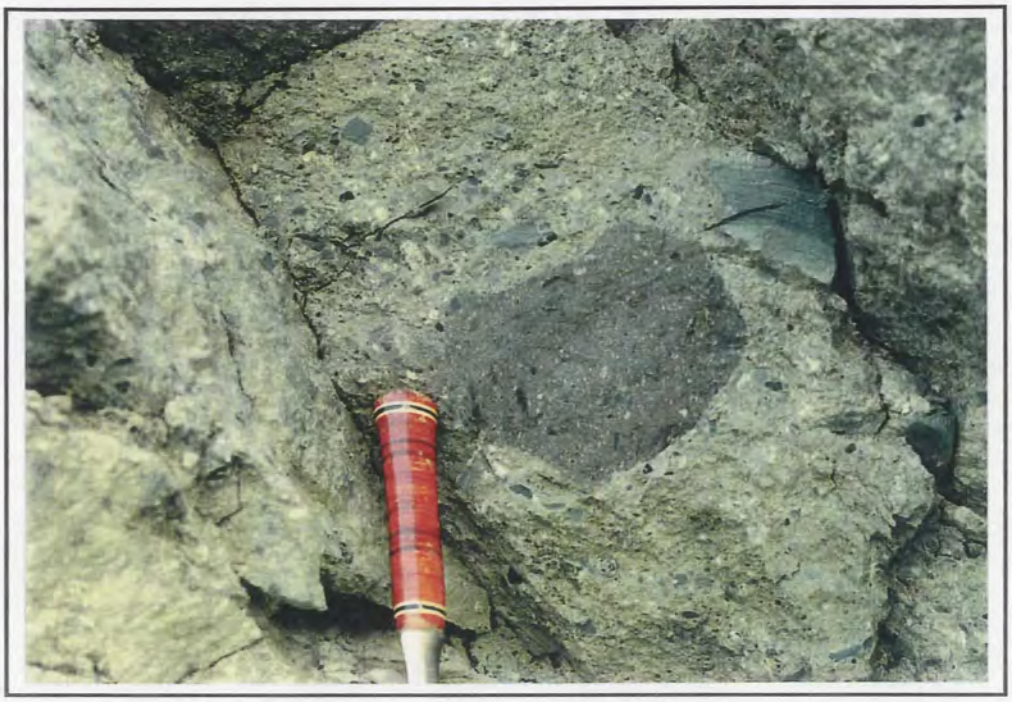

Figure 25: Reddish-brown subrounded VK autolith within medium grained massive RVK facies in a pit exposure of the South Lobe.

Figure 26: Grey-green subangular VK autolith within medium grained massive RVK facies in a pit exposure of the South Lobe.

Figure 27: Volcaniclastic kimberlite (VK) and hypabyssal facies autoliths within medium grained massive RVK facies: core samples (a) DD88/23 (hypabyssal facies autolith) and (b) DD15/8 (VK autolith). Scale in centimeters.

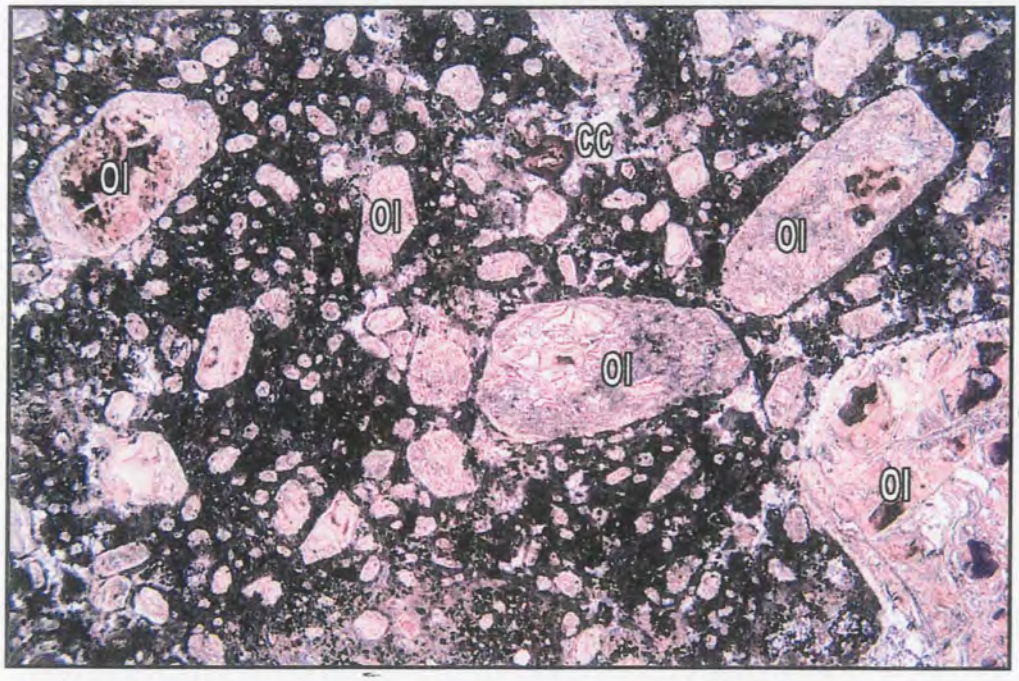

Figure 28: Photomicrograph of a hypabyssal autolith (sample DD88/23) displaying a uniform to weakly segregationary texture. Note the abundant serpentinised and carbonatised olivine (Ol) macrocrysts and phenocrysts, fine grained groundmass spinel and irregular pools of calcite (cc). PPL. FOV = 5.2mm)

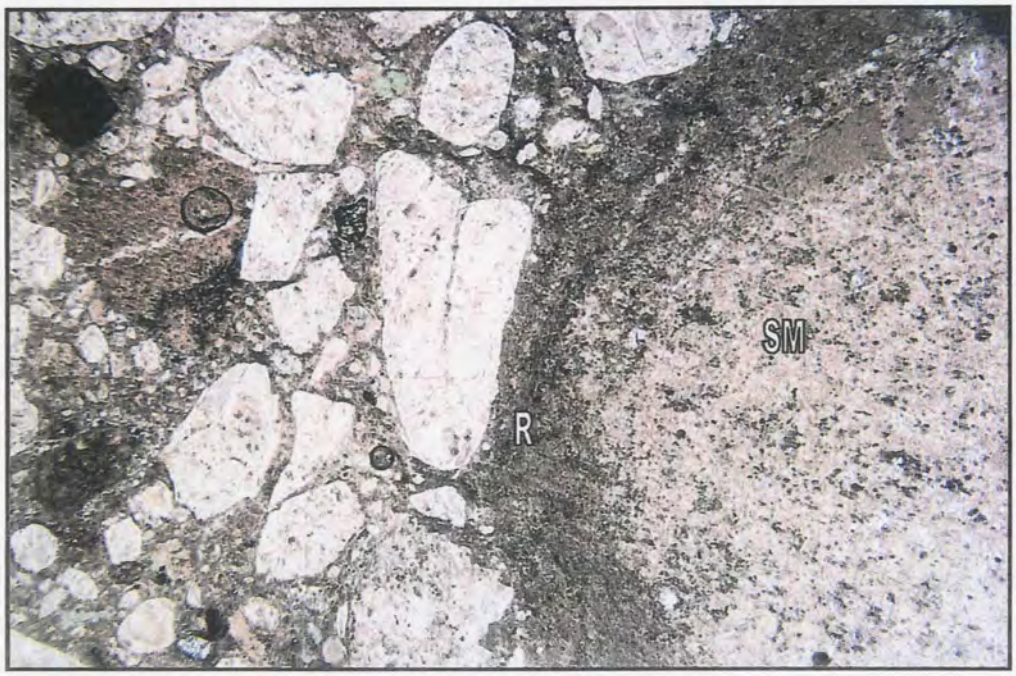

Figure 29: Photomicrograph of an armoured lapillus (sample DD88/18) within massive RVK facies. The lapillus consists of a silty mudstone (SM) clast mantled by a narrow, very fine grained non-magmatic rim (R). PPL. FOV = 5.2mm).

Figure 30: The RVK shale-rich breccia facies (RVK-Mc_{srb}): core samples DD15/25 and DD68/31. Note the abundant subangular to angular shale xenoliths. Scale in centimeters.

2.1.2. Bedded RVK Facies (RVK-B)

The bedded RVK facies includes all RVK deposits which display internal structure in the form of bedding. The RVK-B facies was observed in all of the pit exposures and was intersected in each of the three drillcores, but is volumetrically subordinate to the massive RVK facies. The bedded deposits may be divided into those in which the bedding is vague (RVK-B_v) and those which are distinctly bedded (RVK-B_d).

2.1.2.1. Vaguely Bedded RVK Facies

In the RVK-B_v facies the bedding is defined by the subparallel alignment of elongate clasts, most notably shale xenoliths. The vague bedding has been observed in *fine*-medium, medium and coarse grained RVK deposits (RVK-B_v*f*-m, RVK-B_vm and RVK-B_vc subfacies, respectively). These deposits are generally only a few meters or less in thickness and display gradational contacts with the massive RVK facies. They commonly represent the only occurrence of internal structure within tens of meters of massive RVK facies, e.g. 51.35 – 55.32m in DD68 and 109.07 – 110.28m in DD88. Figure 9 shows an example of vague bedding (RVK-B_vm) as it occurs in the pit exposures. The crude preferred orientation of clasts is often difficult to detect in the drillcore where the lateral extent of the outcrop is not present. The vaguely bedded RVK facies may therefore be more common than is indicated in the drillcore logs.

Microscopic examination of the RVK-B_v facies reveals that it is texturally and compositionally very similar to the massive RVK facies. It is predominantly clast-supported and poorly sorted with modal abundances of lithic and juvenile components which are comparable to those recorded in the massive RVK facies (Table 6). The vague clast alignment is in most cases not recognisable on a microscopic scale. However, in a few of the samples (e.g. DD88/6, DD68/10) the long axes of certain of the xenolithic fragments, olivine macrocrysts and elongate magma clasts display a crude subparallel alignment.

2.1.2.2. Distinctly Bedded RVK Facies

Distinct planar bedding of fine, *fine*-medium, medium and coarse grained RVK facies (RVK-B_df, RVK-B_d*f*m, RVK-B_dm and RVK-B_dc subfacies respectively) is defined by the presence of narrow clast-supported layers displaying an increase in mean grain size and lithic content (Figure 10). The latter is generally accompanied by an increase in the grain size of the juvenile component. In some cases the bedding is accentuated by differences in the fines content of the inter-clast matrix of the beds, which imparts a colour contrast to the rocks (Figure 31). Crude prefered orientation of elongate clasts parallel to the bedding planes is a common feature. The coarser-grained lithic-rich beds range in thickness from 2 to 30cm. They occur either at random or regular intervals between the comparatively finer-grained and lithic-poor beds, in which small-scale size grading of constituents may be present (e.g. samples DD88/14, DD68/28, DD68/23B and DD68/29).

The distinctly bedded RVK facies is not abundant in the pit exposures, with usually only one or two bedded zones being present within a bench face 50 meters in lateral extent. The exposure traversed on Bench 12, however, exhibits some of the best examples of distinct bedding within a relatively narrow zone (refer to Figure 8). The bedding is in all cases laterally discontinuous, occuring in distinct blocks and less well-defined zones of only a few meters in width. Contacts with the adjacent massive RVK facies may be sharp or gradational. In all cases the dip of the beds is steep, ranging between 48° and 70°, with an average dip of 62°. Although the bedding commonly dips towards the centre of the lobe, a number of blocks displaying bedding with other orientations are also present.

The distinctly bedded RVK facies was intersected in each of the three drillcores, with the bedded zones ranging between 0.25m and 12m in thickness. Contacts between the bedded RVK facies and massive RVK facies are generally sharp. The grain size contrast within the bedded zones, i.e. between the coarser-grained lithic-rich and the finer-grained lithic-poor beds, is variable, as is the sharpness of the bed contacts, although diffuse contacts tend to predominate. The thickness of the beds, within and between the various bedded zones, is also variable (Figure 32). For example, the dominantly medium to thickly bedded (10 – 100cm) *fine*-medium and coarse grained RVK facies intersected at 284.23 – 289.90m in DD68 contrasts with the dominantly thinly bedded (3 – 10cm) *fine*-medium and medium grained RVK facies intersected at 111.60 – 112.72m in DD88. Narrow intersections of

very thinly to thinly bedded (1 – 10cm) fine and *fine*-medium/medium grained RVK facies were intersected at 145.05 – 145.28m in DD15 and 265.82 - 265.99m in DD88. In these, as well as in other such bedded zones observed in the pit exposures, the fine grained beds (RVK-B_df) comprise dark lithic-poor, mud-rich RVK.

In a number of samples (e.g. DD68/21 and DD68/23B) the presence of bedding was revealed only once the core had been cut and polished. The vertical extent of the bedding in these zones is thus uncertain. Therefore, it should be noted that since the rough outer core surfaces may have obscured the presence of bedding in other areas of the drillcore, it is possible that the distinctly bedded RVK facies is more common than the drillcore logs indicate.

Microscopic examination of the coarser-grained lithic-rich beds reveals a distinctly clast-supported granular texture, resulting from the presence of closely-packed olivine, country rock xenoliths and juvenile magma clasts (Figure 33). These coarse constituents are set in an inter-clast matrix composed predominantly of clay minerals and lesser serpentine. In a few of the samples the interstices between the clasts are filled with strained quartz (probably related to post-depositional diagenesis). Although on a macroscopic scale these beds appear to be relatively well sorted, particularly in comparison to the massive RVK facies, they are in fact poorly sorted, with each clast type displaying a considerable range in grain size.

Subrounded and subangular to angular fragmented macrocrysts and phenocrysts of altered olivine are abundant (40 – 50 volume %), occuring both discretely and as coarse inclusions within magma clasts. The lithic component of the beds is dominated by Transvaal Supergroup shales and wackes and lesser dolomite. Mudstones, altered dolerite, chert, quartzite and rare altered basement fragments may also be present. The xenoliths constitute between 30 and 40 volume % of the beds. They are most commonly subangular to angular, although subrounded and occasional contorted clasts (mudstones) do occur. Xenocrystic garnet, ilmenite, chrome diopside, amphibole, biotite and magnetite constitute up to 5 volume % of the beds. Rounded to irregular juvenile magma clasts (10 – 20 volume %) are closely packed between the olivine and lithic clasts and are texturally and mineralogically similar to those which occur in the massive RVK facies (Table 6). Both mineralogical varieties of magma clasts identified in the latter are present. The fabric

imparted by the prefered orientation of elongate components (mostly country rock xenoliths, but also certain olivines and magma clasts) is identifiable microscopically in some samples. Contacts between these coarser-grained lithic-rich beds and the finer-grained, comparatively lithic-poor beds are in most cases relatively diffuse.

Apart from the obvious grain size difference, the finer-grained beds are texturally very similar to the coarser-grained beds. The degree of sorting does, however, appear to be greater than in the coarser-grained beds. A weak fabric, imparted by the prefered orientation of elongate clasts, is present in many of the beds (Figure 34). The modal abundance of olivine and magma clasts is comparable to that of the coarser-grained beds. The modal abundance of country rock xenoliths is lower, however, and ranges from 10 to 20 volume %. Small-scale size-sorting of constituents into diffuse layers is occasionally present in the finer-grained beds, particularly in cases where the bedded RVK facies is thinly bedded (3 – 10cm thick beds).

The thin beds of fine grained RVK (RVK-B_df) which are occasionally interbedded with the beds described above display a distinctly matrix-supported, inequigranular texture. Loosely packed olivine, magma clasts and minor country rock xenoliths are set in a dark brown, mud-rich inter-clast matrix (Figure 35). These beds are generally relatively well sorted, however rare outsized clasts may be present (Figure 36). Vague subparallel alignment of elongate components is common. Fine grained altered olivine forms the dominant constituent of these beds (20 – 25 volume %). Juvenile magma clasts and country rock xenoliths occur in very low proportions, each comprising less than 10 volume % of the beds. The magma clasts are often difficult to distinguish from the clays in the inter-clast matrix, but appear to be texturally and compositionally similar to those in the coarser-grained beds. The lithic clast population includes mainly shale and lesser dolomite.

Figure 31: Distinctly bedded fine-medium and medium grained RVK facies (RVK-B_d *f*m-m) in a pit exposure of the South Lobe. The colour contrast of the beds is related to differences in the inter-clast matrix fines content of the individual beds.

Figure 32: Distinctly bedded RVK facies in core samples (a) DD88/14, (b) DD68/29 and (c) DD68/23B showing variations in bed thickness. Scale in centimeters.

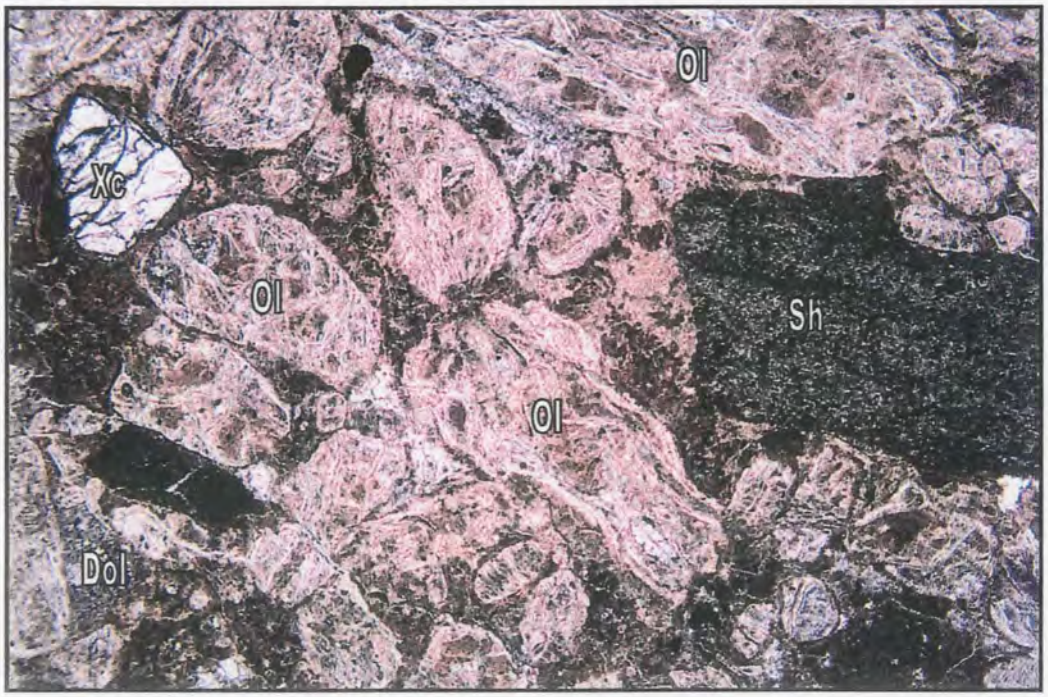

Figure 33: Photomicrograph showing the closely-packed, granular texture of the coarser-grained beds in the distinctly bedded RVK facies (sample DD88/14). Abundant altered olivine (Ol), dolomite (Dol) and shale (Sh) xenoliths, and a garnet xenocryst (Xc) occur in a clay- and serpentine-rich matrix. PPL. FOV = 5.2 mm.

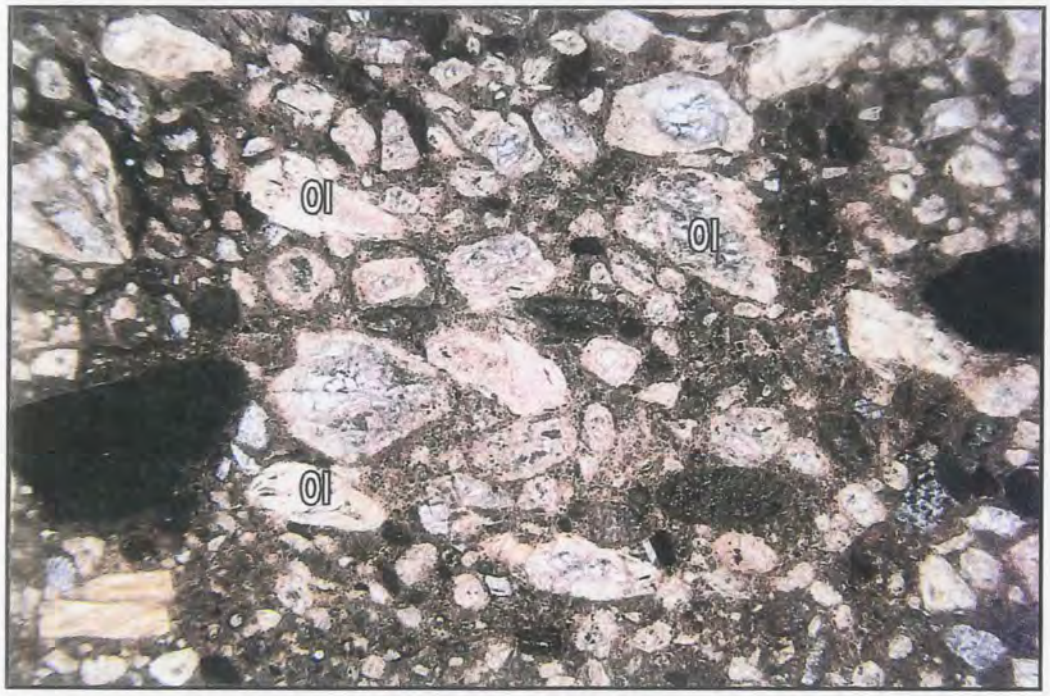

Figure 34: Photomicrograph showing the texture and fabric of the finer-grained beds in the distinctly bedded RVK facies (sample DD15/11). Note the crude subparallel alignment of elongate altered olivine (Ol) grains. PPL. FOV = 5.2 mm.

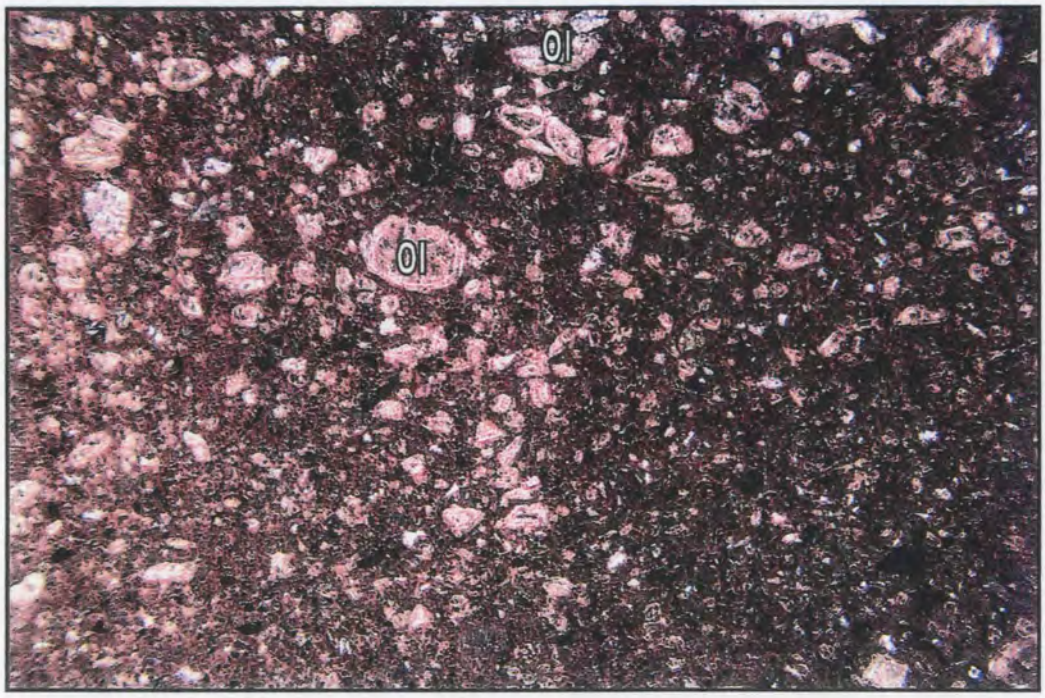

Figure 35: Photomicrograph showing the texture of the fine grained, mud-rich beds of the distinctly bedded RVK facies (sample DD15/11). Note the altered olivine (Ol) fragments and the high proportion of mud-rich inter-clast matrix. PPL. FOV = 5.2mm.

Figure 36: Distinctly bedded RVK facies containing a thin fine grained, mud-rich RVK bed: core sample DD15/11. Note crude subparallel alignment of elongate clasts and rare outsized clasts. Scale in centimeters.

2.2. The QRVK Facies

The quartz-bearing QRVK facies is volumetrically subordinate to the quartz-free RVK facies. It is restricted to a discontinous marginal zone of the pipe which, where present, has a thickness of 7 to 15 meters adjacent to the wall-rock contact. The QRVK facies has been subdivided into two subfacies, based on the proportion of quartz present in the rocks. These are termed the quartz facies (**QRVKq facies**), in which quartz predominates, and the juvenile/quartz facies (**QRVKj/q facies**) in which the juvenile component is dominant, but quartz is present. The contacts between the QRVK facies and the RVK facies are either sharp or gradational. Where the contact is sharp it is defined by the abrupt disappearance of quartz. Gradational contacts are characterised by the alternation of quartz-rich (QRVKq facies) and quartz-poor (QRVKj/q facies), and in some cases quartz-free (RVK facies) zones, over several meters. It should be noted that the QRVK facies contains feldspar in addition to quartz, but in subordinate quantities.

2.2.1. QRVKquartz Facies (QRVKq)

The QRVKq facies includes predominantly *fine*-medium, medium and lesser coarse grained massive and bedded deposits. This facies also includes fine grained deposits which occur as large inclusions within the massive QRVKq and QRVKj/q facies, as well as within the massive RVK facies, and display evidence of slumping (QRVKq-S). As is the case in the RVK facies, the **massive QRVKq** facies dominates over the **bedded QRVKq** facies. The **slumped QRVKq** facies is volumetrically subordinate to the massive QRVKq facies, but is more common than the bedded QRVKq facies. The characteristic features of these facies are summarised in Table 6.

2.2.1.1. Massive QRVKq facies

The massive QRVKq facies (QRVKq-M) was observed close to the wall-rock contact in most of the pit exposures and was intersected in two of the three drillcores, namely DD15 and DD88, at depths greater than 168.80m and 408.37m, respectively.

The rocks of this facies are pale to medium greenish-grey in colour with a characteristic patchy red-brown discolouration, which is particularly well-developed in the few meters directly adjacent to the wall-rock contact. The rocks are generally competent and display good textural preservation, despite relatively high degrees of clay, serpentine and carbonate alteration. They exhibit a distinctly fragmental, inequigranular texture resulting from the presence of predominantly subangular to angular and lesser subrounded coarser components (olivine, magma clasts, country rock xenoliths, quartz and feldspar and VK autoliths), which are set in a very fine grained inter-clast matrix. The ubiquitous quartz and lesser feldspar grains are in most cases not readily identifiable in handspecimen. The rocks are predominantly matrix-supported and well to poorly sorted on a macroscopic scale. Variably coloured mudstone clasts of all sizes, which commonly display highly irregular contorted or 'wisp-like' shapes, are abundant in these rocks and are a diagnostic feature of the facies (Figure 37). They are more common than in the RVK facies.

This facies has been termed massive due to a lack of any obvious internal structure or bedforms. It does, however, exhibit broad-scale, gradational variations in mean grain size, lithic content and/or juvenile content. For example, in DD15 between 168.80m and 176.43m the mean grain size, lithic content and juvenile content increase gradationally to 4mm, 30 volume % and 15 volume %, respectively, and then decrease again to 3mm, 20 volume % and 10 volume %. Although these subtle variations are not as easily recognised in the pit exposures as in the drillcore, they do not appear to define distinct bedding.

Subangular to angular and lesser subrounded quartz and feldspar fragments constitute between 20 and 40 volume % of the rocks (Figure 38). The quartz and feldspar are poorly sorted, displaying a polymodal size distribution from fine silt- to very coarse sand-sized (0.01 – 1.5mm), although the majority of grains are coarse silt- to medium sand-sized (0.04 – 0.5mm). The quartz population includes predominantly monocrystalline grains and lesser polycrystalline aggregates. Plagioclase and potassium feldspar occur in subordinate proportions to the quartz, and most grains display secondary clay alteration. The majority of the quartz and feldspar is strained and displays undulose extinction.

The modal abundance of macrocrystal and phenocrystal olivine pseudomorphs is variable within the massive QRVKq facies, but is in all cases lower than in the massive RVK facies, ranging between 10 and 30 volume %. The grain size varies considerably from

coarse macrocrysts (up to 6mm) to small crystal fragments less than 0.5mm in size. The olivine occurs both as discrete grains within the inter-clast matrix and as coarse inclusions within juvenile magma clasts (Figure 39).

Country rock xenolith lithologies include green and black shales, micaceous and quartz wackes, dolomite and chert, mudstones and siltstones, dolerite, quartz arenite, quartzite, amphibolitised basement granitoids and biotite schist. In contrast to the massive RVK facies, the Transvaal Supergroup shales are in many cases not the dominant lithic clast type. Coal fragments are common in places. Grey-green to brown to red-brown mudstone clasts are abundant and range in size from a few millimeters to 100mm. They often display highly contorted or 'wisp-like' shapes and many have irregular, diffuse contacts with the host rock. In places they appear to be intimately mixed with the inter-clast matrix. Most of the xenoliths occur discretely, although some have a juvenile magmatic selvage. The modal abundance of country rock xenoliths varies from 10 to 15 volume %, with localised increases up to 20 volume %.

The modal abundance of juvenile magmaclastic material is lower than in the massive RVK facies, and ranges between 5 and 10 volume %. The magma clasts are often difficult to recognise in uncut core and in the pit exposures, probably as a result of the patchy appearance of the rocks. The magma clasts vary from 0.15mm to 15mm in size, and include predominantly rounded and subrounded types, with lesser irregular and subangular varieties. The magma clasts are texturally and mineralogically similar to those in the massive RVK facies, with both the monticellite and monticellite-calcite types being present. No microlitic diopside was found in any of the samples examined.

Mantle- and crustal-derived xenocrysts constitute up to 3 volume % of the rocks and occur either discretely within the inter-clast matrix or as coarse inclusions within juvenile magma clasts. The inter-clast matrix is compositionally similar to that of the massive RVK facies and commonly displays a red-brown patchy appearance resulting from the oxidation of iron-bearing clay minerals.

Subrounded to irregular autoliths of VK occur in places and range from a few millimeters to 70mm in size. They are recognisable in handspecimen by their darker colour in comparison to the host. Contacts are generally sharp, but may be irregular on a small-scale.

Microscopically they are seen to be highly altered and to differ from the host, particularly in terms of grain size, quartz/feldspar content and inter-clast matrix mud content.

As is the case in the massive RVK facies, the massive QRVKq facies contains a number of country rock xenoliths, juvenile magma clasts and autoliths which have narrow non-magmatic rims composed of mud and very fine grained lithic and juvenile fragments. These rimmed or armoured clasts are rare, and were observed in a few samples only (e.g. DD15/26, DD88/45 and DD88/46). They were also recognised by Field (1988b, 1989a-b, 1991) in his examination of the QRVK facies.

2.2.1.2. Bedded QRVKq facies

Very few occurrences of bedded QRVKq facies (QRVKq-B) were observed in the pit exposures, where it occurs as laterally discontinuous zones of one or two meters in maximum extent. In all instances the bedding is planar and displays steep dips into the pit, generally greater than 60°. The dip directions of the beds are variable. Contacts with the adjacent massive QRVK facies may be sharp or gradational. The QRVKq-B facies was intersected in only one of the drillcores, namely DD15, between 160.03 - 164.40m. This relatively narrow intersection is overlain by massive RVK facies and followed with depth by bedded QRVKj/q facies.

The bedding is defined by the presence of narrow clast-supported layers displaying an increase in mean grain size and lithic content, which alternate with finer-grained, comparatively lithic-poor beds. The contrast in grain size between the beds is variable, but most commonly ranges from *fine*-medium to medium grained, i.e. QRVKq-B*f*m-m. The QRVKq-B facies is generally medium to thickly bedded, with the coarser-grained beds typically being less than 15cm thick and the finer-grained beds having thicknesses of up to a meter. The rocks are generally competent and medium to dark greenish-grey, with a red-brown patchy appearance in places. They display a fragmental, inequigranular texture and are texturally well-preserved.

The coarser-grained beds display a clast-supported, granular texture and are relatively well sorted. They consist of closely-packed altered olivine, country rock xenoliths, magma clasts and xenocrystic quartz and feldspar grains set in a very fine grained clay and

serpentine matrix. Subangular to angular quartz and lesser feldspar grains are abundant, comprising up to 40 volume % of the beds, and range in size from 0.01mm to 2mm (fine silt- to very coarse sand-sized). Olivine and country rock xenoliths constitute 20 to 25 volume % and 30 volume % of the beds, respectively. The range of xenolith lithologies present is similar to that in the massive QRVKq facies. Rounded to subangular juvenile magma clasts comprise a maximum of 10 volume % of the beds and the majority are highly altered. They are texturally and mineralogically similar to those in the massive QRVKq facies. Minor (2 – 3 volume %) garnet, ilmenite and chrome diopside xenocrysts also occur within the beds. Crude subparallel alignment of elongate components may be present, but is not a widespread feature.

In contrast, the finer-grained beds are matrix-supported and well to poorly sorted, and have a lower country rock xenolith content (approximately 10 volume %) compared to the coarser-grained beds (Figure 40). They are in fact very similar in their overall appearance, composition and texture to the massive QRVKq facies (Table 6). Subangular to angular quartz and feldspar fragments are abundant, but slightly less so than in the coarser-grained beds, reaching a maximum of 20 volume % (Figure 41). Prefered orientation of elongate components is occasionally observed in the finer-grained beds exposed in the pit, but has not been observed microscopically. The contacts between the coarser-grained and finer-grained beds are in most cases relatively sharp.

Figure 37: The massive QRVK quartz facies: core samples (a) DD88/46, (b) DD15/20 and (c) DD15/27. Note the chararacteristic patchy red-brown colour of the matrix and common contorted mudstone clasts, particularly in sample DD15/27. Scale in centimeters.

Figure 38: Photomicrograph showing abundant subangular to angular quartz (Q) and feldspar (F) grains in the massive QRVK quartz facies (sample JS-KM1). Note also the altered olivine (Ol) macrocryst and phenocryst fragments and dolomite (Dol) and quartzite (Qt) xenoliths. PPL. FOV = 2.75 mm.

Figure 39: Photomicrograph showing the characteristic texture and composition of the massive QRVK quartz facies (sample DD88/47). Quartz (Q) and feldpar (F) fragments, altered olivine (Ol) grains, juvenile magma clasts (MC) and shale (Sh) xenoliths are set in a clay and serpentine dominated matrix. PPL. FOV = 5.2mm.

Figure 37.

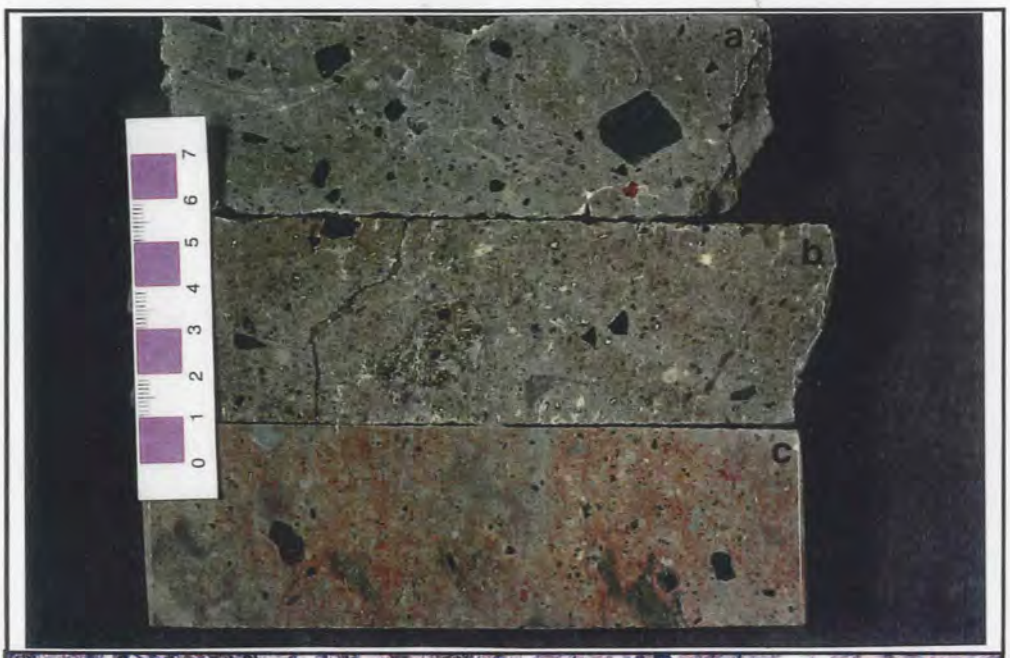

Figure 38.

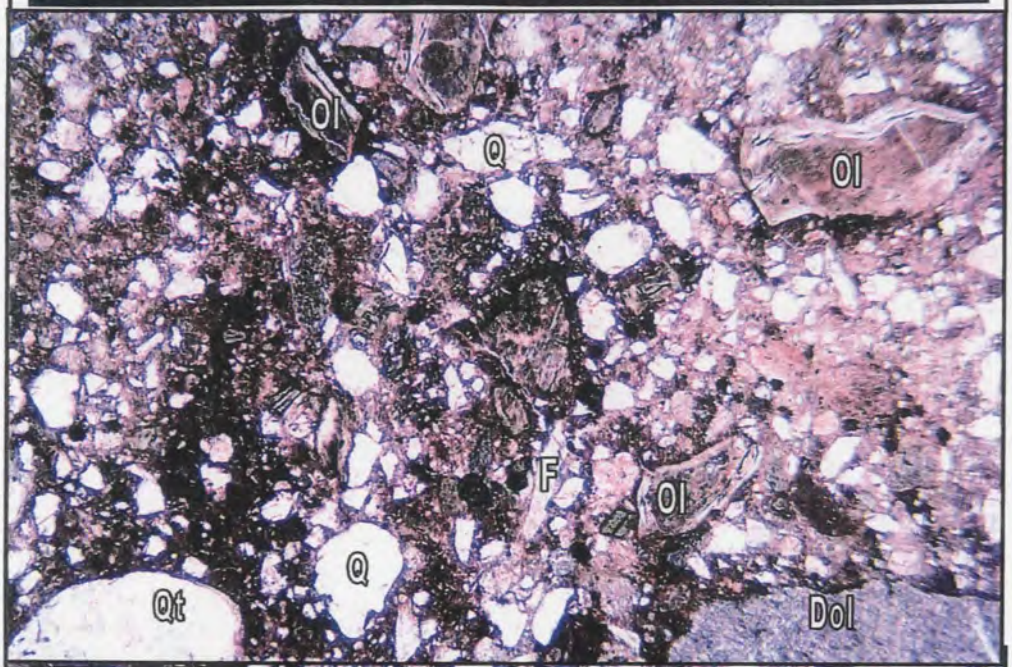

Figure 39.

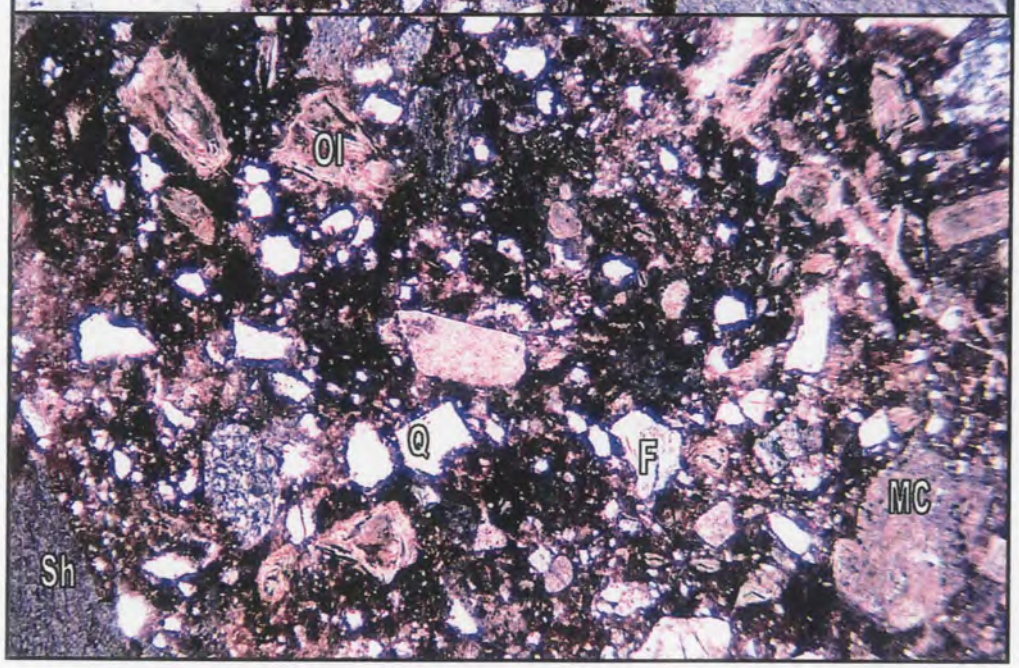

Figure 40: Finer-grained bed of the distinctly bedded QRVK quartz facies: core sample DD15/17. Scale in centimeters.

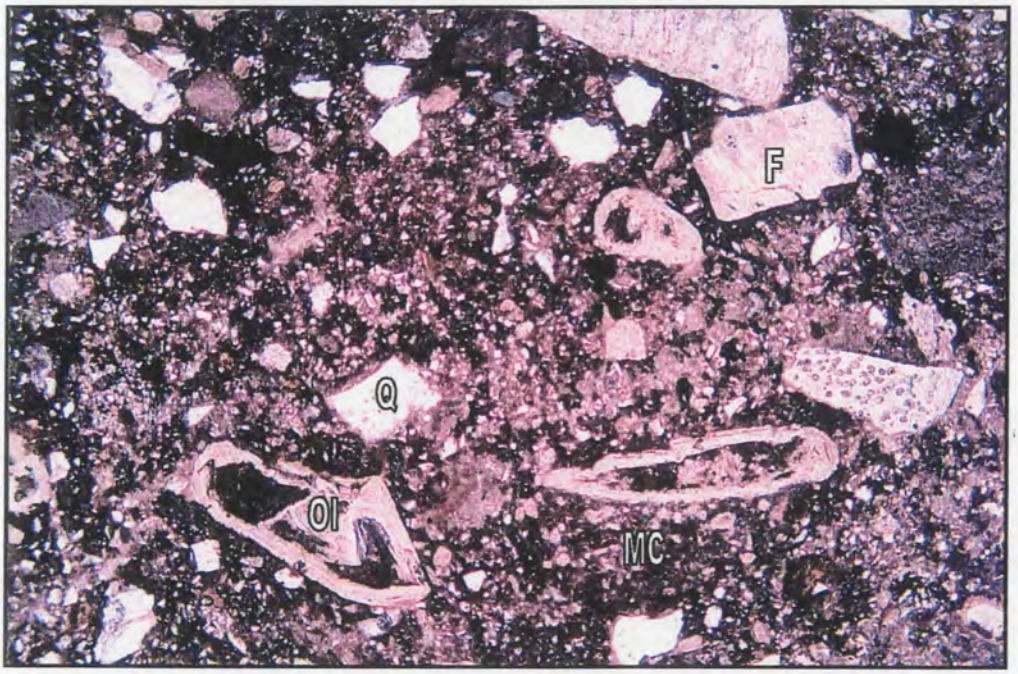

Figure 41: Photomicrograph showing the characteristic texture and composition of the finer-grained beds of the distinctly bedded QRVK quartz facies (sample DD15/17). Note the altered olivine (Ol) fragments, juvenile magma clasts (MC) and abundant subangular to angular quartz (Q) and feldspar (F) grains, which display a wide range in grain size. PPL. FOV = 5.2mm.

2.2.1.3. Slumped QRVKq facies

The slumped QRVKq facies (QRVKq-S) was observed in all of the pit exposures. This fine grained, mud-rich QRVKq facies occurs as subrounded to irregular inclusions or 'clots', ranging up to a few meters in size, within medium and coarse grained massive RVK and QRVK facies. The QRVKq-Sf facies was intersected below 300m depth in DD88 only, where it occurs as relatively common intersections which range between 10cm and 2m in thickness. Contacts between the QRVKq-Sf facies and the massive RVK and QRVK facies are almost always sharp, and commonly irregular.

The rocks are typically dark grey-green or grey-brown in colour and brittle to friable. They display a distinctive blocky weathered appearance in the pit exposures (Figure 42). Despite high degrees of alteration (mainly serpentine and clay minerals), textural preservation is good. The rocks display a fragmental, inequigranular and matrix-supported texture, resulting from the presence of loosely packed olivine, lithic clasts, quartz and feldspar, magma clasts and mantle xenocrysts which occur within a very fine grained mud-rich matrix. The deposits are compositionally variable and range from those in which scattered olivines and mantle xenocrysts are the only recognisable kimberlitic components, through those which contain irregularly shaped diffuse lenses/pods and irregular laminations composed of coarser-grained lithic and juvenile components, to those which contain more uniformly distributed juvenile and lithic constituents (Figure 43). The rocks are characterised by an overall paucity of lithic clasts and outsized clasts are very rare (Figure 44). Soft sediment deformation structures, such as slumping and micro-faulting, are common (Figure 13, Section1).

Altered olivine varies in size from coarse macrocrysts (up to 5mm) to minute grain fragments (0.05mm), although the average size in most cases is approximately 0.5mm. The modal abundance of olivine is variable between samples, but is in all cases lower than in the RVK facies, and is often comparable to the massive and bedded QRVKq facies (20 – 25 volume %). The majority of grains occur discretely within the inter-clast matrix. Juvenile magma clasts comprise up to 10 volume % of the rocks and range considerably in size from 0.05mm to 5mm, although the majority rarely exceed 2mm. Most of the magma clasts are highly altered and the smaller clasts are often difficult to distinguish from the

clays in the inter-clast matrix. In many cases altered olivine and spinel are the only recognisable primary groundmass constituents. Examination of the coarser, less altered magma clasts reveals that both the monticellite and monticellite-calcite types, which occur in the facies described above, are present.

The country rock xenolith content is generally low, with modal abundances ranging between 10 and 15 volume % (refer to Table 6 for xenolith types). The lithic clasts range in size up to 7mm, but outsized clasts are rare and the lithic component in most samples is fine grained (< 2mm). Quartz and feldspar together comprise 10 to 25 volume % of the rocks. The grains display a polymodal size distribution in most samples, ranging from 0.01mm to 2mm (fine silt- to very coarse sand-sized), although coarse silt- to fine sand-sized grains (0.04 – 0.2mm) are dominant. The majority of the grains occur discretely within the matrix, but a few occur as coarse inclusions within juvenile magma clasts. Mantle- and crustal-derived xenocrysts may comprise up to 5 volume % of the rocks. VK and hypabyssal facies autoliths are extremely rare or absent in this facies. Certain samples occasionally display alignment of coarser lithic and juvenile components in narrow (single grain thick) laminations or 'clast strings' which are generally irregular and laterally impersistant. The proportion of inter-clast matrix is high, typically 40 volume % (Figure 45).

Of particular interest in the QRVKq-Sf facies is the presence of rare accretionary and armoured lapilli. The latter were observed in the massive RVK and QRVKq facies, but they appear to be more common in the fine grained QRVKq-S facies. The accretionary lapilli and rims of the armoured lapilli are composed of material which closely resembles the inter-clast matrix, i.e. clays and very fine grained lithic and juvenile fragments. The rims of the armoured lapilli vary in thickness and mantle a variety of clast types. Sample DD88/33 from 328.05m in drillhole DD88 contains some of the best examples of accretionary and armoured lapilli (Figures 46 and 47).

Figure 42: Large irregular 'clot' of grey-brown fine grained slumped QRVK facies (QRVKq-S) displaying characteristic blocky weathered appearance within weathered medium to coarse grained massive RVK facies in a pit exposure of the South Lobe.

Figure 43: The fine grained slumped QRVK quartz facies: core samples (a) DD88/33, (b) DD88/30 and (c) DD88/19. Samples DD88/33 and DD88/19 display a uniform distribution of juvenile and lithic constituents, whereas sample DD88/30 contains a diffuse pod of coarser-grained components. Scale in centimeters.

Figure 44: The fine grained slumped QRVK quartz facies in a pit exposure in the South Lobe. Note the paucity of outsized lithic clasts.

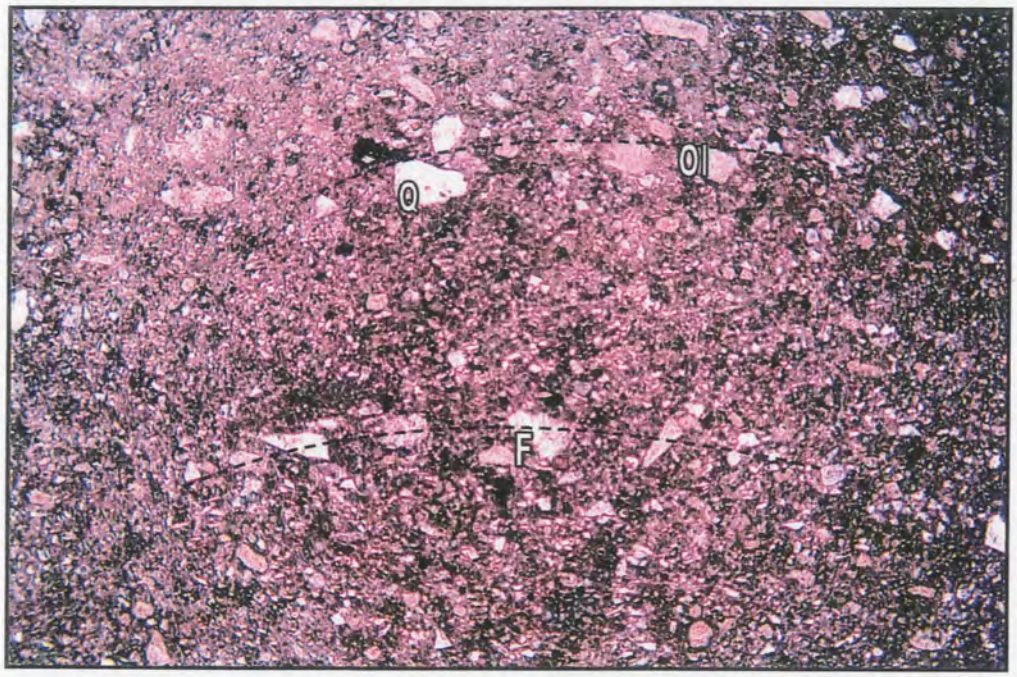

Figure 45: Photomicrograph showing the characteristic texture and composition of the fine grained slumped QRVK quartz facies (sample JS-KM1). Note the scattered altered olivine (Ol) fragments and abundant fine grained quartz (Q) and feldspar (F) grains. The coarser constituents appear to define laterally impersistant laminations (dashed lines). PPL. FOV = 5.2mm.

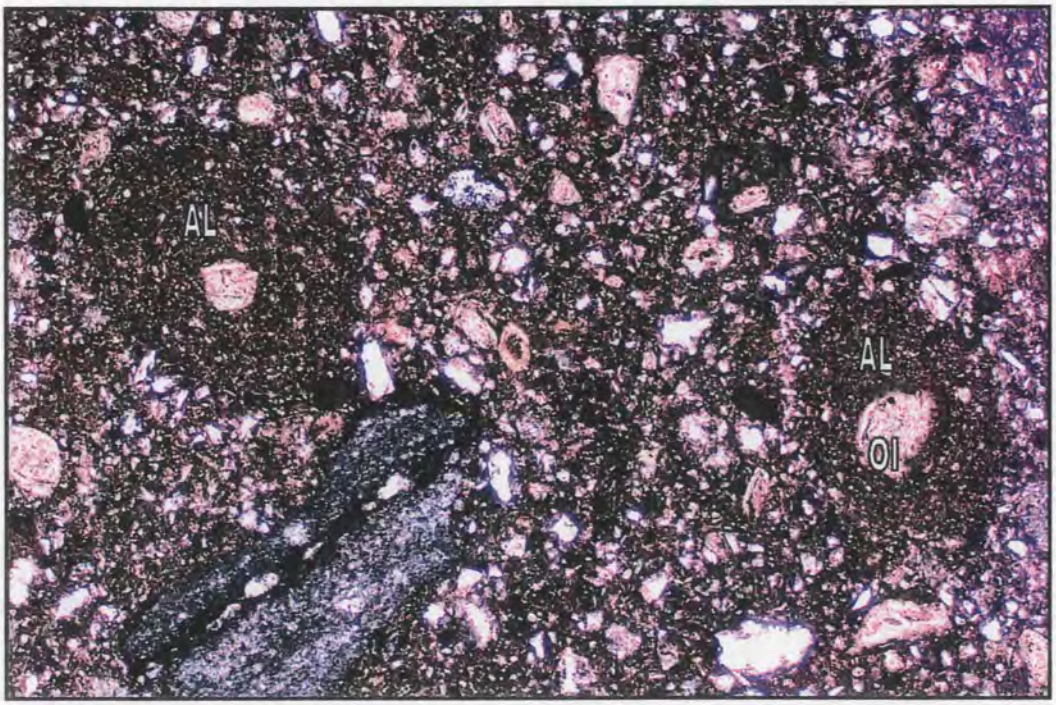

Figure 46: Photomicrograph showing well-developed accretionary lapilli (AL) in the fine grained slumped QRVK quartz facies (sample DD88/33). The lapilli consist of clays and very finely comminuted juvenile and lithic fragments (i.e. ash/mud). Ash-sized altered olivine (Ol) grains occur within each lapillus. PPL. FOV = 2.75mm.

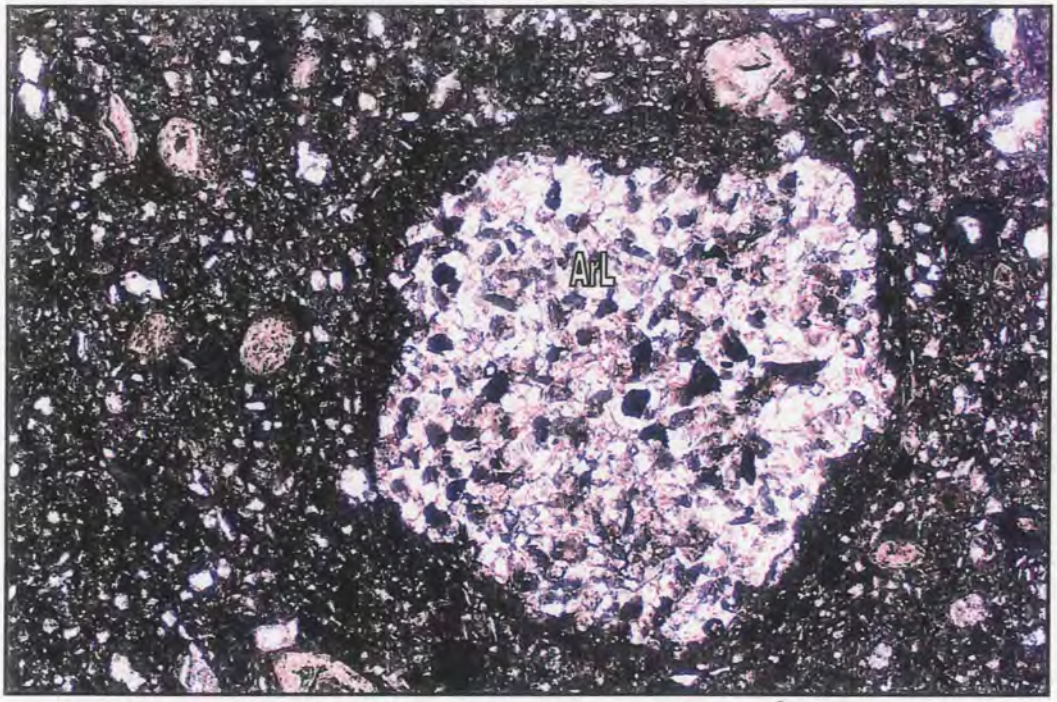

Figure 47: Photomicrograph showing an armoured lapillus (ArL) in the fine grained slumped QRVK quartz facies (sample DD88/33). The lapillus consists of a subrounded arenite clast mantled by a thin ash/mud rim. PPL. FOV = 2.75mm.

2.2.2. QRVKjuvenile/quartz Facies (QRVKj/q)

The QRVKj/q facies includes predominantly *fine*-medium and medium grained massive and bedded deposits. The **massive QRVKj/q** facies dominates over the **bedded QRVKj/q** facies. The facies is volumetrically subordinate to both the RVK facies and QRVKq facies and typically occurs in the contact zone between the latter two facies. Both the massive and the bedded QRVKj/q facies are not readily recognisable in the pit exposures due to their overall similarity in appearance to the massive and bedded RVK facies and the fine grainsize of the quartz and feldspar, the presence of which is the fundamental diagnostic feature. Refer to Table 6 for a summary of the characteristic features of this facies.

2.2.2.1. Massive QRVKj/q facies

The massive QRVKj/q facies (QRVKj/q-M) was intersected in two of the three drillcores, namely DD15 and DD88, at depths greater than 147.15m and 313.06m, respectively. In both drillcores the first intersections of the QRVKj/q-M facies are followed with depth by relatively thick intersections of massive RVK before intersection with the QRVKq facies.

The rocks of this facies are pale to medium greenish-grey in colour and competent. They are moderately to highly altered, but display good textural preservation. They exhibit a distinctly fragmental, inequigranular texture and are clast-supported due to the close-packed arrangement of the coarser juvenile and lithic constituents. Macroscopically the rocks are well to poorly sorted, with rare outsized clasts only (Figure 48).

The main distinguishing feature of the massive QRVKj/q facies is the presence of minor amounts of quartz and feldspar (Figure 49). The combined abundance of these minerals is variable between samples, but generally does not exceed 10 volume %. As is the case in the QRVKq facies, the quartz and feldspar varies considerably in size from 0.01mm to 1.5mm (fine silt- to very coarse sand-sized).

The nature of the olivine and juvenile magma clasts, and the range of country rock xenolith lithologies is similar to that in the massive RVK facies (Table 6). However, the modal abundances of the various components differ slightly from those of the massive RVK

facies. The modal abundances of olivine and juvenile magma clasts are slightly lower than in the massive RVK facies, ranging from 25 to 45 and 10 to 15 volume %, respectively. The proportion of country rock xenoliths is comparable to that in the massive RVK facies, but generally does not exceed 20 volume %. Highly altered small peridotite xenoliths are rare (e.g. sample DD88/31).

Subrounded VK autoliths are relatively common and are similar to those described in the massive QRVKq facies. In most cases the quartz and feldspar content of the autoliths is significantly higher than that of the host. The contacts between the autoliths and the host rock are sharp. Clasts mantled by non-magmatic rims are a rare feature of the massive QRVKj/q facies (samples DD88/31 and DD88/35 only). The rims are similar in texture and composition to those observed in both the RVK and QRVKq facies.

2.2.2.2. Bedded QRVKj/q facies

The bedded QRVKj/q facies (QRVKj/q-B) occurs as two narrow intersections between 164.40 – 168.80m and 289.55 – 296.40m in drillcores DD15 and DD88, respectively. In DD15, the four meter intersection of QRVKj/q-B facies occurs between intersections of bedded QRVKq facies and massive QRVKq facies, in the vicinity of the contact between the RVK facies and QRVKq facies. In DD88, the seven meter intersection of QRVKj/q-B facies is followed with depth by approximately 17m of massive RVK facies before intersection with massive QRVKj/q facies at 313.06m. The QRVKj/q-B facies was not identified in the pit exposures.

The nature of the bedding is similar to that of the RVK-B and QRVKq-B facies (refer to Table 6). The grain size contrast between the beds ranges from *fine*-medium to medium grained, i.e. QRVKj/q-B *f*m-m. The QRVKj/q-B facies is thinly to thickly bedded, with the coarser-grained beds typically being less than 10cm thick and the finer-grained beds having thicknesses of up to 50cm. Contacts between the coarser-grained and finer-grained beds are sharp. The rocks are generally competent and pale to medium greenish-grey in colour. They display a fragmental, inequigranular texture and are texturally well-preserved (Figure 50).

The coarser-grained beds display a clast-supported, granular texture and are relatively well sorted. Closely packed altered olivine (35 – 45 volume %), country rock xenoliths (35 – 40 volume %), juvenile magma clasts (15 – 20 volume %) and minor quartz and feldspar grains (< 10 volume %) are set in a very fine grained matrix. The nature of the olivine and magma clasts, and the range of country rock xenolith lithologies present is similar to that in the massive QRVKj/q facies.

The finer-grained beds are very similar in their overall appearance and texture to the massive QRVKj/q facies (Figure 51). They have a lower country rock xenolith content (10 - 20 volume %) compared to the coarser-grained beds, whereas the modal abundances of the juvenile component and quartz and feldspar are comparable to those in the coarser-grained beds. Crude prefered orientation of elongate components is occasionally observed in the finer-grained beds, but is not recognisable on a microscopic scale.

Figure 48: The massive QRVK juvenile/quartz facies: core samples (a) DD88/31, (b) DD88/34 and (c) DD15/13. Note the fragmental, poorly sorted texture and overall similarity to the massive RVK facies. Scale in centimeters.

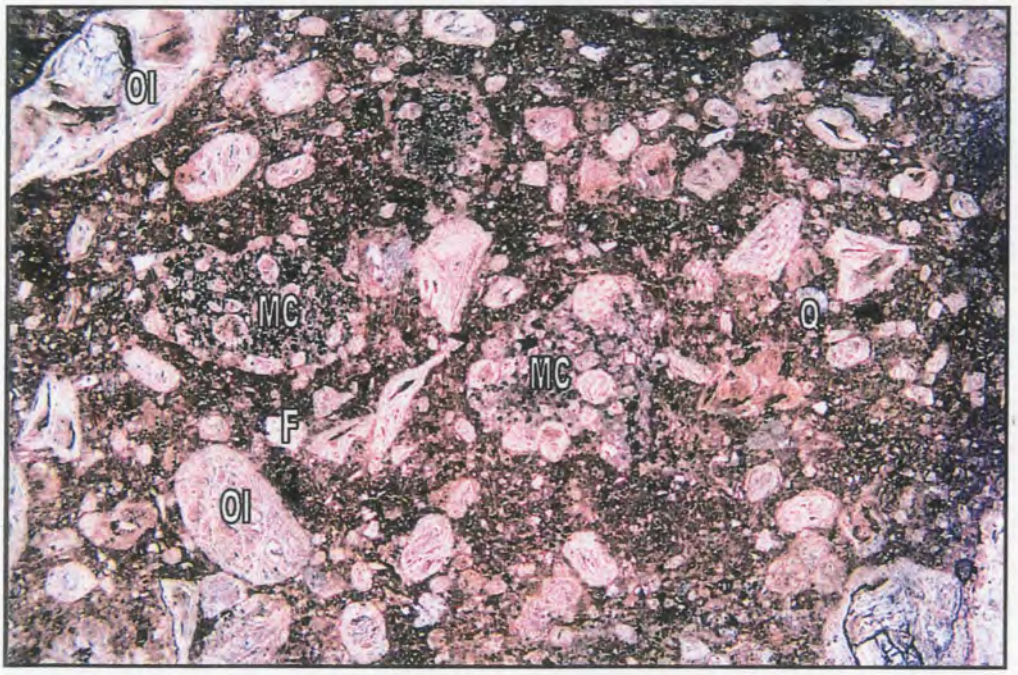

Figure 49: Photomicrograph showing the characteristic texture and composition of the massive QRVK juvenile/quartz facies (sample DD88/31). Abundant altered olivine (Ol) macrocryst and phenocryst fragments, juvenile magma clasts (MC), country rock xenoliths and rare quartz (Q) and feldspar (F) fragments are set in a clay and serpentine matrix. PPL. FOV = 5.2mm.

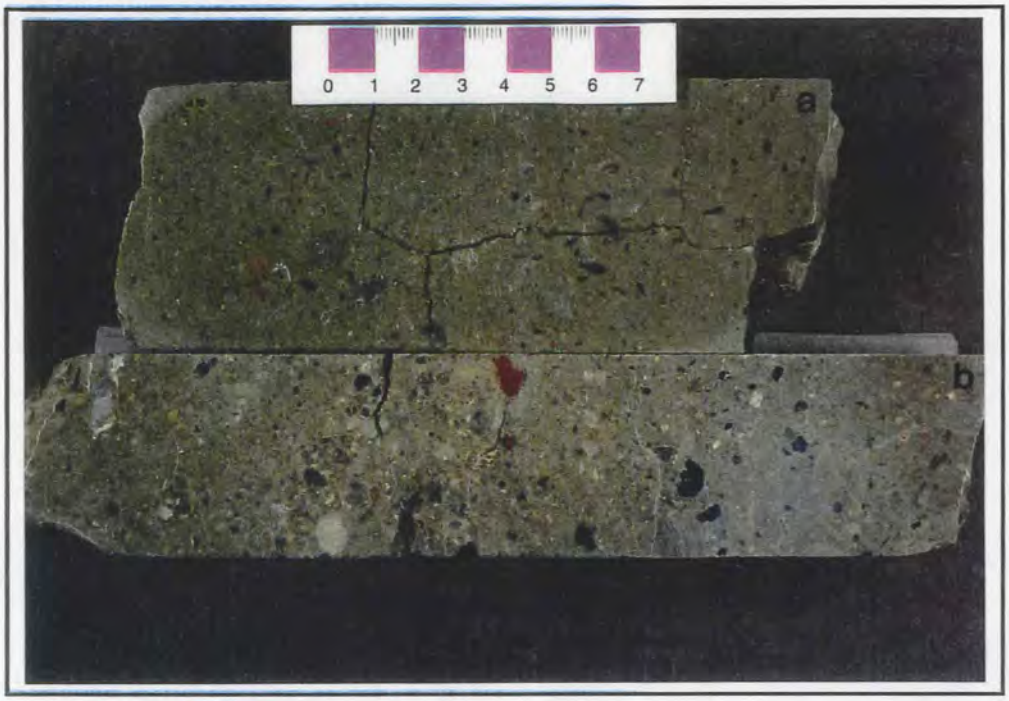

Figure 50: The bedded QRVK juvenile/quartz facies: core samples (a) DD88/28 (finer-grained bed only) and (b) DD15/18 (contains thin diffuse coarser-grained, lithic-rich bed). Scale in centimeters.

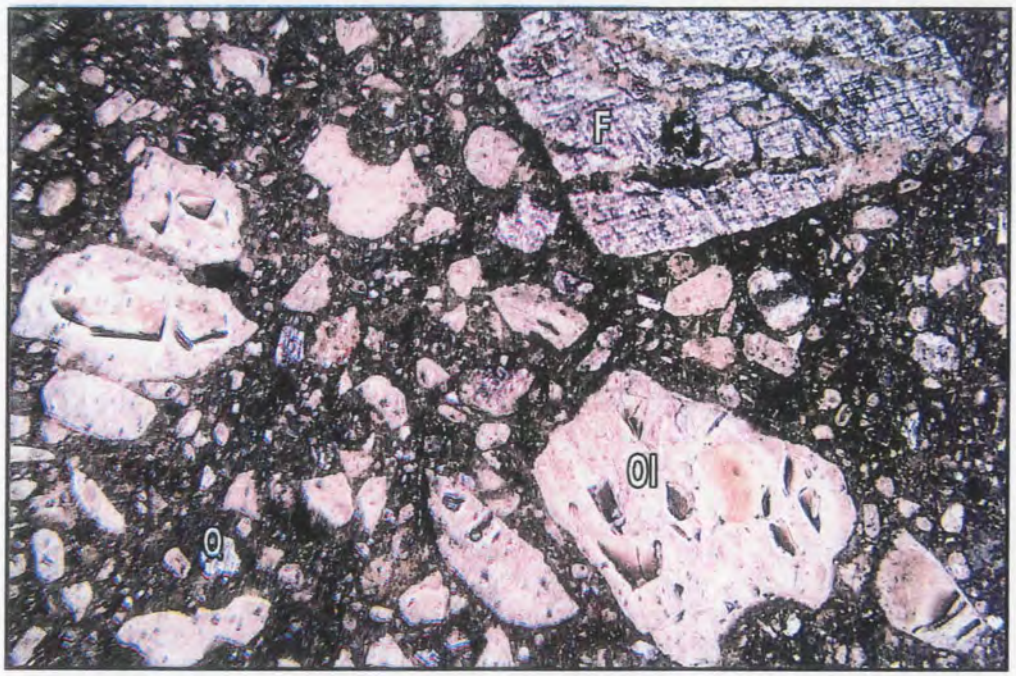

Figure 51: Photomicrograph showing the characteristic texture and composition of the finer-grained beds of the bedded QRVK juvenile/quartz facies (sample DD88/28). Note the abundant altered olivine (Ol) fragments and minor, scattered quartz (Q) and feldpsar (F) grains. PPL. FOV = 5.2mm.

2.3. Summary

The material which forms the infill of the South Lobe exhibits the following features:

- The material is extremely homogenous on a megascopic scale, but exhibits considerable variation on a small-scale, particularly in terms of grain size, texture and internal structure. No marker horizons or readily mapable units are present. Two principal lithofacies have been identified: the RVK and QRVK facies.
- The RVK facies occupies the bulk of the pipe, whereas the QRVK facies is restricted to a narrow discontinuous marginal zone.
- The RVK facies is rich in juvenile components, with a low to moderate country rock xenolith content and contains little or no quartz/feldspar. In contrast, the QRVK facies is characterised by a comparatively low juvenile content and the xenolithic content (including abundant quartz and feldspar) is high.
- Both the RVK and QRVK facies are characterised by a fragmental, inequigranular texture, resulting from the presence of subangular to angular, and lesser subrounded, coarser-grained juvenile and lithic components which are set in a very fine grained inter-clast matrix composed predominantly of clay minerals and lesser serpentine.
- The various country rock xenolith types are uniformly distributed in both facies.
- Massive deposits dominate over bedded deposits in both the RVK and QRVK facies.
- The massive deposits have a chaotic appearance and in places contain slickenside-bound rotated blocks of massive RVK or QRVK.
- The bedding in the bedded RVK and QRVK facies is always laterally discontinuous and displays steep dips, generally greater than 60°. The dip directions of the bedding are variable.
- The nature of the bedding in both facies is similar, being defined by coarser-grained lithic-rich beds which alternate with finer-grained lithic-poor beds. Narrow fine-grained mud-rich beds occur in rare cases. The bedded facies include thinly to very thickly bedded deposits. Evidence for slumping or deformation of individual beds is rare or absent.
- The ubiquitous quartz and lesser feldspar in the QRVK facies occurs as fine silt to very coarse sand-sized, subangular to angular strained grains and grain fragments.
- The QRVKj/q facies occurs in the contact zone between the RVK and QRVKq facies, and contains a low proportion of quartz and feldspar compared to the QRVKq facies.

- The magma clast population of each facies includes mainly rounded and subrounded types and lesser, but significant proportions of irregular and subangular types. Two mineralogical types were recognised, namely monticellite and monticellite-calcite kimberlite magma clasts. The granularity of the magmaclastic material resembles typical hypabyssal facies kimberlite. No microlitic diopside was identified.
- Autoliths of VK occur in both facies, and are relatively common in some areas. They are texturally and compositionally similar to the host facies.
- The QRVKq-S facies is a fine grained, mud-rich facies which occurs as irregular inclusions up to 2m in size within the massive RVK and QRVK facies, and displays soft sediment deformation structures.
- Both the RVK and QRVK facies contain rare juvenile and lithic clasts which are mantled by very fine grained clastic rims composed of clay minerals and very finely comminuted juvenile and lithic fragments. These armoured clasts, as well as rare accretionary lapilli, appear to be most common in the fine grained QRVKq-S facies.

Table 6: Summary of the characteristic features and modal proportions of the lithofacies of the Jwaneng South Lobe.

Facies	Facies Code	Subfacies (MGS)	Grain-matrix relationship	Sorting (macro-scale)	Juvenile Vol %	CRX Vol %	Qtz/Fspar Vol %	Xenocryst types & Vol %	CRX lithologies	ICM composition	Colour	Accretionary/ armoured lapilli	Interpretation
RVK FACIES													
Massive RVK	RVK-M	RVK-M*f* RVK-M*f*/m RVK-Mm RVK-Mc	Clast supp. dominant	poor	OL 40 - 52 MC 10 - 20	10 - 25	-	GAR, ILM, CPX, SPI, PHL, RUT 5 %	SH, WA, DOL, CH, DT, QTZ, SST, GRN, BSC, MUD	clays & serpentine	medium grenish-grey	Yes, rare	Debris flow
Shale-rich breccia	RVK-M_{srb}	RVK-Mc_{srb}	Clast supp.	poor	OL 30 - 40 MC 15 - 20	35 - 45	-	GAR, ILM, CPX, SPI, PHL, RUT 5 %	SH, WA, DOL, DT	clays & serpentine	medium greenish-grey	No	Rockfall-avalanche
Vaguely bedded RVK	RVK-B_v	RVK-B_v*f*/m RVK-B_vm RVK-B_vc	Clast supp. dominant	poor	OL 40 - 52 MC 10 - 20	10 - 25	-	GAR, ILM, CPX, SPI, PHL, RUT 5 %	SH, WA, DOL, CH, DT, QTZ, SST, GRN, BSC, MUD	clays & serpentine	medium greenish-grey	No	Hyperconcentrated flow
Distinctly bedded RVK	RVK-B_d	RVK-B_df RVK-B_d*f*/m RVK-B_dm RVK-B_dc	CGB & FGB Clast supp.	CGB well FGB well	CGB & FGB: OL 40 - 50 MC 10 - 20	CGB: 30 - 40 FGB: 10 - 20	-	CGB & FGB: GAR, ILM, CPX, AMP, BIO, MAG 5 %	CGB & FGB: SH, WA, DOL, MUD, DT, CH, QTZ, GRN	clays & serpentine	medium greenish-grey	No	Grain flow
QRVK FACIES													
Massive QRVK quartz	QRVKq-M	QRVKq-M*f*/m QRVKq-Mm QRVKq-Mc	Matrix supp. dominant	poor to well	OL 10 - 30 MC 5 - 10	10 - 15 20 max	20 - 40	GAR, ILM, CPX, SPI, PHL, RUT, AMP, MUSC 3 %	SH, WA, DOL, CH, MUD, DT, SST, QTZ, GRN, BSC, CL	clays & serpentine	pale-med greenish-grey to red-brown patchy	Yes, rare	Debris flow
Bedded QRVK quartz	QRVKq-B	QRVKq-B*f*/m QRVKq-Bm	CGB clast supp. FGB matrix supp.	CGB well FGB poor to well	CGB: OL 20 - 25 MC 10 FGB: OL 20 MC 10	CGB: 30 FGB: 10	CGB: < 40 FGB: < 20	CGB & FGB: GAR, ILM, CPX 2 - 3 %	CGB & FGB: SH, WA, DOL, CH, MUD, DT, SST, QTZ, GRN, BSC, CL	clays & serpentine	med-dark greenish-grey to red-brown patchy	No	Grain flow
Slumped QRVK quartz	QRVKq-S	QRVKq-Sf	Matrix supp.	well	OL 20 - 25 MC < 10	10 - 15	10 - 25	GAR, ILM, CPX, SPI, AMP, BIO, MUSC, MAG 5 %	SH, WA, MUD, DOL, SST, DT, GRN	clays dominant	dark grey-green or grey-brown	Yes, rare	Disrupted crater lake sediments – suspension settling
Massive QRVK juvenile/quartz	QRVKj/q-M	QRVKj/q-M*f*/m QRVKj/q-Mm	Clast supp. dominant	poor to well	OL 25 - 45 MC 10 - 15	< 20	< 10	GAR, ILM, CPX, SPI, PHL, RUT, AMP, BIO 5 %	SH, WA, DOL, CH, DT, QTZ, SST, GRN, BSC, MUD	clays & serpentine	pale-med greenish-grey	Yes, rare	Debris flow
Bedded QRVK juvenile/quartz	QRVKj/q-B	QRVKj/q-B*f*/m QRVKj/q-Bm	CGB & FGB Clast supp.	CGB well FGB poor to well	CGB & FGB OL 35 - 45 MC 15 - 20	CGB: 35 - 45 FGB: 10 - 20	CGB: < 10 FGB: < 10	CGB & FGB: GAR, ILM, CPX 5 %	CGB & FGB: SH, WA, DOL, CH, DT, QTZ, SST, GRN, BSC, MUD	clays & serpentine	pale-med greenish-grey	No	Grain flow

CGB = coarser-grained bed, FGB = finer-grained bed; GNT = garnet, ILM = ilmenite, CPX = clinopyroxnene, SPI = spinel, PHL = phlogopite, RUT = rutile, AMP = amphibole, BIO = biotite, MAG = magnetite; SH = shale, WA = wacke, DOL = dolomite, CH = chert, DT =dolerite, QTZ = quartzite, SST = sandstone, MUD = mudstone, GRN = granite, BSC = biotite schist, CL = coal.

3. CLAST ANALYSES

3.1. Maximum clast size analysis

The maximum sizes of olivine (OL), magma clasts (MC) and country rock xenoliths (CRX) have been measured in all the samples collected from drillcores DD15, DD68 and DD88 (Figures 52, 53 and 54). Refer also to Table A2. The sample suite is assumed to be representative of the range of lithofacies and the grain sizes present in each.

The range and mean of the coarsest fraction in the grain size spectrum of juvenile and lithic clasts of all the lithofacies is indicated in Table 7 below. These values have been calculated from the maximum sizes of clasts in samples representative of both the RVK and QRVK facies.

Table 7: The range and mean of the coarsest fraction in the grain size spectrum of juvenile and lithic clasts.

Clast type	Range of coarsest fraction	Mean of coarsest fraction
Olivine	2 – 14 mm	6 mm
Magma clasts	2 – 44 mm	9 mm
Country rock xenoliths	5 – 122 mm	21 mm

The variation in the maximum size of both the juvenile and lithic clasts is relatively constant in the sample suite from each borehole. Samples from DD68 (Figure 53) display the least variation in maximum clast size. In each sample suite, the country rock xenoliths display the greatest variation in maximum size, whereas the maximum sizes of olivine and magma clasts are comparable in each sample suite and display a considerably smaller variation. Figure 55 (a) – (c) further illustrate this and also show that the maximum size of the clasts in the coarsest fraction of each component is greatest in samples from DD88.

Figures 56 and 57 compare the maximum juvenile and lithic clast sizes in samples of the RVK facies with those of the QRVK facies in drillcores DD15 and DD88. The plots indicate that the maximum size of the clasts in the coarsest fraction of juvenile and lithic components is greater in the RVK facies than in the QRVK facies, i.e. the QRVK facies displays an overall finer grain size compared to the RVK facies.

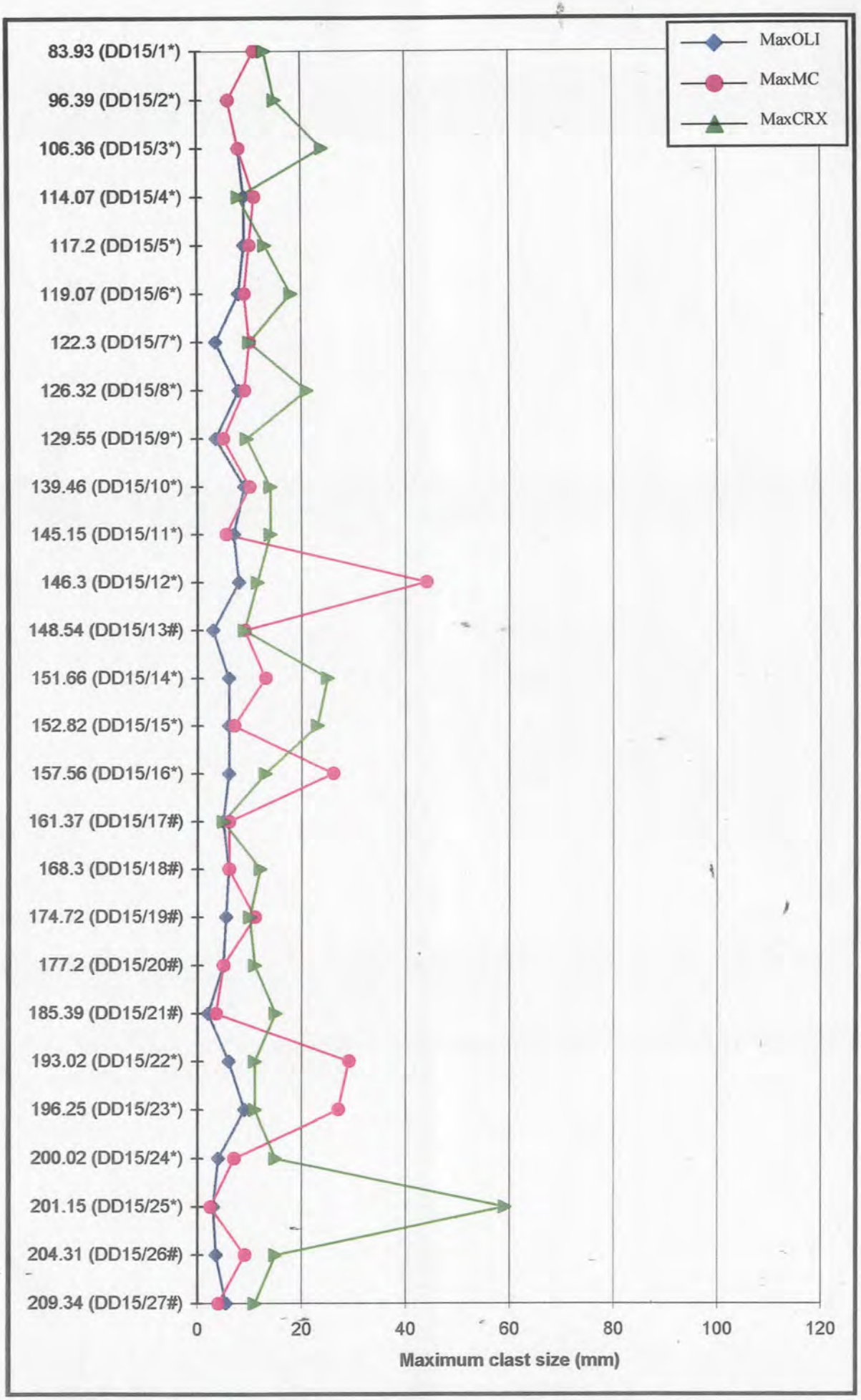

Figure 52: Maximum sizes of olivine (OL), magma clasts (MC) and country rock xenoliths (CRX) for samples from drillhole DD15. Depths in meters. Symbols appending the sample numbers denote the lithofacies of the samples as follows: * = RVK facies, # = QRVK facies.

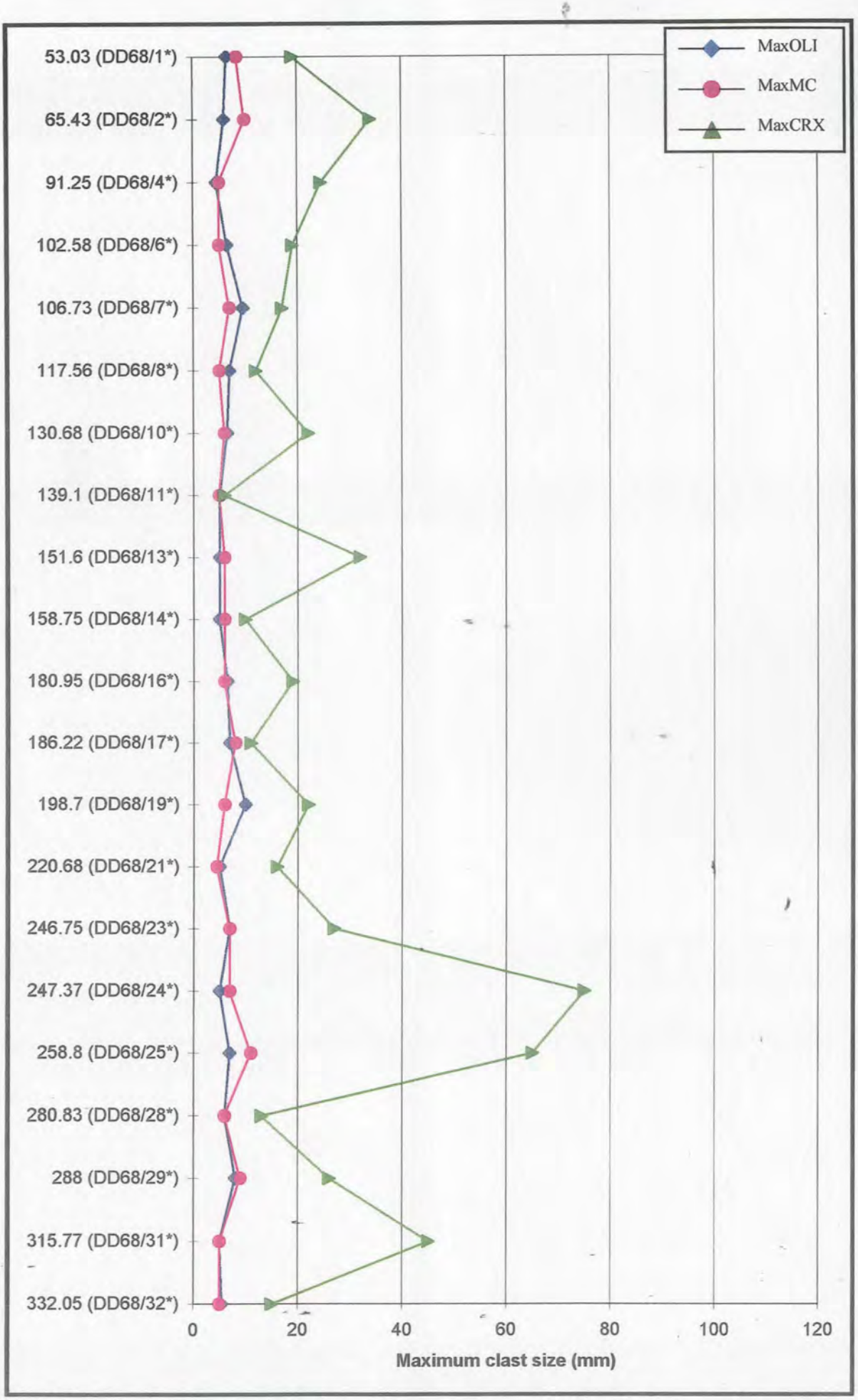

Figure 53: Maximum sizes of olivine (OL), magma clasts (MC) and country rock xenoliths (CRX) for samples from drillhole DD68. Depths in meters. Symbols appending the sample numbers denote the lithofacies of the samples as follows: * = RVK facies, #.= QRVK facies.

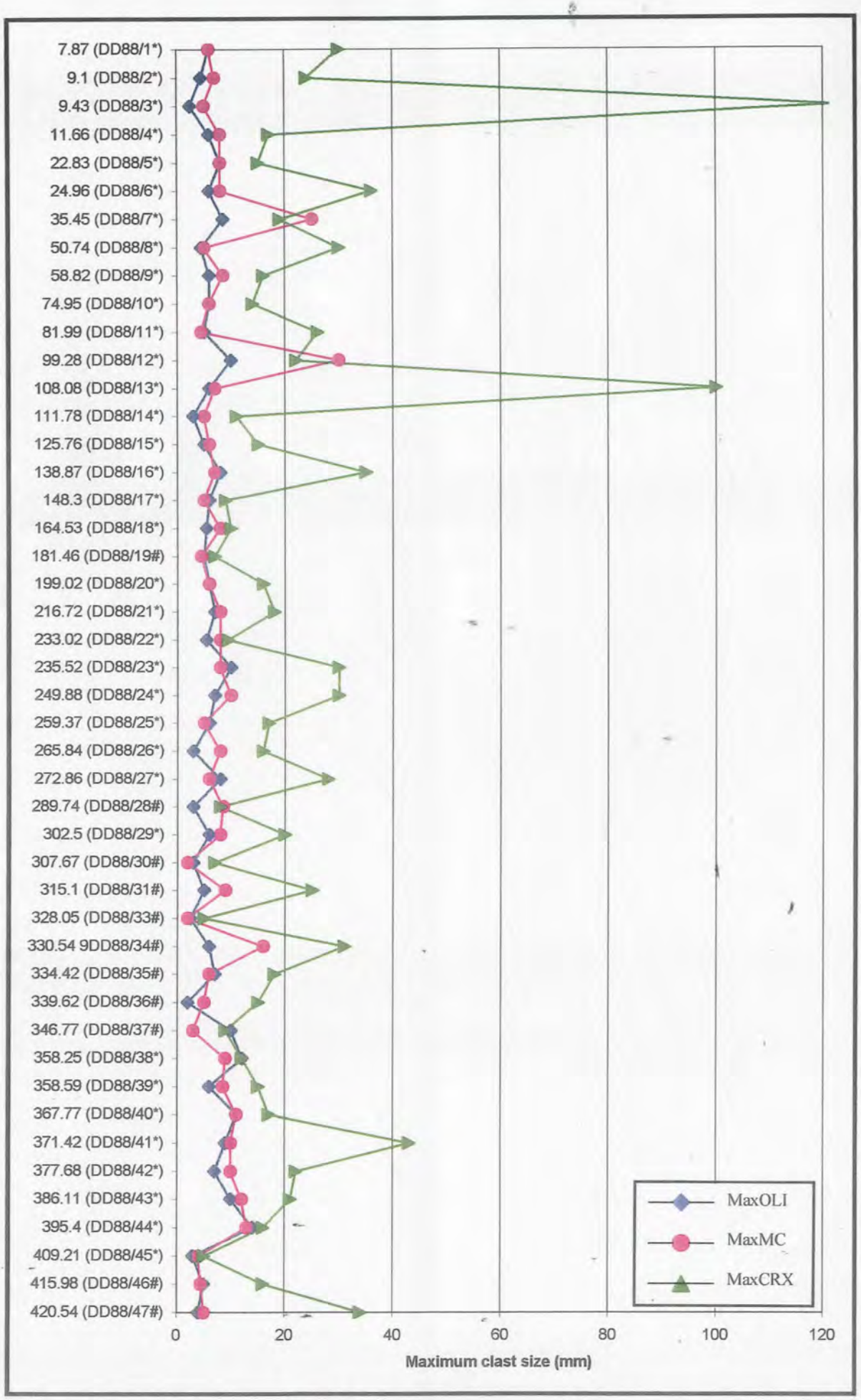

Figure 54: Maximum sizes of olivine (OL), magma clasts (MC) and country rock xenoliths (CRX) for samples from drillhole DD88. Depths in meters. Symbols appending the sample numbers denote the lithofacies of the samples as follows: * = RVK facies, # = QRVK facies.

Figure 55 (a) – (c): Histograms showing the variation in maximum size of the coarsest fraction of juvenile and lithic components in the samples from (a) DD15, (b) DD68 and (c) DD88.

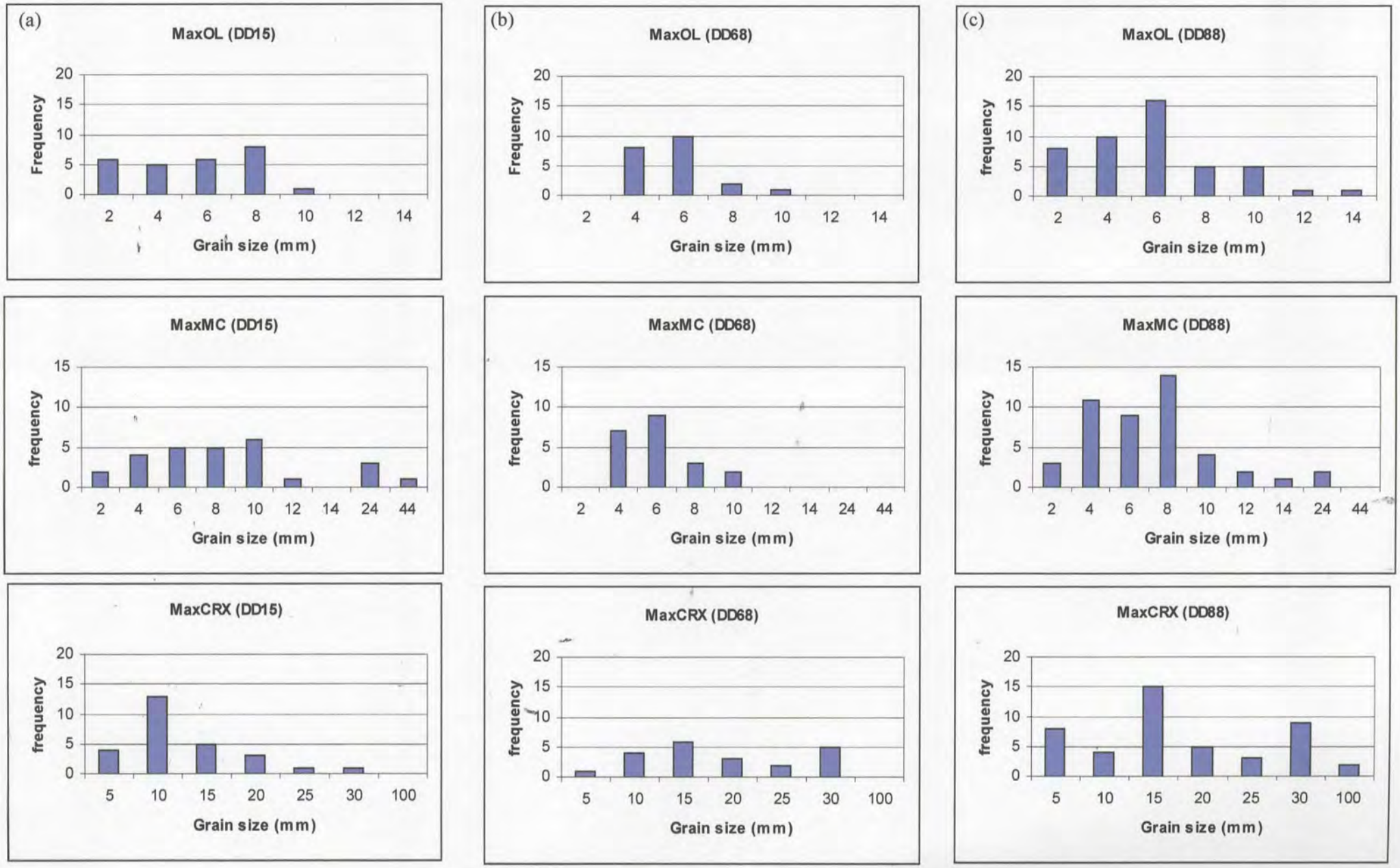

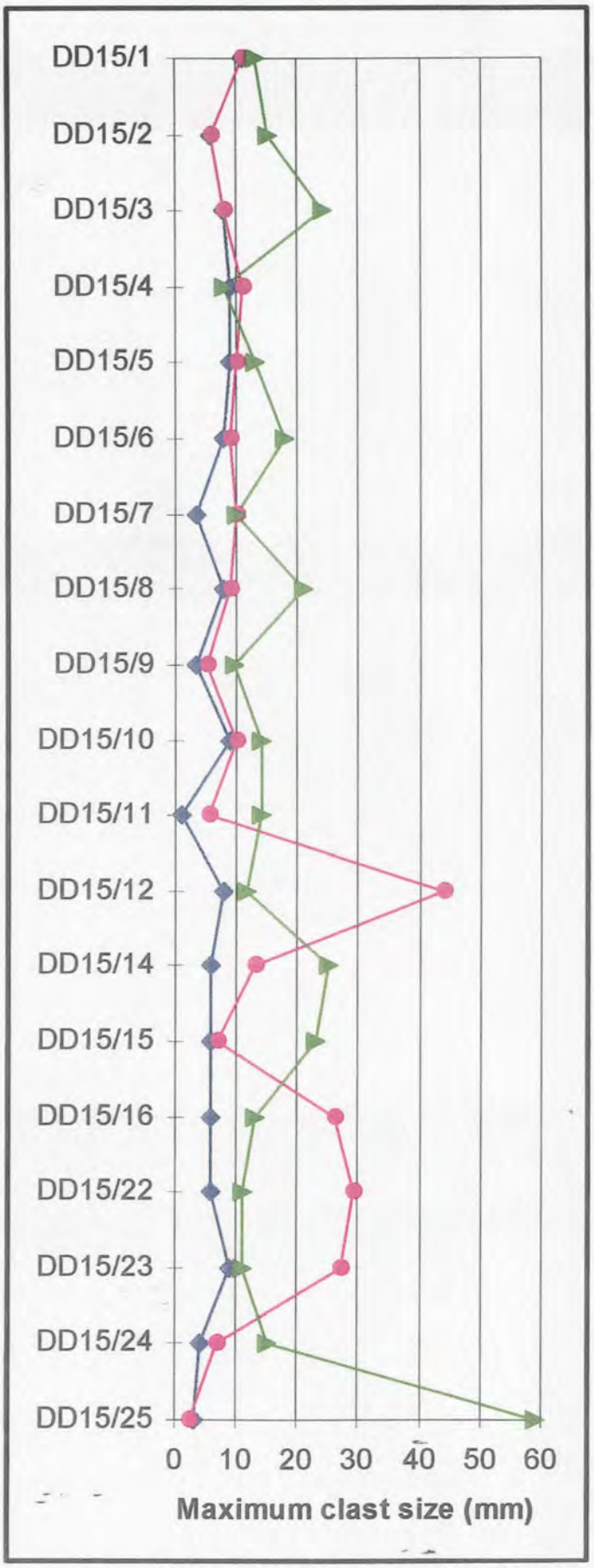

Figure 56 (a) and (b): Maximum sizes of olivine (OL), magma clasts (MC) and country rock xenoliths (CRX) for samples of the (a) RVK facies and (b) QRVK facies from drillhole DD15. Refer to Figure # for sample depths.

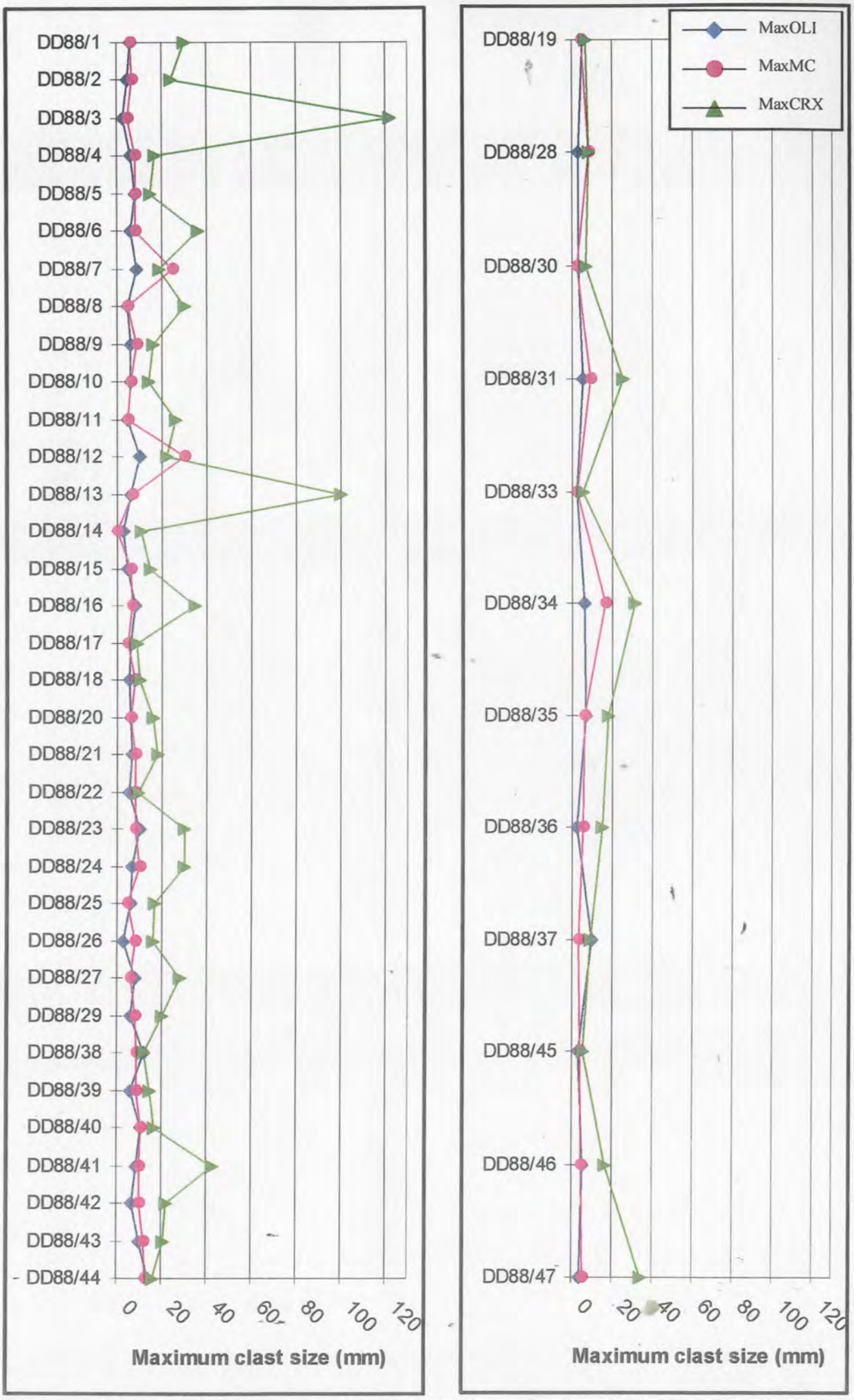

Figure 57 (a) and (b): Maximum sizes of olivine (OL), magma clasts (MC) and country rock xenoliths (CRX) for samples of the (a) RVK facies and (b) QRVK facies from drillhole DD88. Refer to Figure # for sample depths.

2.2. **Modal Analysis**

Modal analysis by pointcounting has been conducted on a suite of 12 representative drillcore samples. The suite includes samples of both the RVK facies and the QRVK facies. The constituents counted include olivine (OL), other xenocrysts (Xc), juvenile magmaclastic material (MC-x), country rock xenoliths (CRX), inter-clast matrix (ICM) and, where applicable, quartz and feldspar (Qtz/Fspar), which were counted together. The results are presented in Table 8. These data are averages of the modal abundances obtained by micro- and macro-pointcounting procedures. Both procedures were employed in this study in order to assess the relative accuracy of each method in its application to volcaniclastic rocks. The results of modal analysis by the macro-pointcounting and micro-pointcounting methods are compared in Figures 58 - 60, and indicate that:

(i) the degree of repeatability of the data within each sample is high for both the macro- and micro-pointcounting methods (refer to Table A3);

(ii) a good correlation exists between the modal analyses by macro- and micro-pointcounting methods for most of the samples;

(iii) modal analysis by the macro-pointcounting method is not recommended on the fine grained QRVK facies rocks, since the diagnostic fine grained quartz and feldspar in these rocks cannot be observed.

Table 8: Results of modal analysis for the sample suite.

Sample number	Lithofacies code	OL	Xc	MC-x	CRX	ICM	Qtz/ Fspar
DD15/5	RVK-Mm	52.9	1.9	18.2	14.9	12.1	-
DD15/14	RVK-Mm	47.8	3.1	16.9	18.2	14	-
DD15/17	QRVKq-B*f*m	18.1	2.3	9.3	12.5	39	18.6
DD15/27	QRVKq-Mm	12.3	2.8	4.7	10.1	29.5	40.6
DD68/11	RVK-M*f*m	45.5	2.6	14.5	14.4	23	-
DD68/16	RVK-Mc	46.8	3.7	12.6	20.4	16.5	-
DD68/21	RVK-Mm	49.4	3	11.8	10.6	25.2	-
DD68/25	RVK-Mc	46.8	3.8	12	25.5	11.9	-
DD88/9	RVK-Mm	47.1	3.5	12.8	22.9	13.7	-
DD88/19	QRVKq-Sf	22.6	3.7	10	14.6	43	12.2
DD88/28	QRVKj/q-B*f*m	45.4	4.2	15.6	16.4	15.4	6
DD88/41	RVK-Mc	46.5	4.1	18.2	17.9	13.3	

The results of the modal analysis reveal the following:

(i) olivine varies from 45 - 53 % in the RVK facies, and is therefore considerably more abundant than in the QRVKq facies (< 23 %), but has similar abundances in the QRVKj/q facies (~ 45 %).

(ii) magmaclastic material is more abundant in the RVK facies (12 – 18 %) than in the QRVKq facies (< 10 %), but has similar abundances in the QRVKj/q facies (~ 15 %)

(iii) the modal abundance of the juvenile component (olivine and magma clasts) in the RVK facies is considerably higher (up to 70 %) than in the QRVKq facies (maximum 33 %), and is similar to that in the QRVKj/q facies (~ 60 %)

(iv) country rock xenolithic material (excluding quartz and feldspar in the case of the QRVK facies) varies from 10 - 25 % in the RVK facies, and from 10 - 16 % in the QRVK facies

(v) quartz and feldspar varies from 12 - 40 % in the QRVKq facies and is < 10 % in the QRVKj/q facies

(vi) the modal abundance of both country rock xenoliths and quartz/feldspar in the QRVKq facies is high (up to 55 %)

(vii) mantle- and crustal-derived xenocrysts constitute between 2 and 4 % of both the RVK facies and QRVK facies

(viii) the inter-clast matrix comprises 12 - 25 % of the RVK facies and 15 - 43 % of the QRVK facies. The inter-clast matrix is more abundant in the QRVKq facies (particularly the QRVKq-S facies) compared to the QRVKj/q facies.

The quantitative estimates of the abundances of the main constituents of the various lithofacies have been used to refine, and where necessary adjust, the visual estimations of juvenile and lithic component modal proportions made during logging of the three drillcores. The results of this procedure are presented in Tables A4, A5 and A6, and on the graphic logs of the drillcores (Appendix I). Figure 61 (a) – (c) indicates the modal abundances (both quantitative estimations and adjusted visual estimates) of olivine and country rock xenoliths for the complete sample suite derived from each of the three drillcores. These plots provide an indication of the variation in olivine and country rock xenolith modal abundances of the various lithofacies with depth in each drillhole.

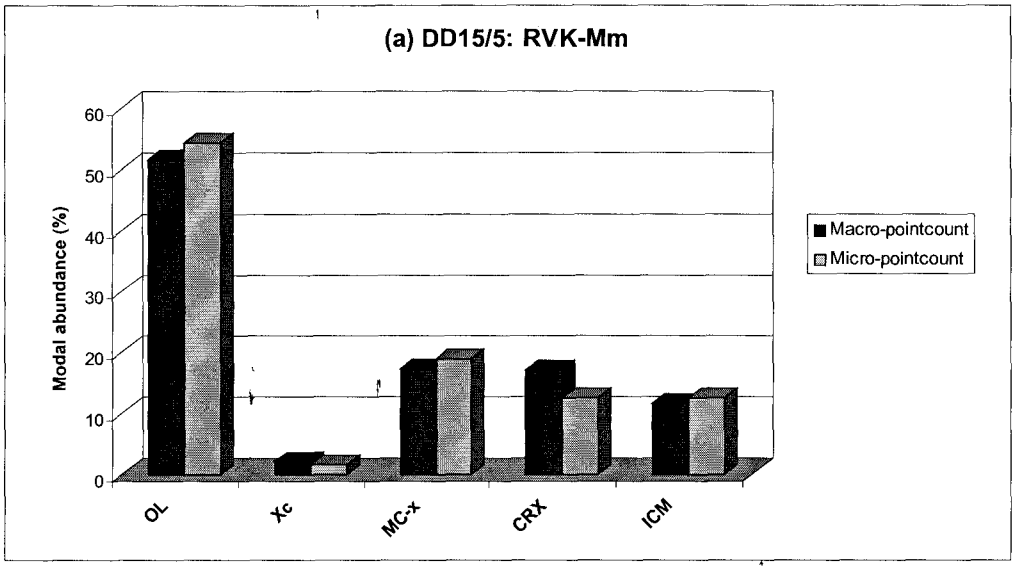

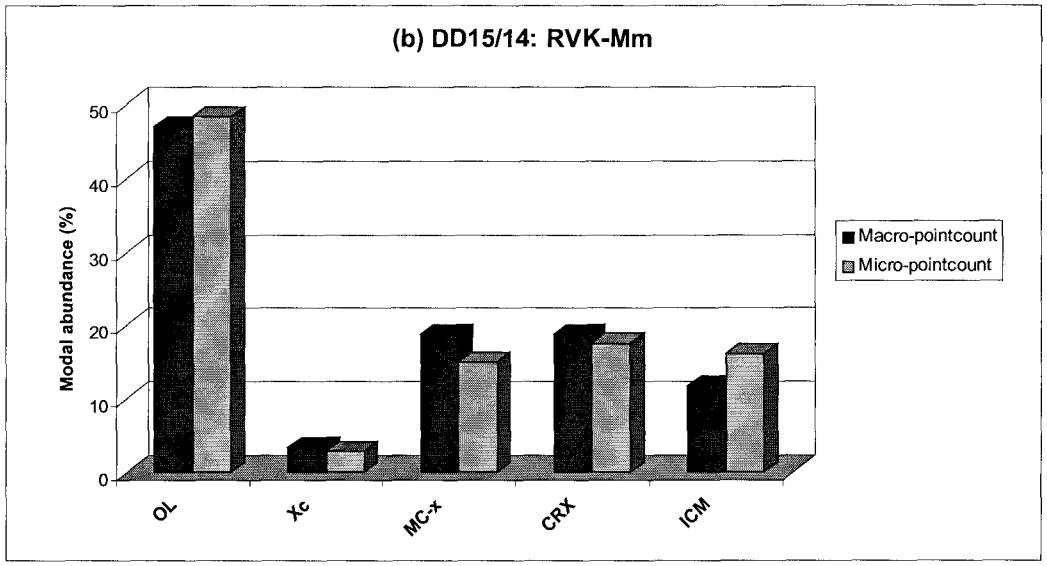

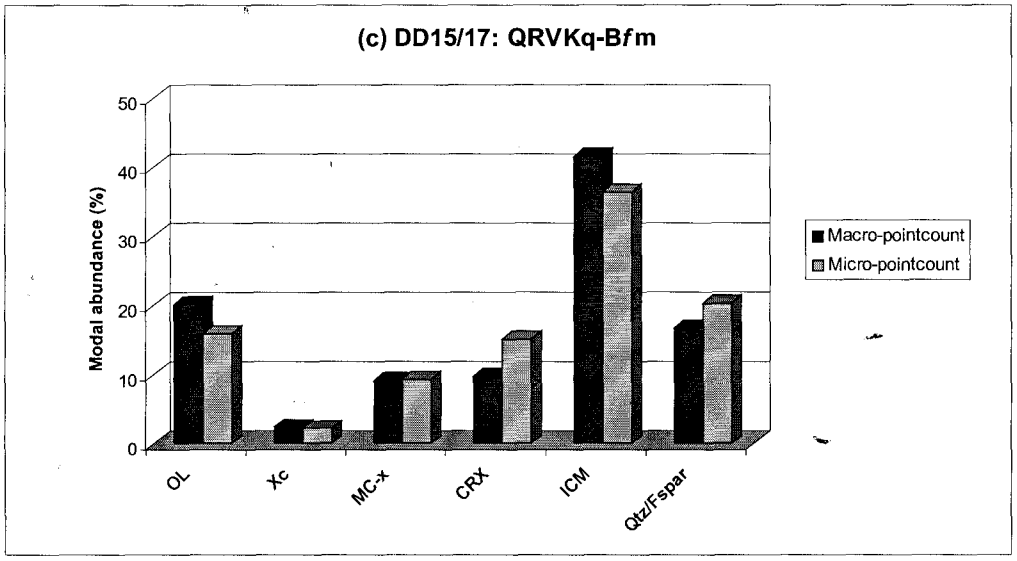

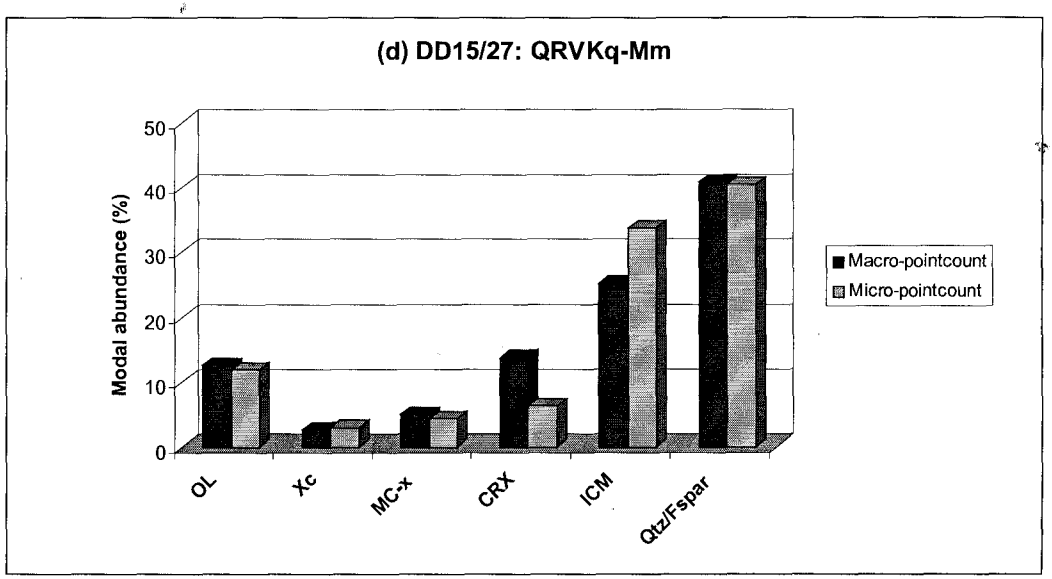

Figure 58 (a) – (d): comparison of results of modal analysis by macro- and micro-pointcounting methods for samples from drillhole DD15.

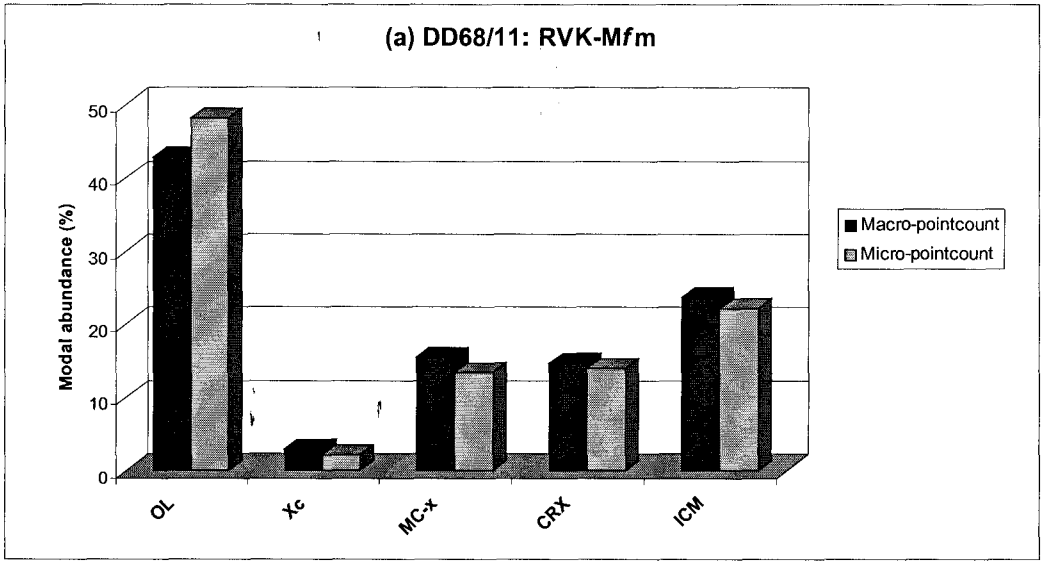

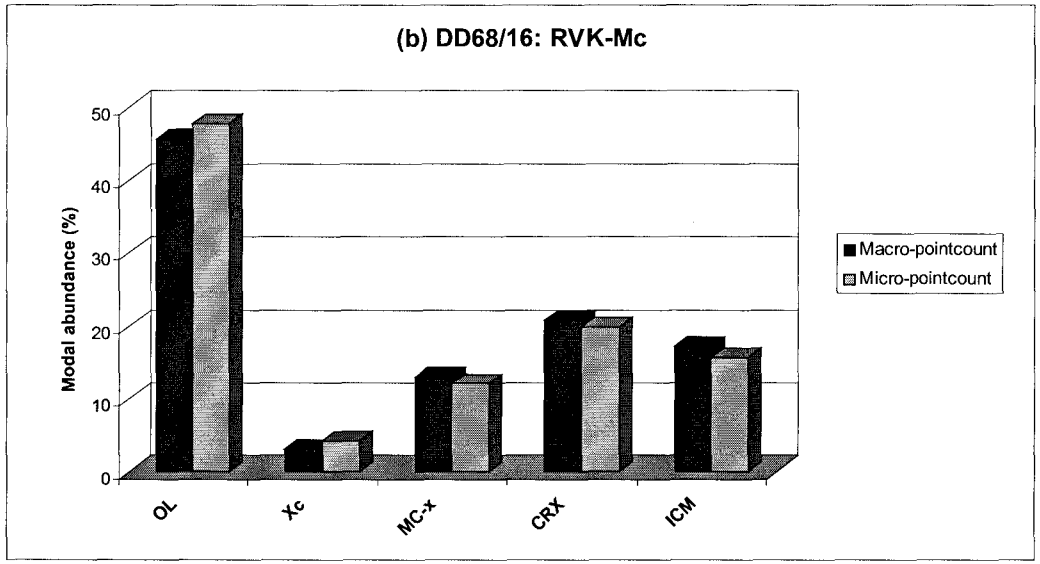

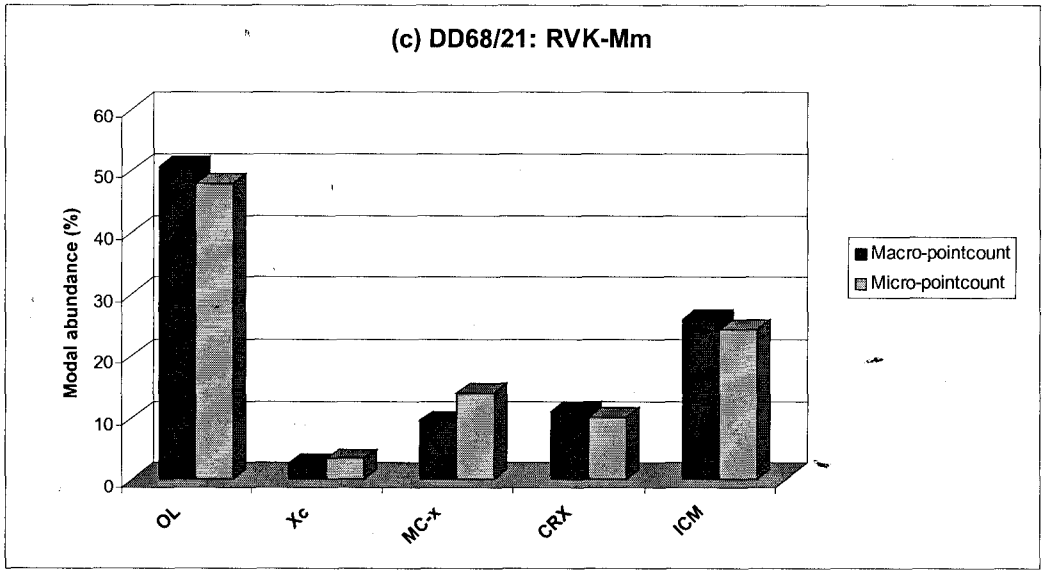

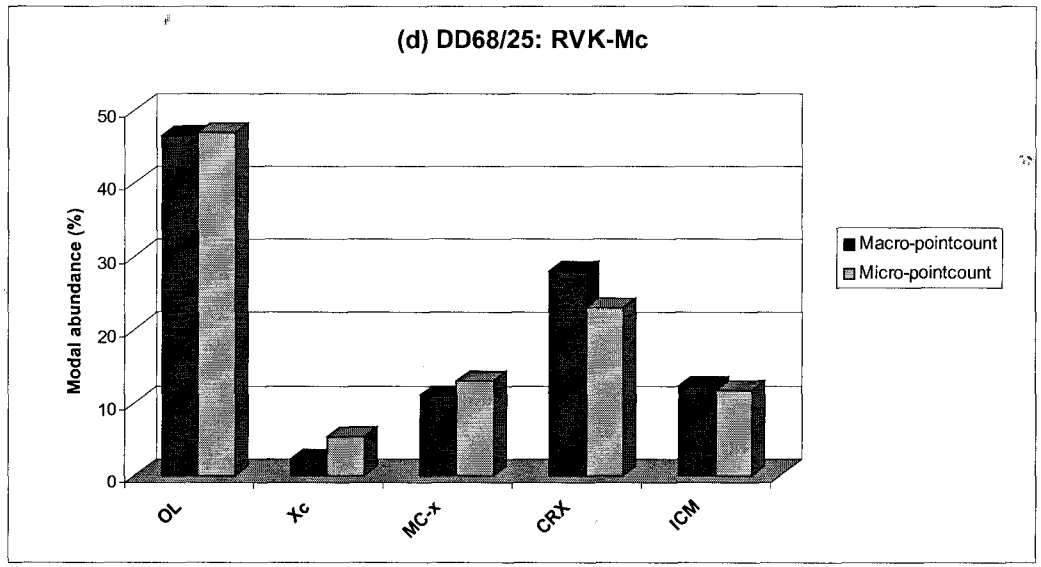

Figure 59 (a) – (d): comparison of results of modal analysis by macro- and micro-pointcounting methods for samples from drillhole DD68.

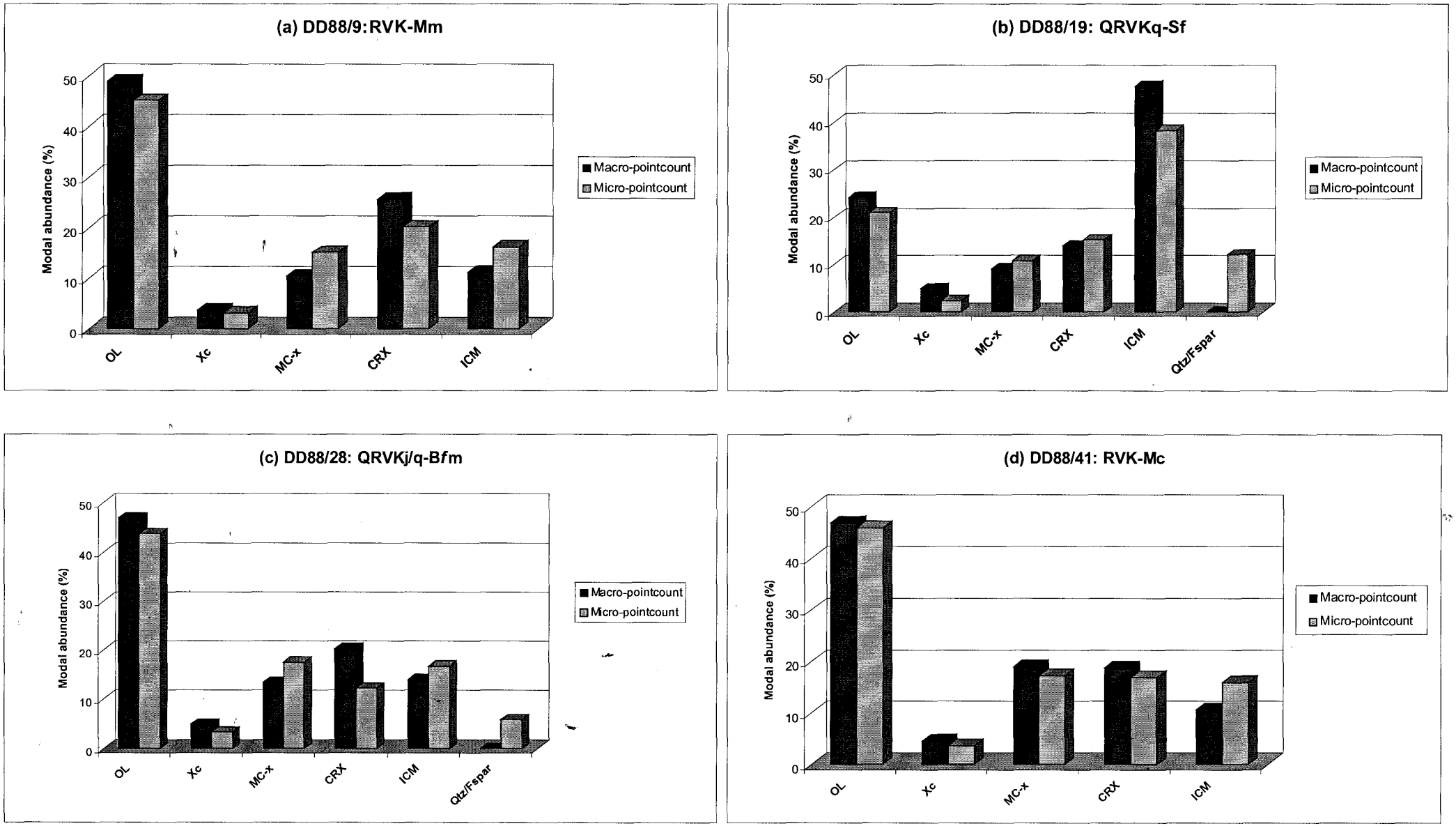

Figure 60 (a) – (d): comparison of results of modal analysis by macro- and micro-pointcounting methods for samples from drillhole DD88.

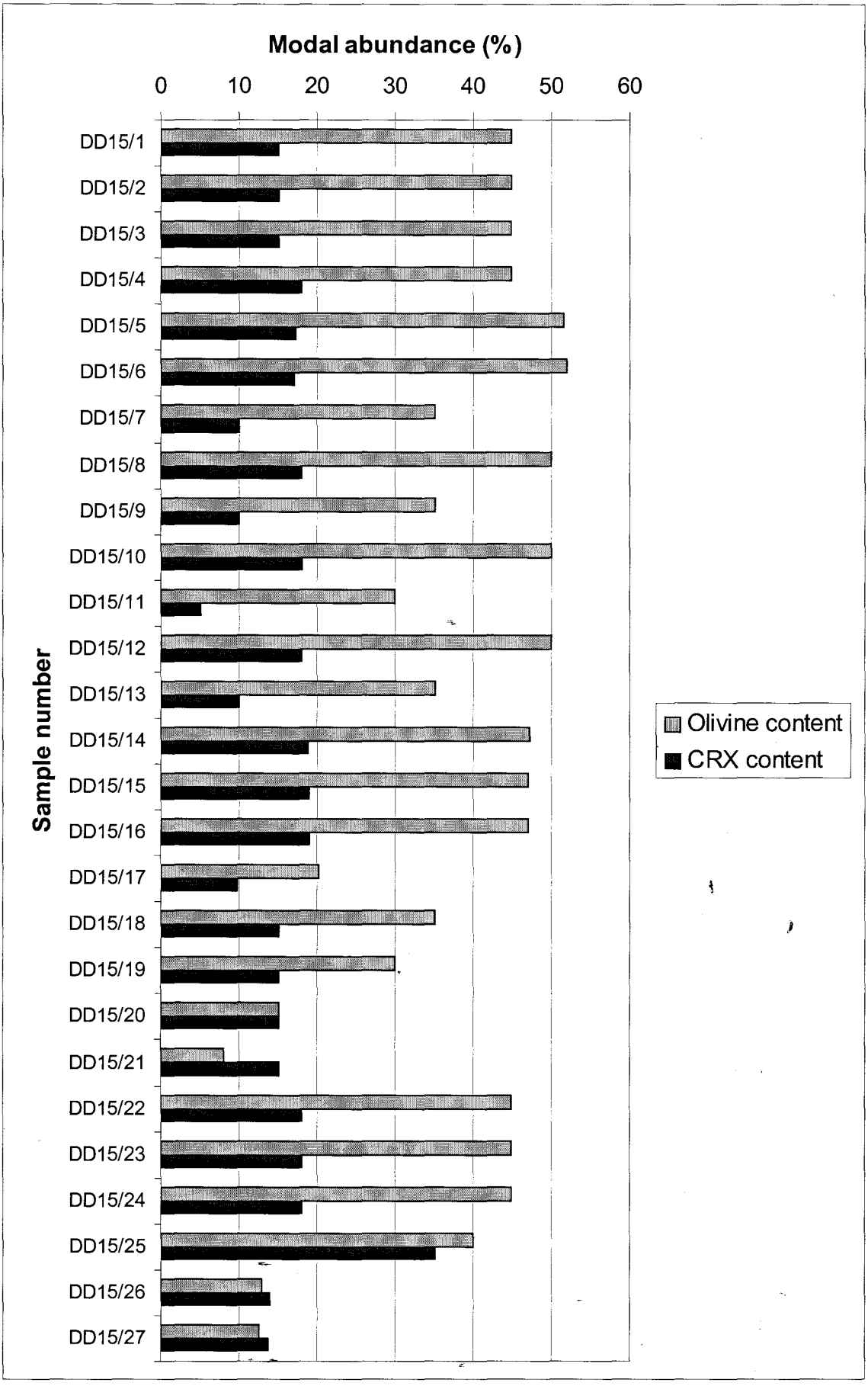

Figure 61 (a): the modal abundances of olivine and country rock xenoliths of the sample suite from drillhole DD15.

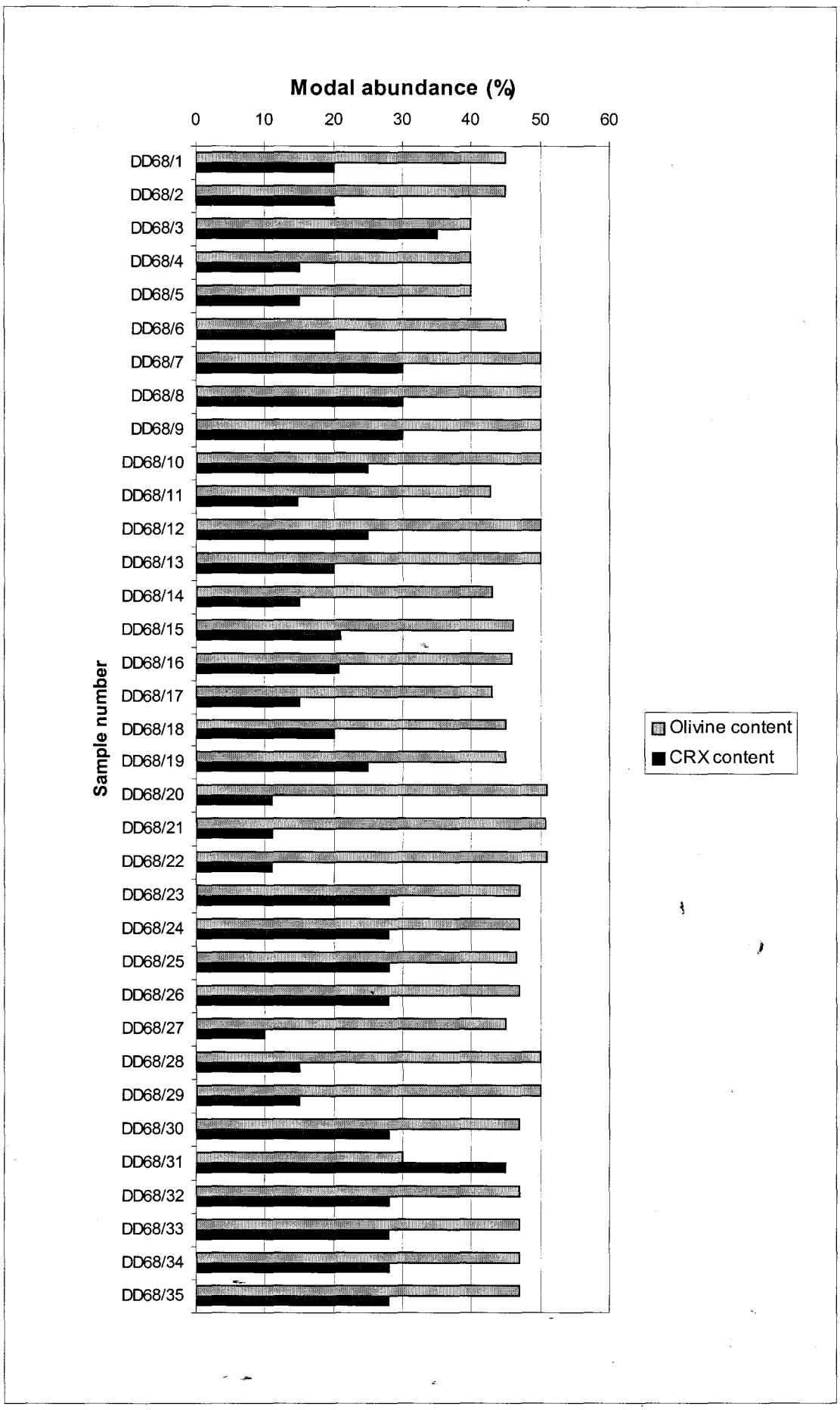

Figure 61 (b): the modal abundances of olivine and country rock xenoliths of the sample suite from drillhole DD68.

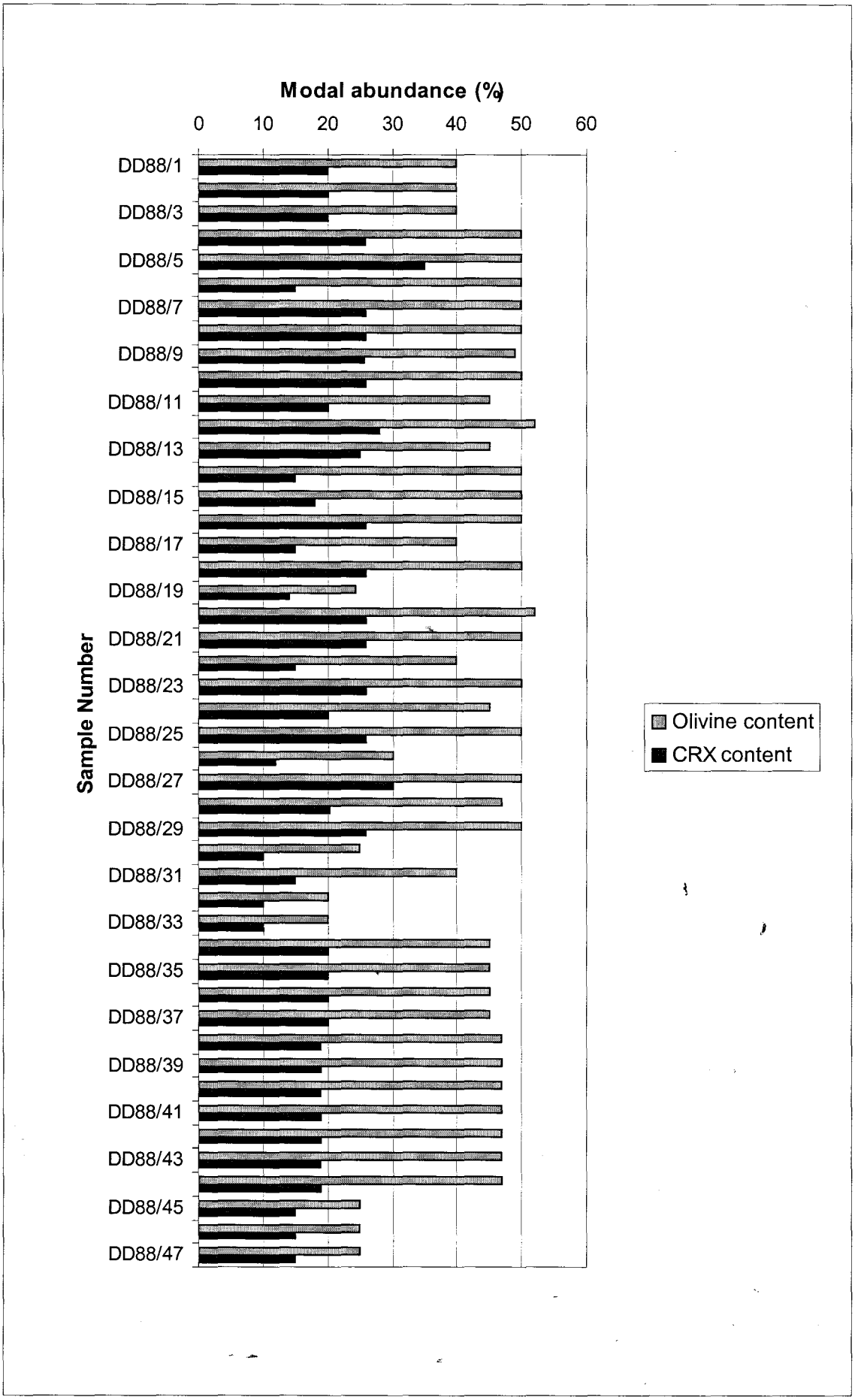

Figure 61 (c): the modal abundances of olivine and country rock xenoliths of the sample suite from drillhole DD88.

2.2. Magma clast shape analysis

The magma clast shape classification scheme used in this study was developed specifically for the analysis of the Jwaneng volcaniclastic rocks. The scheme is primarily concerned with the angularity or roundness of the magma clasts. A standard set of grain silhouettes has been devised to estimate the differing degrees of roundness (Figure 4). The classification scheme was applied to thin sections of the same suite of samples that was used for the modal analysis (Table 5), and a total of 20 magma clasts in each sample were categorised (refer to Chapter II, Section 8).

Figure 62 presents the results of the shape analysis (refer also to Table A7) and shows that the magma clast population is dominated by rounded and subrounded types (34.6 % and 33.3 % respectively), with lesser but significant proportions of irregular (20.8 %) and subangular (11.3 %) varieties. No angular magma clasts were recorded during the analysis, although rare examples were observed during macroscopic examination of the polished core samples. A comparison of the magma clast populations of samples of the RVK facies and QRVK facies indicates that the relative proportions of the various magma clast shapes in each lithofacies is similar (Figure 63).

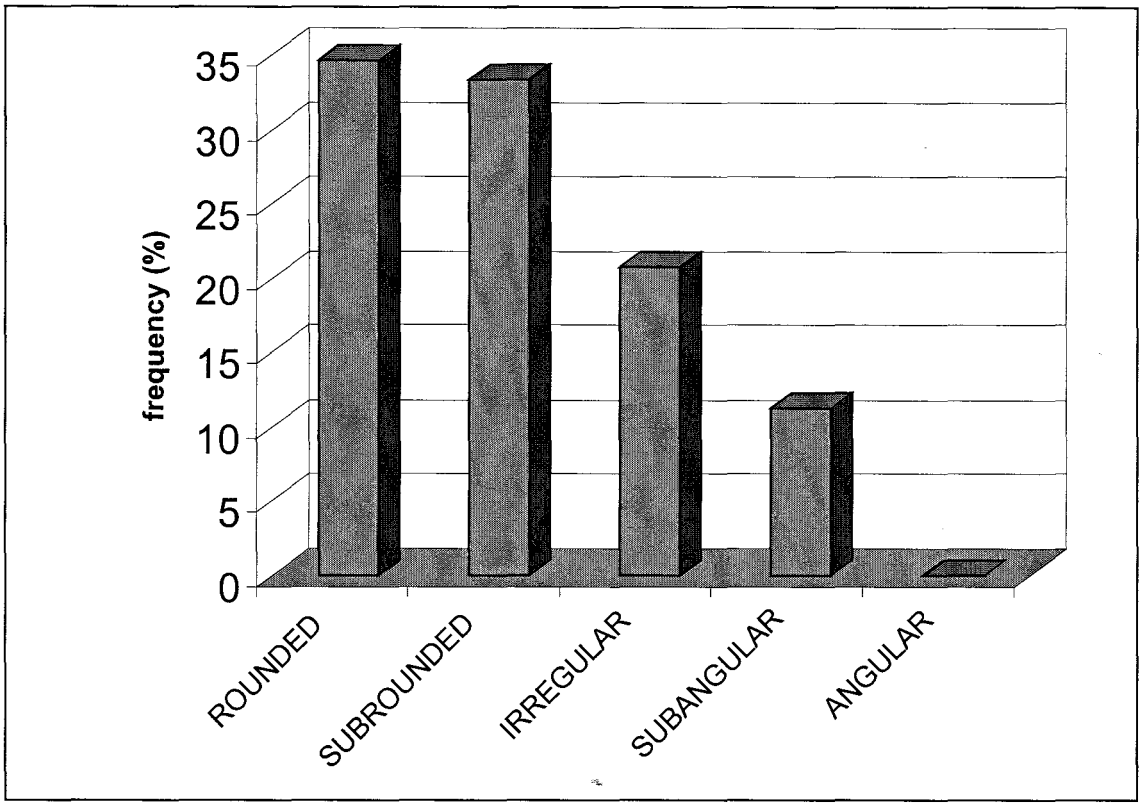

Figure 62: The magma clast shape variation of the sample suite.

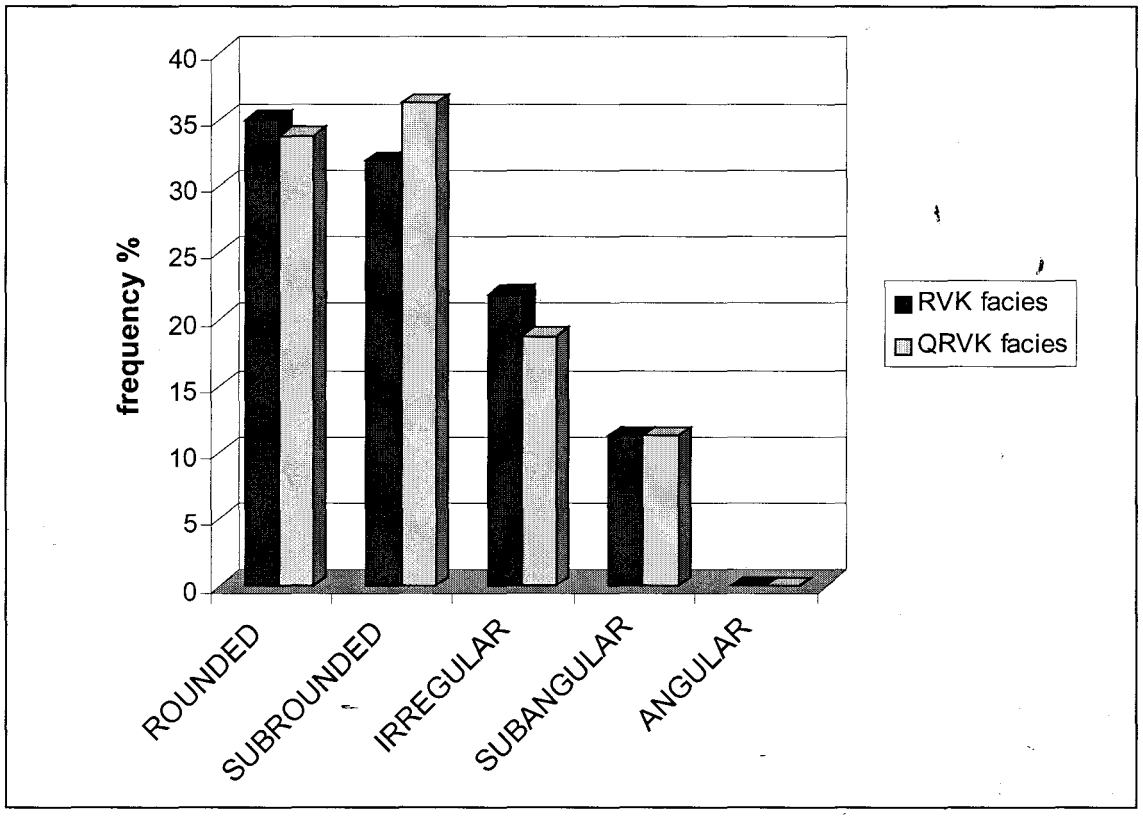

Figure 63: The magma clast shape variation of samples of RVK facies and QRVK facies within the sample suite.

4. GEOCHEMICAL ANALYSIS

4.1. Introduction

To the best of the author's knowledge, no Jwaneng volcaniclastic rocks have been analysed to date. Nine samples (Table 9) comprising various lithologies were collected from the three Lobes for whole-rock geochemical analysis. Three of the samples (JS-KM1, JC-KM2 and JN-KM3) consist of fine grained muddy RVK, two of which are quartz-bearing. These fine grained kimberlitic sediments occur as large (up to 1.5 m) irregular inclusions or 'clots' within the coarser-grained massive host RVK and belong to the slumped RVK/QRVKq facies (Section 2.3.1.3).

Table 9: Details of the samples selected for whole rock geochemical analysis.

Sample Name	Location	Lithology/Facies
JS-KM1	South Lobe	fine grained QRVKq-S facies
JC-KM2	Centre Lobe	fine grained QRVKq-S facies
JN-KM3	North Lobe	fine grained RVK-S facies
JC-GM	Centre Lobe	green mudstone from megablock
JC-GMB	Centre Lobe	brecciated green mudstone from megablock
JS-M	South Lobe	finely laminated mudstone xenolith
JN-FM	North Lobe	contorted purple-brown mudstone clast
JN-KBs	North Lobe	siltstone from megablock
JN-KBm	North Lobe	grey mudstone from megablock

The remaining six samples comprise mudstones or siltstones which either occur as discrete clasts within the RVK or are derived from certain of the megablocks which occur in the peripheral zones of the pipes. One of the unique features of the Jwaneng RVK in comparison to other volcaniclastic kimberlite deposits, is the abundance of mudstone clasts of various colours and textures. Many of the clasts display contorted shapes and soft sediment deformation structures, such as slumping and syn-sedimentary faulting, suggesting that they were poorly consolidated at the time of incorporation in the kimberlite. It is generally impossible to determine microscopically whether these muds are kimberlitic in origin or represent poorly consolidated Karoo sediments. Due to the uncertain origin of the megablocks (Section 5), it was also deemed pertinent to obtain geochemical data for a number of these. Thus, the principal aims of the geochemical

analyses were: (1) to determine the bulk and trace element composition of the fine grained RVK/QRVKq-S facies, and (2) to test for a kimberlitic geochemical signature in the various mudstone clasts and megablock lithologies.

The nine samples were crushed, ground in two stages (swing mill and automatic agate pestle and mortar) and analysed for major and trace elements using X-ray fluorescence procedures. Major elements (except Na) were determined on fused duplicate lithium tetraborate glass discs prepared in accordance with the method of Norrish & Hutton (1969). Trace elements and Na were determined on pressed powder pellets. The analyses were conducted on a Phillips PW 1480 X-ray spectrometer at Rhodes University. All analytical runs were calibrated using a variety of international and in-house standards. Corrections for dead time, background, spectral line interference, instrumental drift and mass absorption were made in all determinations. The results of the analyses are summarised in Tables A8 and A9.

4.2. **Bulk chemical composition**

The contamination index (C.I.) of Clement (1982) is used to evaluate the effects of crustal contamination and/or weathering of kimberlites:

$$C.I. = (SiO_2 + Al_2O_3 + Na_2O)/(MgO + 2K_2O)$$

Contamination by crustal rocks usually results in the addition of SiO_2, Al_2O_3 and Na_2O to kimberlites. Weathering to mixtures of chlorite, montmorillonite and serpentine will lead to increased SiO_2 and Al_2O_3, as Mg^{2+} and other soluble cations are removed. Either process will result in increased SiO_2 and Al_2O_3 relative to the pristine kimberlite (Mitchell, 1986). Contaminations indices close to unity are considered to indicate uncontaminated or fresh kimberlite. The C.I. for the three fine grained, mud-rich (Q)RVK samples (JS-KM1, JC-KM2 and JN-KM3) are 3.09, 2.15 and 2.16 (respectively), indicating relatively high levels of contamination and/or weathering. This is supported by modal analyses which indicate that these rocks may comprise up to 50 volume % crustal-derived material, including country rock xenoliths and individual quartz and feldspar fragments, as well as finely comminuted sub-microscopic crustal xenoliths and clays within the inter-clast matrix

(Section 2.3.1.3.). These data should thus be regarded with caution and not be considered as representative of the primitive Jwaneng kimberlite composition.

Kimberlite-normalised multi-element diagrams (Figures 64 and 65) have been used to compare and discriminate the (Q)RVK and various xenolith/megablock lithologies. The selected elements of interest include compatible (Cr, Ni) and incompatible elements (Rb, Ba, Sr, Zr, Nb, U, Th, Pb, P, K, Y) and REE (La, Ce, Nd), as well as Ti and MgO. These elements are commonly used in normalised multi-element diagrams for simple mafic igneous systems, and are arranged from left to right in order of increasing compatibility. Kable et al. (1975) demonstrated that certain elements, including Ti, Nb, Zr, P and the rare earths are insignificantly affected by crustal contamination of kimberlites. Incorporation of country rocks will either have a minor effect on overall concentrations of these elements or act as a dilutent, depending on the compositional contrast between kimberlite and country rock. Elements such as Nb, Rb, Ba, Sr, U and Th occur in significant amounts in kimberlites and are useful for kimberlite/non-kimberlite discrimination purposes.

The element abundances of the nine samples were normalised to values for hypabyssal kimberlite from the adjacent DK7 kimberlite, the composition of which is most likely to approximate that of the primitive Jwaneng kimberlite. The DK7 hypabyssal kimberlite is a serpentinised, macrocrystic opaque-mineral rich monticellite kimberlite and is uncontaminated, having a C.I. of 1.01 (Smith et al., 1985b). Its bulk composition approximates that of average on-craton Group I kimberlites, and is thus considered to be representative. Element distributions of NASC (North American Shale Composite) and the average compositions of the Timeball Hill Shale Formation of the Transvaal Supergroup (Wronkiewicz and Condie, 1990) and the Eendragtpan Formation (shale/mudstone) of the Beaufort Group of the Karoo Supergroup (Faure et al., 1996) have also been included in the multi-element diagrams for comparison with the various xenoliths/megablocks of uncertain origin.

Figure 64(a) indicates that the element abundance patterns of the NASC and the Transvaal Supergroup and Karoo Supergroup shales are similar, although the latter is enriched in Pb and depleted in Ba, K, P, Cr and MgO relative to the other shales. The shales are all depleted in Nb, Cr, Ni and MgO and enriched in Pb, Y and K relative to the DK7 kimberlite. Element distribution patterns of the three (Q)RVK samples are shown in Figure

64(b). The patterns of the samples are similar, with sample JN-KM3 displaying the least deviation from the DK7 kimberlite composition. Sample JS-KM1 is enriched in Rb and K compared to samples JC-KM2 and JN-KM3. Samples JS-KM1 and JC-KM2 are depleted in P, Ni and Cr relative to JN-KM3. The shales and the (Q)RVK samples are compared in Figure 64(c). Although the overall shapes of the abundance patterns are similar, the (Q)RVK samples are characterised by an enrichment in Nb, Sr, P, Ni, Cr and MgO relative to the shales.

The element distribution pattern of sample JC-GM, derived from a green mudstone megablock in the Centre Lobe, is extremely similar to that of the shales (Figure 65(a)). Sample JC-GMB, derived from the same megablock, is brecciated and contains minor kimberlitic components between the brecciated mudstone fragments, as observed both in handspecimen and microscopically. The kimberlitic geochemical signature of the sample is shown by an enrichment in Nb, Ni, Cr, MgO, Sr and P relative to sample JC-GM.

Figure 65(b) compares the element abundance patterns of the shales, sample JC-GM and sample JN-KBm. The latter is a mudstone from a megablock in the North Lobe. It differs significantly from all the other samples in terms of its major element composition, particularly its Al_2O_3 and Fe_2O_3 concentrations: it is extremely enriched in Al_2O_3 relative to the other samples, as well as the shales, and has a very low Fe_2O_3 concentration. This suggests that sample JN-KBm is highly altered in comparison to the other samples. The patterns of samples JC-GM and JN-KBm are similar to that of the shales and also to one another. However, sample JN-KBm displays an enrichment in Nb, Th, Pb, Zr and Y and a slightly lower abundance of Ba, P and Ni.

Figure 65(c) compares the element abundance patterns of samples JS-M, JN-FM and JN-KBs with that of the shales, and indicates that the abundances of the majority of elements are similar in each case, with the exception of Ni, Cr and MgO, and in the case of sample JN-FM, P. The abundances of these elements in the samples display significant differences to those in the shales: Ni and MgO abundances are higher and the abundance of Cr is lower relative to the shales; sample JN-FM is enriched in P relative to the shales. These element abundances yield a characteristic distribution trend which differs from that of samples JC-GM and JN-KBm and the (Q)RVK samples. The trend is most pronounced in samples JS-

M and JN-FM, both of which are contorted mudstone xenoliths, and is least pronounced in sample JN-KBs which is a siltstone derived from the same megablock as sample JN-KBm.

Following from these multi-element diagrams, simple bivariate plots (Figure 66 (a) – (f)), using the most effective discriminant elements, have been used to further illustrate the compositional distinction between the (Q)RVK samples, shales and xenolith/megablock lithologies. Note that fields defined by the compositions of a number of southern African on-craton Group I kimberlites (Smith et al., 1985b), including two additional analyses of the DK7 kimberlite and the average on-craton Group I kimberlite composition, have been added to the plots in order to demonstrate the compositional variation of Group I kimberlite.

Figure 66(a) plots Cr vs Ni and indicates that two mixing trends exist within the group of samples: Trend 1 is a mixing trend between kimberlite and the shales, whereas Trend 2 is defined by samples JN-FM, JS-M and to a lesser degree JN-KBs. These samples are characterised by higher Ni and lower Cr concentrations relative to the shales, and lower Cr concentrations relative to the (Q)RVK samples. The trend thus suggests mixing between typical shale compositions and an unknown high Ni (and MgO), low Cr component.

A plot of Ni vs Nb (Figure 66(b)) similarly indicates the existance of two distinct mixing trends. Trend 2, defined here by samples JN-FM and JS-M, suggests that the unknown high Ni and MgO, low Cr mixing component is also characterised by a low Nb concentration. Sample JC-GMB falls along the kimberlite-shale mixing trend, substantiating the kimberlitic geochemical signature of the sample indicated in Figure 65(a). Sample JN-KBm deviates from the shales due to its Nb enrichment.

Plotting Cr vs Nb (Figure 66(c)) produces a relatively well defined mixing trend between kimberlite and the shales. The DK7 kimberlite has somewhat higher Cr concentrations compared to average concentrations of this element in kimberlites (Smith et al., 1985b), and thus does not lie at the end of the mixing trend.

In a plot of Th vs Nb (Figure 66(d)) the Transvaal and Karoo shales and sample JN-KBm deviate significantly from the mixing trend. In the case of the Transvaal and Karoo shales this may be explained in part by the wide standard deviation on the Th analyses

(Wronkiewicz and Condie 1990, Faure et al. 1996). Sample JN-KBm is significantly enriched in Th relative to all the other samples.

Figure 66(e) plots SiO_2 vs Nb and indicates a well defined mixing trend between kimberlite and shales. Most of the other samples plot along this trend, however sample JN-FM deviates from the low-Nb compositions due to its significantly lower SiO_2 concentration. Figure 66(f) indicates that sample JN-KBm has unusually high concentrations of Al_2O_3 relative to the other samples.

4.3. **Summary**

The normalised multi-element diagrams indicate that:

(i) the overall shapes of the abundance patterns of the (Q)RVK samples (JS-KM1, JC-KM2 and JN-KM3) and the shales (NASC, Transvaal and Karoo shales) are similar, however the (Q)RVK samples are characterised by a distinct enrichment in Nb, Ni, Cr and MgO relative to the shales;

(ii) the element abundance patterns of samples JC-GM and JN-KBm are extremely similar to those of the shales, however sample JN-KBm displays an enrichment in Nb;

(iii) the element abundance patterns of samples JS-M, JN-FM and JN-KBs are broadly similar to those of the shales, however these samples are characterised by a distinctive Ni-Cr-MgO trend, resulting from higher Ni and MgO and lower Cr abundances relative to the shales.

Bivariate plots of the samples indicate that:

(i) a distinct mixing trend (Trend 1) exists between kimberlite and the shales and is best illustrated in terms of Cr, Ni and Nb concentrations of the samples. The trend is defined by the three (Q)RVK samples, as well as sample JC-GMB;

(ii) a second mixing trend (Trend 2) exists between the shales and an unknown component and is defined by samples JS-M, JN-FM and to a lesser degree JN-KBs. These samples are characterised by low Cr and Nb and high Ni (and MgO) concentrations. The unknown component is characterised by low Cr and SiO_2 and high Ni and MgO concentrations. These are the compositional characteristics of olivine;

(iii) sample JC-GM has a composition very similar to that of the shales;

(iv) sample JN-KBm has an unusual composition: it is enriched in Nb relative to the shales and other xenolith/megablock samples, and its Zr, Th, Pb and Y concentrations greatly exceed those of all the other samples. It has significantly higher Al_2O_3 and lower Fe_2O_3 concentrations relative to all the other samples, suggesting that it is highly altered in comparison to the other samples. The Nb enrichment suggests the presence of kimberlitic components, however any other kimberlitic geochemical signature has probably been diluted by the severe alteration of the rock.

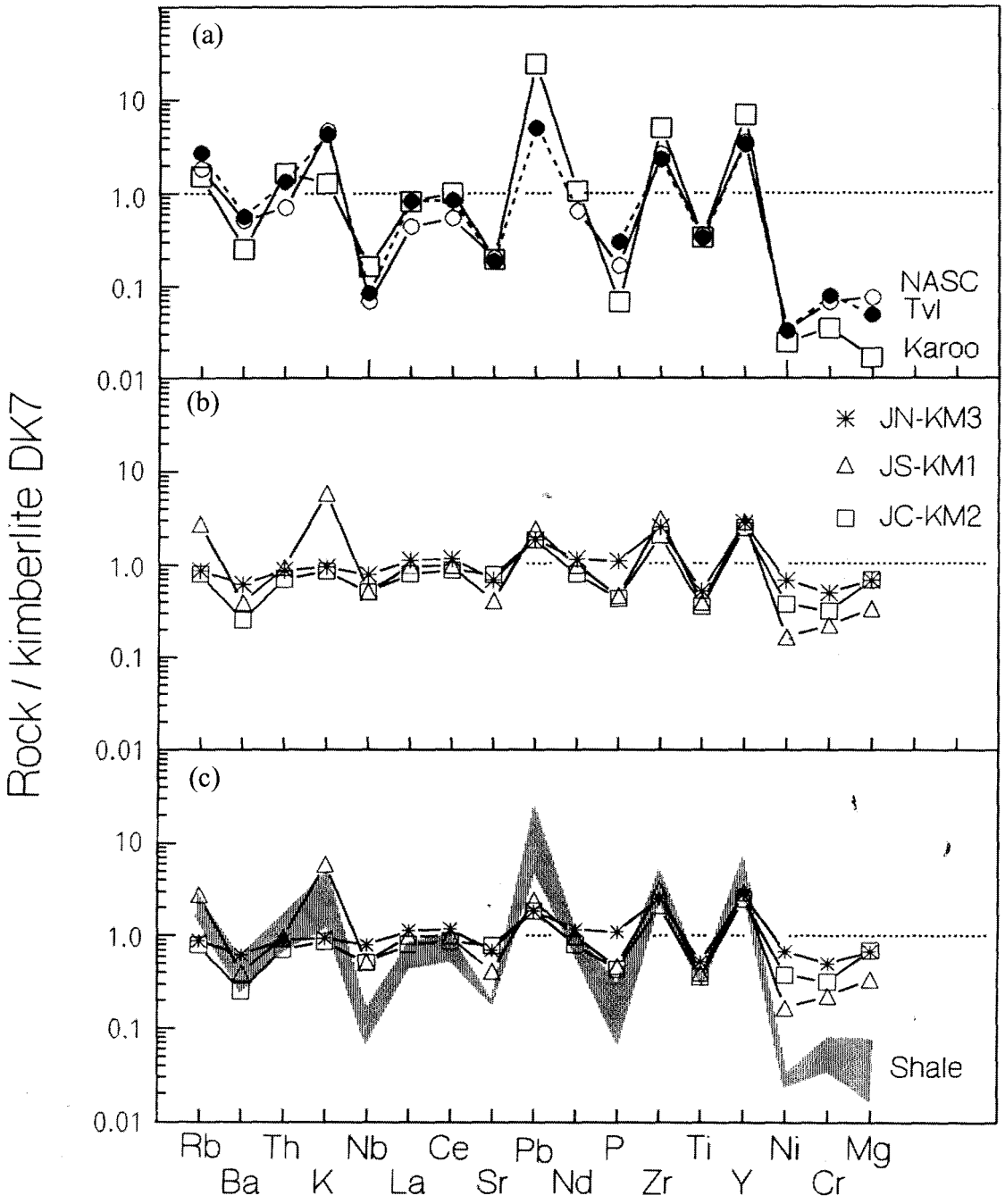

Figure 64 (a) – (c): Normalised multi-element diagrams for (a) NASC, Transvaal and Karoo shale, (b) the three (Q)RVK samples and (c) compares the element abundance patterns of the shales and (Q)RVK samples.

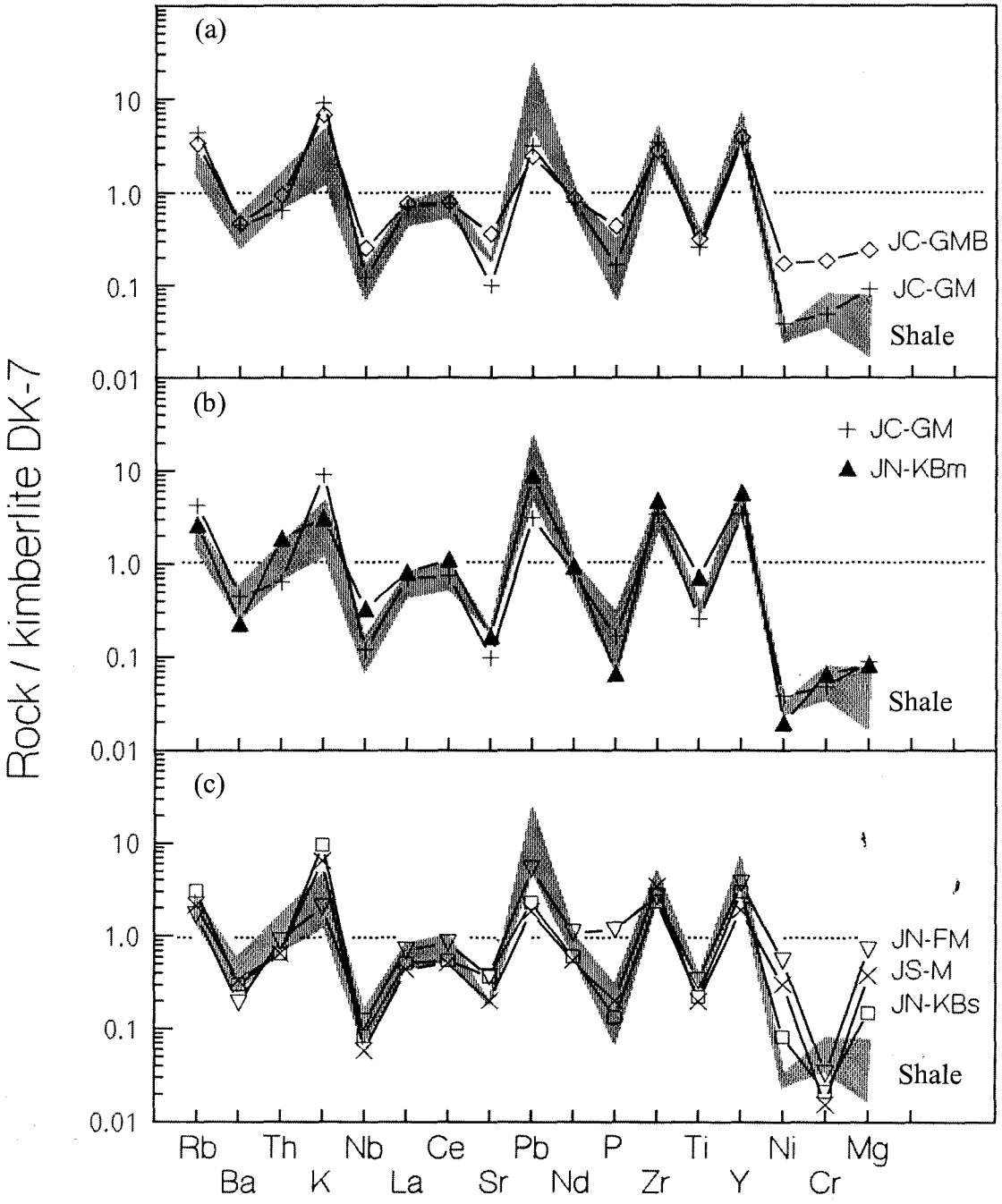

Figure 65 (a) – (c): Normalised multi-element plots for NASC, Transvaal and Karoo shales and (a) samples JC-GM and JC-GMB, (b) samples JC-GM and JN-KBm, (c) samples JS-M, JN-FM and JN-KBs.

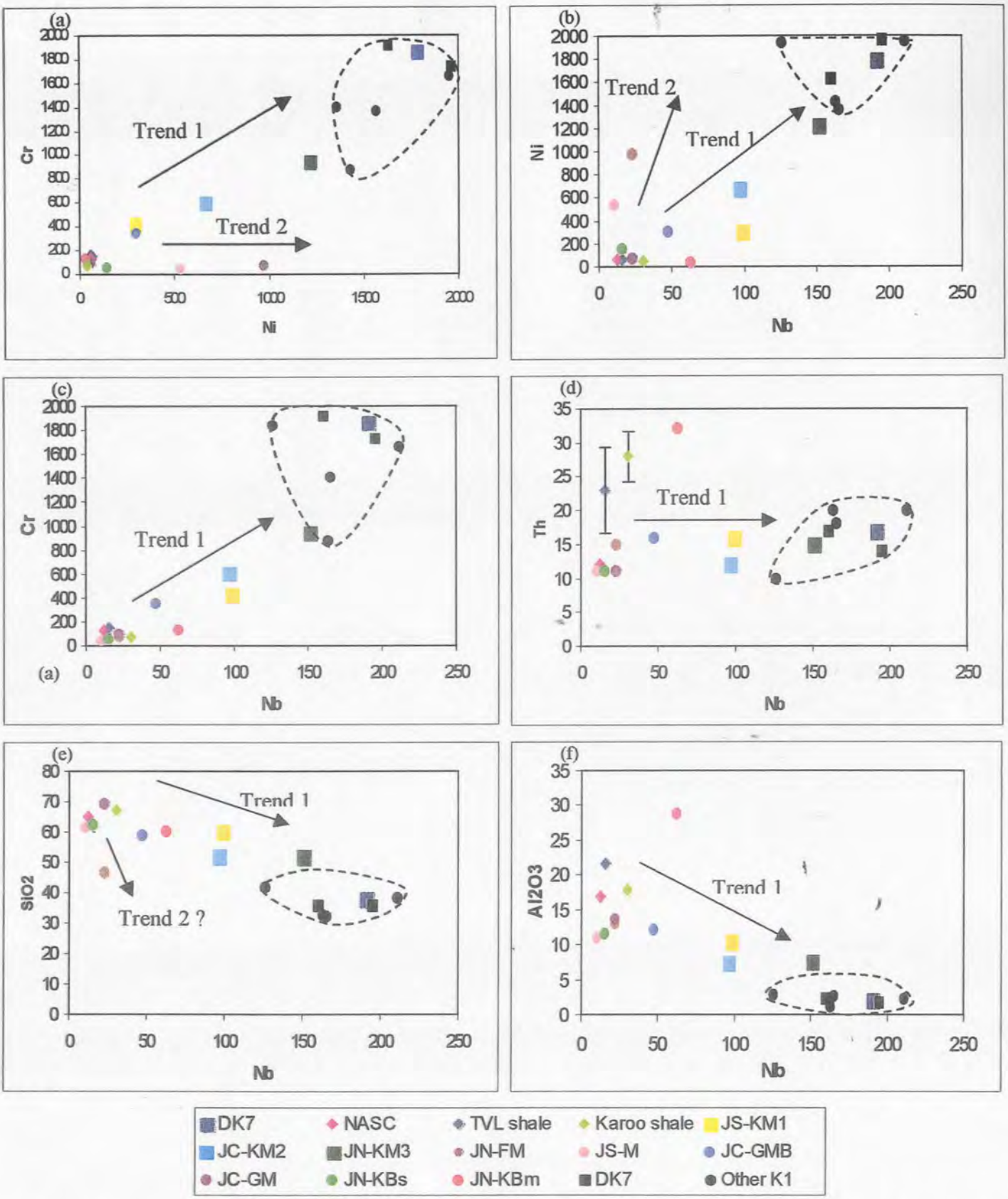

Figure 66 (a) – (f): Bivariate plots for the nine samples analysed in this study as well as the DK7 kimberlite, NASC, Transvaal and Karoo shales, and a number of other on-craton Group I kimberlites.

5. MEGABLOCKS

All three pipes of the Jwaneng kimberlite are characterised by the presence of a number of megablocks of various lithologies which occur exclusively in the peripheral zones of the pipes, close to the kimberlite-wall rock contacts. Three of these megablocks, one from each of the pipes, have been investigated in this study. The megablocks range in size up to 30m, hence the use of the term 'megablock', after the grain size classification scheme for coarse sedimentary particles of Blair & McPherson (1999). It has been postulated that these megablocks represent fragments of the original land surface which was broken up during eruption and incorporated into the kimberlite by gravitational processes (Stiefenhofer, 1999).

The megablock studied in the South Lobe (Figure 67) is approximately 10 meters in maximum dimension. It occurs close to the wall-rock contact along the southwestern margin of the pipe at a depth of approximately 164m below the present surface. It consists of pale to medium green, massive to finely-laminated silty mudstone, and displays evidence of soft sediment deformation in the form of abundant contorted laminations. This, as well as the irregular shape of the megablock, suggests that it is likely to have been poorly consolidated at the time of incorporation in the kimberlite. The Centre Lobe contains an approximately 15m wide megablock close to the wall-rock contact along its northern margin, at a depth of approximately 224m below the present surface (Figure 68). It is very similar in its overall appearance and lithology to the megablock studied in the South Lobe. However, in places it has undergone in-situ micro-brecciation and contains minor kimberlitic and xenolithic components between the fractured mudstone fragments. These components include highly altered olivine and juvenile magma clasts, as well as quartz and feldspar grains, rare altered country rock xenoliths, opaque oxides and rare micas set in a clay-rich matrix. The bulk compositions of two samples (JC-GM and JC-GMB) of this megablock have been determined and are discussed in the previous section. The results indicate that the bulk composition of the silty mudstone approximates that of typical Transvaal Supergroup shales and Karoo Supergroup (Beaufort Group) mudstones, as well as the NASC. The presence of kimberlitic components in the brecciated mudstone (sample JC-GMB) is confirmed by an enrichment in Nb, Ni, Cr and MgO relative to the unbrecciated sample (sample JC-GM).

The megablock studied in the North Lobe occurs at the wall-rock contact along the southeastern margin of the pipe at a depth of approximately 128m below the present surface. It is approximately nine meters wide at this depth, and has a vertical extent equivalent to at least two bench intervals, i.e. ~ 24m (Figure 69). The megablock is vaguely bedded and comprises siltstone, sandstone, mudstone and conglomerate units, as shown in Figure 69. Unit 1 is a competent pinkish-yellow siltstone, Unit 2 is a highly brecciated siltstone which occurs in an irregular zone at or close to the margin of Unit 1. Unit 3 is a pale grey-white mudstone and Unit 4 is a coarse-grained grey sandstone. Unit 5 is a matrix-supported, poorly sorted conglomerate comprising subrounded to subangular pebbles (10 – 250mm) of sandstone, siltstone and quartzite set in a gritty sand-rich matrix (Figure 70). The volcaniclastic kimberlite (VK) to the left of the megablock contains fragments and larger blocks of siltstone which appears similar to Unit 1. The irregularity of the bedding surfaces within the megablock suggest that the sediments were poorly consolidated when the megablock was incorporated into the kimberlite. The bulk compositions of the siltstone from Unit 1 (sample JN-KBs) and the mudstone from Unit 3 (sample JN-KBm) have been determined and are discussed in detail in the previous section.

The following lines of evidence suggest that, unlike the megablocks from the South and Centre Lobes, the megablock in the North Lobe does not represent a typical sedimentary package derived from the original land surface at the time of kimberlite eruption:

(i) the overall geometry and stratigraphy of the megablock suggests formation in a unique micro-sedimentary environment;

(ii) the poorly sorted, matrix-supported conglomeratic unit (Unit 5) is more likely to have formed by mass flow processes than in a fluvial environment;

(iii) the geochemical compositions of the siltstone and mudstone differ from typical shale/mudstone compositions and suggest the presence of minor kimberlitic components within these units;

(iv) rare kimberlitic indicator minerals have been recovered from a siltstone sample from this megablock (Dr J. Stiefenhofer, pers. comm.).

These features suggest formation of the sedimentary package as part of a crater filling event, with subsequent disruption of the deposits, probably during a later eruptive event, and incorporation of the megablock into the kimberlite pipe. However, it should be noted

that the limited geochemical analyses may not be representative and due to a lack of available data for comparative purposes, the above evidence may not be conclusive.

Figure 67: The 10m wide green, massive to finely laminated mudstone megablock which occurs along the southwestern margin of the South Lobe.

Figure 68: The 15m wide green, massive to finely laminated mudstone megablock which occurs along the northern margin of the Centre Lobe. The mudstone is brecciated in parts and contains minor kimberlitic components (samples JC-GM and JC-GMB derived from this megablock).

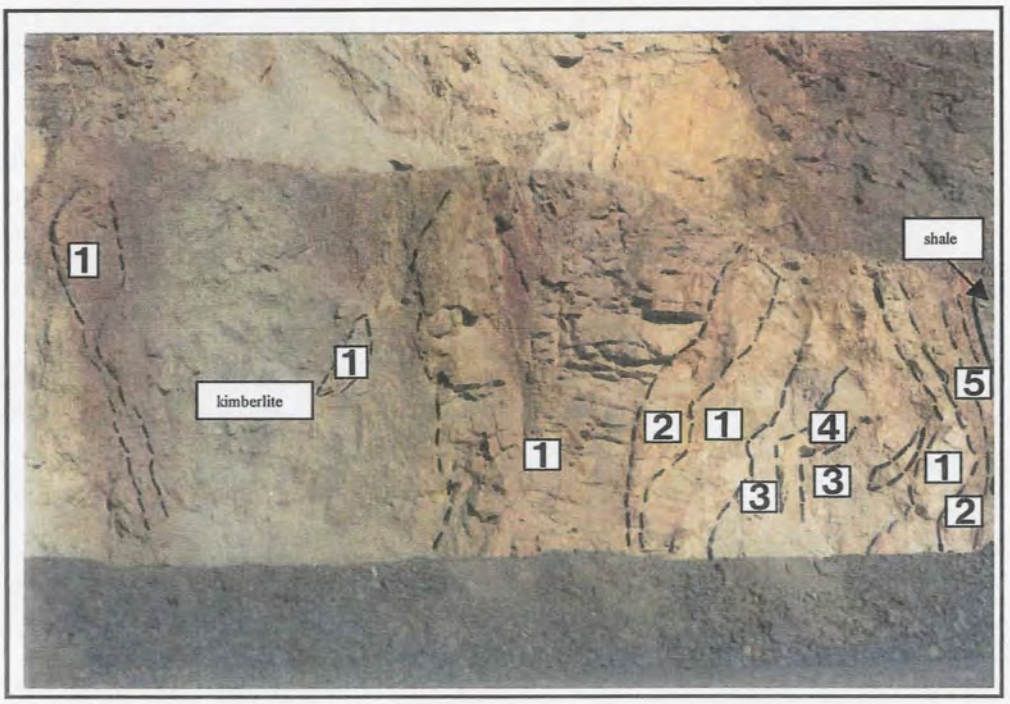

Figure 69: The nine meter wide megablock which occurs along the southeastern margin of the North Lobe. It consists of a composite sedimentary package comprising the following units: Unit 1 = siltstone; Unit 2 = brecciated siltstone; Unit 3 = mudstone; Unit 4 = sandstone; Unit 5 = conglomerate.

Figure 70: The poorly sorted, matrix-supported conglomeratic unit (Unit 5) of the megablock shown in Figure #. Subrounded clasts of sandstone, siltstone and quartzite are set in a sand-rich matrix.

6. PALYNOLOGY

Limited palynological data are available for Jwaneng Mine. In one study (Stiefenhofer, 1999) several samples of mudstone were examined, only one of which contained a good selection of pollen. In the present investigation, three samples of contorted mudstone clasts (Table 10, Figure 71) were collected from the open-pit and submitted to the Witwatersrand University Palaeontology Unit for detailed palynological examination. The analyses were requested in order to: (1) obtain confirmation of the age of intrusion of the Jwaneng kimberlites, and (2) derive indications of the palaeoenvironment at the time of kimberlite emplacement. As discussed in Section 4, the contorted mudstone clasts possibly represent poorly consolidated Karoo-age sediments that were present in the near-surface environment at the time of eruption.

Table 10: Details of samples submitted for palynological examination.

Sample Number	Shape/colour	Lithology	Host lithofacies	Location
JN-FM	Contorted Purple-brown	Mudstone	RVK-Mm	North Lobe Bench 12
JS13-M	Contorted Dark green	Mudstone	RVK-Mc	South Lobe Bench 13
JS14-M	Contorted Pale green	Mudtsone	RVK-Mc	South Lobe Bench 14

Unfortunately, all of the samples submitted were completely barren, lacking even background debris, such as wood and plant pieces (A. Sander, pers.comm.). This suggests either a low abundance of spore-producing plant species or extremely poor preservation of any original pollen. No details regarding the exact source (location) or nature of the single pollen-yielding sample reported by Stiefenhofer (1999) are available, although soft sediment deformation structures in the mudstone have been described. The sample contains a moderate to high abundance of triletes, monosaccates and aletes, which are generally associated with the Permo-Carboniferous Dwyka Group diamictites and Lower Ecca subgroup shales (Karoo Supergroup) of glacial and fluvioglacial origin. The sample therefore probably represents a xenolith from the Lower Ecca subgroup, and places a maximum Lower Permian age on kimberlite emplacement.

The presence of coal fragments within the South Lobe volcaniclastic kimberlite indicates that at least the Middle Ecca subgroup, and probably also the Upper Ecca subgroup had been deposited prior to kimberlite eruption, as these include the major coal-bearing formations of Botswana. This supports the estimated Upper Permian (~ 245 Ma) emplacement age (Chapter 1, Section 3) for the Jwaneng kimberlite, which places it within the depositional period of the Beaufort Group of the Karoo Supergroup. The latter was deposited in a fluvio-lacustrine environment under semi-arid conditions (Smith, 1984). A number of fossil wood specimens derived from the Centre Lobe have been identified as araucarian wood (Stiefenhofer, 1999). This wood is commonly found in many primitive gymnosperms and also in the family Araucariaceae, which were common in South Africa until they became extinct during the Tertiary.

Figure 71: One of the contorted mudstone clasts (Sample JN-FM) which were submitted for palynological examination. Whole rock geochemical analysis was also conducted on this sample.

IV. INTERPRETATION AND DISCUSSION

1. INTRODUCTION

Although kimberlite eruptions have never been observed, certain characteristics of the rocks indicate that some aspects of the eruption processes differ from those of most other magma types. Kimberlite textures are unusual, and must reflect unusual processes of formation (Scott-Smith, 1999). Prior to assessing the possible eruption and resedimentation processes that were involved in the emplacement of the South Lobe of the Jwaneng kimberlite, it is worthwhile briefly reviewing the emplacement models which have been postulated for kimberlites occuring mainly in southern Africa and also for those which have recently been discovered in Canada.

The classical southern African kimberlites

Most southern African kimberlite pipes are steep-sided and carrot-shaped, and show a characteristic gradual and progressive change in kimberlite textures with depth from partly bedded pyroclastic kimberlite (PK) to monotonous, intrusive, tuffisitic kimberlite breccia (TKB) to hypabyssal kimberlite (HK). Resedimented volcaniclastic kimberlite (RVK), which is commonly well-bedded, is generally deposited on top of the PK. Each of these textural types of kimberlite dominates a different zone within the pipe (and is associated with a specific style of magmatic activity). HK and associated breccias occur in the irregular root zone, TKB in the steep-sided diatreme and PK and RVK in the shallower crater zone. The emplacement mechanisms proposed by Clement (1982), Clement and Reid (1989) and Field and Scott-Smith (1999) for the southern African kimberlite pipes include complex intrusive-extrusive magmatic eruptions from closed systems. These authors propose that precursor subsurface processes result in the initial formation of irregular embryonic pipes which develop upwards intermittently (from depths of 2 to 3 km) to within approximately 500m from the palaeosurface. These processes include hydraulic wedging, fracturing and explosive brecciation ascribed to precursor gas caps formed by the exsolution of juvenile volatiles as a consequence of cooling, crystallisation and decompression (see later discussion). Field and Scott-Smith (1999) have highlighted the importance of natural lithological barriers (which in southern Africa include the Karoo dolerite sills and Drakensberg (Stormberg) Group basalts) in these processes. Where the

rising magma meets a barrier, a temporary halt in ascent and build-up of the gas cap occurs. After pressure build-up and fracturing of the country rocks, breaching of the barrier occurs by explosive brecciation. Features such as basalt breccias and 'blind' intrusions/narrowing of pipes below or in the vicinity of dolerite sills or the Drakensberg (Stormberg) Group basalts have been observed at a number of localities (Clement 1982, Clement and Reid 1989, Field and Scott-Smith 1999, pers. observation), and provide empirical evidence for a relationship between the intruding magma and the igneous rocks.

Explosive breakthrough occurs when volatile pressure exceeds the confining pressure. A crater is excavated and rapid degassing of the magma leads to short-lived fluidisation which, together with authigenic brecciation, results in the downward modification of the embryonic pipe and the formation of the diatreme. The fluidisation process produces the diatreme facies TKB, a very specific textural variety of kimberlite. As fluidisation wanes, the kimberlite magma below crystallises to form HK. After initial breakthrough a pyroclastic eruption cloud is formed and PK is deposited both within and around the rim of the crater. The PK is composed of the same constituents as the TKB below. The overlying RVK represents post-eruptive redeposition of the extra-crater deposits. It should be noted that this type of pipe is not restricted to southern Africa, as similar kimberlites occur in Canada in both the Slave and Superior Provinces, as well as in other parts of the world, such as Tanzania and India (Field and Scott-Smith, 1999).

In contrast, Lorenz (1975, 1985, 1999) has postulated that the southern African kimberlite pipes were formed by phreatomagmatic maar-diatreme processes. Lorenz suggests that the pipes are explosion craters which were back-filled by erosion of the crater rim deposits, related to repeated hydrovolcanic explosions at successively increasing depths below the palaeosurface. For a number of reasons, as outlined by Clement and Reid (1989), Field and Scott-Smith (1999) and Scott-Smith (1999) this model is considered untenable. However, although these authors believe that magmatic, rather than phreatomagmatic, processes were dominant in the formation of kimberlite diatremes, they all agree that in certain circumstances phreatomagmatism may play a role in crater excavation and during the later stages of embryonic pipe formation. Recent identification of a base surge deposit at the base of the shale basin at Orapa (Dr R. Cas, pers. comm.) also suggests that minor phreatomagmatic eruptions must have occurred in the final stages of pipe formation and filling.

The Canadian Prairies kimberlites

Recently discovered kimberlites in the Canadian Prairies differ significantly from the southern African kimberlite pipes, both in terms of their pipe shapes and characteristic fills. These are shallow (< 500m) saucer-shaped pipes which comprise only a crater zone, with no evidence for diatremes or significant root zones having been found. The craters are filled exclusively with volcaniclastic kimberlite, predominantly pyroclastic material, and TKB and HK appear to be absent (Field and Scott-Smith 1999, Scott-Smith 1999). These authors propose a two stage process for the formation of these pipes: complete excavation of the craters by phreatomagmatic maar-like processes and subsequent, rapid filling of the craters by predominantly subaerial primary pyroclastic processes. The pyroclastic kimberlite is texturally very different to that which occurs in the southern African pipes, particularly in terms of the juvenile magma clasts (see Section 2).

The Lac de Gras (NWT) kimberlites

Kimberlite pipes discovered at Lac de Gras in the Slave Province of the Canadian Northwest Territories (NWT) differ from both the southern African and the Canadian Prairies kimberlite pipes. Here small (< 600-700m deep), steep-sided pipes are filled predominantly with resedimented volcaniclastic kimberlite and less common pyroclastic kimberlite or, in a few instances, with hypabyssal kimberlite. Little or no TKB is present (Berg and Carlson 1998, Kirkley et al. 1998, Field and Scott-Smith 1999, Graham et. al. 1999). Eruption and emplacement processes for these pipes are, as yet, poorly constrained, although a third mechanism, distinct from those described above, seems likely. Graham et al. (1999) suggest that emplacement of certain pipes on the Diavik property at Lac de Gras was controlled by phreatomagmatic maar-diatreme processes, whilst Kirkley et al. (1998), in their study of kimberlites on the BHP-Dia Met property near Lac de Gras, propose initial complete expulsion of host rock material, i.e. crater excavation (which allows for subsequent filling of an open pipe) as a function of "intense fluid pressure which built up in front of the kimberlite magma advance".

Thus, at least three types of kimberlite pipes have been identified, each of which is probably associated with different emplacement mechanisms. Field and Scott-Smith (1999) and Scott-Smith (1999) have further indicated that there appears to be a correlation

between the type of pipe and the near-surface geological setting. The three types of pipes described above have the following geological settings: (1) competent country rocks which contain common igneous rocks (classical southern African pipes), (2) poorly consolidated sediments (Canadian Prairies), and (3) basement covered by a veneer of poorly consolidated sediments (Lac de Gras, NWT). These authors suggest that the near-surface geological setting into which the kimberlites are emplaced is a major control in determining the mechanism of pipe formation for any kimberlite.

The Jwaneng kimberlite

The South Lobe of the Jwaneng kimberlite is a steep-sided pipe filled predominantly with massive and chaotically-bedded resedimented volcaniclastic kimberlite (RVK) to at least 400m below the present surface. No diatreme facies TKB has thus far been identified and no hypabyssal kimberlite has been intersected to date. The RVK contains juvenile magma clasts which differ in many respects to those found in TKB and PK/RVK of other southern African kimberlites and the Canadian Prairies kimberlites (see Section 2). The adjacent Centre and North Lobes have a similar overall pipe morphology to that of the South Lobe. However, whereas the geology of the Centre Lobe is similar to that of the South Lobe, the North Lobe contains significant PK in addition to RVK. The Jwaneng kimberlite does not appear to conform to the emplacement models proposed for either the southern African or Canadian Prairies kimberlite pipes, and thus different emplacement mechanisms need to be invoked to explain its formation. Based on the similarities between the three pipes of the Jwaneng kimberlite, and their close proximity to each other, it is probable that whatever mechanisms operated were similar in each case. The pipe morphology and geology of the Jwaneng kimberlite is most comparable to that described from the Lac de Gras kimberlites. The near-surface geological setting at Jwaneng is also comparable to that at Lac de Gras i.e. thick sequence of Proterozoic shales and dolomites (Segwagwa Group) and sandstones (Waterberg Group), overlain by a comparatively thin veneer of consolidated to poorly consolidated sediments (Karoo Supergroup).

With respect to pipe models, it is important to estimate the amount of erosion in the Jwaneng area. Although all the Waterberg Group and Karoo Supergroup sediments have been lost, erosion of the Segwagwa Group shales since kimberlite emplacement is presumed to be minimal. The thickness of the Waterberg and Karoo sediments is difficult

to estimate, but comparison with regional data (Smith 1984, Carney et al. 1994) suggests that these may have been less than 300m in thickness. Although these estimations are not well-constrained, the original vertical extent of the pipes which constitute the Jwaneng kimberlite may be in the order of 800 – 1000m.

The significant features observed in the South Lobe and which require to be explained by any proposed mechanisms of emplacement, include:

(i) the formation of a relatively narrow (~ 300m), deep (800 - 1000m) steep-sided pipe filled with RVK to considerable depth (~ 400m below present surface)

(ii) the presence of two principal, distinct lithofacies, namely the quartz-rich RVK facies (QRVK) and the quartz-free RVK facies (RVK)

(iii) the spatial distribution of these principal lithofacies: the QRVK facies occurs in a narrow, discontinuous marginal zone, whereas the RVK facies is volumetrically dominant and occupies the central portion of the pipe

(iv) the specific nature of the juvenile magma clasts, particularly with respect to size, shape, granularity and composition

(v) the presence of similar juvenile magma clasts in the QRVK and RVK facies

(vi) the higher xenolithic content of the QRVK facies compared to the RVK facies and the differences in the types of xenolithic material in each facies (particularly quartz, poorly consolidated mudstone and shale)

(vii) the higher proportion of juvenile components (magma clasts and olivine) in the RVK facies compared to the QRVK facies

(viii) indications of emplacement into a dominantly subaerial, though probably 'wet' environment

(ix) the presence of rare accretionary and armoured lapilli in both the RVK and QRVK facies

(x) the presence of abundant interclast matrix 'fines' of predominantly xenolithic (mud) and possibly kimberlitic (ash) derivation

(xi) the predominantly massive, poorly sorted, and lesser chaotically-bedded nature of the pipe fill

(xii) the lateral discontinuity and oversteepened dips of the beds (planar bedding only)

(xiii) the occurrence of megablocks of poorly consolidated mudstone in the peripheral zone of the pipe.

Field and Scott-Smith (1999) consider that the differences in the characteristics of the three main pipe types could be created by intrusion of kimberlite into different near-surface geological settings. They maintain that kimberlites are petrologically similar throughout the world and that slight differences in petrological character could not account for the differences in emplacement processes. In assessing the possible mechanisms involved in the formation of the Jwaneng South Lobe, it is suggested that variations in the H_20 and CO_2 content of kimberlite magmas, *together* with the near-surface geological and hydrogeological conditions, may have an impact on kimberlite pipe emplacement.

2. ERUPTION PROCESSES

The deep, steep-walled nature of the pipe and the fine fragmental texture of juvenile and lithic clasts in the volcaniclastic kimberlite indicate that the pipe was formed by high energy, explosive volcanism. The presence of two distinct lithofacies and their spatial distribution within the pipe suggest that there were at least two major eruption episodes involved in pipe formation. The critical question is what mechanism caused the explosive eruptions ? There are essentially two possibilities: (1) explosivity resulting from the exsolution of juvenile volatiles (magmatic eruptions), and (2) explosivity resulting from the interaction of hot magma and external water (hydrovolcanic or phreatomagmatic eruptions). There is little doubt that both processes were possible at Jwaneng, given the right set of conditions, however one of the processes was probably dominant during pipe formation.

The nature of juvenile magma clasts present in volcaniclastic kimberlite is important, since it provides an indication of the state of crystallisation/devolatilisation of the magma at the time of fragmentation, and possibly also the mode of fragmentation. The juvenile magma clasts present in the South Lobe RVK and QRVK facies differ from those which occur in the volcaniclastic kimberlite of the classical southern African and Canadian Prairies pipes. They display the following characteristics: (i) a polymodal size distribution from ash to lapilli size, (ii) mainly rounded and subrounded shapes, with lesser but significant proportions of irregular and subangular varieties and minor angular clasts, (iii) two mineralogical types, namely monticellite and monticellite-calcite kimberlite, (iv) the granularity, particularly of groundmass constituents, is comparable to that of typical uniformly textured, deep-seated hypabyssal facies kimberlite, (v) the groundmass is

texturally well-preserved, and (vi) no microlitic diopside, glass or vesicles have been identified.

In contrast, the juvenile magma clasts within the VK of most southern African pipes are relatively small (mainly ash-sized) and predominantly pelletal (rounded) in shape. The groundmass constituents are finer-grained than in typical hypabyssal facies kimberlite and are often replaced or overprinted by abundant acicular microlites of diopside. The latter are considered to be one of the hallmarks of the diatreme-forming event and are thought to be the products of crystallisation of interstitial vapour phase or vapour condensates during the waning stages of fluidisation (Clement and Reid 1989, Field and Scott-Smith 1999). The VK of the Canadian Prairies kimberlite pipes contain juvenile magma clasts that are commonly lapilli-sized, mostly rounded, but in some cases amoeboid in shape, and the groundmass constituents are fine grained. They are devoid of microlitic diopside, glass is rare, but may be present and calcite-filled vesicles may be common. These magma clasts are thought to be the products of extrusive magmatic eruption of kimberlite magma from open systems at relatively shallow levels (Field and Scott-Smith 1999, Scott-Smith 1999). Volcaniclastic rocks described from maar-diatreme volcanoes formed by phreatomagmatic explosions (Lorenz 1975, 1985; White 1991), including lamproite pipes (Boxer et al, 1989), contain magma clasts which are dominantly blocky, poorly to non-vesicular and generally glassy, indicating that these clasts have been formed dominantly by quench fragmentation during explosive interaction of magma and water.

The magma clasts in the South Lobe QRVK and RVK facies appear to represent fragments of earlier consolidated hypabyssal kimberlite, suggesting that explosive fragmentation at depth and subsequent eruption brought these fragments to the surface. Although the magma clasts are suggestive of fragmentation by magmatic rather than phreatomagmatic explosions, arguments presented below show that the sedimentological and volcanological features and relationships observed in the South Lobe cannot be fully explained by magmatic processes alone.

It seems relevant at this point to reiterate the definition of resedimented volcaniclastic kimberlite (RVK) as used in this study: RVK is used here to describe VK for which depositional mechanisms can be ascribed to short-lived mass flow redeposition processes involving little textural modification, i.e. gravitational *resedimentation* is distinguished

from tractional *reworking* which may involve abrasion and rounding of clasts. In essence, RVK is used to indicate that the VK of the South Lobe is not a primary deposit, i.e. the material is no longer in its initial emplacement position. The evidence in support of this, as well as the mass flow processes involved in resedimentation, are discussed in detail in Section 3.

2.1. Magmatic eruption processes

In assessing the possibility of magmatic eruptions dominating the formation of the South Lobe, the following needs to be considered: what mechanism could (i) cause explosive excavation of a deep (800m - 1 km) steep-sided pipe, and (ii) produce the type of juvenile magma clasts present in the RVK.

In an analysis of second or retrograde boiling in felsic magmas, Burnham (1985) has argued that this is a magmatic process that is bound to occur in aqueous magmas at low pressure as a consequence of cooling, crystallisation and volatile exsolution. Overpressures generated when the volatile pressure in the magma chamber exceeds the confining pressure may, in some cases, lead to subsurface brecciation of the wall rocks surrounding magma columns and, in other cases, cause explosive eruption to surface. Clement and Reid (1989) refer to "vapour phase related explosive subsurface brecciation" as one of the processes responsible for embryonic pipe development in the southern African kimberlite pipes. They propose that the explosive brecciation probably took place as a consequence of second or retrograde boiling in the manner suggested by Burnham (1985), provided certain constraints were met. These constraints relate to variations in bulk composition (presumably influenced by CO_2/H_2O ratios), depth of the magma, mass fraction of H_2O in the initial melt, mass fraction of melt in the magma at the time of emplacement (presumably influenced by crystal content), and tensile strength of the wall rocks. Variations in these constraints or conditions will influence whether or not the second boiling process can occur, at what depths it may occur, the extent of mechanical energy that may be generated, at what depths this process leads to subsurface fracture failure and brecciation of the surrounding wall rocks, and at what depth explosive penetration to surface might occur (Skinner, 2000).

Clement and Reid (1989) and Field and Scott-Smith (1999) consider that pre-existing structures such as relatively impervious natural lithological 'traps' could provide *temporary* barriers to gas-magma penetration and yield sites of more intensive brecciation. They propose that in the classical southern African kimberlites, embryonic pipes formed by this process (from depths of 2 – 3 km) continue to develop upwards to very near surface (500m) until explosive breakthrough occurs. With regard to these comments and the discussion which follows, it is important to note that: (i) intermittent, progressively higher stages of brecciation can occur only if new batches of magma are emplaced into the system, and (ii) the kimberlite associated with the subsurface contact breccias is in all cases typical uniformly textured hypabyssal facies kimberlite, and not diatreme facies kimberlite (Skinner, 2000).

With regard to the Jwaneng South Lobe, the second or retrograde boiling process may also be responsible for magma fragmentation and explosive pipe excavation, *but* under different conditions to those involved in the emplacement of the classical southern African pipes. The conditions are considered to differ as a function of: (1) a difference in the H_2O/CO_2 content of the magma, and (2) the absence of natural lithological barriers in the near-surface environment during magma ascent.

Kimberlites are amongst the most volatile-rich rocks known (Clement 1982, Smith et al, 1985b). Significant proportions of juvenile H_2O and lesser amounts of CO_2 are likely to be retained in kimberlite magmas in near-surface environments, despite the obvious losses due to reduced volatile solubility with decompression. The proportion of juvenile volatiles in the kimberlite magma will affect the solidus and liquidus of the magma. Although experiments involving kimberlite compositions have not been conducted, insights can be gained from work carried out on peridotite compositions. Wyllie (1987) indicates that the solidus of a H_2O-rich peridotite magma at relatively low pressure will exhibit a significant increase in temperature (T) with decreasing pressure (P), whereas the solidus of a CO_2-rich peridotite magma will display a much lower increase in T with decreasing P and approach the position of the dry peridotite solidus. The solidi of peridotite magmas with intermediate H_2O/CO_2 ratios will vary between these two extremes. Magma temperatures at the onset of crystallisation will also vary depending on the position of the liquidi. Assuming that the cooling rates of the different magma types are the same, H_2O-rich magmas will intersect the solidus at relatively higher P compared to CO_2-rich magmas (Figure 72).

Assuming that similar relationships apply in kimberlite magmas, and excluding consideration of any other criteria, variation in the proportion of H_2O and CO_2 will influence the depth of onset of crystallisation. As indicated by Burnham (1985), variation in bulk composition of the magma and mass fraction of water will influence the depth of magma penetration and the amount of mechanical energy that could be generated by second boiling. Magmas emplaced at shallower depths would generate relatively greater mechanical energy (due mainly to larger volume increases), and would therefore have a greater potential for breakthrough to surface.

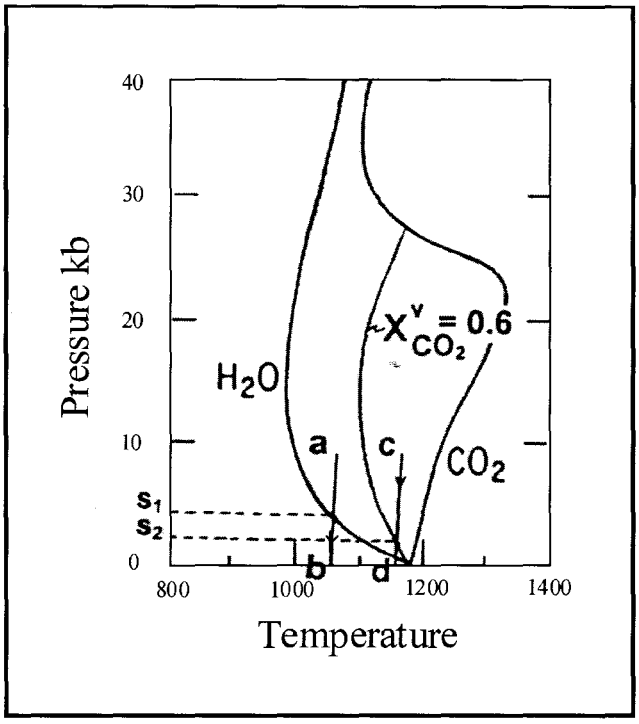

Figure 72: Solidus surfaces for peridotite-H2O and peridotite-CO2 (X=1.0) and peridotite-CO2 (X=0.6) after Wylie (1987). Hypothetical cooling curves ab and cd at similar cooling rates intersect the respective solidi at S_1 and S_2 pressures.

In the case of Jwaneng, if the second boiling process was responsible for the formation of the South Lobe, it must have resulted in a major explosion from a depth of approximately 1 km or less below the original surface (see later discussion). In order to facilitate the continued rise of the magma to these levels, a higher proportion of CO_2 relative to H_2O in the magma, compared with the starting compositions of magmas of the classical southern African pipes, would be necessary (Skinner, 2000). Presumably, the magmas of the Canadian Prairies kimberlite pipes would have had even higher proportions of CO_2, in

order for these magmas to sustain supersolidus conditions to very low pressures, i.e. depths of as little as 300m below the original surface (Field and Scott-Smith, 1999).

As stated above, an additional contributing factor in the formation of the South Lobe may be the absence of natural lithological barriers or 'traps' in the near-surface environment. Presumably, in the absence of such structures, the kimberlite magma could rise unimpeded to higher levels (~ 1 km) below the original surface, where it would cool, crystallise and degas to form a solidified carapace along the lines as proposed by Burnham (1985), i.e. crystallisation of the kimberlite magma itself causes plugging of the system to prevent the further escape of exsolved volatiles.

Burnham (1985) regards the intensely fractured marginal parts of stocklike bodies and their superjacent wall rocks, as well as the numerous breccia bodies that these fractured rocks commonly host, as manifestations of the mechanical energy released during emplacement and solidification of hydrous felsic magmas in subvolcanic environments. He states that this mechanical energy is released as a natural consequence of crystallisation or decompression of a hydrous magma or both and that, in a structurally weakened edifice, this could be the principal cause of explosive volcanism. Provided certain contraints were met, Skinner (2000) suggests that a similar scenario could have developed at Jwaneng as follows: the magma rises unimpeded and sustains supersolidus conditions during ascent to a depth of approximately 1 km (~ 250 bars) below the surface, at which point cooling, crystallisation and volatile exsolution, particularly within the upper and marginal parts of the rising magma column, would form a carapace of solidified kimberlite, with excess volatiles possibly moving to the hot interior. Continued cooling, crystallisation and volatile exsolution would occur in the unconsolidated magma column below, and the potential is high for the accumulation of a 'gas bubble' below the solidified kimberlite carapace. Exsolution of volatiles by crystallisation and second boiling is defined by the reaction:

volatile-saturated melt → crystals + supercritical fluid/gas

Whether a supercritical fluid or gas phase is produced depends on the pressure (depth) at which the reaction takes place and the critical point of the volatile phases. The latter may be influenced by a number of factors in natural magma systems, as outlined by Krauskopf (1979).

When the volatile overpressure within the unconsolidated kimberlite and the 'gas bubble' exceeds the lithostatic pressure, fracture failure will occur, mainly in the country rocks above the carapace, and possibly also in the marginal parts of the carapace (Burnham, 1985). Expansion of the gases on decompression associated with fracture failure, plus further exsolution of gases from the melt will add to the mechanical energy produced. This self-perpetuating cycle of fracture failure-decompression-volatile exsolution will continue until the fractures extend to surface, at which point catastrophic explosive eruption to surface is possible. The juvenile magma clasts present in the RVK represent fragments of the solidified kimberlite carapace, which are carried to surface by the explosive eruption.

The intruding kimberlite magma is also likely to encounter meteoric water. Depending on the pressure (depth) at which this occurs, phreatomagmatism is possible. At pressures and temperatures above the critical point of water (> 220 bars and > 374° C), meteoric water (as a fluid phase) would probably either complement second boiling processes or be driven away into fractures in the country rock, rather than produce phreatomagmatic eruptions (Skinner, 2000).

The volcaniclastic fill of the South Lobe comprises two petrographically and spatially distinct lithofacies. The QRVK facies occurs in a narrow, discontinuous marginal zone, whereas the RVK facies is volumetrically dominant and occupies the central portion of the pipe. This, together with the characteristic features of each lithofacies as outlined below (refer also to Chapter III, Sections 2 and 3), suggests that at least two eruption episodes occurred during pipe formation. The fact that the diamond grade and quality is different in each of the lithofacies (M. Gare, pers. comm.) further supports this interpretation. This would require the processes described above to have been repeated. If this was the case, evidence within the lithofacies, particularly in terms of xenolith content and type, and juvenile content suggests that: (1) the first eruption (QRVK facies) was the dominant vent-clearing episode in terms of the overlying country rocks, and (2) the second eruption (RVK facies) may have been more intense and cored out the pipe fill resulting from the first eruption.

The modal proportion of xenolithic constituents is higher in the QRVK facies (< 55 %), than in the RVK facies (< 25 %), and is dominated by abundant fine grained, angular quartz and lesser feldspar grains, presumably derived from disaggregation of the

sedimentary rocks of the Ecca Group and possibly also the Waterberg Group. Poorly consolidated mudstone clasts derived from the uppermost Beaufort Group are also adundant in this facies. In contrast, the RVK facies is quartz-free and the comparatively low xenolithic component is dominated by Segwagwa Group shales. The modal proportion of juvenile constituents is higher in the RVK facies compared to the QRVK facies. This may relate to dilution of the juvenile component by xenolithic material in the QRVK facies, possibly combined with lower magma volumes. The nature of the juvenile magma clasts is similar in the QRVK and RVK facies, and both contain two mineralogical varieties, namely monticellite and monticellite-calcite kimberlite. This implies that two compositionally distinct magma batches were involved in each eruption episode and that these magma batches were similar in each case. Filling of the South Lobe to produce the RVK is ascribed to gravitational resedimentation, involving little textural modification. This is supported by the predominantly subangular and angular shapes of the xenolithic clasts. However, the juvenile magma clasts range in shape from rounded to angular, with rounded and subrounded clasts being dominant (Chapter III, Section 3.3). Although a minor degree of rounding probably occurred during resedimentation, the majority of abrasion may have been caused by mechanisms such as in-vent 'milling' (Cas and Wright, 1987).

The second eruption may have been more intense than the first, due to the reduction in effective tensile strength afforded by the overlying volcaniclastic pipe fill compared with the original wall rocks. This would require the expenditure of less mechanical energy in causing fracture failure, thereby releasing a higher proportion of the total energy by decompression into the fracture system (Burnham, 1985). The second eruption appears to have cored out the pipe fill from the first eruption (QRVK facies), ejecting most of the debris out of the crater and leaving only a marginal remnant. The absence of quartz within the RVK facies suggests that the second eruption resulted in intense fragmentation and wide dispersal of the QRVK facies. Conflicting evidence for the difference in intensity of the eruptions is provided by the maximum size of the clasts in the coarsest fraction of juvenile and lithic components, which is greater in the RVK facies than in the QRVK facies. This may indicate that the intensity of the first explosion (QRVK facies) was greater than the second (RVK facies), although it should be noted that the values have been obtained from a limited dataset (Chapter III, Section 3), and that other processes, such as

those involved in resedimentation of the material, may also have had an impact on clast size.

2.2. Phreatomagmatic eruption processes

Although the nature of the juvenile magma clasts in the South Lobe (Q)RVK pipe fill is suggestive of dominantly magmatic explosive eruptions, there are certain aspects of the volcaniclastic pipe fill that display similarities to the deposits of phreatomagmatic eruptions. These include:

(i) evidence of subsidence such as slumping and the steep dips and lateral discontinuity of bedding;

(ii) the presence of rare accretionary and armoured lapilli.

Shallow (maar) and deep (diatreme) levels of maar-diatreme volcanoes are generally considered to be formed by phreatomagmatic eruptive processes, which involve complex interactions between rising magma and external water that give rise to powerful water vapour explosions (Lorenz 1975, 1985; White 1991; Zimanowski 1998). The diatremes are thought to form by repeated explosions from successively greater depths, which are controlled by hydrostatic pressure and water availability, and are associated with subsidence of overlying pyroclastic beds and collapse of the wall rocks. The deposits of phreatomagmatic eruptions can be recognised by a number of characteristic features (Cas and Wright 1987, Fisher and Schmincke 1984, Lorenz 1985, Zimanowski 1998). Such features tend to be associated with pyroclastic beds deposited from pyroclastic surges and falls, which are usually best developed in crater rim deposits. Crater rim deposits are not preserved at Jwaneng so their absence is not surprising. However, it should be noted that none of the bedded blocks within the pipe display bedding features (such as cross-bedding or impact sags) which are typically associated with surge deposits.

Nevertheless, comparisons made between the South Lobe (Q)RVK pipe fill and the volcaniclastic rocks of the diatremes of maar volcanoes and lamproites (Lorenz 1975, 1985, 1999, White 1991, Boxer et al., 1989) indicate that a number of similarities exist which cannot be ignored. White (1991) describes the lower diatremes of maar-diatreme volcanoes at Hopi Buttes in Arizona as comprising largely chaotic deposits with a near-absence of bedding resulting from recycling and mixing of debris during successive

phreatomagmatic eruptions. Furthermore, there is a crude concentric arrangement of rock types, with late-emplaced breccias having deeper-seated lithic fragments than more marginal breccias emplaced earlier. In the Argylle lamproite diatreme in Western Australia, subsidence of overlying pyroclastic deposits and adjacent country rocks has resulted in steep dips within the diatreme, disruption to the continuity of bedding and slumping of unconsolidated ejecta back into the crater. The subsidence is attributed to the downward migration of the phreatomagmatic explosive activity (Boxer et al., 1989).

Although the South Lobe displays some strong similarities to the abovementioned deposits, these (and those at other similar volcanic centres) are characterised by the presence of poorly to non-vesicular, generally blocky, glassy to microcrystalline juvenile clasts, indicative of fragmentation and simultaneous rapid chilling through explosive interaction of magma and water. Such juvenile clasts appear to be absent in the South Lobe (Q)RVK. The absence of glass may not be a function of a difference in magma composition, since kimberlite magmas are thought to form glass in some cases (e.g. Canadian Prairies kimberlites, B. Scott-Smith, pers. comm.). It has also been noted, however, that the relatively high degree of alteration of the South Lobe volcaniclastic rocks may obscure the presence of minor amounts of glass. Most phreatomagmatic explosions require the presence of an aquifer. At Jwaneng, the consolidated but probably weakly cemented sandstones of the Karoo Ecca Group would have been the most likely aquifer. At Argyle, mixing of sand derived from the sandstone aquifer unit and magma during explosive interaction resulted in abundant quartz xenocrysts within the juvenile clasts of the quartzose tuffs (Boxer et al., 1989). This does not appear to be the case in the QRVK facies of the South Lobe. The regular shape and steep (~ 80°) contacts of the pipe are perhaps more consistent with a major explosion from depth (Rice, 1999), rather than intermittent phreatomagmatic explosions with successively deeper foci.

Accretionary and armoured lapilli form by the aggregation (and subsequent cementation by precipitation of salts) of liquid-coated particles as a result of collisions due to terminal fall velocity differences in eruption plumes (Gilbert and Lane, 1994). Accretionary lapilli are defined as lapilli-sized (i.e. 2-64mm diameter) aggregates composed entirely of ash and are distinguished from armoured lapilli which consist of a recognisable lithic, crystal or vitric core coated with ash/mud (Fisher and Schmincke, 1984, Cas and Wright 1987, Schumacher and Schmincke 1991). Whilst both are recognised from a variety of

pyroclastic deposits, they are most frequently found developed in the steam-rich columns of phreatomagmatic and phreatic eruptions (Cas and Wright, 1987). They are not indicative solely of pyroclastic fall deposits, but may also occur in pyroclastic flow and surge deposits. Some accretionary/armoured lapilli can survive a limited amount of redeposition and can therefore be found in resedimented volcaniclastic deposits.

Accretionary and armoured lapilli are present in the South Lobe QRVK and RVK facies, but are extremely rare. Accretionary lapilli have been recognised only within the fine grained slumped QRVK facies, whereas rare examples of armoured lapilli also occur in medium to coarse grained massive QRVK and RVK facies. The accretionary lapilli and narrow ash/mud coatings on lithic/crystal fragments consist of material which closely resembles the very fine grained inter-clast matrix of the deposits, i.e. clays and finely comminuted juvenile and lithic fragments. The scarcity of accretionary and armoured lapilli may be a function of: (i) very limited phreatic/phreatomagmatic activity, (ii) low abundance of steam in the eruption column, (iii) predominantly coarse nature of the volcaniclastic debris (accretionary structures form preferentially in fine grained material), and/or (iv) if present, the majority were destroyed during resedimenation.

Although phreatomagmatism may not have been the dominant emplacement mechanism of the South Lobe, it is possible that minor phreatic/phreatomagmatic eruptions did occur. Phreatic explosions may have occurred at surface as a result of superheating of water-saturated sediments by deposition of the hot pyroclastic debris. Some or all of the accretionary/armoured lapilli may have formed in this way. Minor phreatomagmatic eruptions may have occurred either during, or in the waning stages of, resedimentation and pipe filling following each major eruptive event. This would require intrusion of late-stage magma pulses to relatively shallow levels and interaction with groundwater or possibly localised accumulations of water within the pipe. Apart from the rare accretionary/armoured lapilli, there is no other evidence to support this, but the possibility cannot be discounted. Minor eruptions in the waning stages of pipe filling could account for the inferred subsidence of the volcaniclastic deposits due to the resulting mass deficit and consequent collapse processes (Lorenz 1985, Boxer et al. 1989). However, subsidence could also be explained by other processes, which are discussed in Section 4.

3. RESEDIMENTATION PROCESSES

The volcaniclastic fill of the South Lobe consists predominantly of resedimented volcaniclastic kimberlite (RVK) to at least 400m below the present surface. No pyroclastic kimberlite (PK), such as that identified in the North Lobe (Stiefenhofer, 1999), has yet been intersected. However, it is quite likely that PK is present in the South Lobe below current mining/drilling depths. The term RVK is used in this study to describe volcaniclastic kimberlite for which depositional mechanisms can be ascribed to short-lived mass flow redeposition processes. Features of the volcaniclastic kimberlite which suggest an origin by gravitational resedimentation rather than direct deposition from primary pyroclastic processes include: (i) the high inter-clast matrix fines content of the rocks, which is dominated by mud, and contrasts with the 'clean' serpentine-rich inter-clast matrix of the PK in the North Lobe (Stiefenhofer, 1999), (ii) the predominantly chaotic, massive nature of the material and lack of continuous bedding and mapable units, (iii) the oversteepened dips of the beds (suggesting tilting due to subsidence), and (iv) the presence of autolithic fragments and blocks of previously deposited RVK.

It is proposed that the formation of the South Lobe probably involved major explosions of sufficient intensity to excavate a deep pipe and result in *initial* ejection and deposition of both country rock material and pyroclastic kimberlite out of the pipe. If this were the case, the following needs to be considered:

(i) what triggering mechanism(s) would have caused rapid redeposition of the material back into the pipe to produce the RVK, and

(ii) what processes would have been involved during redeposition ?

Resedimentation is considered to have been fairly rapid and to have occurred soon after pipe excavation. Had resedimentation taken place over a significant period of time, one would expect greater stratification of the volcaniclastic fill, as well as the presence of non-kimberlitic sediments at depth, as is the case at Lac de Gras (Field and Scott-Smith, 1999).

The presence of fossil wood and abundant xenoliths of poorly consolidated mudstones suggests that the South Lobe was emplaced into a subaerial, though probably wet environment. The emplacement age for the Jwaneng kimberlite places it within the

depositional period of the Beaufort Group of the Karoo Supergroup. According to Smith (1984), the Beaufort strata in the Southern Belt of the Central Kalahari Sub-basin were deposited in a fluvio-lacustrine environment under semi-arid climatic conditions. Thus, despite a semi-arid climate, the local environment during pipe emplacement is likely to have been wet (e.g. aggrading floodplain), and probably influenced by seasonal rainstorms.

The bulk chemical composition, morphology and internal structure of the mudstone megablocks which occur around the periphery of the pipe suggest that these represent blocks of the poorly consolidated mudstone underlying the pre-eruption surface. It is conceivable that the weight of the extra-crater ejecta may have caused failure and collapse of the mudstones forming the pipe walls. This, combined with slope instability due to the unconsolidated nature of the debris, the availability of water (surface water and rain), as well as possible eruption-generated shock waves, may have led to the rapid collapse and remobilisation of the crater rim pyroclastic successions into the open pipe. The chaotic, predominantly unstructured nature of the RVK is consistent with gravitational resedimentation of large volumes of material into a relatively narrow pipe. The specific mass flow processes which may have produced the various facies within the South Lobe are discussed below. Based on the similarities in overall structure and characteristics of the QRVK and RVK facies, the processes operating in each case were probably similar.

Massive (Q)RVK facies:

The massive QRVK and RVK facies dominate the South Lobe. They are characterised by poor sorting, lack of internal stratification, a wide range of clast sizes, from clay to large xenoliths of a meter or more in size, and include both clast- and matrix-supported deposits. These features are consistent with mass deposition by debris flows. Debris flows have been described by many authors (Middelton and Hampton 1976, Allen 1985, Smith 1986, Smith and Lowe 1991) as highly concentrated, viscous, sediment-fluid dispersions that move downslope under the influence of gravity, with larger clasts being supported by a combination of matrix yield strength, buoyancy and dispersive pressure. Only a small amount (~ 5 %) of interstitial matrix (i.e. mud and water) is required to reduce the strength of unconsolidated sediment and allow flow over even gentle slopes (Middleton and Hampton 1976, Smith 1986, Stow 1994). At Jwaneng, the presence of relatively abundant kimberlitic and xenolithic fines (ash and mud), as well as water incorporated into the

pyroclastic debris during eruption and probably also during occasional rainstorms, may have resulted in large-volume, predominantly cohesive debris flows. The broad-scale gradational variations in mean grain size of juvenile and lithic components observed within the massive (Q)RVK facies may be explained in terms of normal and reverse grading, which are commonly recognised in debris flow deposits, usually in the upper and basal portions, respectively (Middleton and Hampton 1976, Smith 1986). Lateral variations in mean and maximum clast size, concomitant with the development of better sorting, as observed in the massive (Q)RVK facies, have been reported from some debris flow deposits and are thought to reflect the wide range of flow character within debris flows (Smith, 1986). It is important to note that whilst the majority of the massive (Q)RVK facies was probably deposited by debris flows, these deposits later underwent subsidence (Section 4), i.e. there are no in-situ debris flows. Because debris flows move and deposit material *en masse*, deposits ascribed to debris flow processes should not contain traction-produced sedimentary structures (Smith, 1986). No such structures have been observed within the massive (Q)RVK facies.

Bedded (Q)RVK facies:

The bedded QRVK and RVK facies are volumetrically subordinate to the massive QRVK and RVK facies. The bedded RVK facies displays both vague and distinct bedding, whereas the bedded QRVK facies appears to be dominated by distinctly bedded deposits. Bedding in both facies is in all cases laterally discontinuous and displays abnormally steep dips ($> 60^{o}$), suggesting tilting due to subsidence (refer to Section 4).

In the vaguely bedded RVK facies the bedding is defined by the subparallel alignment of elongate clasts. These deposits are generally only a few meters or less in thickness, display gradational contacts with the massive RVK facies, and usually represent the only occurrence of internal structure within tens of meters of massive RVK facies. Elongate clast orientation has been recorded in debris flow deposits, however it is generally considered as being characteristic of hyperconcentrated flow deposits (Smith 1986, Smith and Lowe 1991). Hyperconcentrated flow is intermediate in nature between dilute fully turbulent stream flow and viscous debris flow, and involves rapid transport and deposition of sediment during high sediment and discharge events. These authors propose that hyperconcentrated flow can be produced in volcanic terranes by debris flow dilution,

resulting from mixing of debris flows with stream water, ponds or lakes. At Jwaneng, it is possible that occasional rainstorms may have contributed to the formation of hyperconcentrated flow deposits, as represented by the vaguely bedded RVK facies in the South Lobe.

The distinctly bedded QRVK and RVK facies are characterised by alternating coarser-grained lithic-rich and finer-grained lithic-poor beds. The bedding is in all cases laterally discontinuous, occuring in distinct blocks and less well-defined zones of only a few meters in maximum dimension. The thickness of individual beds is variable (2 – 100cm) within and between the bedded deposits. Both the coarser-grained and finer-grained beds are clast-supported and may display crude prefered orientation of elongate clasts parallel to the bedding planes. Contacts between the beds may be sharp or diffuse. These features suggest formation of the bedding by grain flow processes. Grain flow involves the downslope movement of concentrated dispersions of cohesionless sediment, solely under the influence of gravity, with the grains supported by dispersive pressure (Middleton and Hampton 1976, Nemec 1990). Grain flow deposits are characterised by steeply inclined stratification (30° to 35°) with internally diffuse, relatively thin layers which may display reverse grading produced by intense shearing at the contact with the substrate. Grain flow may occur in volcanic environments on steep slopes strewn with pyroclastic debris, giving rise to scree slopes with slope angles close to the angle of repose (Cas and Wright, 1987). In the South Lobe, grain flow may have occurred on the steep slopes of the pyroclastic pile around the pipe, and may also have developed on the slopes of debris cones within the pipe during periods of relative quiescence in localised areas. The distinctly bedded (Q)RVK facies occasionally contains intercalated, very thin mud-rich layers (suspension sediments), suggesting that debris slopes also occurred subaqueously during resedimentation, perhaps in shallow pools or a larger crater lake (Nemec, 1990). No tractional bedforms, such as cross bedding, have been observed.

Shale-rich breccia facies:

This facies occurs in localised areas only, close to the wall-rock contact. It is composed of abundant, poorly sorted, angular and subangular shale xenoliths, ranging in size from a few centimeters to a meter, which occur in a finer-grained matrix composed of closely-packed juvenile kimberlitic and xenolithic constituents. These breccias may represent small-scale

debris avalanche deposits, resulting from rock falls which occurred on the steep inner walls of the crater. Although both debris flow and avalanche deposits are characteristically massive, poorly sorted, and display a wide range in clast sizes, the abundance of brecciated shale clasts and location of the shale-rich breccia facies near the pipe contacts is more consistent with a rockfall-avalanche origin (Cas and Wright 1987, Smith and Lowe 1991). The localised nature and overall low abundance of this facies within the pipe may be explained as follows: the shale wall-rocks occurred below the palaeosurface at depths greater than approximately 300m, and may have been relatively stable in comparison to the the poorly consolidated sediments present at surface. The presence of downrafted mudstone megablocks and abundant mudstone xenoliths, particularly in the QRVK facies, attests to the instability of the surface environment. It is interesting to note that no megablocks of shale have yet been found within any of the Lobes.

The QRVK juvenile/quartz facies:

This facies includes both bedded and massive deposits and is volumetrically minor relative to the other facies. It occurs in the contact zone between the RVK and QRVK quartz facies in some parts of the pipe, where its presence defines a gradational contact between the two facies in terms of their quartz content. The facies is similar macroscopically to the RVK facies, and may be distinguished only by the presence of minor proportions of microscopic quartz. It is possible that the QRVK juvenile/quartz facies represents the incorporation and disaggregation of parts of the QRVK quartz facies marginal remnant during resedimentation of the RVK facies following the second major eruption event.

The slumped QRVK quartz facies:

This fine grained, mud-rich facies occurs as subrounded to irregular inclusions or 'clots', ranging up to a few meters in size, within medium and coarse grained massive RVK and QRVK facies. The rocks contain abundant fine grained detrital quartz and variable, but generally low, proportions of juvenile and lithic components. They usually contain diffuse lenses/pods and irregular laminations of coarser-grained constituents, and soft sediment deformation structures, such as slumping and micro-faulting, are common. Rare accretionary and armoured lapilli may also be present. The characteristics of this facies suggest original deposition by suspension settling within standing water bodies (shallow

ponds or lake), following sediment gravity flows such as turbidity currents. The majority of original internal structure (lamination) appears to have been destroyed or disturbed during remobilisation of the material into its present position within the coarser-grained facies. This is thought to have occurred as a result of slumping associated with subsidence within the volcaniclastic pipe fill. The deformation structures and irregular contacts with the host facies indicate that the fine grained sediments were cohesive and poorly consolidated during slumping, disruption and incorporation into the coarser-grained material. The occurrence of the slumped QRVK quartz facies within the massive RVK facies, in which quartz is rare or absent, requires consideration. The possible sequence of events that may have occurred during pipe emplacement to produce such a situation are discussed in Section 5.

It is thus proposed that the volcaniclastic fill of the South Lobe resulted mainly from gravitational resedimentation of pyroclastic deposits and country rocks from the crater walls into the open pipe. However, it is difficult to envisage that an 800 – 1000m deep pipe would be filled by these processes alone, without any primary pyroclastic kimberlite having been deposited at some level within the pipe. The future intersection and recognition of unequivocal PK within the South Lobe is therefore considered vital to the full understanding of the emplacement mechanism of the South Lobe.

4. SUBSIDENCE

Several lines of evidence exist within the volcaniclastic fill of the South Lobe which suggest that relatively large-scale subsidence occurred within the pipe. These include:

(i) the oversteepened dips of the bedding (> 60°);

(ii) the lateral discontinuity and variable orientations of the bedding;

(iii) the presence of slickenside-bound rotated blocks of massive RVK and QRVK facies;

(iv) the presence of the slumped QRVK quartz facies as irregular inclusions within coarser-grained massive RVK and QRVK facies.

Grain flow produces bedding which dips at or close to the angle of repose, which for sands and gravels is between 30° and 35°. Thus, the > 60° dip angles of the beds in the bedded (Q)RVK facies are clearly not a primary depositional feature and probably reflect post-

depositional tilting of the bedding. Since deformation of individual beds is rare or absent, the tilting must have occurred only after the bedded deposits were at least partially consolidated. The lateral discontinuity of the bedding may be a function of the localisation of grain flow processes on debris cones and lobes. It may also be partially related to reconstitution of the volcaniclastic debris due to subsidence, which could have destroyed some of the original bedding features. Both of these factors may also explain the overall low proportion of bedded deposits within the pipe. Preservation of certain bedded deposits and destruction of all or portions of others suggests differential rates and degrees of both consolidation and subsidence. Although the bedding commonly dips towards the centre of the pipe, a number of bedded blocks displaying other orientations are also present. This may also indicate some differential subsidence, rather than an entirely funnel-like collapse process.

Some mechanism is required to explain the occurrence of the slumped QRVKq facies as irregular inclusions, ranging up to a few meters in size, within the coarser-grained massive RVK and QRVK facies. The fine grained, mud-rich QRVK which constitutes these inclusions or 'clots' is thought to have originally been deposited subaqueously, either within shallow pools, or perhaps more likely, within a crater lake. It is possible that relatively large-scale subsidence of the volcaniclastic pipe fill would enable slumping, disruption and mixing of the cohesive crater lake sediments with the comparatively non-cohesive (Q)RVK facies.

The presence of slickenside-bound blocks up to several meters in size of massive RVK facies, or QRVK facies in the case of the marginal zones, may also be attributed to subsidence. These blocks display a variation in mean grain size and/or xenolith content relative to the immediately adjacent rocks, and thus appear to have been displaced from their original site of deposition. The generation of slickensides on the contacts between the blocks and the adjacent rocks may be related to differences in consolidation of the rocks and possibly also volume increases during post-depositional diagenetic alteration.

The cause of the inferred subsidence includes a number of possibilities. Firstly, it is likely that gravity-induced compaction would have occurred during and after resedimentation, resulting in differential subsidence of the pipe contents. However, subsidence of this nature was probably not sufficient to result in slumping, disruption and incorporation of the fine

grained crater lake sediments into the massive (Q)RVK facies. Large-scale subsidence would require some process which results in mass deficit at the base of the volcaniclastic fill, leading to collapse of the overlying material. It has been proposed that at least two major explosive events were involved in the formation of the South Lobe, and that the QRVK and RVK facies are the resedimented products of these eruptions. It has also been suggested that additional minor eruptions, probably phreatomagmatic in nature, may have occurred during, or in the waning stages of, resedimentation. If this was the case, the eruptions were probably relatively small-scale, resulting from intrusion of late-stage magmas, and occurring within and possibly near the margins of the pipe. They could, however, cause collapse of parts of the volcaniclastic fill and result in significant subsidence of the pipe contents. An alternative cause of large-scale subsidence may relate to magma withdrawal in the root zone of the pipe. Although such a mechanism is poorly understood in relation to kimberlites, it should not be discounted, particularly considering the close proximity of the three pipes of the Jwaneng kimberlite. The relationship of the three pipes at depth (i.e. in the root zones) is not known, however it is conceivable that eruption of an adjacent pipe may have caused mass deficit below the South Lobe and subsequent collapse of the pipe fill.

5. PIPE EMPLACEMENT MODEL

5.1. Introduction and review

The emplacement of pipes/diatremes in general has been investigated by a number of authors. With regard to kimberlite explosive eruptions, there has been considerable debate for many years between those favouring a hydrovolcanic or phreatomagmatic mechanism and those favouring explosive outburst of a system in which juvenile volatiles play a controlling role. However, it has recently become increasingly evident that in many cases neither process operates alone during pipe formation, although one of the mechanisms may be dominant. This is not considered unusual, since many other volcanic centres (of a variety of parental magma types) experience both phreatomagmatic and magmatic explosive activity during the same eruption, the style depending on the balance between magma eruption rate and aquifer recharge rate (e.g. Cas and Wright, 1987).

The Jwaneng kimberlite does not appear to conform to the emplacement models proposed for either the classical southern African or the Canadian Prairies kimberlite pipes. The pipe morphology and internal geology are most comparable to that of the kimberlites at Lac de Gras, Canadian NWT, for which contrasting emplacement models have been proposed (Section 1). The presence of rare accretionary and armoured lapilli in the volcaniclastic kimberlite of the Jwaneng South Lobe provides unequivocal evidence of interaction with water during eruption, which is not surprising considering the near-surface geological setting and palaeoenvironmental conditions. However, the nature and extent of such interaction is difficult to determine due to a number of possible influencing factors (Section 2.2). Certain features of the volcaniclastic pipe fill bear some resemblance to those described from phreatomagmatic maar-diatreme volcanoes, particularly the evidence for significant subsidence of the material filling the pipe (Sections 2.2 and 4).

The nature of juvenile magma clasts in volcaniclastic rocks is critical, as it provides an indication of the state of crystallisation/devolatilisation of the magma at the time of fragmentation, and possibly also the mode of fragmentation. The juvenile magma clasts in the South Lobe RVK suggest crystallisation and complete devolatilisation at depth prior to explosive fragmentation. A scenario in which this may have occured and led to catastrophic explosive eruption and pipe excavation has been proposed (Section 2.1). It is suggested that two important factors influencing the formation of the South Lobe (as opposed to other types of kimberlite pipes) include: (i) the H_2O/CO_2 content of the magma, and (ii) the near-surface geological setting, particularly the absence of natural lithological barriers during magma ascent. It has further been proposed that the pipe was filled mainly by resedimentation of extra-crater pyroclastic deposits and country rocks from the pipe walls into the open conduit (Section 3). It has been speculated that primary pyroclastic kimberlite may occur at some level within the pipe, although this has yet to be confirmed.

The presence of two distinct lithofacies (QRVK and RVK facies) within the South Lobe suggests that at least two major eruptions occurred during pipe formation. This, combined with the evidence for possible minor phreatic/phreatomagmatic eruptions and significant subsidence of the volcaniclastic fill, suggests that the evolution of the South Lobe was complex. The close proximity of the two adjacent kimberlite pipes (Centre and North Lobes) also requires consideration. Although the relative timing of emplacement of the

three pipes is uncertain, it is possible that the eruption of one or both of the adjacent pipes may have had an impact on the emplacement of the South Lobe.

5.2. Emplacement model for the Jwaneng South Lobe

A model for the emplacement of the Jwaneng South Lobe is outlined below. This model is based on features observed in the present study, and will undoubtedly evolve as mining proceeds and further research is conducted. The model is illustrated schematically in Figure 73.

Stage 1: This stage includes a variety of processes which may have led to the explosive excavation of the pipe and the production of the juvenile magma clasts present in the volcaniclastic kimberlite: Intrusion of relatively H_2O- and CO_2-rich kimberlite magma to approximately 1 km below the palaeosurface, followed by cooling, crystallisation and volatile exsolution by second boiling, and the formation of a solidified kimberlite carapace (Section 2.1.). The presence of two mineralogical varieties of magma clasts suggests the development of a composite intrusion. When the volatile overpressure below the carapace exceeds the lithostatic pressure, fracturing of the overlying country rock occurs, which aids further expansion and exsolution of gases. As these processes are repeated, the overlying country rocks become intensely fractured. The fractures eventually reach surface and the resultant major decompression produces significant mechanical energy and results in catastrophic explosive eruption and excavation of a deep, steep-sided pipe. Fragmentation of the solidified kimberlite carapace yields juvenile magma clasts which are carried to surface by the explosive eruption. Based on the range of magma clast shapes present, it is possible that a mechanism such as in-vent 'milling' may have caused abrasion and rounding of some of the magma clasts.

Stage 2: Initial ejection of fragmented country rock and pyroclastic kimberlite out of the pipe and formation of a steep tuff cone around the rim of the pipe. Intense fragmentation of consolidated and poorly consolidated Ecca and Beaufort Group sediments yields abundant quartz grains and mudstone xenoliths. Phreatic explosions may have occured in the pyroclastic ejecta, due to the interaction of hot debris and surface water or water-saturated sediments, resulting in the formation of accretionary and armoured lapilli. Although this may account for the presence of such lapilli in the resedimented volcaniclastic kimberlite,

no further evidence exists to support the speculation. Probable deposition of some pyroclastic kimberlite by pyroclastic fall and flow processes within the pipe (still to be confirmed).

Stage 3: Relatively rapid gravitational resedimentation of pyroclastic kimberlite back into the pipe by mass flow processes dominated by debris flows. Resedimentation is initiated by a combination of slope instability, incorporation of water into the unconsolidated debris (during eruption and rainstorms), eruption-generated shockwaves and slumping and collapse of parts of the underlying pipe walls (yielding megablocks of poorly consolidated mudstones). The large-volume debris flows produce a chaotic, unstructured deposit (massive QRVK quartz facies), and localised grain flow on debris cones forms laterally discontinuous, reverse graded planar bedding (distinctly bedded QRVK quartz facies). Shallow pools (or crater lake) form at some stage during resedimentation. Small mud flows are produced and some deposition by suspension settling of fine grained, mud-rich QRVK sediments (slumped QRVK quartz facies) occurs.

Stage 4: Probable gravity-induced compaction of the QRVK pipe fill, and associated differential subsidence and consolidation, prior to the next major eruption event, although the time interval between stages 3 and 5 is difficult to estimate.

Stage 5: Repetition of the processes described in Stage 1 following intrusion of new, relatively H_2O- and CO_2-rich kimberlite magmas at depth (not indicated in diagram). The resultant highly intense explosive eruption cores out the existing QRVK pipe fill, ejecting most of the material out of the pipe and leaving only a marginal remnant. The absence of quartz in the RVK facies may be explained by intense fragmentation and wide dispersal of the QRVK material during this eruption. Deposition of pyroclastic kimberlite occurs, mainly in a tuff cone around the rim of the pipe, but probably also within the pipe (PK?). Based on the dominant xenolith type within the RVK facies, this eruption fragments mainly Segwagwa Group shale country rocks, possibly widening the pipe at depth. However, most of the fragmented country rocks are ejected and dispersed beyond the pipe rim (hence the low xenolithic content of the RVK facies). Rare accretionary and armoured lapilli are present in the RVK facies and their formation may be explained by phreatic explosions which occur in the pyroclastic ejecta. However, they may also have formed during minor late-stage phreatomagmatic eruptions (Stage 7).

Stage 6: Relatively rapid resedimentation of pyroclastic kimberlite back into the pipe by mass flow processes dominated by debris flows. Some incorporation and disaggregation of QRVK quartz facies from the marginal remnant probably occurs during resedimentation. This yields the QRVK juvenile/quartz facies along the contact between the QRVK quartz facies and the RVK facies. As in the case of the QRVK facies, the large-volume debris flows produce a dominantly chaotic, unstructured deposit (massive RVK facies) within the relatively narrow pipe. Dilution of debris flows by occasional rainstorms yields some hyperconcentrated flow deposits (vaguely bedded RVK facies) and localised grain flow on debris cones forms laterally discontinuous, reverse graded, planar bedding (distinctly bedded RVK facies). Shallow pools probably form during resedimentation and deposition of small mud flows and thin mud-rich beds in the bedded RVK facies occurs. A crater lake develops towards the end of resedimentation and suspension settling yields fine grained, mud-rich QRVK sediments (slumped QRVK quartz facies). The quartz is probably derived from resedimentation of the remaining QRVK material from the base of the now-removed tuff cone. However, quartz may also be sourced from the adjacent Centre Lobe. This speculation is based on the observation that the emplacement of the Centre Lobe also produced QRVK facies, which similarly occurs in the marginal zone of the pipe. Some accretionary/armoured lapilli survive resedimentation and occur in the slumped QRVK quartz facies.

Stage 7: Some subsidence probably occurs during resedimentation due to gravity-induced compaction. Differential rates and degrees of consolidation and subsidence of the pipe fill result in tilting of some of the bedding to abnormal dip angles and possibly destruction of other bedding by reconstitution of the material. Large-scale collapse and subsidence also occurs, probably due to mass deficit at the base of the volcaniclastic pipe fill. This may be related either to minor phreatomagmatic eruptions within the pipe or to eruption of the adjacent Centre Lobe, or both. The phreatomagmatic eruptions may result from explosive interaction of late-stage magma and groundwater or water accumulated within the pipe. The subsidence causes further rotation and tilting of bedding, as well as slumping, disruption and incorporation of the cohesive crater lake sediments (slumped QRVK quartz facies) into the non-cohesive massive QRVK and RVK facies. Blocks of massive QRVK and RVK facies are also displaced and rotated during subsidence.

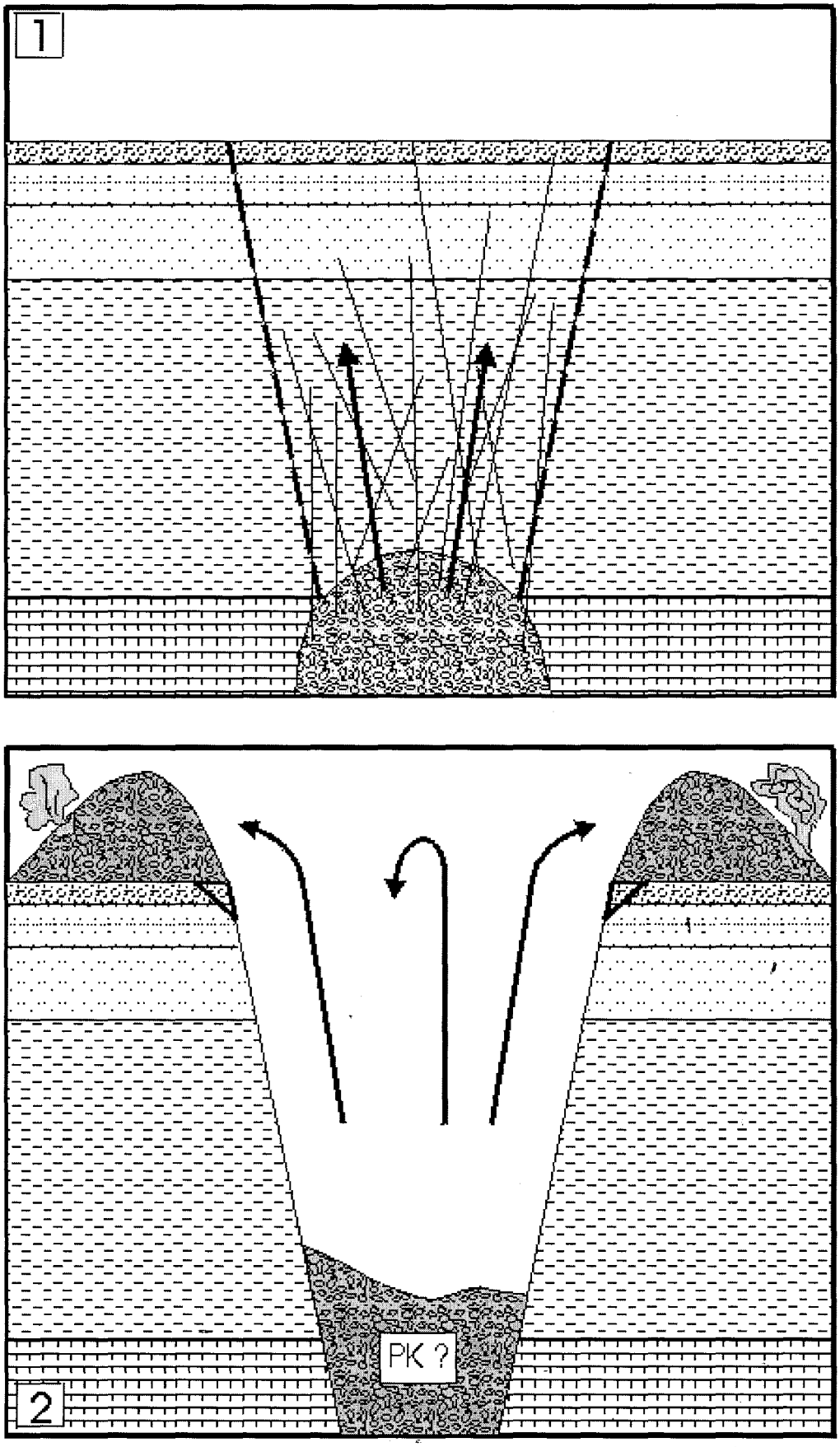

Figure 73: A schematic representation of the emplacement model for the Jwaneng South Lobe. The numbers refer to the stages of emplacement described in the text.

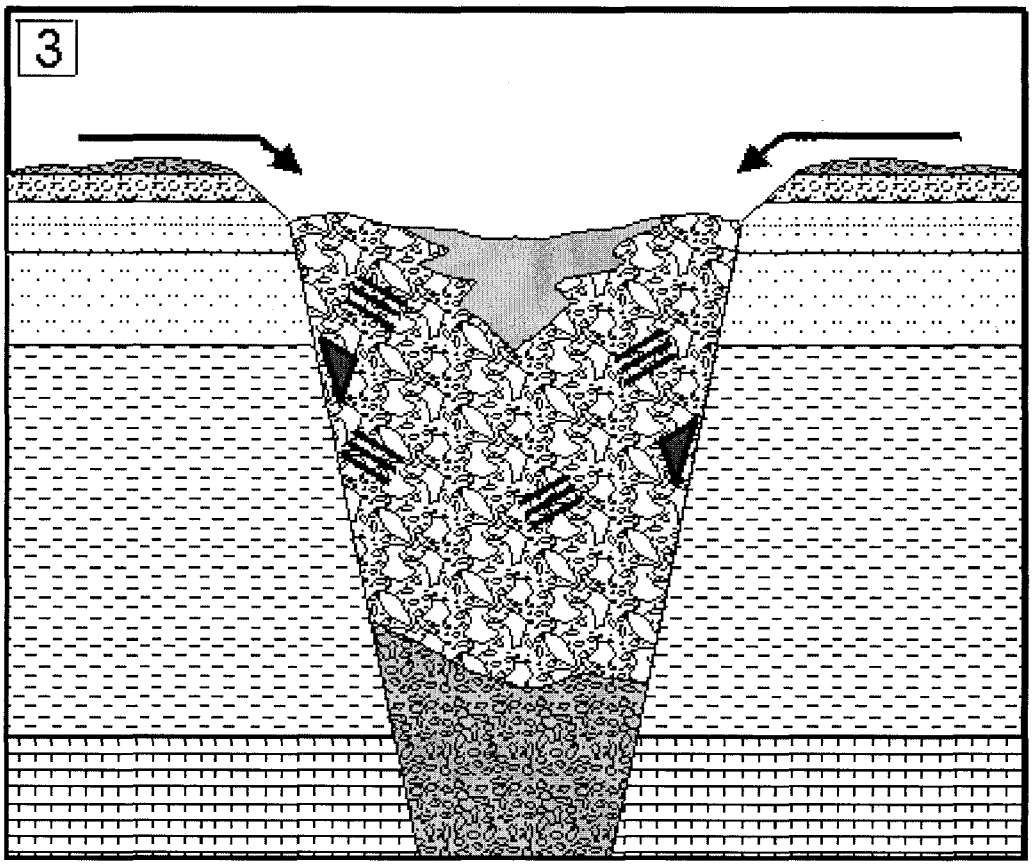
3

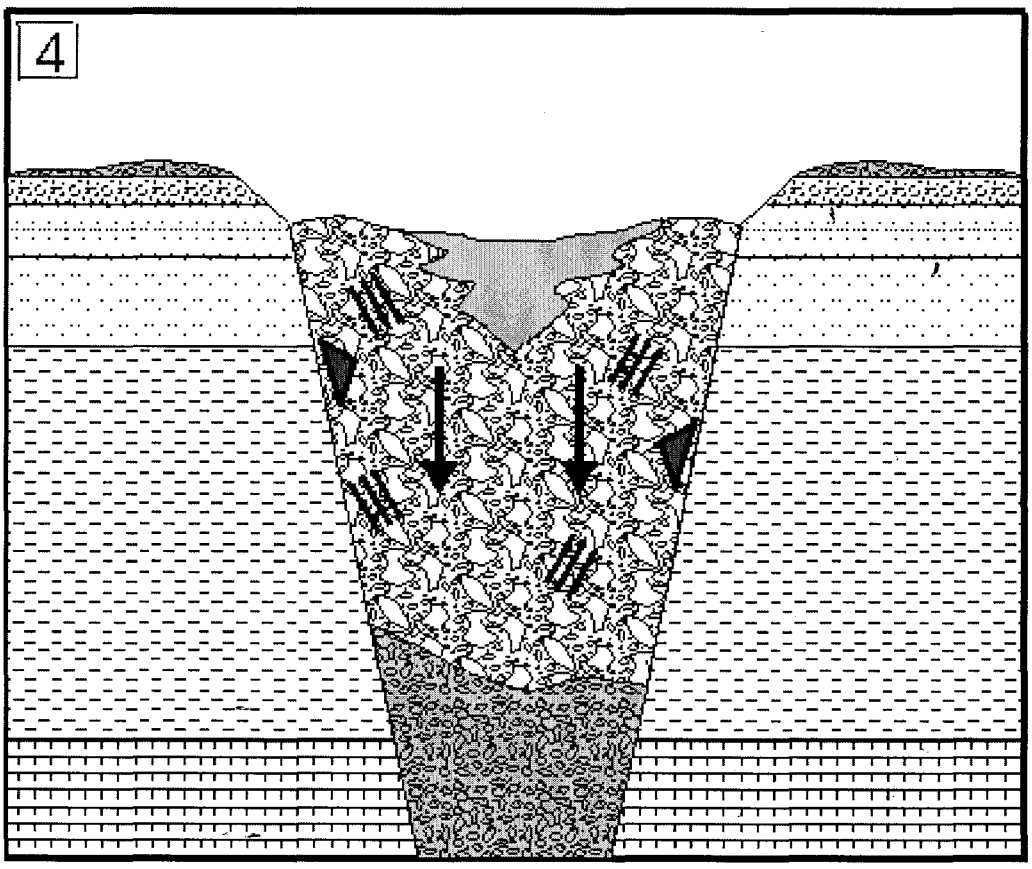
4

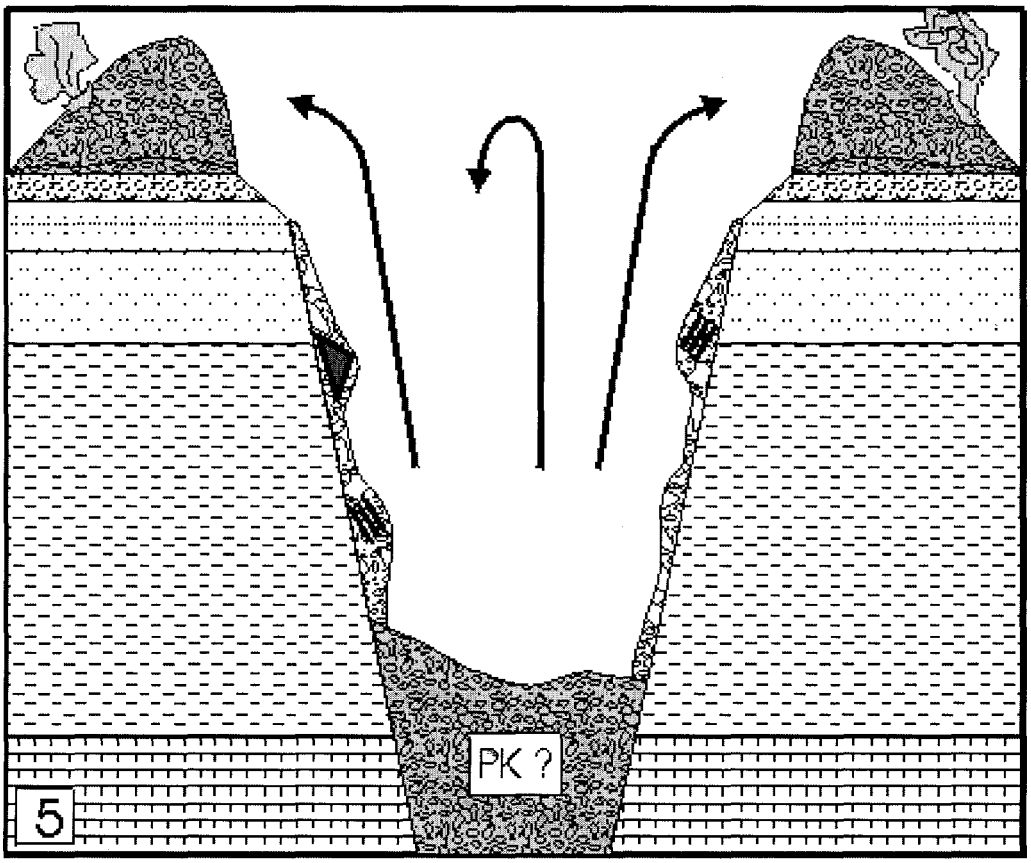
PK ?
5

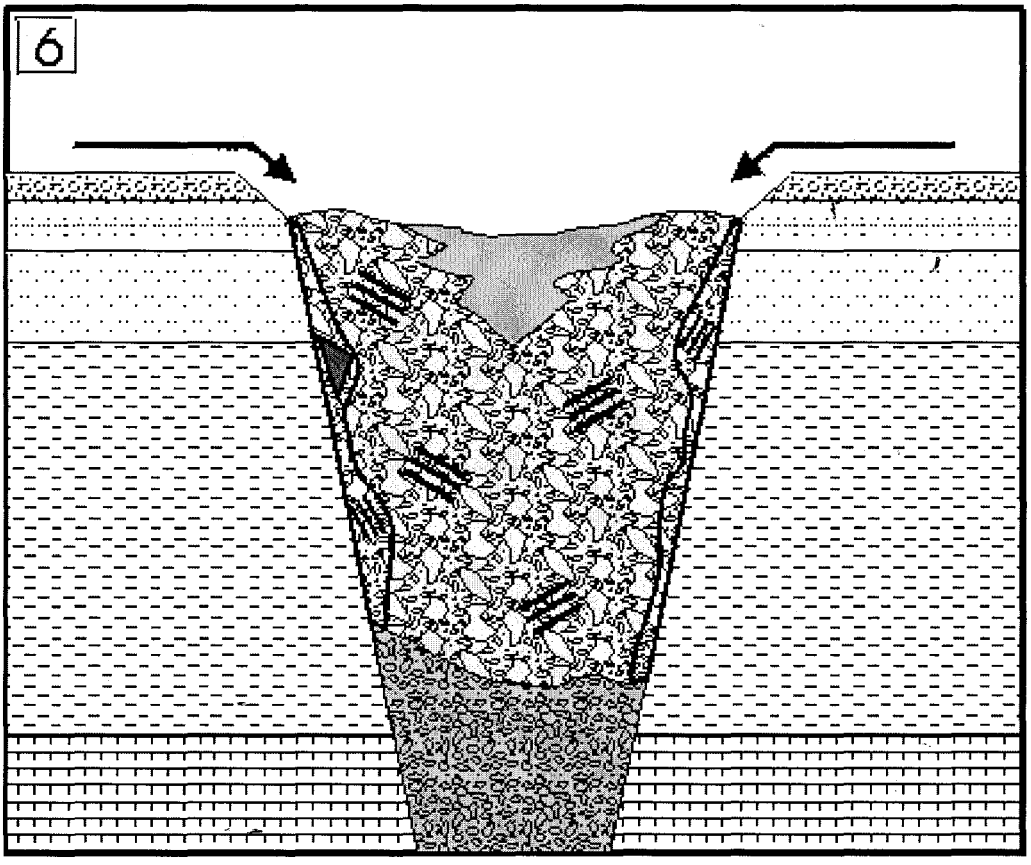
6

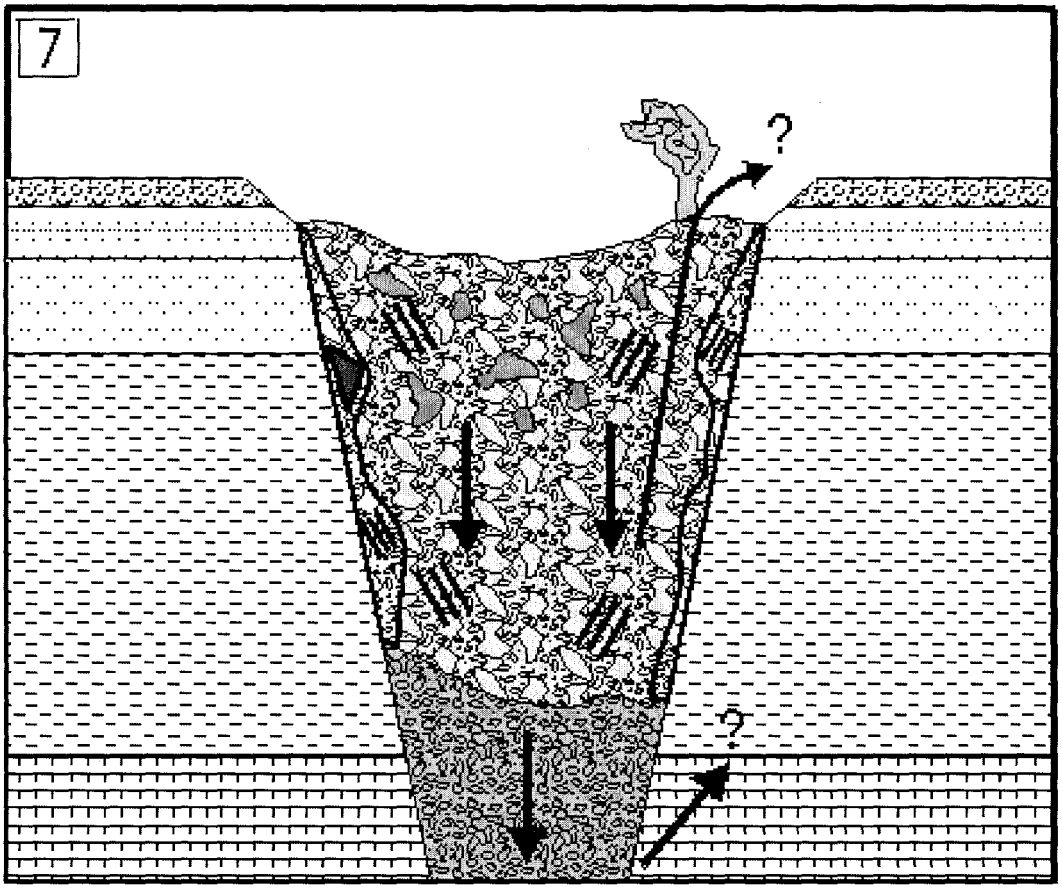

KEY

- Karoo (Beaufort)
- Karoo (Ecca)
- Waterberg Group
- Upper Transvaal (shale)
- Lower Transvaal (Dolomite)
- Hypabyssal kimberlite
- Pyroclastic kimberlite (PK)
- QRVK-M facies
- RVK-M facies
- (Q)RVK-B facies
- QRVK-S facies
- Megablock
- Phreatic eruption

V. SUMMARY AND CONCLUSIONS

The present study of the Jwaneng kimberlite, as well as research on kimberlites recently discovered in Canada (Field and Scott Smith, 1999), indicate that the spectrum of kimberlite pipe types and emplacement styles is greater than that previously described from southern Africa. The South Lobe of the Jwaneng kimberlite does not appear to conform to the pipe models or emplacement mechanisms postulated for either the southern African or Canadian Prairies kimberlites, and thus different processes have been invoked to explain its formation. The pipe morphology and internal geology are most comparable to that of the kimberlites at Lac de Gras, Canadian NWT, for which contrasting emplacement styles have been proposed.

The Jwaneng South Lobe is one of three steep-sided pipes which together constitute the Permian (~245Ma) Jwaneng kimberlite. Although the shapes of these pipes are comparable to other southern African kimberlite pipes, the Jwaneng pipes are filled predominantly with crater facies volcaniclastic kimberlite. No tuffisitic kimberlite breccia (TKB), the characteristic rock type of the diatremes of other southern African pipes, has yet been identified. The volcaniclastic pipe fill comprises two principal, distinct lithofacies, namely the QRVK facies and the RVK facies. These differ in many respects, particularly in terms of juvenile content and country rock xenolith content and type. Based on these observations and the spatial distribution of the facies within the pipe, they are interpreted as being the products of at least two separate eruption events. Both facies include fine to coarse grained, predominantly massive and subordinate chaotically-bedded deposits. The volcaniclastic rocks have been classified as resedimented volcaniclastic kimberlite, since their deposition can be ascribed to mechanisms dominated by mass flow processes. The morphology, internal structure and bulk chemical composition of mudstone megablocks which occur in the peripheral zone of the pipe suggest that these represent blocks of the poorly consolidated Karoo sediments which occurred below the palaeosurface and collapsed into the pipe. The bulk chemical composition of fine grained, mud-rich kimberlitic sediments indicate a high degree of contamination and weathering, and mixing between pristine kimberlite and silicic shale/mud compositions.

The nature of the juvenile magma clasts in the QRVK and RVK facies has been highlighted, since certain of their characteristic features are thought to be indicative of complete crystallisation and devolatilisation of the magma at depth prior to explosive fragmentation. A scenario in which this may have occured and led to catastrophic explosive eruption and pipe excavation has been proposed. The absence of microlitic diopside in the volcaniclastic kimberlite is, amongst other factors, thought to preclude the formation of the pipe by the fluidisation processes of the southern African kimberlite model (Clement 1982, Clement and Reid 1989, Field and Scott Smith 1999, Scott-Smith 1999). It is proposed in this study that both the H_2O/CO_2 content of the magma and the near-surface geological setting, particularly the absence of natural lithological barriers during magma ascent, may have influenced the formation of the South Lobe. Furthermore, the presence of rare accretionary and armoured lapilli in the QRVK and RVK facies provides evidence for interaction with water during eruption, but due to a number of possible influencing factors (Chapter IV, Section 2.2), the nature and degree of such interaction remains uncertain.

Based on the features observed in this study a model for the emplacement of the Jwaneng South Lobe has been proposed. Since the QRVK and RVK facies which constitute the volcaniclastic pipe fill display broad similarities, the various eruption and resedimentation processes involved in each case are thought to have been similar. The model describes a number of stages during pipe evolution which are summarised as follows:

The catastrophic explosive eruption and excavation of the deep, steep-sided pipe is thought to have resulted essentially from magma crystallisation and second boiling processes following intrusion of relatively H_2O- and CO_2-rich kimberlite magma to approximately 1 km or less below the palaeosurface. Fragmentation of the solidified kimberlite carapace formed at depth yields juvenile magma clasts which are carried to surface by the explosive eruption. Fragmented country rock and pyroclastic kimberlite are initially ejected out of the pipe and a steep tuff cone is formed around the rim of the pipe. Phreatic explosions may occur in the pyroclastic ejecta, resulting in the formation of accretionary and armoured lapilli. It is speculated that some pyroclastic kimberlite is deposited by pyroclastic fall and flow processes within the pipe. Relatively rapid resedimentation of the tuff cone material back into the relatively narrow pipe occurs by mass flow processes dominated by debris flows. Resedimentation is initiated by a combination of slope

instability, incorporation of water into the unconsolidated debris, eruption-generated shockwaves and slumping and collapse of parts of the underlying pipe walls. The large-volume debris flows produce a chaotic, unstructured deposit and localised grain flow on debris cones forms laterally discontinuous, reverse graded planar bedding. Shallow pools form during resedimentation and deposition of small mud flows and thin mud-rich beds occurs. A crater lake develops towards the end of resedimentation and suspension settling yields fine grained, mud-rich QRVK sediments. Some accretionary/armoured lapilli survive resedimentation and occur in these sediments. Gravity-induced compaction and associated subsidence of the pipe fill results in tilting of some of the bedding to abnormal dip angles and destruction of other bedding by reconstitution of the material. Large-scale collapse and subsidence occurs as a result of mass deficit at the base of the volcaniclastic pipe fill. This may be related either to minor phreatomagmatic eruptions within the pipe or to eruption of the adjacent Centre Lobe, or both. The subsidence causes further rotation and tilting of bedding, slumping, disruption and incorporation of the crater lake sediments into the massive QRVK and RVK facies, as well as displacement and rotation of blocks of massive QRVK and RVK facies.

This model is expected to evolve as mining proceeds and further research is conducted. The following issues are considered critical to the further development of the emplacement model: the future identification of pyroclastic kimberlite in the South Lobe would render the current model more conceivable, as it is difficult to envisage an 800 – 1000m deep pipe being filled by gravitational resedimentation processes alone. The identification of unequivocal evidence for phreatomagmatism, such as base surge deposits (perhaps in bedded blocks representing downrafted portions of a crater rim succession), would support the contention that at least minor phreatomagmatic eruptions may have occurred during pipe emplacement. Furthermore, since the eruption of one or both of the adjacent two pipes may have impacted on the emplacement of the South Lobe, further detailed research on these pipes would contribute both to the advance of the South Lobe model, as well as to the understanding of the evolution of the Jwaneng kimberlite as a whole.

VI. ACKNOWLEDGEMENTS

De Beers Consolidated Mines Ltd and Debswana Diamond Mining Company are thanked for permission to undertake this study. The opportunity they provided me, as well as the financial support, is gratefully acknowledged. Thanks to Mahwi Benjamin, Michael Gare, Ken Masogo, Jacob Balesamang and Edwin of the Jwaneng Mine Geology Section for their assistance and hospitality. My sincere thanks to my supervisor, Dr Ian Skilling, for his invaluable guidance, support and encouragement throughout the course of this thesis, albeit from a distance towards the end. Prof. Goonie Marsh took over supervision of the project after Ian's departure. I am grateful for his help and expert advise, especially with the geochemistry. This research also benefitted greatly from many discussions with Mike Skinner, whose detailed knowledge of kimberlites led to many useful comments and constructive criticism. Special thanks to my two office mates, Emese Bordy and Laura Quinton, for their wonderful friendship, constant support and stimulating brainstorming sessions. I couldn't have done it without you. Thanks also to all the staff at the Rhodes University Geology Department, especially Jenny Wright, Ashley Goddard, John Hepple and his technical staff, and Malcolm Roberts, for always being willing to help, whatever the request. Caiphus Majola, Nathaniel Senosi and Justice Mswane are thanked for expertly making the majority of the numerous thin sections and polished slabs which were examined during this study. And lastly, I am indebted to my family and my other half, Ryan. I thank them for their enthusiastic support, encouragement and incredible patience.

VII. REFERENCES

Allen, J.R.L. 1985. *Principles of Physical Sedimentology*. George Allen & Unwin, London. 385 p.

Berg, G.W. and Carlson, J.A. 1998. The Leslie kimberlite pipe of Lac de Gras, Northwest Territories, Canada: evidence for near surface hypabyssal kimberlite emplacement. In: Extended Abstracts of the VIIth International Kimberlite Conference, Cape Town. pp 81 – 83.

Blair, T.C. and McPherson, J.G. 1999. Grain-size and textural classification of coarse sedimentary particles. *Jour. Sed. Research*, **69**, No. 1, 6 – 19.

Boxer, G.L., Lorenz, V. and Smith, C.B. 1989. The geology and volcanology of the Argyle (AK1) lamproite diatreme, Western Australia. In: Ross J. et al. (eds), Kimberlites and Related Rocks, Vol. 1. *Geol. Soc. Australia Spec.Pupl.*, **14**, p. 140 – 152.

Burnham, C.W. 1985. Energy release in subvolcanic environments: implications for breccia formation. *Econ. Geol.*, **80**, 1515 – 1522.

Carlson, J.A., Kirkley, M.B., Thomas, E.M. and Hillier, W.D. 1999. Recent Canadian kimberlite discoveries. In: Proceedings of the VIIth International Kimberlite Conference, Cape Town. Vol. 1, pp 81 – 89.

Carney, J.N., Aldiss, D.T. and Lock, N.P. 1994. The Geology of Botswana. *Bulletin Geological Survey of Botswana*, **37**. p 113.

Cas, R. and Wright, J.V. 1987. *Volcanic Successions: Modern and Ancient*. Allen & Unwin, London. 528 p.

Clement, C. R. 1982. A comparative geological study of some major kimberlite pipes in the Northern Cape and Orange Free State. Ph.D thesis (2 vols), University of Cape Town, South Africa.

Clement, C.R. and Reid, A.M. 1989. The origin of kimberlite pipes: an interpretation based on a synthesis of geological features displayed by southern African occurrences. In: Ross J. et al. (eds), Kimberlites and Related Rocks, Vol. 1. *Geol. Soc. Australia Spec. Pupl.*, **14**, p. 632 – 646.

Clement, C. R. and Skinner, E.M.W. 1978. The nature of the kimberlite in the Jwaneng pipe. De Beers Internal Report. DBG/PI/50.

Clement, C. R. and Skinner, E.M.W. 1979. A textural-genetic classification of kimberlite rocks. Kimberlite Symp. II, Cambridge, Extended Abstract.

Clement, C. R. and Skinner, E.M.W. 1985. A textural-genetic classification of kimberlites. *Trans. Geol. Soc. S. Afr.* **88**, 403 – 409.

Dawson, J.B. 1971. Advances in kimberlite geology. *Earth Sci. Rev.*, **7**, 187 – 214.

Edwards, C.B. and Howkins, J.B. 1966. Kimberlites in Tanganyika with special reference to the Mwadui occurrence. Eco. Geol., **61**, 537 – 554.

Faure, K., Armstrong, R.A., Harris, C. and Willis, J.P. 1996. Provenance of mudstones in the Karoo Supergroup of the Ellisras Basin, South Africa: geochemical evidence. *Journ. Afr. Earth Sci.*, Vol 23, **2**, 189 – 204.

Field, M. 1988a. A recommended strategy for logging borehole core at Jwaneng Mine. De Beers Internal Report, PI/88–121.

Field, M. 1988b. The petrography of kimberlite from boreholes DD11 and DD12, Jwaneng Mine, Botswana. De Beers Internal Report, PI/88 136.

Field, M. 1989a. The petrography of kimberlite specimens from borehole DD1, Jwaneng Mine, Botswana. De Beers Internal Report, PI/89–051.

Field, M. 1989b. The petrography of core from borehole DD13, Southern Lobe, Jwaneng Mine, Botswana. De Beers Internal Report, PI/89–070.

Field, M. 1989c. The petrography of core from borehole DD5, Southern Lobe, Jwaneng Mine, Botswana. De Beers Internal Report, PI/89–076.

Field, M. 1989d. The petrography of core from borehole DD7, Southern Lobe, Jwaneng Mine, Botswana. De Beers Internal Report, PI/89–078.

Field, M. 1991. The petrography, HMA and mineral chemistry of samples from borehole DD1, South Lobe, Jwaneng Mine, Botswana. De Beers Internal Report, KR91/257.

Field, M., Gibson, J.G., Wilkes, T.S., Gababotse, J. and Khujwe, P. 1997. The geology of the Orapa A/K1 kimberlite, Botswana: further insight into the emplacement of kimberlite pipes. In: Proceedings of the Sixth International Kimberlite Conference, *Russ. Geol. and Geoph.*, Vol. **38** (1), Kimberlites, Related Rocks and Mantle Xenoliths, p 24–39.

Field, M. and Scott-Smith, B.H. 1998. Textural and genetic classification schemes for kimberlites: a new perspective. In: Extended Abstracts of the VIIth International Kimberlite Conference, Cape Town. pp 214 – 216.

Field, M. and Scott-Smith, B.H. 1999. Contrasting geology and near-surface emplacement of kimberlite pipes in Southern Africa and Canada. In: Proceedings of the VIIth International Kimberlite Conference, Cape Town. Vol. 1, pp 214 – 237.

Fisher, R.V. 1961. Proposed classification of volcaniclastic sediments and rocks. *Geol. Soc. America. Bull.*, **72**, 1409 – 1413.

Fisher, R.V. and Schmincke, H.U. 1984. *Pyroclastic rocks.* Springer-Verlang, New York. 472 p.

Gilbert, J.S. and Lane, S.J. 1994. The origin of accretionary lapilli. *Bull. Volcanol.*, **56**, 398 – 411.

Graham, I., Burgess, J.L., Bryan, D., Ravenscroft, E., Thomas, E., Doyle, B.J., Hopkins, R. and Armstrong, K.A. 1999. Exploration History and Geology of the Diavik Kimberlites, Lac de Gras, Northwest Territories, Canada. In: Proceedings of the VIIth International Kimberlite Conference, Cape Town. Vol. 1, pp 262 – 279.

Hawthorne, J.B. 1975. Model of a kimberlite pipe. *Phys. Chem. Earth*, **9**, 1 – 15.

Kable, E.J.D., Fesq, H.W. and Gurney, J.J. 1975. The significance of interelement relationships of some minor and trace elements in South African kimberlites. *Phys. Chem Earth*, **9**, 709 – 734.

Kinney, P.D., Compston, W., Bristow, J.W. and Williams, I.S. 1989. Archaean mantle xenocrysts in a Permian kimberlite: two generations of kimberlitic zircon in Jwaneng DK2, southern Botswana. In: Ross J. et al. (eds), Kimberlites and Related Rocks, Vol. 2. *Geol. Soc. Australia Spec. Pupl.*, **14**, p. 833 – 842.

Kirkley, M.B., Kolebaba, M.R., Carlson, J.A., Gonzales, A.M., Dyck, D.R. and Dierker, C. 1998. Kimberlite emplacement processes interpreted from Lac de Gras examples. In: Extended Abstracts of the VIIth International Kimberlite Conference, Cape Town. pp 429 – 431.

Krauskopf, K.B. 1979. *Introduction to Geochemistry.* 2nd Ed., McGraw-Hill, Inc. 617 p.

Krumbein, W.C. 1934. Size frequency distribution of sediments. *Jour. Sed. Petrol.*, **4**, 65 – 77.

Le Blanc Smith, G. 1980. Logical-letter coding system for facies nomenclature: Witbank coalfield. *Trans. Geol. Soc. S. Africa*, **83**, 301 – 311.

Lorenz, V. 1975. Formation of phreatomagmatic maar-diatreme volcanoes and its relevance to kimberlite diatremes. *Phys. Chem. Earth*, **9**, 17 – 27.

Lorenz, V. 1985. Maars and diatremes of phreatomagmatic origin: a review. *Trans. Geol. Soc. S. Afr.*, **88**, 459 – 470.

Lorenz, V. 1999. Discussion on the formation of kimberlite pipes: the phreatomagmatic model. Commission on Explosive Volcanism Newsletter, sponsored by IAVCEI.

McPhie, J., Doyle, M. and Allen, R. 1993. *Volcanic Textures*. Key Centre for Ore Deposit and Exploration Studies, University of Tasmania, Hobart, Tasmania. 196 p.

Miall, A.D. 1977. A review of the braided river depositional environment. *Earth Sci. Review*, **13**, 1 – 62.

Miall, A.D. 1978. Lithofacies types and vertical profile models in braided river deposits: a summary. In: Miall, A.D. (ed.), Fluvial Sedimentology. *Can. Soc. Petrol. Geol. Mem.*, **5**, pp 597 – 604.

Middleton, G.V. and Hampton, M.A. 1976. Subaqueous sediment transport and deposition by sediment gravity flows. In: Stanley, D.J. and Swift, D.J.P. (eds). *Marine Sediment Transport and Environmental Management.* New York, John Wiley. pp 197 – 218.

Mitchell, R. H. 1986. *Kimberlites: Mineralogy, Geochemistry and Petrology*. Plenum Press, New York. 410 p.

Mitchell, R. H. 1995. *Kimberlites, Orangeites and Related Rocks*. Plenum Press, New York. 410 p.

Nemec, W. 1990. Aspects of sediment movement on steep delta slopes. In*: Coarse-Grained Deltas*. Colella, A. and Prior, D.B. (eds). Blackwell Scientific Publications, London. 357 p.

Norrish, K. and Hutton, J.T. 1969. An accurate x-ray spectrographic method for the analysis of a wide range of geological samples. *Geoch. Cocm. Acta*, **33**, 431 – 453.

Pettijohn, F.J., Potter, P.E. and Siever, R. 1987. *Sand and sandstone*. 2nd ed. Springer-Verlang, New York. 553 p.

Prothero, D.R. and Schwab, F. 1996. *Sedimentary Geology: An Introduction to Sedimentary Rocks and Stratigraphy*. W.H. Freeman and Company, New York. 575 p.

Powers, M.C. 1953. A new roundness scale for sedimentary particles. *Jour. Sed. Petrol.*, **23**, 117 – 119.

Rice, A. 1999. Can the blasting excavation engineering sciences provide insight into the processes of kimberlite emplacement and eruption? In: Proceedings of the VIIth International Kimberlite Conference, Cape Town. Vol. 2, pp 699 – 708.

Schumacher, R. and Schmincke, H.U. 1991. Internal structure and occurrence of accretionary lapilli – a case study at Laacher See Volcano. *Bull. Volcanol.*, **53**, 612 – 634.

Scott-Smith, B. H. 1999. Near-surface emplacement of kimberlites by magmatic processes. Commission on Explosive Volcanism Newsletter, sponsored by IAVCEI. 3 – 10.

Skinner, E.M.W. 2000. Second or retrograde boiling as an eruption process associated with kimberlite pipe emplacement. Wolfe Trust report for De Beers GeoScience Centre, WT00/013.

Smith, R.A. 1984. The Lithostratigraphy of the Karoo Supergroup in Botswana. *Bulletin Geological Survey of Botswana*, **26**, 239 p.

Smith, G.A. 1986. Coarse-grained nonmarine volcaniclastic sediment: terminology and depositional process. *Geol. Soc. Am. Bull.*, 97, 1 – 10.

Smith, C.B., Allsopp, J.D., Kramers, J.D., Hutchenson, G. and Roddick, J.C. 1985a. Emplacement ages of Jurassic-Cretaceous South African kimberlites by the Rb-Sr method on phlogopites and whole-rock samples. *Trans.Geol. Soc. S. Afr.*, **88**, 249 – 266.

Smith, C.B., Gurney, J.J., Skinner, E.M.W., Clement, C.R. and Ebrahim, N. 1985b. Geochemical character of southern African kimberlites: a new approach based on isotopic constraints. *Trans. Geol. Soc. S. Afr.*, **88**, 267 – 280.

Smith, G.A. and Lowe, D.R. 1991. Lahars: volcano-hydrologic events and deposition in the debris flow-hyperconcentrated flow continuum. Sedimentation in Volcanic Settings, SEPM Special Publication, **45**, 59 – 70.

Stiefenhofer, J. 1999. Report on the petrographic investigation and first pass unit identification of the North and Central Lobes of the Jwaneng Mine, Botswana, and the effects on diamond distribution. De Beers Internal Report, KR99/0223.

Stow, D.A.V. 1994. Deep sea processes of sediment transport and deposition. In: *Sediment Transport and Depositional Processes.* Pye, K. (ed.). Blackwell Scientific Publications, London. 397 p.

Terry, R.D. and Chilingar, G.V. 1955. Summary of "Concerning some additional aids in studying sedimentary formations" by M.S. Shvetsov. *Jour.Sed. Petrology*, **25**, 229 – 234.

Udden, J.A. 1914. Mechanical composition of clastic sediments. *Geol. Soc. America Bull.* **25**, 655 – 744.

Wadell, H. 1935. Volume, shape and roundness of rock particles. *Jour. Geology*, **40**, 443 – 451.

Wagner, P. A. 1914. *The Diamond Fields of South Africa*. Transvaal Leader, Johannesburg, South Africa. 355 p.

Wentworth, C. K. 1922. A scale of grade and class terms for clastic sediments. *Jour. Geology*, **30**, 377 – 392.

White, J.D.L. 1991. Maar-diatreme phreatomagmatism at Hopi Buttes, Navajo Nation (Arizona), USA. *Bull. Volcanol.*, **53**, 239 – 258.

Wronkiewicz, D.J. and Condie, K.C. 1990. Geochemistry and mineralogy of sediments from the Ventersdorp and Transvaal Supergroups, South Africa: Cratonic evolution during the early Proterozoic. *Geoch. et Cosmo. Acta*, Vol. 54, **2**, 343 – 354.

Wyllie, P.J. 1987. Transfer of subcratonic carbon into kimberlites and rare earth carbonatites. In: Magmatic Processes: Physiochemical Principles. Mysen, B.O. (ed.) *Geochem.Soc. Special Publication*, **1**, 107 – 119.

Zimanowski, B. 1998. Phreatomagmatic explosions. In: *From Magma to Tephra: Modelling Physical Processes of Explosive Volcanic Eruptions*. Freundt, A. and Rosi, M. (eds). Elsevier Science Ltd. 318 p.

APPENDIX I

Table A1: List of core samples and corresponding depths in drillholes DD15, DD68 and DD88.

Drillhole DD15	
Sample number	**Depth**
DD15/1	83.93
DD15/2	96.39
DD15/3	106.36
DD15/4	114.07
DD15/5	117.2
DD15/6	119.07
DD15/7	122.3
DD15/8	126.32
DD15/9	129.55
DD15/10	139.46
DD15/11	145.15
DD15/12	146.3
DD15/13	148.54
DD15/14	151.66
DD15/15	152.82
DD15/16	157.56
DD15/17	161.37
DD15/18	168.3
DD15/19	174.72
DD15/20	177.2
DD15/21	185.39
DD15/22	193.02
DD15/23	196.25
DD15/24	200.02
DD15/25	201.15
DD15/26	204.31
DD15/27	209.34
Drillhole DD68	
DD68/1	53.03
DD68/2	65.43
DD68/3	81.2
DD68/4	91.25
DD68/5	96.38
DD68/6	102.58
DD68/7	106.73
DD68/8	117.56
DD68/9	125.68
DD68/10	130.68
DD68/11	139.1
DD68/12	148
DD68/13	151.6
DD68/14	158.75
DD68/15	166.73
DD68/16	180.95
DD68/17	186.22
DD68/18	193.17
DD68/19	198.7
DD68/20	212.65
DD68/21	220.68
DD68/22	231
DD68/23	246.75
DD68/24	247.37
DD68/25	258.81
DD68/26	262.83
DD68/27	269.32
DD68/28	280.83
DD68/29	288
DD68/30	300.03

Table A1 continued

Drillhole DD68 cont.	
DD68/31	315.77
DD68/32	332.05
DD68/33	345.4
DD68/34	356.7
DD68/35	372.65
Drillhole DD88	
Sample number	**Depth**
DD88/1	7.87
DD88/2	9.1
DD88/3	9.43
DD88/4	11.66
DD88/5	22.83
DD88/6	24.96
DD88/7	35.45
DD88/8	50.74
DD88/9	58.82
DD88/10	74.95
DD88/11	81.99
DD88/12	99.28
DD88/13	108.08
DD88/14	111.78
DD88/15	125.76
DD88/16	138.87
DD88/17	148.3
DD88/18	164.53
DD88/19	181.46
DD88/20	199.02
DD88/21	216.72
DD88/22	233.02
DD88/23	235.52
DD88/24	249.88
DD88/25	259.37
DD88/26	265.84
DD88/27	272.86
DD88/28	289.74
DD88/29	302.5
DD88/30	307.67
DD88/31	315.1
DD88/32	316.47
DD88/33	328.05
DD88/34	330.54
DD88/35	334.42
DD88/36	339.62
DD88/37	346.77
DD88/38	358.25
DD88/39	358.59
DD88/40	367.77
DD88/41	371.42
DD88/42	377.68
DD88/43	386.11
DD88/44	395.4
DD88/45	409.21
DD88/46	415.98
DD88/47	420.54

Table A2: Maximum clast size measurements for the samples from drillholes DD15, DD68 and DD88 (OL = olivine, CRX = country rock xenoliths, MC = magma clasts)

Drillhole DD15			
Sample number	**MaxOL**	**MaxMC**	**MaxCRX**
DD15/1	11	11	13
DD15/2	6	6	15
DD15/3	8	8	24
DD15/4	9	11	8
DD15/5	9	10	13
DD15/6	8	9	18
DD15/7	3.5	10	10
DD15/8	8	9	21
DD15/9	3.5	5	9.5
DD15/10	9	10	14
DD15/11	1.2	5.5	14
DD15/12	8	44	11.5
DD15/13	3	9	9
DD15/14	6	13	25
DD15/15	6	7	23
DD15/16	6	26	13
DD15/17	5	6	5
DD15/18	6	6	12
DD15/19	5.5	11	10
DD15/20	5	5	11
DD15/21	2	3.5	15
DD15/22	6	29	11
DD15/23	9	27	11
DD15/24	4	7	15
DD15/25	3	2.5	59
DD15/26	3.5	9	15
DD15/27	5.5	4	11
Drillhole DD68			
Sample Number	**MaxOL**	**MaxMC**	**MaxCRX**
DD68/1	6.5	8.5	19
DD68/2	6	10	34
DD68/4	4.5	5	24.5
DD68/6	6.5	5	19
DD68/7	9.5	7	17
DD68/8	7	5	12
DD68/10	6.5	6	22
DD68/11	5	5	6
DD68/13	5	6	32
DD68/14	5	6	10
DD68/16	6.5	6	19
DD68/17	7	8	11
DD68/19	10	6	22
DD68/21	5	4.5	16
DD68/23	7	7	27
DD68/24	5	7	75
DD68/25	7	11	65
DD68/28	6	6	13
DD68/29	8	9	26
DD68/31	5	5	45
DD68/32	5.5	5	15

Table A2 continued

Drillhole DD88			
Sample Number	MaxOL	MaxMC	MaxCRX
DD88/1	6	6	30
DD88/2	4.5	7	24
DD88/3	2.5	5	122
DD88/4	6	8	17
DD88/5	8	8	15
DD88/6	6	8	36
DD88/7	8.5	25	19
DD88/8	4.5	5	30
DD88/9	6	8.5	16
DD88/10	6	6	14
DD88/11	5	4.5	26
DD88/12	10	30	22
DD88/13	6	7	100
DD88/14	3	5	11
DD88/15	5	6	15
DD88/16	8	7	35
DD88/17	6	5	9
DD88/18	5.5	8	10
DD88/19	5	4.5	7
DD88/20	6	6	16
DD88/21	7	8	18
DD88/22	5.5	8	9.5
DD88/23	10	8	30
DD88/24	7	10	30
DD88/25	6	5	17
DD88/26	3	8	16
DD88/27	8	6	28
DD88/28	3	8.5	8
DD88/29	6	8	20
DD88/30	3	2	7
DD88/31	5	9	25
DD88/33	2.5	2	5
DD88/34	6	16	31
DD88/35	7	6	18
DD88/36	2	5	15
DD88/37	10	3	9
DD88/38	12	9	12
DD88/39	6	8.5	15
DD88/40	11	11	17
DD88/41	9	10	43
DD88/42	7	10	22
DD88/43	10	12	21
DD88/44	14	13	16
DD88/45	3	4	5
DD88/46	5	4.5	16
DD88/47	4	5	34

Table A3(a): Results of modal analysis by macro- and micro-pointcounting methods applied to samples from drillhole DD15.

MACRO-POINTCOUNT											
DD15/5 (RVK-Mm)						DD15/14 (RVK-Mm)					
counts	OL	Xc	MC-x	CRX	ICM	counts	OL	Xc	MC-x	CRX	ICM
100	52	2	18	14	14	100	48	2	15	25	10
200	47	4	20	18	11	200	48	3	23	13	13
300	47	1	17	24	11	300	44	4	21	18	13
400	60	1	17	13	9	400	50	4	14	19	13
500	52	3	15	17	13	500	46	4	21	19	10
TOTAL	258	11	87	86	58	TOTAL	236	17	94	94	59
Vol. %	51.6	2.2	17.4	17.2	11.6	Vol. %	47.2	3.4	18.8	18.8	11.8

DD15/17 (QRVKq-Bfm-m)							DD15/27 (QRVKq-Mm)						
counts	OL	Xc	MC-x	CRX	ICM	Qtz/F	counts	OL	Xc	MC-x	CRX	ICM	Qtz/F
100	21	3	11	8	41	16	100	12	3	5	13	30	37
200	22	1	8	11	40	18	200	14	2	3	11	25	45
300	24	1	9	9	38	19	300	9	3	7	14	24	43
400	15	4	9	9	46	17	400	12	2	3	16	28	39
500	19	3	9	12	43	14	500	16	3	7	15	19	40
TOTAL	101	12	46	49	208	84	TOTAL	63	13	25	69	126	204
Vol. %	20.2	2.4	9.2	9.8	41.6	16.8	Vol. %	12.6	2.6	5	13.8	25.2	40.8

MICRO-POINTCOUNT											
DD15/5 (RVK-Mm)						DD15/14 (RVK-Mm)					
counts	OL	Xc	MC-x	CRX	ICM	counts	OL	Xc	MC-x	CRX	ICM
100	51	0	19	15	15	100	43	0	16	20	21
200	54	3	19	14	10	200	48	5	12	18	17
300	56	4	20	9	11	300	49	2	18	19	12
400	57	0	17	11	15	400	52	3	16	14	15
500	53	1	20	14	12	500	50	4	13	17	16
TOTAL	271	8	95	63	63	TOTAL	242	14	75	88	81
Vol. %	54.2	1.6	19	12.6	12.6	Vol. %	48.4	2.8	15	17.6	16.2

DD15/17 (QRVKq-Bfm-m)							DD15/27 (QRVKq-Mm)						
counts	OL	Xc	MC-x	CRX	ICM	Qtz/F	counts	OL	Xc	MC-x	CRX	ICM	Qtz/F
100	14	3	10	17	33	23	100	9	3	5	4	36	43
200	17	2	8	12	40	21	200	15	2	4	6	32	41
300	15	2	9	20	34	20	300	11	4	4	7	35	39
400	17	1	8	18	39	17	400	11	3	4	7	34	41
500	17	3	12	9	38	21	500	14	3	5	8	32	38
TOTAL	80	11	47	76	184	102	TOTAL	60	15	22	32	169	202
Vol. %	16	2.2	9.4	15.2	36.4	20.4	Vol. %	12	3	4.4	6.4	33.8	40.4

Table A3(b): Results of modal analysis by macro- and micro-pointcounting methods applied to samples from drillhole DD68.

MACRO-POINTCOUNT											
DD68/11 (RVK-Mfm)						DD68/16 (RVK-Mc)					
counts	OL	Xc	MC-X	CRX	ICM	counts	OL	Xc	MC-x	CRX	ICM
100	43	2	15	15	25	100	36	4	13	31	16
200	41	4	18	13	24	200	48	2	13	19	18
300	42	3	17	18	20	300	48	3	14	17	18
400	43	4	13	15	25	400	47	2	12	22	17
500	45	2	15	13	25	500	50	5	13	15	17
TOTAL	214	15	78	74	119	TOTAL	229	16	65	104	86
Vol. %	42.8	3	15.6	14.8	23.8	Vol. %	45.8	3.2	13	20.8	17.2

DD68/21 (RVK-Mm)						DD68/25 (RVK-Mc)					
counts	OL	Xc	MC-x	CRX	ICM	counts	OL	Xc	MC-x	CRX	ICM
100	50	3	10	10	27	100	39	2	11	38	10
200	53	3	9	12	23	200	54	2	9	23	12
300	51	2	11	12	24	300	45	2	13	26	14
400	46	3	10	12	29	400	45	2	12	28	13
500	54	2	8	9	27	500	50	3	10	25	12
TOTAL	254	13	48	55	130	TOTAL	233	11	55	140	61
Vol. %	50.8	2.6	9.6	11	26	Vol. %	46.6	2.2	11	28	12.2

MICRO-POINTCOUNT											
DD68/11 (RVK-Mfm)						DD68/16 (RVK-Mc)					
counts	OL	Xc	MC-x	CRX	ICM	counts	OL	Xc	MC-x	CRX	ICM
100	48	1	10	16	25	100	53	4	13	16	14
200	48	2	14	14	22	200	40	9	15	19	17
300	50	0	15	14	21	300	51	3	10	20	16
400	48	4	12	16	20	400	50	2	13	17	18
500	47	4	16	10	23	500	45	3	10	28	14
TOTAL	241	11	67	70	111	TOTAL	239	21	61	100	79
Vol. %	48.2	2.2	13.4	14	22.2	Vol. %	47.8	4.2	12.2	20	15.8

DD68/21 (RVK-Mm)						DD68/25 (RVK-Mc)					
counts	OL	Xc	MC-x	CRX	ICM	counts	OL	Xc	MC-x	CRX	ICM
100	49	1	15	7	28	100	46	2	13	26	13
200	51	5	15	8	21	200	43	7	6	35	9
300	47	4	13	11	25	300	44	6	18	19	13
400	43	4	15	16	22	400	50	9	10	21	10
500	50	3	12	9	26	500	52	3	18	14	13
TOTAL	240	17	70	51	122	TOTAL	235	27	65	115	58
Vol. %	48	3.4	14	10.2	24.4	Vol. %	47	5.4	13	23	11.6

Table A3(c): Results of modal analysis by macro- and micro-pointcounting methods applied to samples from drillhole DD88.

MACRO-POINTCOUNT											
DD88/9 (RVK-Mm)						DD88/19 (QRVKq-Sf)					
counts	OL	Xc	MC-x	CRX	ICM	counts	OL	Xc	MC-x	CRX	ICM
100	48	2	10	28	12	100	24	3	8	13	52
200	58	4	9	18	11	200	25	7	9	10	49
300	48	3	9	26	14	300	23	7	9	18	43
400	43	4	12	34	7	400	22	5	10	14	49
500	48	6	12	22	12	500	27	3	10	15	45
TOTAL	245	19	52	128	56	TOTAL	121	25	46	70	238
Vol. %	49	3.8	10.4	25.6	11.2	Vol. %	24.2	5	9.2	14	47.6

DD88/28 (QRVKj/q-Bfm-m)						DD88/41 (RVK-Mc)					
counts	OL	Xc	MC-x	CRX	ICM	counts	OL	Xc	MC-x	CRX	ICM
100	51	4	14	16	15	100	46	3	17	24	10
200	45	6	15	18	16	200	43	7	20	19	11
300	46	4	14	22	14	300	50	4	19	17	10
400	46	6	11	23	14	400	47	4	20	18	11
500	47	5	14	23	11	500	49	5	19	16	11
TOTAL	235	25	68	102	70	TOTAL	235	23	95	94	53
Vol. %	47	5	13.6	20.4	14	Vol.%	47	4.6	19	18.8	10.6

MICRO-POINTCOUNT												
DD88/9 (RVK-Mm)						DD88/19 (QRVKq-Sf)						
counts	OL	Xc	MC-x	CRX	ICM	counts	OL	Xc	MC-x	CRX	ICM	Qtz/F
100	41	5	24	14	16	100	21	2	10	13	42	12
200	54	3	13	14	16	200	23	5	9	17	37	9
300	42	2	11	28	17	300	17	1	12	17	38	15
400	42	0	17	26	15	400	21	1	10	19	38	11
500	47	6	11	19	17	500	23	3	13	10	37	14
TOTAL	226	16	76	101	81	TOTAL	105	12	54	76	192	61
Vol. %	45.2	3.2	15.2	20.2	16.2	Vol. %	21	2.4	10.8	15.2	38.4	12.2

DD88/28 (QRVKj/q-Bfm-m)							DD88/41 (RVK-Mc)					
counts	OL	Xc	MC-x	CRX	ICM	Qtz/F	counts	OL	Xc	MC-x	CRX	ICM
100	43	4	18	14	17	4	100	50	4	17	14	15
200	43	2	22	10	17	6	200	45	0	22	15	18
300	48	6	18	5	13	10	300	46	2	16	21	15
400	45	3	17	13	18	4	400	47	4	15	15	19
500	40	2	13	20	19	6	500	42	8	17	20	13
TOTAL	219	17	88	62	84	30	TOTAL	230	18	87	85	80
Vol. %	43.8	3.4	17.6	12.4	16.8	6	Vol. %	46	3.6	17.4	17	16

Table A4: Sample numbers, logging codes, modal proportions and facies codes for drillhole DD15. Modal analyses by pointcounting in bold.

DEPTH FROM	DEPTH TO	Sample No.	Mean grain size	Logging code	% Olivine	% CRX	Facies code
0	79.4		-	-	-	-	OH
79.4	83.5		9	Ccpm	45	15	RVK-Mc
83.5	84.15	DD15/1	9	Ccwb	45	15	RVK-B_vc
84.15	88.41		9	Ccpm	45	15	RVK-Mc
88.41	91.53		6.5	Mcwm	40	12	RVK-Mm
91.53	92.85		9	Ccpm	45	15	RVK-Mc
92.85	94.9		5	Mcwm	40	12	RVK-Mm
94.9	95.88		8	Mcwm	45	15	RVK-Mm
95.88	109.53	DD15/2,3	8.5	Ccpm	45	15	RVK-Mc
109.53	110.77		-	-	-	-	CB
110.77	115.53	DD15/4	9	Ccpm	45	18	RVK-Mc
115.53	116.72		8	Mcpm	50	18	RVK-Mm
116.72	116.82		2.5	Mmwm*	40	8	RVK-M*f*m
116.82	116.96		8	Mcpm	50	18	RVK-Mm
116.96	117.05		3	Mmwm*	40	8	RVK-M*f*m
117.05	121.19	**DD15/5**,6	8	Mcpm	**51.6**	**17.2**	**RVK-Mm**
121.19	121.32		2.5	Mmwm*	35	10	RVK-M*f*m
121.32	122.35		8	Mcpm	50	18	RVK-Mm
122.35	122.62	DD15/7	2.5	Mmwm*	35	10	RVK-M*f*m
122.62	128.06	DD15/8	8	Mcpm	50	18	RVK-Mm
128.06	128.18		2	Mmwm*	18	8	RVK-M*f*m
128.18	128.28		6	Mcpm	50	18	RVK-Mm
128.28	128.46		3	Mmwm*	20	10	RVK-M*f*m
128.46	129.55		8.5	Ccpm	50	18	RVK-Mc
129.55	133.17	DD15/9	3.5	Mmwm	35	10	RVK-M*f*m
133.17	136.4		-	-	-	-	CB
136.4	142.5	DD15/10	8	Mcpm	50	18	RVK-Mm
142.5	143.54		6	Mcwm	50	15	RVK-Mm
143.54	145.05		8	Mcpm	50	18	RVK-Mm
145.05	145.28	DD15/11	0.5 - 2.5	Fmwb-Mcwb	20-40	5--10	RVK-B_df-*f*m
145.28	147.15	DD15/12	8	Mcpm	50	18	RVK-Mm
147.15	149.38	DD15/13	3	Mmwm	35	10	QRVKj/q-M*f*m
149.38	160.03	**DD15/14**,15,16	8	Mcpm	**47.2**	**18.8**	**RVK-Mm**

160.03	164.4	**DD15/17**	3//5	Mmwb	**20.2**	**9.8** - 30	**QRVKq-B*f*m-m**
164.4	168.8	DD15/18	4//6	Mmwb	35	15-35	QRVKj/q-B*f*m-m
168.8	170.08		3	Mmwm	20	10	QRVKq-M*f*m
170.08	176.17	DD15/19	4	Mmpm	30	15	QRVKq-M*f*m
176.17	176.43		3	Mmwm	20	10	QRVKq-M*f*m
176.43	183.1	DD15/20	4	Mmpm	15	15	QRVKq-M*f*m
183.1	184.76						*SHALE*
184.76	186.5	DD15/21	7	Mcwb	8	15	QRVKq-Mm
186.5	190.38		8	Mcpm	45	18	QRVKj/q-Mm
190.38	190.7		3	Mmwm	20	10	QRVKq-M*f*m
190.7	200.94	DD15/22,23,24	8	Mcpm	45	18	RVK-Mm
200.94	203.6	DD15/25	16	Ccpm	40	35	RVK-Mc_{srb}
203.6	215.47	**DD15**/26,**27**	5	Mmpm	**12.6**	**13.8**	**QRVKq-Mm**
215.47	251.57						*SHALE*

Calcretised kimberlite: 0.00 - 115.53 m

OH = open hole, CB = core broken

Mmwm* probably represents intersection with a VK autolith.

Shaded units are enlarged on graphic logs

Table A5: Sample numbers, logging codes, modal proportions and facies codes for drillhole DD68. Modal analyses by pointcounting in bold.

DEPTH FROM	DEPTH TO	Sample No.	Mean grain size	Logging code	% OL	% CRX	Facies code
0	5.71		-	-	-	-	OH
5.71	14.4		-	-	-	-	KAL
14.4	46.56		-	-	-	-	Ox-K, CB
46.56	51.35		8	Mcpm	40	15	RVK-Mm
51.35	55.32	DD68/1	10	Ccpb	45	20	RVK-B_vc
55.32	56.27		12	Ccpm	40	35	RVK-Mc
56.27	70.56	DD68/2	10	Ccpm	45	20	RVK-Mc
70.56	73.3		12	Ccpm	45	25	RVK-Mc
73.3	74.51		8	Mcpm	45	20	RVK-Mm
74.51	77.98		12	Ccpm	45	25	RVK-Mc
77.98	82.35	DD68/3	12	Ccwm	40	35	RVK-Mc
82.35	97.5	DD68/4,5	5	Mmwm	40	15	RVK-Mm
97.5	105.21	DD68/6	8	Ccpm	45	20	RVK-Mm
105.21	109.64	DD68/7	10	Ccpm	50	30	RVK-Mc
109.64	110.12		-	-	-	-	CB
110.12	114.98		9	Ccwm	50	25	RVK-Mc
114.98	127.86	DD68/8,9	10	Ccpm	50	30	RVK-Mc
127.86	136.22	DD68/10	9	Ccpb	50	25	RVK-B_vc
136.22	138.02		-	-	-	-	CB
138.02	140.5	**DD68/11**	4	Mmwm	**42.8**	**14.8**	**RVK-M*f*m**
140.5	142.6		-	-	-	-	CB
142.6	150.25	DD68/12	9	Ccpm	50	25	RVK-Mc
150.25	152.25	DD68/13	7	Mcwb	50	20	RVK-B_vm
152.25	155.8		10	Ccpm	50	25	RVK-Mc
155.8	160.1	DD68/14	5.5	Mcwm	43	15	RVK-Mm
160.1	185.75	**DD68**/15,**16**	11	Ccpm	**45.8**	**20.8**	RVK-Mc
185.75	187.5	DD68/17	4	Mcwm	43	15	RVK-M*f*m
187.5	196.56	DD68/18	9	Ccpm	45	20	RVK-Mc
196.56	197.4		-	-	-	-	CB
197.4	202.38	DD68/19	8	Mcpm	45	25	RVK-Mm
202.38	206.75		10	Ccpm	45	20	RVK-Mc
206.75	244.4	**DD68**/20,**21**,22	4.5	Mcwm (b)	**50.8**	**11**	**RVK-Mm**

244.4	267.68	**DD68**/23A,23B,24,**25**,2	10	Ccpm (Mcwb)	**46.6**	**28**	**RVK-Mc**
267.68	271.78	DD68/27	4.5	Mcwm	45	10	RVK-Mm
271.78	274.98		9	Ccpm	47	28	RVK-Mc
274.98	276.38		5	Mcwm	45	10	RVK-Mm
276.38	280.51		10	Ccpm	47	28	RVK-Mc
280.51	281.03	DD68/28	3//7	Mcwb	50	15-30	RVK-B_d*f*m-m
281.03	281.34		5//10	M-Ccwb	50	15-40	RVK-B_dm-c
281.34	281.62		3	Mcwm	50	18	RVK-M*f*m
281.62	284.23		10	Ccpm	47	28	RVK-Mc
284.23	289.9	DD68/29	3//10	M-Ccwb	50	15-40	RVK-B_d*f*m-c
289.9	315.17	DD68/30	11	Ccpm	47	28	RVK-Mc
315.17	317.24	DD68/31	18	Ccpm	30	45	RVK-Mc_{srb}
317.24	318.54		11	Ccpm	47	28	RVK-Mc
318.54	318.95		18	Ccpm	30	45	RVK-Mc_{srb}
318.95	320.06		11	Ccpm	47	28	RVK-Mc
320.06	320.37		18	Ccpm	30	45	RVK-Mc_{srb}
320.37	326.1		11	Ccpm	47	28	RVK-Mc
326.1	326.48		4	Mcwm*	50	18	RVK-M*f*m
326.48	327.06		11	Ccpm	47	28	RVK-Mc
327.06	327.21		4	Mcwm*	50	18	RVK-M*f*m
327.21	376.3	DD68/32,33,34,35	11	Ccpm	47	28	RVK-Mc

Oxidised kimberlite: 14.40 - 46.56 m
Calcretised kimberlite: 46.56 - 86.65m
OH = open hole, KAL = Kalahari beds, Ox-K = oxidised kimberlite, CB = core broken.
Sample DD68/23B is RVK-B*f*m-m. It occurs at 246.92 - 247.10m within RVK-Mc.
Lower limit of the RVK-B*f*m-m is defined by sample DD68/24 (RVK-Mc)
Shaded units are enlarged on graphic logs.

Table A6: Sample numbers, logging codes, modal proportions and facies codes for drillhole DD88. Modal analyses by pointcounting in bold.

DEPTH FROM	DEPTH TO	Sample No.	Mean grain size	Logging code	% OL	% CRX	Facies code
0	5.7		-	-	-	-	OH
5.7	10.9	DD88/1,2,3	11	Ccpm	40	20	RVK-Mc
10.9	22.28	DD88/4	9.5	Ccpm	50	26	RVK-Mc
22.28	22.47		6	Mcwb	50	18	RVK-B_vm
22.47	22.79		9.5	Ccpm	50	26	RVK-Mc
22.79	23.37	DD88/5	8	Mcwm	50	35	RVK-Mm
23.37	24.9		9.5	Ccpm	50	26	RVK-Mc
24.9	25.3	DD88/6	4	Mcwb	50	15	RVK-B_v*f*m
25.3	31.96		9.5	Ccpm	50	26	RVK-Mc
31.96	37.68	DD88/7	9.5	Ccpm	50	26	RVK-Mc
37.68	40.97		9	Ccpm	50	20	RVK-Mc
40.97	42.52		10	Ccpm	50	26	RVK-Mc
42.52	42.9		10	Ccpm	50	15	RVK-Mc
42.9	51.7	DD88/8	7	Mcpm	50	26	RVK-Mm
51.7	53.8		10	Ccpm	45	26	RVK-Mc
53.8	55.9		8	Mcpm	50	26	RVK-Mm
55.9	70.6	**DD88/9**	7	Mcpm	**49**	**25.6**	RVK-Mm
70.6	81.53	DD88/10	9	Ccpm	50	26	RVK-Mc
81.53	92.85	DD88/11	4	Mcwm	45	20	RVK-M*f*m
92.85	93.3		10	Ccpm	52	28	RVK-Mc
93.3	95.96		-	-	-	-	CB
95.96	103.55	DD88/12	10	Ccpm	52	28	RVK-Mc
103.55	105.33		4.5	Mcwm	50	18	RVK-Mm
105.33	105.75		4	Mmwm	40	15	RVK-M*f*m
105.75	107.57		4.5	Mcwm	50	18	RVK-Mm
107.57	109.07	DD88/13	8	Mcpm	45	25	RVK-Mm
109.07	110.28		4.5	Mcwb	50	18	RVK-B_vm
110.28	111.6		3.5	Mmwm	40	15	RVK-M*f*m
111.6	112.72	DD88/14	3//6	Mcwb	50	15-30	RVK-B_d*f*m-m
112.72	116.78		4.5	Mcwm	40	15	RVK-Mm
116.78	124.72		9	Ccpm	50	26	RVK-Mc
124.72	137.12	DD88/15	5//8	Mcwb	50	18-35	RVK-B_dm-m

137.12	147.96	DD88/16	9	Ccpm	50	26	RVK-Mc
147.96	149.13	DD88/17	5	Mmwm	40	15	RVK-Mm
149.13	152.06		9	Ccpm	50	26	RVK-Mc
152.06	154.7		4//6	Mcwb	40	15-30	RVK-B_d*f*m-m
154.7	181.46	DD88/18	9.5	Ccpm	50	26	RVK-Mc
181.46	181.59	**DD88/19**	1.5	Fmwm	**24.2**	**14**	**QRVKq-Sf**
181.59	185.2		9.5	Ccpm	50	26	RVK-Mc
185.2	196.7		-	-	-	-	CB
196.7	204.83	DD88/20	9.5	Ccpm	52	26	RVK-Mc
204.83	205		1.5	Fmwm	24	14	**QRVKq-Sf**
205	232.55	DD88/21	9.5	Ccpm	50	26	RVK-Mc
232.55	233.19	DD88/22	4	Mmwm	40	15	RVK-M*f*m
233.19	234.63		-	-	-	-	CB
234.63	235.2		4	Mmwm	40	15	RVK-M*f*m
235.2	241.94	DD88/23	9.5	Ccpm	50	26	RVK-Mc
241.94	245.22		11	Ccpm	52	30	RVK-Mc
245.22	250.15	DD88/24	7.5	Mcpm	45	20	RVK-Mm
250.15	255.65		9.5	Ccpm	50	26	RVK-Mc
255.65	256.16		7.5	Mcpm	45	20	RVK-Mm
256.16	265.82	DD88/25	9.5	Ccpm	50	26	RVK-Mc
265.82	265.99	DD88/26	1//5	Fmwb-Mcwb	25-35	10--18	RVK-B_df-m
265.99	271.7		9.5	Ccpm	50	26	RVK-Mc
271.7	276.2	DD88/27	11	Ccpm	50	30	RVK-Mc
276.2	289.55		9.5	Ccpm	50	26	RVK-Mc
289.55	296.4	**DD88/28**	4//7	Mcwb	**47**	**20.4 - 40**	**QRVKj/q-B*f*m-m**
296.4	297.7		9.5	Ccpm	50	26	RVK-Mc
297.7	302.1		3.5	Mcwm	47	20	RVK-M*f*m
302.1	306.74	DD88/29	5.5	Mcpm	50	26	RVK-Mm
306.74	308.65	DD88/30	1.5	Fmwm	25	10	QRVKq-Sf
308.65	310.55		9.5	Ccpm	50	26	RVK-Mc
310.55	313.06		5.5	Mcpm	50	26	RVK-Mm
313.06	316.47	DD88/31	5.5	Mcwm	40	15	QRVKj/q-Mm
316.47	316.69	DD88/32	0.5	Fmwm	20	10	QRVKq-Sf
316.69	325.64		5.5	Mcwm	40	15	QRVKj/q-Mm
325.64	325.74		0.5	Fmwm	20	10	QRVKq-Sf
325.74	326.21		5.5	Mcwm	40	15	QRVKj/q-Mm

326.21	327.51		3.5	Mmwm	25	15	QRVKj/q-M*f*m
327.51	329.35	DD88/33	0.5	Fmwm	20	10	QRVKq-Sf
329.35	335.6	DD88/34,35	8	Mcpm	45	20	QRVKj/q-Mm
335.6	354.7	DD88/36,37	5	Mcpm	45	20	QRVKj/q-Mm
354.7	408.37	**DD88/41**,38-44	10	Ccpm	**47**	**18.8**	**RVK-Mc**
408.37	409.46	DD88/45	4	Mmwm	25	15	QRVKq-M*f*m
409.46	420.68	DD88/46,47	9	Cmpm	25	15	QRVKq-Mc
420.68	427.25		-	-	-	-	*SHALE*

Calcretised kimberlite: 5.7 - 31.96 m
Oxidised kimberlite: 37.68 - 40.97 m
OH = open hole, CB = core broken
Shaded units are enlarged on graphic logs.

Table A7: The results of the magma clast shape analysis.

		ROUNDED	SUBROUNDED	IRREGULAR	SUBANGULAR	ANGULAR
Sample number	**Facies code**					
DD15/5	RVK-Mm	7	7	4	2	0
DD15/14	RVK-Mm	8	6	4	2	0
DD15/17	QRVKq-B*f*m	6	8	4	2	0
DD15/27	QRVKq-Mm	8	6	3	3	0
DD68/11	RVK-M*f*m	7	6	5	2	0
DD68/16	RVK-Mc	7	9	3	1	0
DD68/21	RVK-Mm	8	6	5	1	0
DD68/25	RVK-Mc	8	6	4	2	0
DD88/9	RVK-Mm	6	5	4	5	0
DD88/19	QRVKq-Sf	9	7	2	2	0
DD88/28	QRVKj/q-B*f*m	4	8	6	2	0
DD88/41	RVK-Mc	5	6	6	3	0
TOTAL		**83**	**80**	**50**	**27**	**0**

Table A8: Major and trace element compositions of the nine samples analysed in this study (total Fe as Fe_2O_3; all volatiles as LOI).

Major element abundance (%)	JS-KM1	JC-KM2	JN-KM3	JN-FM	JS-M	JC-GMB	JC-GM	JN-KBs	JN-KBm
SiO_2	51.58	39.8	40.55	39.15	53.34	50.99	65.4	54.38	52.46
TiO_2	0.75	0.61	0.91	0.62	0.39	0.61	0.54	0.43	1.4
Al_2O_3	8.92	5.74	5.94	10.92	9.59	10.56	12.81	10.16	25.26
Fe_2O_3	4.73	5.99	6.38	6.37	5.08	4.99	3.86	3.78	1.13
MnO	0.12	0.08	0.05	0.11	0.02	0.22	0.04	0.14	0.01
MgO	11.06	20.26	20.33	22.86	12.64	7.88	3.22	4.95	2.75
CaO	3.9	3.33	2.99	1.54	1.19	6.19	0.87	6.62	2.21
Na_2O	0.27	0.53	0.23	0.24	0.13	0.38	0.43	0.1	0.09
K_2O	4.31	0.57	0.64	1.45	4.78	5.01	7.35	7.09	2.33
P_2O_5	0.27	0.22	0.6	0.68	0.12	0.26	0.1	0.08	0.04
LOI	8.81	10.02	8.88	10.68	5.74	11.33	4.28	11.41	6.33
H_2O-	5.47	12.66	11.78	5.53	7.39	1.72	1.58	1.59	6.33
TOTAL	100.19	99.81	99.28	100.15	100.41	100.14	100.48	100.73	100.34
Trace element abundance (ppm)	**JS-KM1**	**JC-KM2**	**JN-KM3**	**JN-FM**	**JS-M**	**JC-GMB**	**JC-GM**	**JN-KBs**	**JN-KBm**
V	73	55	77	86	37	58	57	63	128
Cr	358	457	737	52	25	294	84	35	107
Co	36	41	78	37	42	17	13	25	12
Ni	256	519	958	818	469	263	64	130	31
Cu	46	36	34	12	6	25	20	19	16
Zn	53	55	64	90	48	85	69	43	40
Rb	161	42	46	97	126	197	277	184	159
Sr	251	428	386	219	124	222	66	230	103
Y	25	19	22	31	17	33	32	26	51
Zr	205	125	153	172	231	188	250	158	323
Nb	85	75	119	19	10	42	22	14	55
Ba	417	241	601	196	358	501	527	328	249
Th	14	9	12	13	10	14	10	10	28
Sc	11	8	10	12	7	12	11	8	21
La	59	44	63	42	27	47	47	32	51
Ce	106	84	114	88	55	85	89	60	121
Nd	43	32	46	47	24	38	38	27	42
Pb	15	10	10	31	11	15	21	14	55

Table A9: Majbr and trace element data for the nine samples normalised to 100% free of volatiles. This data used in all manipulations.

Major element abundance (%)	JS-KM1	JC-KM2	JN-KM3	JN-FM	JS-M	JC-GMB	JC-GM	JN-KBs	JN-KBm
SiO_2	60.04	51.6	51.58	46.63	61.13	58.54	69.13	61.99	59.83
TiO_2	0.87	0.79	1.16	0.74	0.44	0.7	0.57	0.49	1.6
Al_2O_3	10.38	7.44	7.56	13.01	10.99	12.12	13.54	11.58	28.81
Fe_2O_3	5.51	7.77	8.12	7.59	5.82	5.73	4.08	4.31	1.29
MnO	0.14	0.1	0.06	0.13	0.02	0.25	0.04	0.16	0.01
MgO	12.87	26.27	25.86	27.23	14.49	9.05	3.4	5.64	3.14
CaO	4.54	4.32	3.8	1.83	1.36	7.11	0.92	7.55	2.52
Na_2O	0.31	0.69	0.29	0.29	0.15	0.44	0.45	0.11	0.1
K_2O	5.02	0.74	0.81	1.73	5.48	5.75	7.77	8.08	2.66
P_2O_5	0.31	0.29	0.76	0.81	0.14	0.3	0.11	0.09	0.05
TOTAL	99.99	100.01	100	99.99	100.02	99.99	100.01	100	100.01
Trace element abundance (ppm)	**JS-KM1**	**JC-KM2**	**JN-KM3**	**JN-FM**	**JS-M**	**JC-GMB**	**JC-GM**	**JN-KBs**	**JN-KBm**
V	85	71	98	102	42	67	60	72	146
Cr	417	593	937	62	29	338	89	40	122
Co	42	53	99	44	48	20	14	29	14
Ni	298	673	1219	974	537	302	68	148	35
Cu	54	47	43	14	7	29	21	22	18
Zn	62	71	81	107	55	98	73	49	46
Rb	187	54	59	116	144	226	293	210	181
Sr	292	555	491	261	142	255	70	262	117
Y	29	25	28	37	19	38	34	30	58
Zr	239	162	195	205	265	216	264	180	368
Nb	99	97	151	23	11	48	23	16	63
Ba	485	312	764	233	410	575	557	374	284
Th	16	12	15	15	11	16	11	11	32
Sc	13	10	13	14	8	14	12	9	24
La	69	57	80	50	31	54	50	36	58
Ce	123	109	145	105	63	98	94	68	138
Nd	50	41	59	56	28	44	40	31	48
Pb	17	13	13	37	13	17	22	16	63

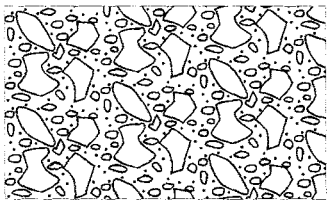

Poorly sorted

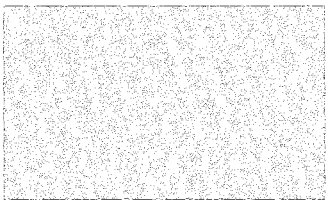

Clast supported

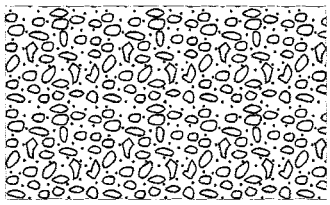

Well sorted

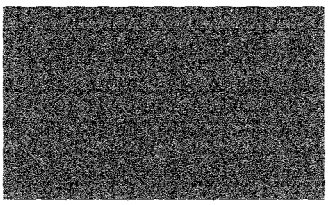

Matrix supported

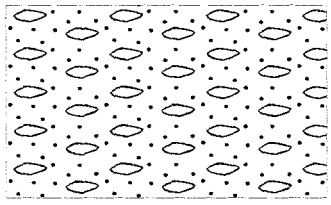

Vaguely bedded

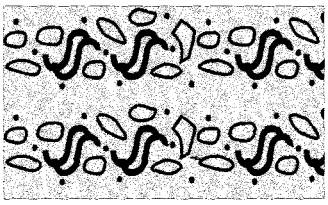

Soft sed deformation

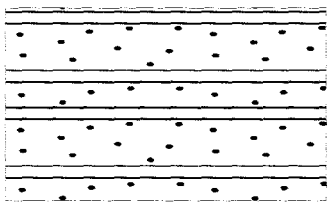

Distinctly bedded

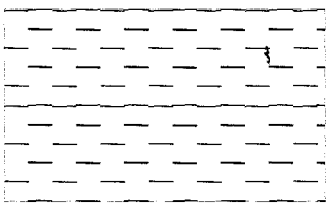

Wall rock shale

Olivine modal abundance

CRX modal abundance

50 18
Olivine CRX
Modal abundance

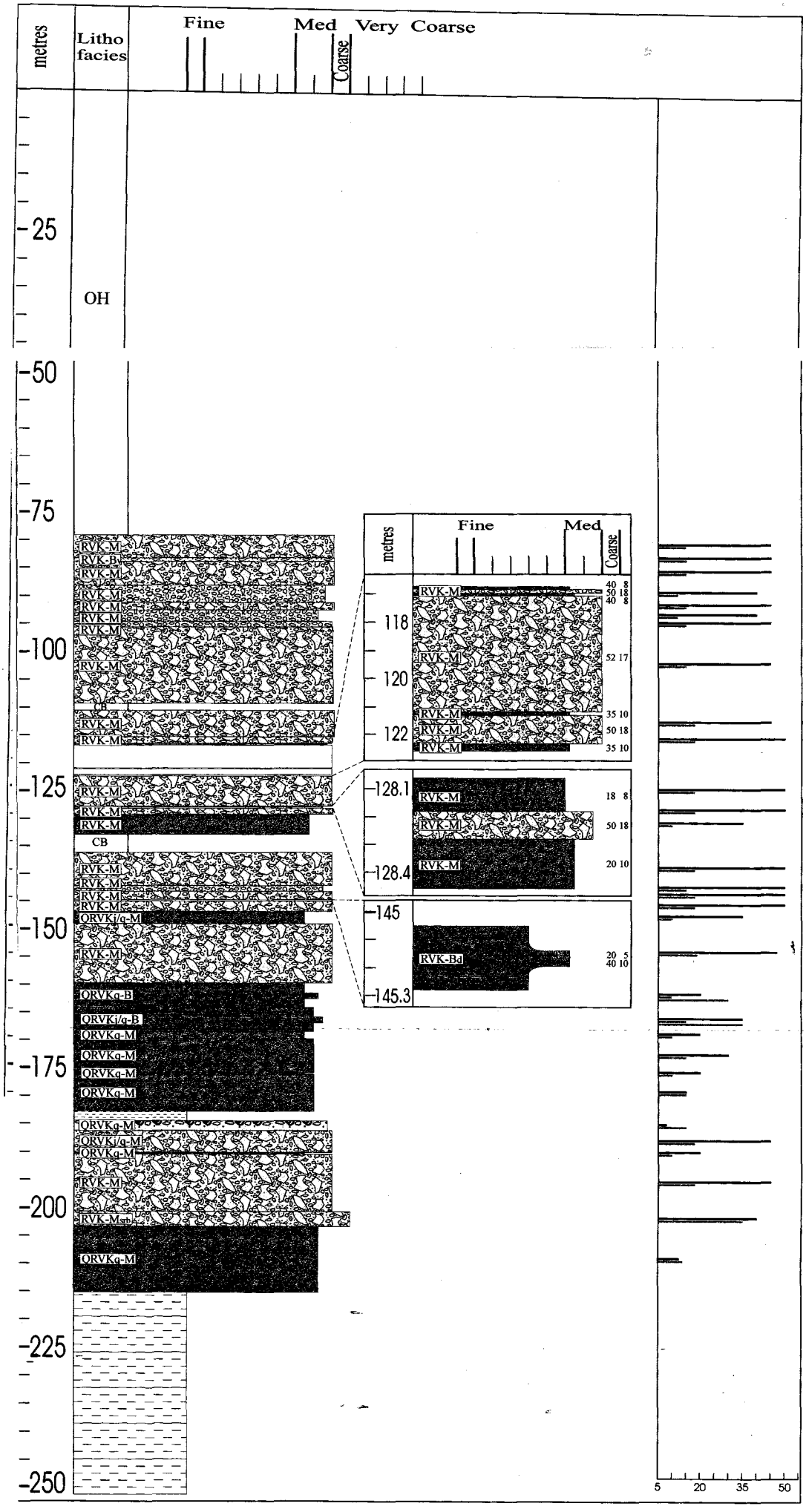
metres
Litho facies
Fine
Med
Very Coarse
Coarse
OH
CB
RVK-M
RVK-Bd
ORVKq-B
ORVKj/q-B
ORVKq-M
ORVKj/q-M
RVK-Msh
-25
-50
-75
-100
-125
-150
-175
-200
-225
-250
118
120
122
128.1
128.4
145
145.3
5
20
35
50

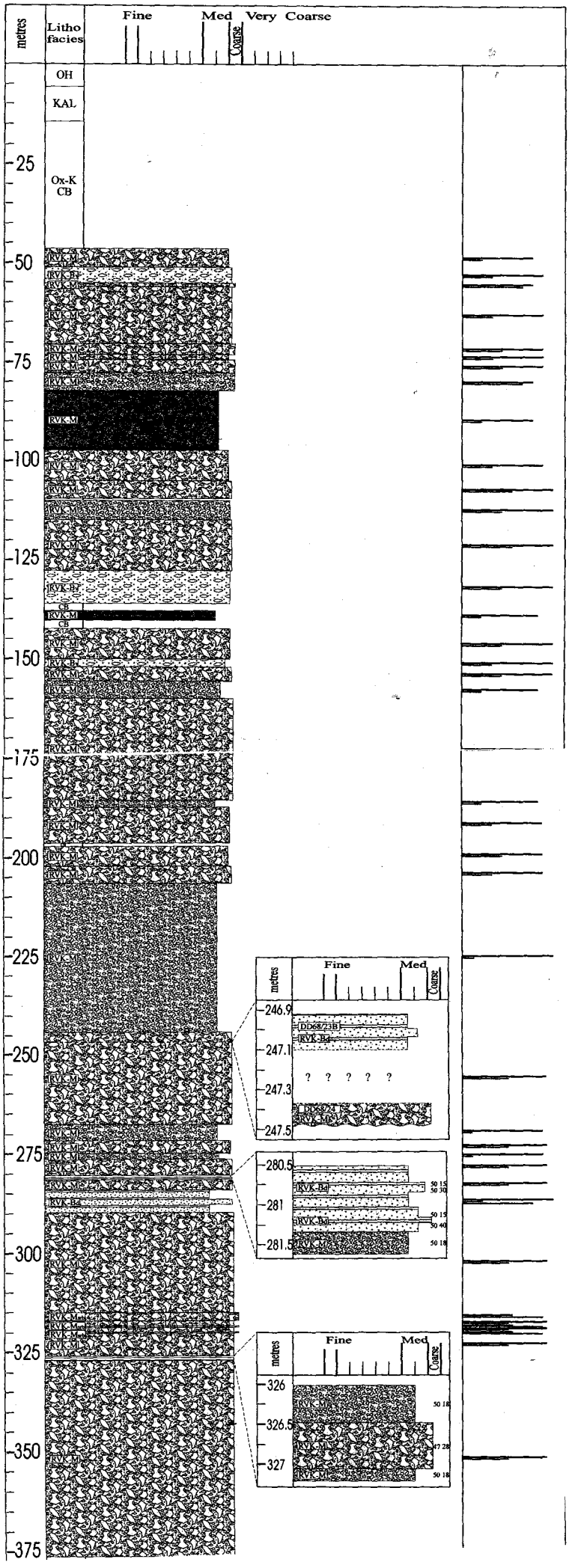
metres
Litho facies
Fine
Med
Very Coarse
Coarse
OH
KAL
Ox-K CB
25
50
75
100
125
150
175
200
225
250
275
300
325
350
375
RVK-Ml
RVK-Bd
RVK-Bl
CB
246.9
247.1
247.3
247.5
DD68/23B
DD68/24
280.5
281
281.5
326
326.5
327

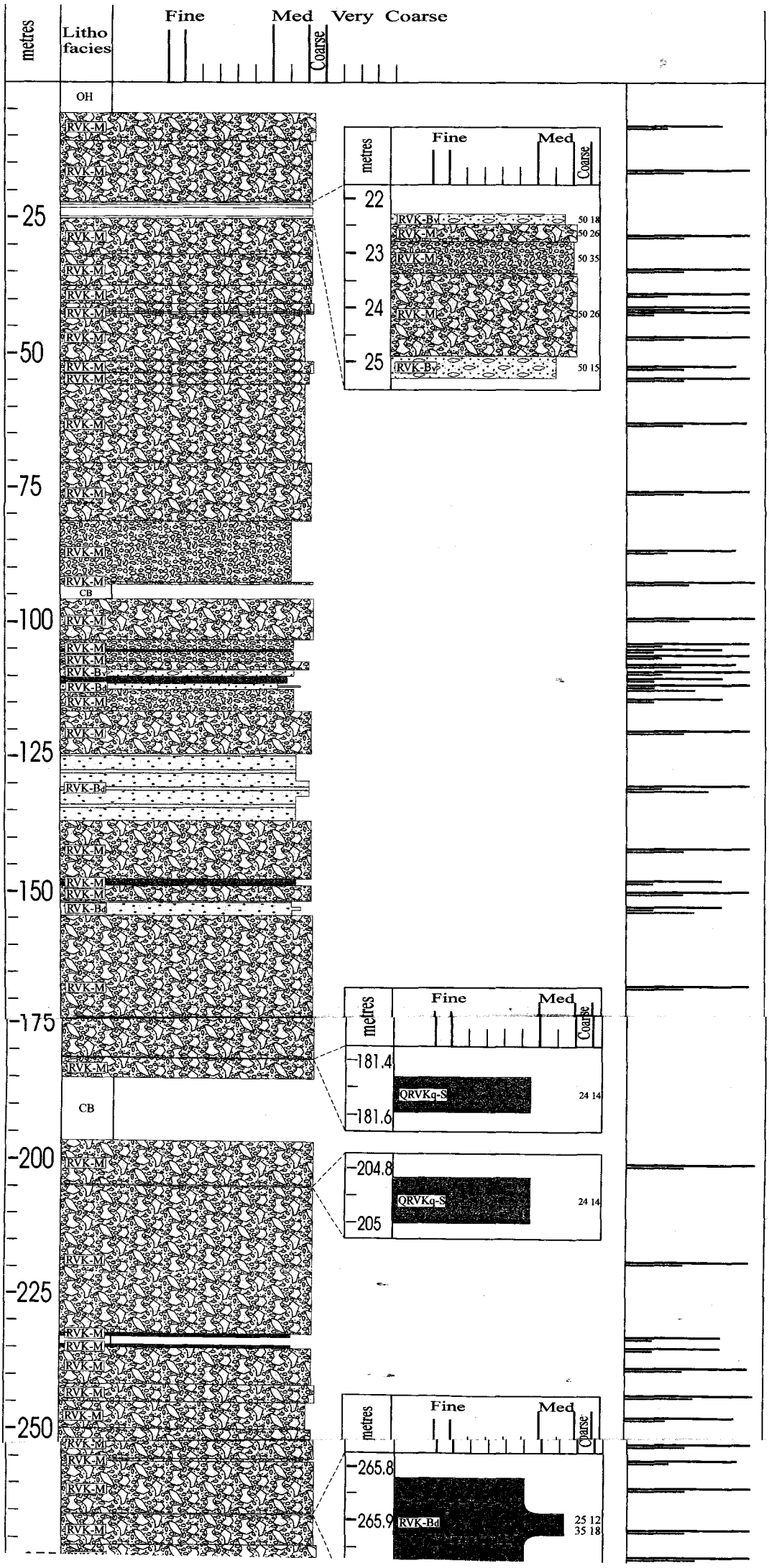

Join to next page

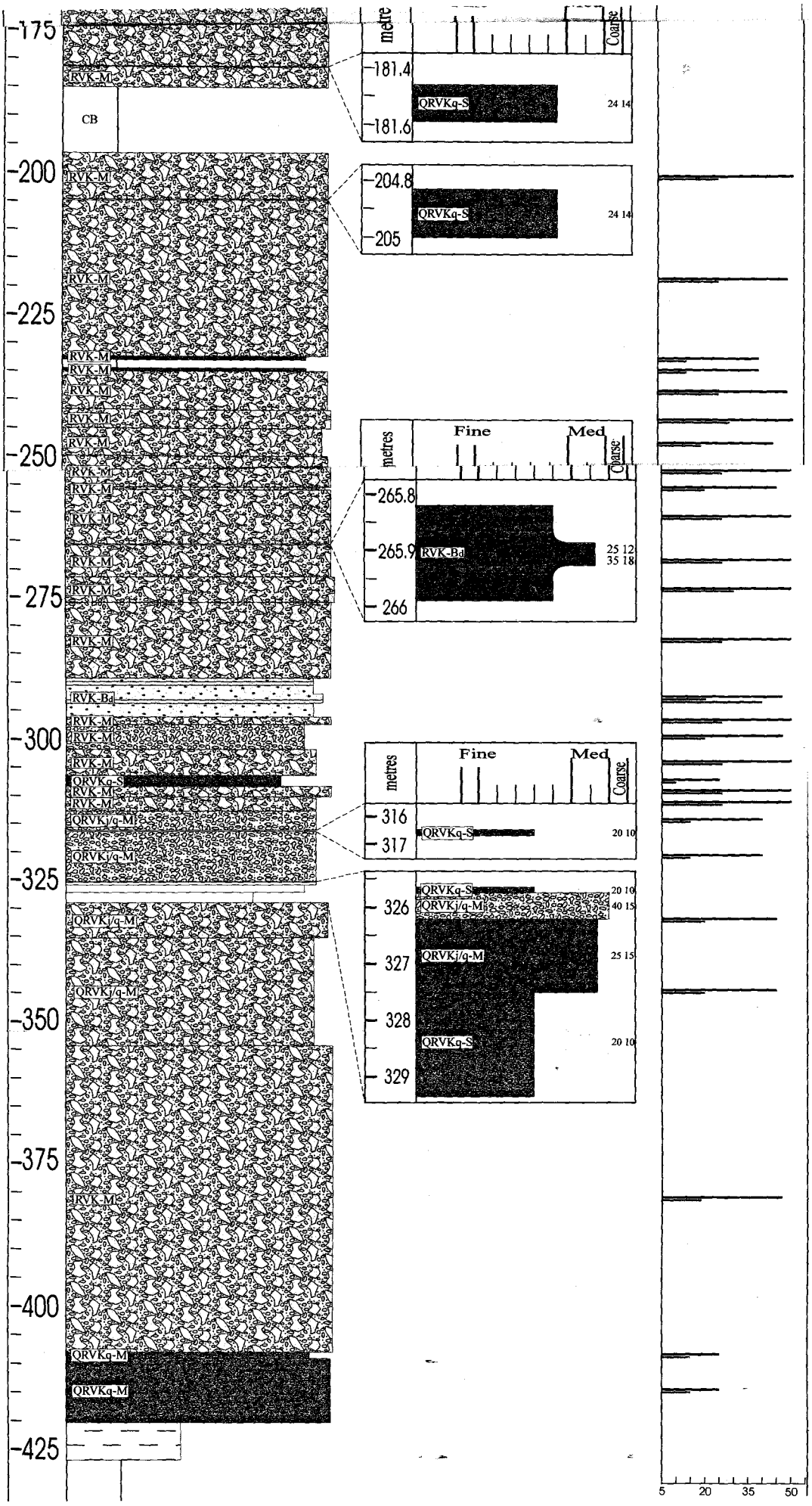

Join on previous page